University of Windsor

Scholarship at UWindsor

2008

Modeling, control, and implementation of enhanced premixed combustion in diesel engines

Raj Kumar
University of Windsor

MODELING, CONTROL, AND IMPLEMENTATION OF ENHANCED PREMIXED COMBUSTION IN DIESEL ENGINES

by

Raj Kumar

A Dissertation

Submitted to the Faculty of Graduate Studies

through Mechanical, Automotive and Materials Engineering

in Partial Fulfillment of the Requirements for

the Degree of Doctor of Philosophy at the

University of Windsor

Windsor, Ontario, Canada

2008

Canada

AUTHOR'S DECLARATION OF ORIGINALITY

I hereby certify that I am the sole author of this thesis and that no part of this thesis has been published or submitted for publication.

I certify that, to the best of my knowledge, my thesis does not infringe upon anyone's copyright nor violate any proprietary rights and that any ideas, techniques, quotations, or any other material from the work of other people included in my thesis, published or otherwise, are fully acknowledged in accordance with the standard referencing practices. Furthermore, to the extent that I have included copyright material that surpasses the bounds of fair dealing within the meaning of the Copyright Canada Act, I certify that I have obtained a written permission from the copyright owner(s) to include such material(s) in my thesis and have included copies of such copyright clearances to my appendix.

I declare that this is a true copy of my thesis, including any final revisions, as approved by my thesis committee and the Graduate Studies office, and that this thesis has not been submitted for a higher degree to any other University of Institutions.

ABSTRACT

Three different combustion modes for simultaneous low-nitrogen oxides (NOx) and low-particulate-matter (PM) called enhanced-premixed combustion (EPC) are described in this thesis for diesel engines.

a) Multi-pulse EPC: This combustion mode was implemented with multi-pulse fuel-injection events early during the compression stroke and a heavy use of EGR. This type of combustion was characterized by a short combustion duration which increased the rate-of-pressure rise and maximum pressures in comparison to the conventional diesel combustion mode. The combustion phasing for this mode was kinetics controlled and this combustion mode was largely applicable to mid-load engine operating conditions.

b) EGR enabled EPC with single injection: This combustion mode was implemented with a single-injection close to top-dead center and a heavy use of EGR. The use of closed-loop control on combustion phasing via a cylinder pressure based control was found to be an important enabler for stabilizing this type of combustion. This combustion mode was applied mainly at low-load engine operating conditions.

c) Combustion mode with a split heat-release characteristic: This combustion mode consisted of a part of the fuel delivery very early during the compression stroke and a part of the fuel delivery close to the top-dead-centre (TDC). The part of fuel injected close to TDC experienced conventional high-temperature combustion and oxidized the carbon-monoxide produced earlier in the cycle, thereby improving combustion efficiency. The split nature of the combustion limited the rate-of-pressure rise associated with the multi-pulse EPC combustion.

The implementation of EPC were associated with fuel-efficiency penalty either due to off-phasing of combustion event, UHC and carbon-monoxide or oil-dilution. Specific strategies have been presented to overcome each of these limitations.

A production version of 2.0 Liter, 4-cylinder FORD common-rail diesel engine was modified for the EPC experiments to run in a single-cylinder mode using a prototype intake and exhaust manifold and using independent fuel-injection strategies.

DEDICATION

This dissertation is dedicated to my parents, Mr. M. Muthurajan and Mrs .M.Nagaratinam my sister, Dr. M.Uma Maheshwari and brother M.Anand, who are my great role models and friends, and for always believing in me, inspiring me, and encouraging me to reach higher in order to achieve my goals. I am also thankful to my dear friend Simran without whom I may have never pursued this endeavor of higher education

ACKNOWLEDGEMENTS

TABLE OF CONTENTS

LIST OF FIGURES

LIST OF TABLES

NOMENCLATURE

ABDC	After Bottom Dead Centre
ATDC	After Top Dead Centre
BDC	Before Bottom Dead Centre
BMEP	Brake Mean Effective Pressure
BSFC	Brake Specific Fuel Consumption
CAD	Crank Angle Degrees (°CA)
CAI	California Analytical Instruments
CI	Compression Ignition
CN	Cetane Number
DI	Direct Injection
EGR	Exhaust Gas Recirculation
EOC	End of Combustion
EPA	USA Environmental protection Agency
EVO	Exhaust Valve Open
Exh	Exhaust
FBP	Final Boiling Point
FPGA	Field Programmable Gate Array
FSN	Filter Smoke Number
HCCI	Homogeneous Charge Compression Ignition
H-FID	Heated-Flame Ionization Detector
HRR CA50	Crank Angle of 50% Heat-Released
HTC	High Temperature Combustion
IBP	Initial Boiling Point
ICE	Internal Combustion Engine

IMEP	Indicated Mean Effective Pressure
Int	Intake
IVC	Intake Valve Close
LHV	Lower Heating Value
LTC	Low Temperature Combustion
MAF	Mass Air Flow
NDIR	Non-Dispersive Infra-Red
NO	Nitrogen Oxide
NO_2	Nitrogen Di-Oxide
O	Oxygen Radical
OH	Hydroxyl Radical
P	Average Cylinder Pressure (during τ_{ID})
P_{intake}	Intake Pressure
PM	Particulate Matter
ppm	Parts Per Million
R_u	Universal Gas Constant
SAES	Synthetic Atmosphere Engine Simulations
SOC	Start of Combustion
SOI	Start of Injection
T	Average Cylinder Temperature (during τ_{ID})
TDC	Top Dead Centre
THC	Total Hydrocarbons
T_{intake}	Intake Temperature
TWC	Three-Way Catalytic converter
UHC	Un-burnt Hydrocarbons

CHAPTER I

1 PREFACE

1.1 Motivation

Diesel engines have high thermal efficiencies due to their higher compression ratio and fuel-lean operation. In addition, diesel engines do not suffer from throttling losses such as in the case of conventional gasoline engines which increases their part-load efficiency. However, the main challenge for the modern diesel engines is to meet increasingly stringent emission norms for oxides of nitrogen (NOx), particulate-matter (PM), carbon-monoxide (CO) and un-burnt hydrocarbons (HC). A significant challenge for emission reduction in current production diesel engines is the presence of NOx-PM trade-off, which means that any emission control measure that leads to a reduction in NOx, results in an increase in PM emissions and vice-versa.

In the present work, the enhanced-premixed combustion strategies have been demonstrated that were able to reduce NOx and PM emissions simultaneously, with limited penalty on the indicated efficiency.

1.2 Objective and approach

The primary goal of the work was to develop an enhanced-premixed combustion (EPC) strategy that helped to overcome the traditional NOx-PM trade-off and reduce NOx and PM simultaneously. This was done by the preparation of a premixed lean cylinder-charge or premixed diluted cylinder-charge prior to the combustion process. However, the preparation of a premixed cylinder charge with in-cylinder injection strategy represents a significant challenge due to the low volatility of the diesel fuel. The petroleum derived diesel fuel is composed of saturated, unsaturated and aromatic hydrocarbons. The carbon chain for the diesel fuel consists of C10 and higher carbon atoms. The chain length has a strong correlation with the boiling point of the fuel, with the longer chains having a higher boiling point. Therefore, the boiling point of diesel is significantly higher than fuels such as gasoline which consists of C7 to C11 carbon chains. For the Diesel fuel

1

used for the present experiments, the vaporization was initiated at ~175°C and continued up to 350°C depending on their molecular structure of the hydrocarbons. These high-temperatures limit the implementation of external mixture preparation strategies such as intake-port injection for the diesel engine. Even for the in-cylinder mixture preparation strategies the temporal window of the fuel vaporization and mixture preparation is normally short, for instance limited to 40~80°CA depending on the engine operating condition.

In this thesis, the effect of important engine parameters such as the fuel-injection scheduling, exhaust gas recirculation (EGR), boost, and injection-pressure was experimentally investigated on the mixture preparation process for the EPC combustion. Based on the experimental studies, guidelines were developed to facilitate the implementation of the EPC strategies over a range of engine operating conditions. The implementation of the EGR enabled EPC strategy resulted in engine operations with high cycle-to-cycle variation and therefore, cylinder-pressure based control strategies were developed and used to assist the engine operation.

1.3   Thesis Organization

The thesis is divided into the IX sections.

Section-I, Preface: This section details the main motivation for the thesis.

Section-II, Introduction: In this section the basics of the diesel combustion and the pollutant formation are discussed.

Section-III, Literature review: In this section work done by other authors in the area for in-cylinder emission control for the diesel combustion is reviewed. This helped to develop the methodology for the present work.

Section-IV, Objective: This section provides the detailed objective for the thesis.

Section-V: Methodology: In this section the details of the experimental and the modeling preparation are provided. The important details for post-processing the experimental data can also be found in this section.

Section-VI, Results and discussion: The experimental test results are presented in a chronological manner in this section.

Section-VII, Efficiency characterization: The examination of the results in the section VI showed that there is a thermal-efficiency penalty during the implementation of the EPC combustion strategy. The major factors that affect the cycle thermal efficiency are documented in this section. This section also provides steps to improve thermal-efficiency of the EPC cycles.

Section-VIII, Modeling studies: In this section, the results for the chemical-kinetic based modeling to evaluate the boundary conditions of boost and EGR for the EPC combustion are presented. The results for the numerical investigation of EGR-reformer are also presented in this section. Furthermore, the computational-fluid dynamics results to explain the EPC combustion are also described in this section.

Section-IX, Heat-release rate characterization: In this section the relationship between the heat-release rate and each of the important emission and performance parameter for the EPC combustion is examined. Based on this analysis, it is possible to formulate the desired set of heat-release characteristics for the EPC combustion.

Section-X, Conclusions and future work: In this section the major conclusions of the thesis have been summarized and the planned future-work for this project has been presented.

CHAPTER II

2   INTRODUCTION

2.1   Diesel Engine

The concept of compression-ignition was proposed by the German engineer, Rudolf Diesel. He was deeply influenced by his contemporaries, Sadi Carnot and Nicolaus Otto. He understood that the engine's cycle efficiency was decided primarily by the compression/expansion cycle. In 1876, Nicolaus Otto had demonstrated the concept of 4-stroke engine with a premixed fuel-air charge. Since a premixed cylinder charge was used, Otto had to limit the compression ratio so that the spontaneous combustion of the cylinder-charge would not be initiated before ignition. Diesel realized that by limiting the compression ratio, Otto had indirectly limited the thermal efficiency for the engine-cycle [1,2,3]. Diesel's solution to the problem was to inject the fuel only during the compression stroke and thus higher compression ratio could be used, thereby achieving higher cycle efficiency. He published his work in a paper called, "The Theory and Construction of a Rational Heat Engine Substitute for the Steam Engine and Today's Combustion Engines" and applied for the patent for his ideas in 1892. He was granted the first patent for his "Working Method and Design for Combustion Engines" in 1893 and tested his first prototype engine in same year. This engine was fuelled by powdered coal and Diesel was able to show that internal combustion was possible with auto-ignition.

2.2   Combustion in Diesel Engines

The diesel combustion process is usually explained on the heat-release rate diagrams such as Figure 2-1. The heat-release rate can be considered as the rate at which the chemical energy of the fuel is liberated during the combustion process and is estimated based on the in-cylinder pressure data. Traditionally, four regions are identified on the heat-release rate diagram [4]; ignition delay period (A), premixed combustion phase, (B) diffusion combustion phase (C), and tail-of-combustion (D).

(A), Ignition delay period: For the conventional diesel engine combustion air alone is compressed in the combustion chamber during the compression stroke, which greatly increases its temperature and pressure. The diesel fuel (commonly at injection pressures between 400~1500 bar) is injected into this highly compressed and heated air in the liquid state during the compression stroke. The liquid fuel droplets then absorb/extract heat from their surroundings and vaporize quickly. This reduces the temperature of the thin layer of air surrounding the droplet but its temperature is again raised by heat transfer from the main bulk of air. The diesel auto-ignition takes place only after the vaporized fuel is mixed with the air to flammability limits and the local temperature is above the auto-ignition temperature. Thus, there is a delay, called the ignition delay period before the combustion is initiated.

(B), Premixed combustion phase: At the end of the ignition delay period, the fuel-air mixture that is premixed during the ignition delay period burns rapidly. Once ignition has taken place and flames are established, the thermal energy available for further evaporation is enhanced by the energy released by combustion. The initial fuel droplets meet air whose temperature is only slightly above their self-ignition temperature and ignite after ignition delay, however, the subsequent fuel droplets find air that is already heated to much higher temperatures by the burning of initial droplets and therefore their ignition delay is much shorter.

(C), Diffusion combustion phase: Typically, at the end of premixed combustion phase the rate of combustion is determined by the fuel-air mixing rate. The mixing controlled part of the combustion phase is known as the diffusion combustion phase.

(D), Tail-of-combustion: A small amount of heat-release may take place after the diffusion combustion due to oxidation of soot or other fuel-rich products during the advanced stages of the expansion stroke. This part of the combustion process is typically called the tail-of combustion.
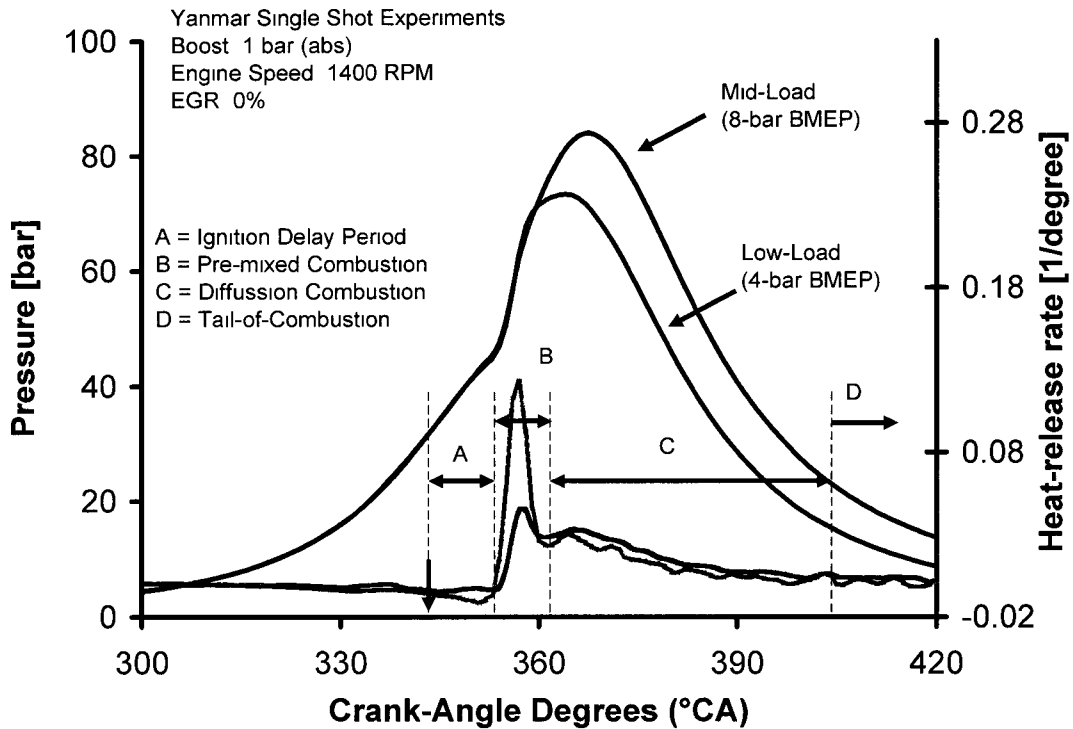
Figure 2-1: Typical heat-release rate from a classical diesel engine based on testing in the Clean Diesel Laboratory.

The spatial and temporal evolution of pollutants such as NOx, particulate matter (PM), and un-burnt hydrocarbons (UHC) are an area of intensive research. The mechanism of pollutant formation has been explained by direct in-cylinder sampling studies, laser diagnostic studies and computational fluid dynamic studies [5~17]. Based on these research tools it is commonly accepted that the diesel emissions are the result of the combustion of the heterogeneous air/fuel mixture and the amount of pollutant formation depends on the residence time in different air-fuel ratio and combustion temperature conditions. The commonly accepted temporal emission evolution during the diesel combustion process (Figure 2-2) suggests that the NOx is formed during the near-stoichiometric premixed combustion. The soot also begins to form during the premixed combustion and reaches its maximum during the diffusion combustion stage. During the diffusion combustion both soot formation and soot oxidation processes take place and the soot concentration at the end of the cycle is the difference between the total soot produced and the total soot oxidized. Similar conclusions were observed on engines with

6

optical-access [15]. The mechanism of formation of each of the species and the available techniques of their reduction are also discussed below.
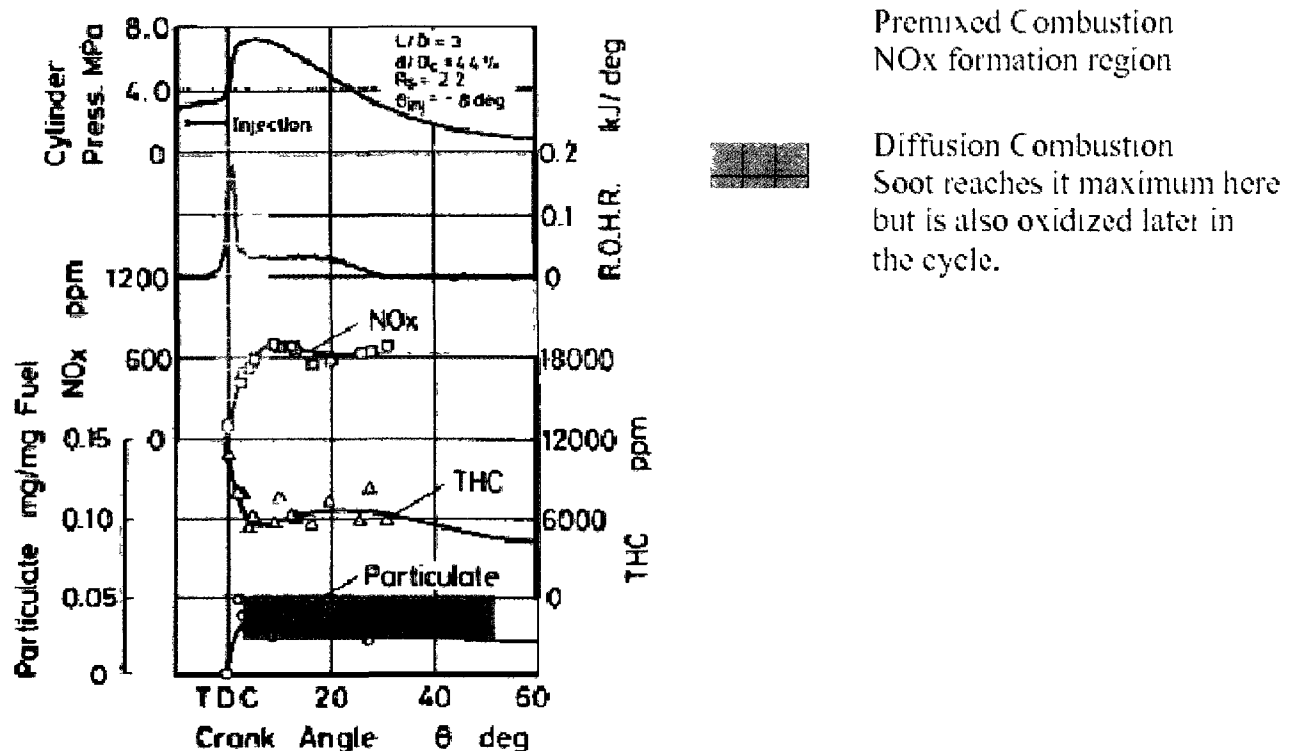
Figure 2-2: Mechanism of emission formation in diesel engines [6].

2.3 Oxides of Nitrogen

Nitrogen oxide (NO) and nitrogen dioxide (NO_2) are the two main oxides of nitrogen that are formed during diesel combustion process. NO usually constitutes about 90% of the total exhaust NOx. Emission regulating bodies such as Environmental Protection Agency of United States regulates only nitrogen dioxide (NO_2) as a surrogate for this family of compounds because it is the most prevalent form of NOx in the atmosphere that is generated by human activities [19]. For the combustion of fuel with very little or no nitrogen, the NO formation has been explained based on three mechanisms namely: extended Zeldovich/thermal mechanism, N_2O intermediate mechanism and the prompt NO mechanism [4,16,17]. The details of the mechanisms are as described below.

a) Extended Zeldovich/thermal mechanism:

The thermal mechanism is considered responsible for the majority of NOx emissions from conventional diesel engines when the peak combustion temperatures are in excess of 2000K. The three chemical reactions that are important in this mechanism are:

$$O + N_2 \leftrightarrow NO + N \tag{2.1}$$

$$N + O_2 \leftrightarrow NO + O \tag{2.2}$$

$$N + OH \leftrightarrow NO + H \tag{2.3}$$

The overall reaction rate for equations (2.1)~(2.3) are temperature sensitive and as a consequence, thermal NO only appears in significant quantities after the start of heat-release (Figure 2-2). The temperature sensitivity of this mechanism also means that as the in-cylinder temperature decreases during the expansion stroke, the thermal NO concentrations freeze shortly after the end of heat-release.

b) N_2O intermediate mechanism:

N_2O pathway is considered important for NO formation during the lean pre-mixed low-temperature combustion process. At sufficiently high pressures, N_2O is formed as a result of the three body reaction:

$$O + N_2 + M \leftrightarrow N_2O + M \tag{2.4}$$

where, "M" is a third body (molecule) of any compound that is needed to remove energy in order to complete the reaction. In the absence of the third body, it is observed that the produced N_2O quickly decomposed back to the original reactants O and N_2. Following equations (2.5) and (2.6)

$$H + N_2O \leftrightarrow N_2 + OH \tag{2.5}$$

$$O + N_2O \leftrightarrow N_2 + O_2 \tag{2.6}$$

However, when the air-fuel ratio is lean, NO forms through the reaction of O with N_2O. The O is produced mainly as a result of the equilibrium reaction (2.8)

$$N_2O + O \leftrightarrow 2NO \qquad\qquad (2.7)$$

$$O_2 + M \leftrightarrow 2O + M \qquad\qquad (2.8)$$

c) Prompt NO mechanism:

The prompt NO is considered significant during the rich combustion process, in the presence of a high concentration of hydrocarbon, O and OH radicals. Since the prompt NO mechanism is significant during the rich combustion, it is believed to contribute a small amount of NO in the diffusion portion of the diesel burning process [15]. The pathway for prompt NO is initiated by the rapid reaction of hydrocarbon radicals from the fuel with molecular nitrogen, leading to the formation of amines compounds that subsequently react to form NO.

2.4 Particulate Matter

As per the emission regulating bodies such as Environmental Protection Agency, particulate-matter (PM) is defined as any matter in the exhaust of an internal combustion engine that can be trapped on a sampling filter medium at 125°F (52°C) or less. The diesel PM is not considered a well defined physical species. Instead, it is treated as a complex emission, including a number of components. PM is traditionally divided into three main fractions as listed in Table 2-1 [18]:

Table 2-1: Particulate-matter constituent characterization

Category	Main Constituents
Solid fraction	Elemental carbon and ash
Soluble organic fraction(SOF)	Organic material derived from engine lubricating oil and fuel
Sulfate Particulates (SO4)	Sulfates, Sulfuric acid and water

2.5   Un-burnt-Hydrocarbons

The sources of HC in DI diesel engines have been attributed mainly to over/under-mixing of fuel-air mixture and flame-quenching during the combustion process [4]. The fuel injected during the ignition delay period (premixed portion) mixes with air and produces a wide range of equivalence ratios. Based on the air-fuel ratios the cylinder-charge mixture can be classified as follows (Figure 2-3):

Lean mixture -A mixture that is too lean to support a stabilized combustion

Stoichiometric -A mixture that is close to the stoichiometric ratio and ready to combust

Rich mixture -A mixture that is too rich and still need to evaporate and mix with air before it can engage in the combustion process

Combustion is initiated at close to stoichiometric regions and the combustion continues till the localized air-fuel ratio decreases rapidly due to over-mixing with the surrounding air or if the flame is quenched at the thermal boundary layer. This over-mixing/quenching can result in the formation of HC. The lean mixture may engage in the combustion process, if it mixes with the additional evaporated fuel during the combustion process or during the expansion-stroke. Similarly, the rich mixture will engage in the combustion process if it mixes with enough oxygen and can form a flammable mixture. However, if the lean mixture fails to find the necessary fuel or the rich mixture fails to find the air, then both the rich and the lean mixture have a tendency to form HC. It may be noted that that the HC characteristics due to the incomplete combustion of the rich mixture would be significantly different from that of the lean mixture. The HC formed due to the incomplete combustion of the rich mixture may consist of lower hydrocarbon chains as compared to the incomplete combustion of the lean mixture.
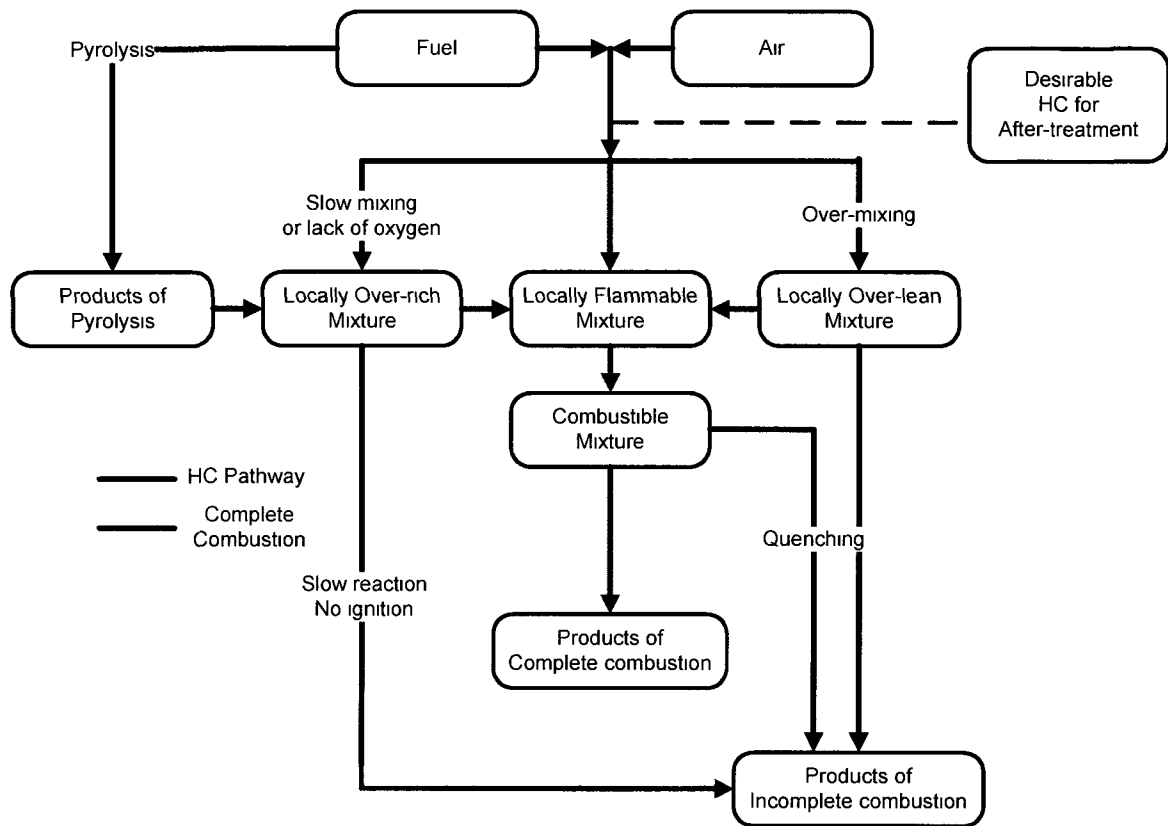
Figure 2-3: Hydrocarbon formation in diesel engine [4].

2.6 Exhaust Emissions Regulation

The diesel engines have been used in large heavy-duty trucks, buses and non-road equipment due to their fuel economy and durability advantages. However, they emit significant amounts of NOx, PM, and HC as pollutants that have a harmful effect on the environment and our health. Therefore, the government organizations are implementing increasingly stringent emission norms to regulate the diesel engine emissions. Figure 2-4 and Figure 2-5 show the important emission control features that were introduced or have evolved over time with the implementation of increasingly stringent emission norms. Currently, most of the diesel engine research is focused on meeting the forthcoming stringent emission norms. An important consideration for the emission regulation is how these emissions regulations are applied to various vehicle categories and are implemented gradually over a period of time. Some details about vehicle categories have been included in the Appendix 11.3 for completeness along with the emission phase-in periods. Another

11

aspect of the emission regulation has been its significant impact on the engine oil development. More details about the evolution of engine oil needs with time as the emission regulations have been progressively tightened are provided in Appendix 11.4.
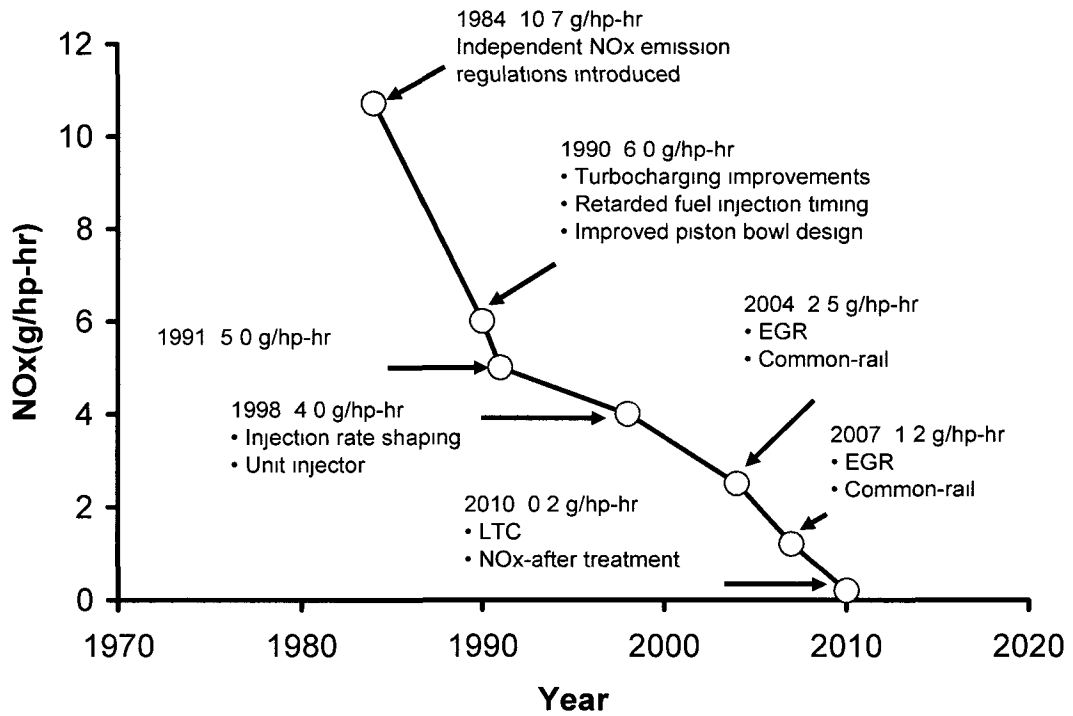
Figure 2-4: Evolution of NOx emission standards and control techniques.
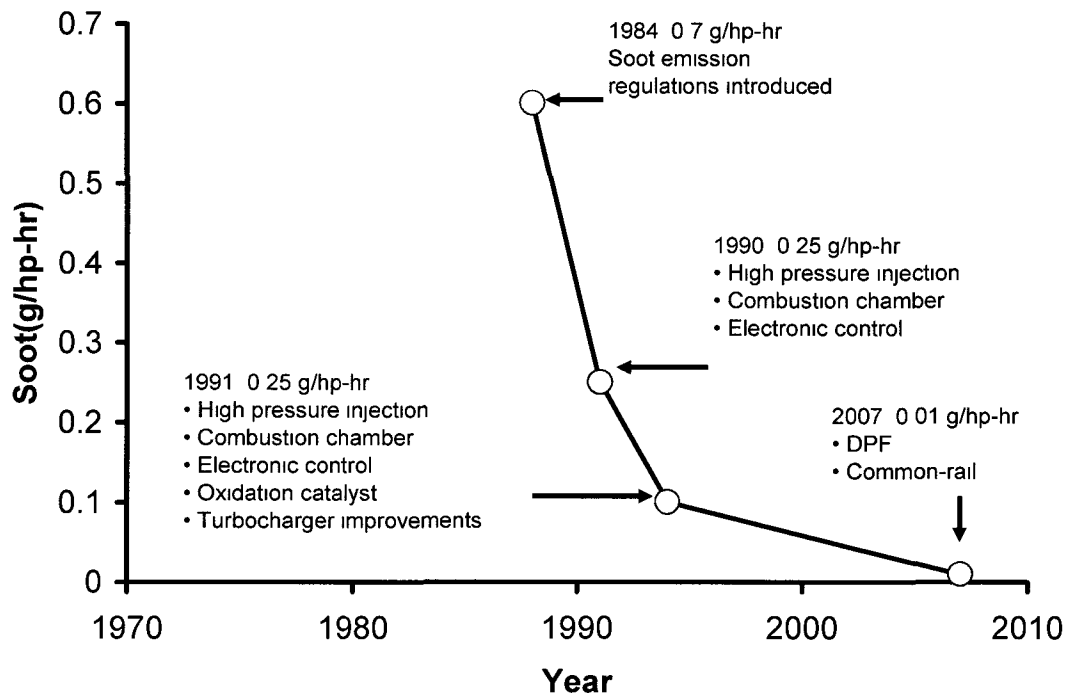
Figure 2-5: Evolution of soot emission standard and control techniques.

13

2.7 NOx-PM trade-off

As discussed in the previous section most of the diesel combustion research is being conducted to formulate solutions for the emission regulations. A serious obstacle towards using in-cylinder emission control measures to meet the emission regulation requirements is the presence of NOx-PM trade-off. The NOx-PM trade-off means that if a particular emission control technique resulted in a lower NOx, it has a tendency to increase PM or vice-versa. For instance, the use of EGR reduced NOx by lowering the combustion flame temperature and oxygen concentration [4,20~25]. However, the use of EGR led to increased PM emissions due to lowered oxygen concentration. Other emission control techniques such as retarding the injection timing or using oxygenated fuels had shown a similar NOx-PM trade-off. Figure 2-6 shows the NOx-PM trade-off with the use of EGR for classical low-injection pressure diesel combustion and diesel engines with modern common-rail injection. Note that the use of higher injection pressure had a tendency to suppress the soot formation but had a higher NOx for a given EGR value. Therefore, it is considered very challenging to reduce NOx and PM simultaneously to meet the future stringent emission norms, while retaining the power-density levels of the modern diesel engine.

	A	B	C	D
Engine Type	Classical Diesel	Common-Rail	Common-Rail	Common-Rail
No of Injections	1	1	2	6
BMEP [bar]	3 4	4 4	6 1	3 6
Fuel Pressure [bar]	NOP 200	Rail 1200	Rail 1200	Rail 1200
Intake Pressure [bar] (abs)	1	2 75	2 0	2 7
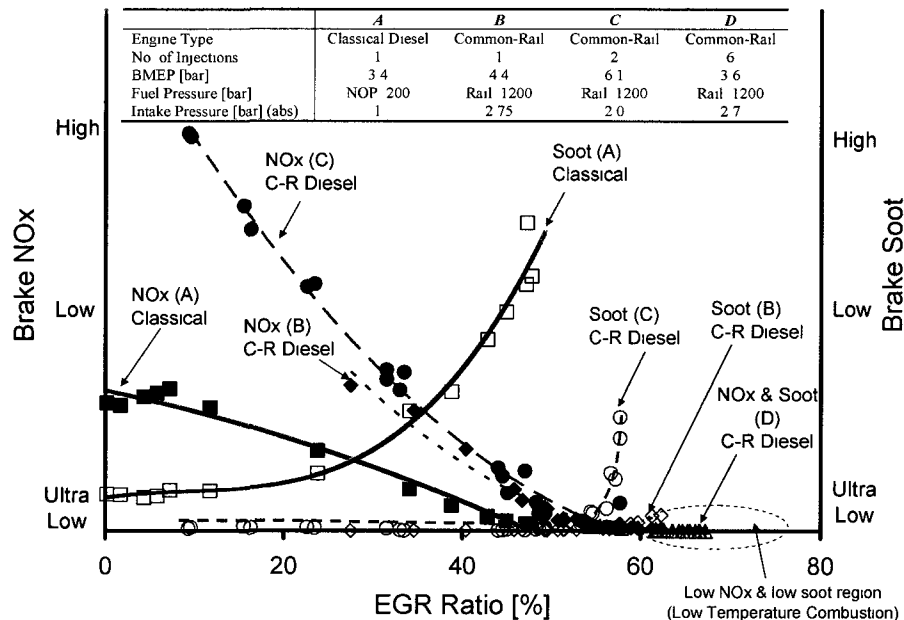
Figure 2-6: Experimental results showing traditional NOx soot trade-off with the application of EGR at the Clean Diesel Engine Laboratory [25].

14

CHAPTER III

3 LITERATURE REVIEW

3.1 Mechanism of particulate matter and NOx reduction

Clean diesel combustion strategies are being pursued to overcome the classical NOx-soot trade-off and to reduce the engine-out NOx and soot emissions simultaneously. In order to accomplish this, researchers have tried to understand the mechanisms of soot and NOx formation and based on this fundamental study, they have tried to formulate the pathways for simultaneous low NOx and soot combustion.

Some of the studies were performed on a diesel engine, while others were performed in apparatus such as a rapid compression machine or a shock-tube. Aoyagi et al. studied the soot formation in a diesel engine using in-cylinder sampling studies and observed that the soot formation was significant when the maximum combustion temperature ranged from 2100 to 2300K and the maximum equivalence ratio ranged from 1.5 to 3.5 [5]. Kamimoto et al. studied the soot formation phenomenon in a rapid compression machine using laser schrielen photograph. Based on their measurements of equivalence ratio and flame temperatures, they concluded that the soot was formed in a region in the flame where the average equivalence ratio was rich and the flame temperature was high enough to promote fuel pyrolysis of the evaporated fuel [10]. Similarly, Uyehara observed that the soot was formed in the temperature ranges from 2000 to 2400K in diffusion flames [12]. The effect of temperature and pressure on soot formation due to pyrolysis was studied in shock tubes by Frenklach et al. and their study showed that the soot yield became significant at 1800K and no soot was generated below 1500K or above 2300K [13]. Kamimoto et al. advanced their previous work with in-cylinder sampling studies in the actual diesel engine and combined it with their NOx modeling work and produced the "ϕ-T" diagram or local-equivalence-ratio versus local-temperature [11]. This work is widely considered as the one of the first attempts to formulate the pathway for simultaneous low-NOx and low-soot (Figure 3-1).

Figure 3-1: Pathway for simultaneous NOx and soot reduction [11].

Recently, Kitamura et al. (Figure 3-2) have revisited the soot formation characteristics on the ϕ-T map based on computational fluid dynamic analysis. They have also identified three different regions on their ϕ-T map for the soot formation. There was no soot below 1500K regardless of equivalence ratio. Similarly, for an equivalence ratio below 2 no soot was formed regardless of temperature. The maximum sooting tendency was around 1800 – 2000K and as temperature gets higher than that, the sooting tendency was reduced for a given equivalence ratio. Based on all the mentioned analysis there was a general consensus that a lean-homogenous cylinder charge during diesel combustion would have very little sooting tendency. The lean-homogenous cylinder charge also produces a low flame temperature which results in low-NOx simultaneously. Thus, the preparation of a lean-homogenous mixture before the combustion was considered as the primary requirement for simultaneous low-NOx and low-soot combustion.

16

Figure 3-2: Mechanism of the soot formation for surrogate diesel fuel, n-heptane [14].

3.2 Simultaneous NOx and particulate-matter reduction in diesel engine

Diesel engine researchers have tried to translate the above knowledge to actual diesel operation. They have tried to prepare the lean-homogenous charge before the combustion process to achieve simultaneous low-NOx and low-soot during the diesel engine combustion. This simultaneous low-NOx and low-soot combustion has been called under different names by various authors such as homogenous-charge-compression-ignition (HCCI), smoke-less rich combustion, premixed lean diesel combustion (PREDIC) and modulated-kinetics (MK) and low-temperature-combustion (LTC), depending on the methodology adopted.

HCCI: HCCI type of combustion has been achieved by compression ignition of a mixture of air, fuel and EGR of appropriate equivalence ratio. The mixture equivalence ratio has a significant effect on the combustion process. If the mixture was too rich, the rate of combustion became too rapid and resulted in knock-related problems. A very lean mixture resulted in incomplete combustion or misfire. Thus a close-control on the air-fuel ratio within a narrow band is a strongly desired attribute for the HCCI type of combustion. Another characteristic for the HCCI type of combustion is the lack of a discernible flame front and rapid distributed low-temperature reactions.

17

The first studies on HCCI were performed on a two stroke engine by Onishi et al. in 1979 and they called it Active-Thermo Atmosphere Combustion (ATAC) [26]. Their studies showed the lack of flame propagation, and the near instantaneous combustion of the entire cylinder charge mixture. Noguchi et al. demonstrated the same combustion process in an opposed-piston two stroke engine [27]. They also conducted measurements of radical concentration during combustion and highlighted the significance of chemical kinetics during HCCI type of combustion. In 1994, Iida used methanol as a fuel to extend the load limits of the stable two-stroke HCCI combustion [28]. HCCI was used in two-stroke engines to improve combustion stability, reduce HC emissions and improve fuel economy at part load conditions. In 1983, Najt and Foster showed HCCI type of combustion in a four-stroke engine with iso-octane and n-heptane as fuel [29]. Thring used both gasoline and diesel fuel, and investigated possible combinations of intake temperature, equivalence-ratio and EGR for a given load [30]. This work was later continued by Ryan and Callahan, and they showed that a low compression ratio (8:1), 45~50% EGR rates, and operation from lean to stoichiometric fresh-air-to-fuel ratios was needed for HCCI type of combustion in diesels [31]. Christensen et al. were the first ones to demonstrate HCCI type of combustion at high loads with natural gas as fuel [32~33]. A detailed review of the benefits and the disadvantages for HCCI type of combustion has been provided by Stanglmaier and Roberts [34]. The evolution of the HCCI combustion process is summarized in Table 3-1.

Table 3-1: History of HCCI combustion

(A) HCCI-Port Injection

SAE-790501 (First HCCI in 2-stroke)	Gasoline	Compression Ratio
SAE-830264 (First HCCI in 4-stroke)	Iso-octane ,n-heptane, isopropyl-benzene	7.5:1
SAE-892068	Gasoline	15:1
SAE-961160 (Low CR, EGR Guidelines)	Diesel Fuel	7.5:1~17:1
SAE-980787 (IMEP~12 bar)	Iso-octane, Ethanol, Natural Gas	17:1, 19:1
SAE-1999-01-0192	Iso-octane, Natural Gas and Ethanol	18:1
SAE 1999-01-3679	Gasoline, Diesel, Iso-octane, n-heptane	9.6:1, 22.5:1
SAE 2000-01-1835	Natural Gas, Iso-Octane	16:1, 24:1
SAE 2001-01-1894	Propane, Butane	18.8:1

(B) Premixed Combustion

SAE-961163	Diesel	16.5:1
SAE 1999-01-0185	Diesel	12:1
SAE 1999-01-3681	Diesel	17.5:1, 16:1
SAE 2005-01-0117 (multiple early injection)	Diesel	Not available
SAE 2005-01-09515	Diesel	Not available

(C) Late Injection with Heavy EGR

SAE 1999-01-3681	Diesel	18:1
SAE 2001-01-0200	Diesel	18:1

(D) Fuel Reforming

SAE 2007-01-2044	Diesel + Hydrogen	*
SAE 2007-01-1083	Diesel + Hydrogen	18.45:1

Based on the method of homogenous-mixture preparation, the diesel HCCI research can be divided into port-injection, single or multiple early in-cylinder injection and late in-cylinder injection. The port-injection was used by several researchers initially as a means of mixture preparation due to its simplicity [30,31]. However, a significant disadvantage for the port-injection strategy was the lack of combustion phasing control by fuel-injection strategy. The port injection with diesel also led to very high HC and CO

emissions and was associated with the problems of oil-dilution. Figure 3-3 and Figure 3-4 show the test results for the port injection experiments at the University of Windsor. It can be seen that for similar load levels port injection HCCI had lower NOx and soot compared to the conventional diesel combustion. However, the CO and HC emission was significantly higher in comparison to the conventional diesel combustion. The dilution of engine-oil with fuel was another significant drawback noticed during the port-injection experiments.
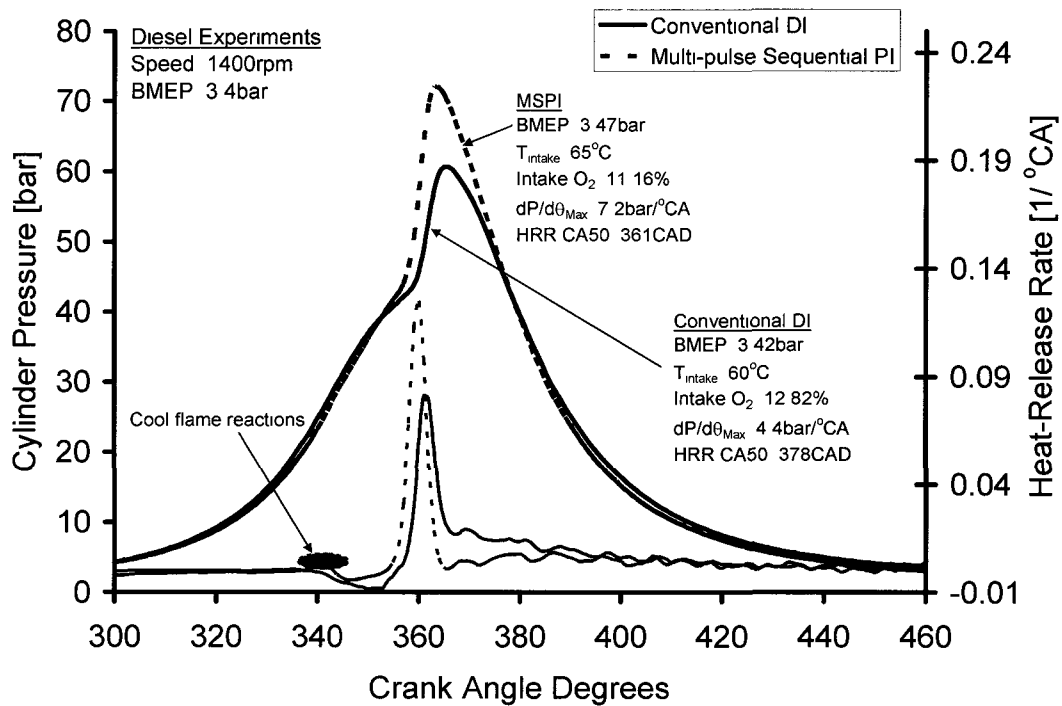
Figure 3-3: Port injection experiments at the University of Windsor [35].
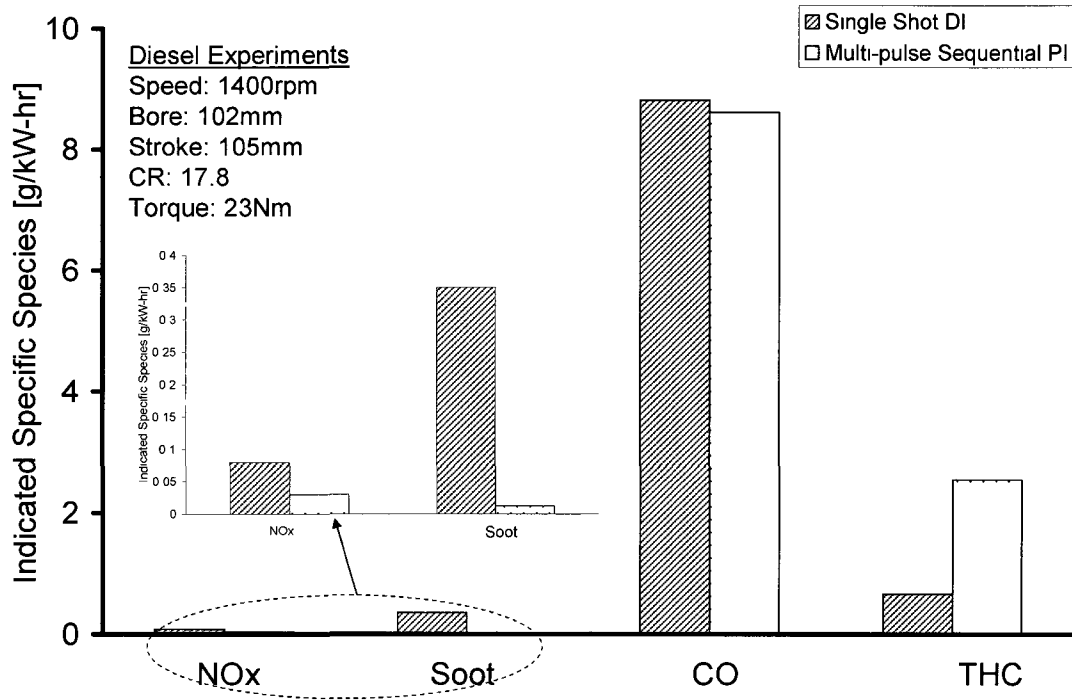
Figure 3-4: Emission results for port injection experiments [35].

PREDIC: PREDIC stands for PREmixed lean DIesel Combustion (PREDIC) and in this method, in-cylinder fuel injection strategy was implemented. The fuel injection timing was advanced very early to promote the preparation of a lean homogenous charge necessary for simultaneous low NOx and low-soot. For this method fuel impingement on the cylinder wall was a significant hindrance because of low cylinder charge densities at the time of fuel-injection [36~38].

Recently, multiple-injection strategies along with heavy EGR have also been reported by various authors as a means to prepare the lean-premixed cylinder charge for HCCI type of combustion. This has partly helped to alleviate the problem of high hydrocarbons due to cylinder wall-impingement. This technique has particularly helped to promote homogenous mixture preparation at high loads [39~45].

MK-combustion: MK combustion or modulated-kinetic combustion was characterized by low-temperature, premixed combustion system to simultaneously reduce NOx and PM emissions. Typically, a single injection strategy close to TDC was used, therefore, direct control on the combustion phasing was still retained by the injection event [46~48]. The

combustion temperature was lowered by the use of EGR. The time necessary for the premixed mixture was secured by prolonging the ignition delay by the use of heavy EGR and high injection pressure. The fuel injection timing was also significantly retarded to prolong the ignition delay. Since the injection event takes place close to TDC, the problem of high HC due to cylinder-wall impingement was avoided.

Smoke-less EGR and LTC: The smokeless combustion avoids the soot formation regions on the "ϕ-T" map by reducing the combustion temperature below the critical temperature for soot formation. This was realized by using a large amount of cooled EGR and the air-fuel ratio approaching near stoichiometric or rich operating conditions instead of the lean-premixed conditions [49].

3.3 Enhanced Premixed Combustion Strategies

The EPC combustion strategies can be considered as an attempt to unify all the previously discussed clean diesel combustion strategies such as HCCI, PREDIC, MK-combustion and LTC. The enhanced premixed combustion techniques refer to the techniques that assist in the transition from the conventional heterogonous combustion to a more homogenous cylinder charge before the combustion. Typically, for diesel engines, even though the air-fuel ratio is globally lean, the combustion is localized at near stoichiometric regions. Thus, during the convention diesel combustion λ_{local} is ~1, while the λ_{global} >1. However, if an early injection strategy is applied and a sufficiently long ignition delay is available for mixture preparation, then a lean homogenous mixture is prepared before the combustion. Thus, at the end of the ignition delay period λ_{local} is approximately equal to λ_{global} and both the quantities are significantly greater than 1. The combustion of a lean-homogenous mixture has a potential to produce a simultaneous low-NOx and low-soot combustion as shown in Figure 3-5.

In another scenario the cylinder charge mixture is heavily diluted with EGR and the λ_{global} is close to 1. For this case also it is possible to attain homogeneity by the use of multiple injection strategy. In the case the cylinder charge mixture is called weak-homogenous mixture. Since, significant homogeneity is attained before the combustion; it

is possible to lower the soot. The use of heavy EGR ensures that the NOx is also low. Thus it is possible to possible to attain simultaneous low-NOx and low-soot combustion with a weak-homogenous cylinder charge (Figure 3-6). More details for the experiments shown in Figure 3-5 and Figure 3-6 are provided later in Chapter 6

Therefore, for the EPC combustion the emphasis is on enhancing the homogeneity, since it is possible to attain low-NOx and low-soot combustion with both lean and weak homogenous mixture (Figure 3-7 and Figure 3-8). The important factors that are responsible for the implementation of enhanced premixed combustion techniques are injection scheduling, in-cylinder charge composition management, cylinder-temperature management and cylinder-pressure based control. All these factors are discussed in detail in the subsequent chapters of this thesis.
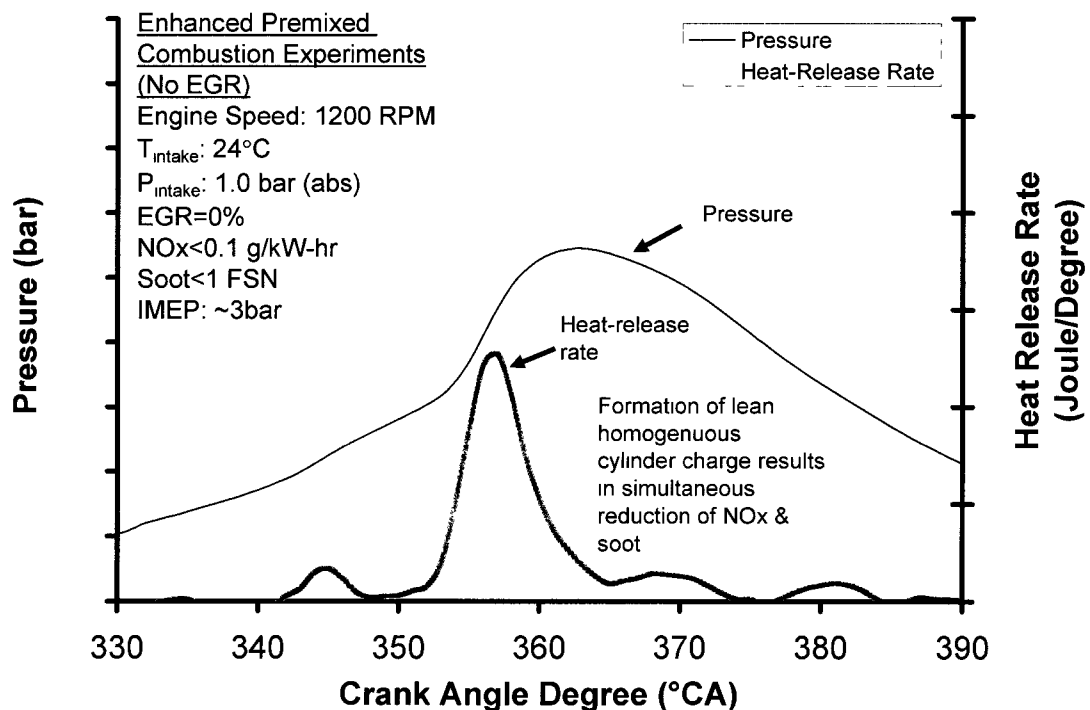
Figure 3-5: Simultaneous reduction of NOx and soot using lean homogenous cylinder charge.
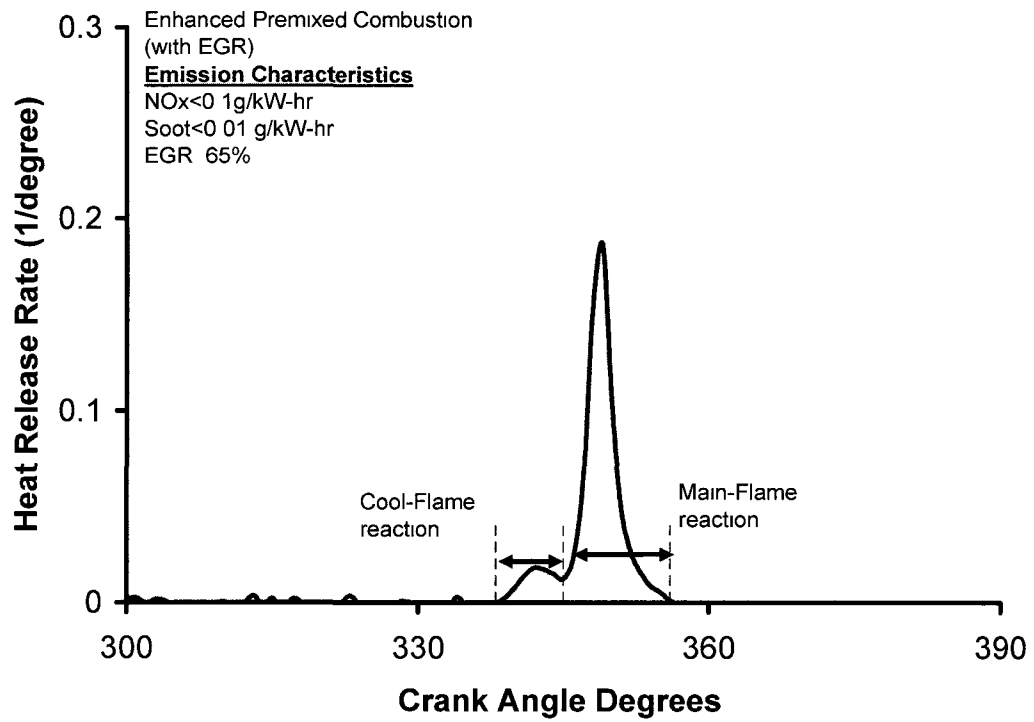
Figure 3-6: Simultaneous reduction of NOx and soot with weak-homogeneous cylinder charge.

Heterogeneous

Conventional Diesel
- λ(local)~1
- 21% O_2+79% N_2
- High NOx
- High Soot

↓ Add EGR

Conventional Diesel
- λ(local)~1
- 17% O_2+78% N_2 +1.8% CO_2+2.4% H2O
- Low NOx
- High Soot

Transition from
Heterogeneous to Homogenous cylinder charge

⇩

by
Enhanced Premixed Mechanism

⇩

Helps to attains LTC or HCCI type of combustion

Homogenous

HCCI
- **Lean + Homogenous** ✓
- λ(local)~2.5~4.0
- 21% O_2+79% N_2
- Low NOx
- Low Soot

↓ Heavy EGR

LTC
- **Weak + Homogenous** ✓
- λ(local)~1.0~1.2
- 9% O_2+75% N_2 +6.5% CO_2+8.8% H2O
- Low NOx
- Low Soot

Figure 3-7: Transition to conventional combustion to low emission diesel combustion.
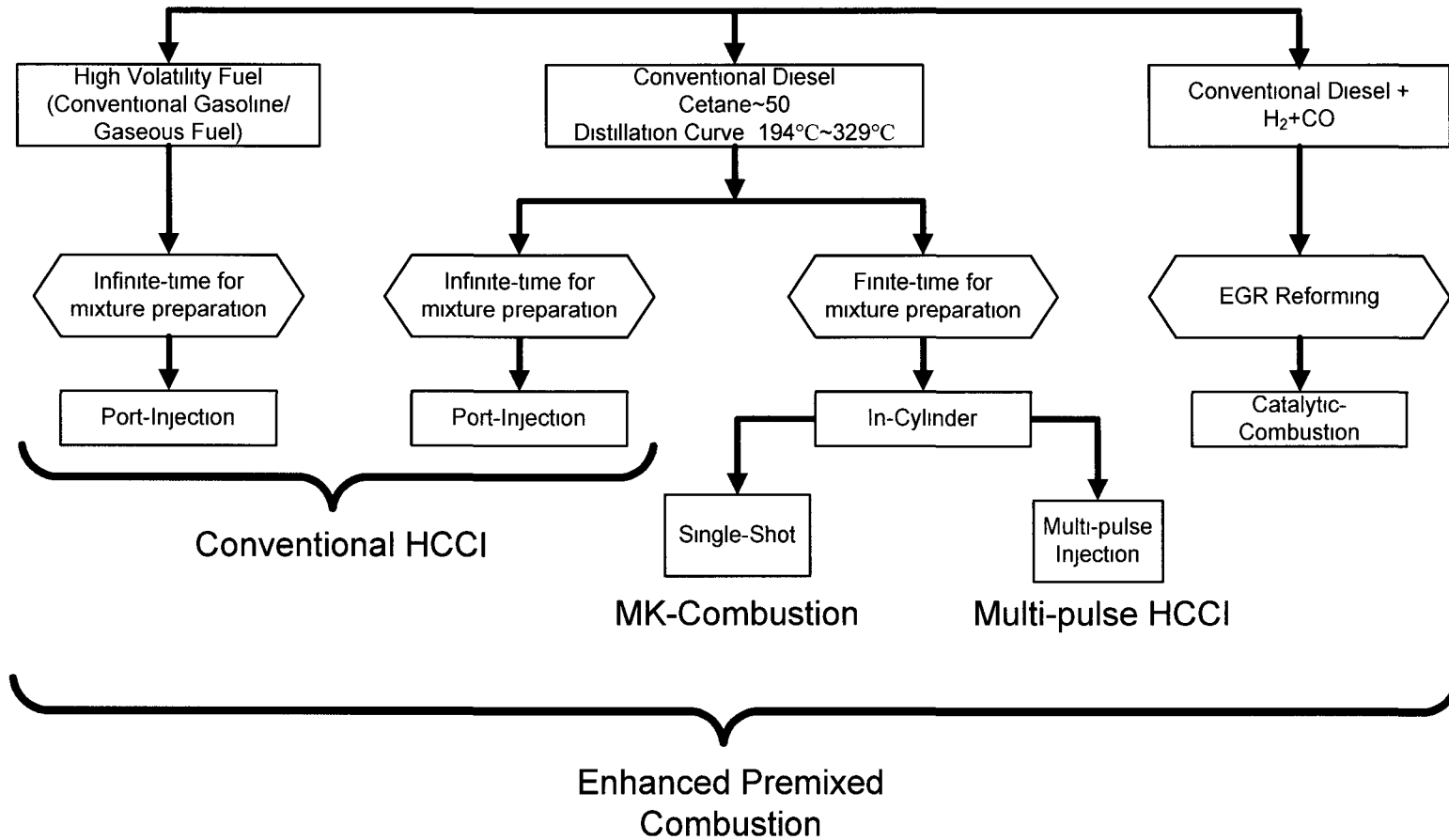
Figure 3-8: Overall mixture preparation strategies for diesel HCCI type of combustion.

CHAPTER IV

4 OBJECTIVES OF THE STUDY

4.1 Objectives

The overall objective of this study was the development of EPC strategies for the diesel combustion that can meet the future stringent emission norms with lesser reliance on diesel-exhaust after-treatment system. The important aspects to these alternate combustion modes are the air-fuel ratio or the homogeneity modulation and the temperature history modulation as seen on the "ϕ-T" diagram. In an actual engine the air-fuel ratio history modulation is carried out by the implementation of the desired injection strategy, boost and EGR. The temperature history modulation is carried out primarily by devices such as variable-valve timing, variable compression ratio and intake heating. For the present work the emphasis was on the air-fuel ratio history modulation while the compression ratio and the valve-timing were treated as the fixed parameters. The intake temperature was modulated to a limited extent by a conventional EGR-cooler. As a first step the present study shows how to implement EPC combustion at a given speed and load by air-fuel ratio modulation.

To implement the EPC combustion two important parameters namely; engine boundary condition and injection characteristic have to be decided. The engine boundary condition establishes the temperature, pressure and composition at the intake-valve closing conditions. These parameters are in turn decided by the intake pressure/boost, intake temperature and the EGR values are used. Similarly, the injection characteristics are completely defined by the

    a. Commanded rail pressure

    b. Number of injections

    c. Dwell between the injections

    d. Weight ratio of injections.

So in this study, the first objective was to demonstrate the EPC combustion strategy and develop a methodology for selection of the engine boundary conditions and injection characteristics for the implementation of EPC combustion at any given load condition (Figure 4-1). Secondly, an attempt was made to quantify the effect of important factors namely; EGR, boost and injection strategy on the homogeneity modulation during the implementation of EPC combustion. Once the EPC was implemented it was observed that the engine operating conditions were less robust than the conventional combustion therefore, the third objective was to implement cylinder pressure based control strategies to ensure stable engine operation. For the EPC combustion the efficiency was observed to be lower than the conventional combustion. Therefore, the final objective was to understand and quantify the factors that were affecting the efficiency of the EPC system and make efforts to recover the efficiency. An effort was also made to correlate the cycle thermal efficiency with the important heat-release characteristics such as combustion-phasing, shaping and duration. It was also found that the important EPC enabler EGR had a dual impact on the cycle thermal efficiency. One effect of the increased use of EGR was the improved combustion phasing and thereby higher work done per cycle. However, the increased use of EGR also led to increased CO and HC which lowered the combustion efficiency. The methodology of equivalent emissions has been proposed to understand the above mentioned effect of EGR.

Implementation of Enhanced Premixed Combustion (Simultaneous Low NOx-Low Soot Combustion)

Load/ IMEP at given RPM

Boundary Conditions
- Boost
- EGR Ratio (Boost & EGR Ratio together = AFR)
- Intake Temperature (not a control variable)

Injection Characteristics
- Injection Event Strategy
- Number of injections
- Dwell
- Ratio of each pulse
- Injection Pressure

Fixed Parameters
- Compression Ratio
- Valve Timing

Homogeneity Characterization
Time for Enhanced Premixed Combustion
- EGR Prolonged Ignition Delay
Supporting Factors
- Injection Pressure
- Boost
- Multiple Injections

Efficiency Characterization
- Combustion phasing
- Combustion shaping
- Combustion duration
- EGR
- Phasing versus CO+HC trade-off
- Additional Accessory Work

Necessity of In-cylinder feed-back
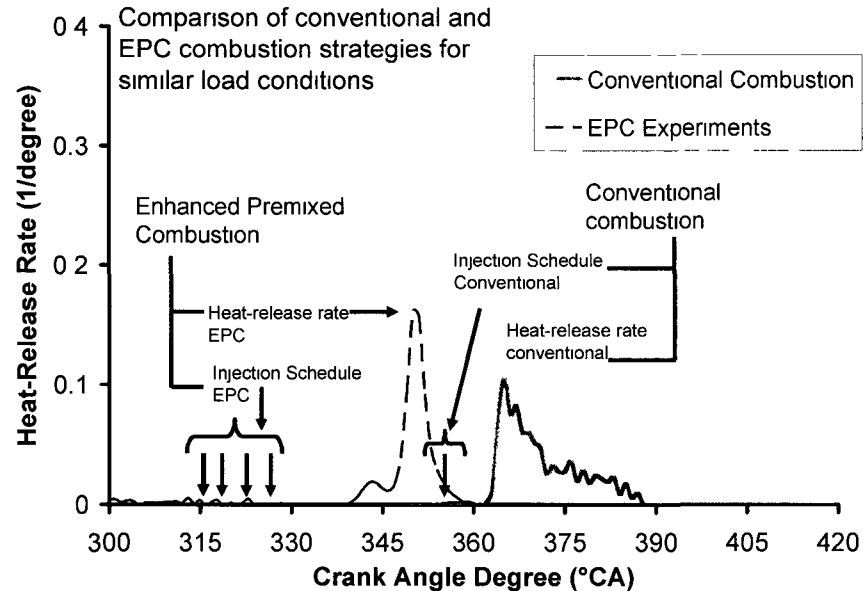
Figure 4-1: Implementation and characterization of EPC experiments.

30

CHAPTER V

5 METHODOLOGY

The principle of EPC strategy was investigated primarily by experimental means. Therefore, this section provides the details for the preparation of the experimental work. This is followed by the post-processing techniques for experimental test-results. The theoretical analysis was performed to understand the empirical results and to develop the boundary condition for the tests. In this section the details of the modeling tools used for the analysis have also been provided.

5.1 Experimental Preparation

The experimental work was performed on a production version of Ford common-rail diesel engine. (4-cylinder 2.0L, V185 Duratorq engine). The details of the engine are as shown in Table 5-1.

Table 5-1: Geometrical characteristics of the engine used for EPC experiments

Engine Type	4-Cylinder, 4-Stroke Ford DuraTorq "Puma"
Displacement [cm^3]	1998
Bore [mm]	86
Stroke [mm]	86
Compression Ratio	18.2:1
Combustion System	Direct Injection
Injection System	DELPHI Common-rail (Rail pressure up to ~ 1600bar)

The base-engine consisted of a single-stage variable geometry turbocharger (VGT). The VGT system provided the required levels of boost and EGR by adjusting the EGR valve and the vane position. An important limitation of using the baseline air-system was that the boost and the EGR system were coupled and could not provide the simultaneous high-EGR and high-boost required for the EPC experiments. Therefore, an independent boost and EGR system was prepared. The boost was provided by an oil-free dry-air

compressor (Manufacturer, Atlas Copco, Model No. GA11FF) while the EGR was controlled by an independent pneumatic back-pressure valve. The original intake and the exhaust manifold were replaced by new prototype unit that allowed the implementation of the EPC experiments in Cylinder No.1 while the other cylinders continued to be connected with the original Ford air-cleaner and operated in the conventional combustion mode (Figure 5-1). This step of running Cylinders No.2, 3 and 4 in the conventional mode was essential for running the engine at a stable rpm. For a motoring dynamometer it is possible to lock the engine operation at any revolutions per minute (rpm) even at unstable combustion conditions. However, for the present experiments the engine was coupled to an eddy-current dynamometer which was readily available in the lab. An eddy current dynamometer can only absorb power, and has a limited speed-response and control stability in comparison to the motoring dynamometer. Therefore, the engine operation at a fixed "set-point" rpm is difficult when the engine is operating at high cycle-to-cycle variation conditions which are inherent with the use of heavy EGR. The strategy of running Cylinder No.2, 3 and 4 in the conventional combustion mode helped to stabilize the engine rpm fluctuations. Note, that the power required to drive the compressors was not considered in the energy-efficiency calculations performed later in this thesis.

Specific provisions were made in Cylinder No.1 to ensure that there was no cylinder-to-cylinder cross-contamination during emission measurements. A dual-bank exhaust analyzer system consisting of NOx, HC, CO, CO_2, O_2 and soot analyzer was used for measuring the exhaust emissions and to monitor the intake gas concentrations.

The details of engine-electronics hardware that were set-up for running the modified single-cylinder engine are shown in Figure 5-2. The precise fuel injection scheduling was implemented using a real-time controller embedded with a field programmable gate array (FPGA) device. The FPGA generated the desired transistor-transistor logic (TTL) pulse patterns corresponding to the on-fly updated injection schedule. The timing of the commanded injection pulses was crank-angle resolved at 0.1 °CA intervals and the duration of the injection was time-resolved in microseconds deterministically. This TTL output signal was amplified using the injector power driver to execute the pulse trains,

which were programmed to drive the injectors with the suitable voltage and current profiles. The EPC specific injection strategies were implemented for Cylinder No.1 while for the Cylinder No. 2, 3 and 4, a single-shot injection strategy was implemented. A brief description of all the injection strategies used for EPC combustion is provided in Appendix 11.1. The FPGA device was additionally used to perform cylinder pressure data-acquisition and to implement cylinder-pressure based control strategies. All the programming required for configuring the FPGA logic gates was done using LabVIEW programming environment [50]. The FPGA device was accommodated in a Peripheral component interconnect extension for instrumentation (PXI) chassis that also included a real-time controller used for floating point calculations.

An additional real-time controller was also set-up for fuel-rail pressure regulation. The engine hardware modifications allowed bypassing the original ECU and running independent fuel-injection and air-fuel ratio management strategies. The LabVIEW programming environment was also utilized in the laboratory for PC-based boost and EGR control for the EPC experiments, data acquisition and on-line monitoring of the heat-release rates, pressures, temperatures and emissions. The engine coolant and lubricant oil conditions were monitored and controlled closely with external conditioning systems to minimize the discrepancies of the testing results. For all the tests described in this thesis, the coolant and the oil temperature was set to 80°C, while oil pressure was set to 4 bar (absolute). Additional details about the major components that were set-up as part of the engine instrumentation are included in Appendix 11.2.
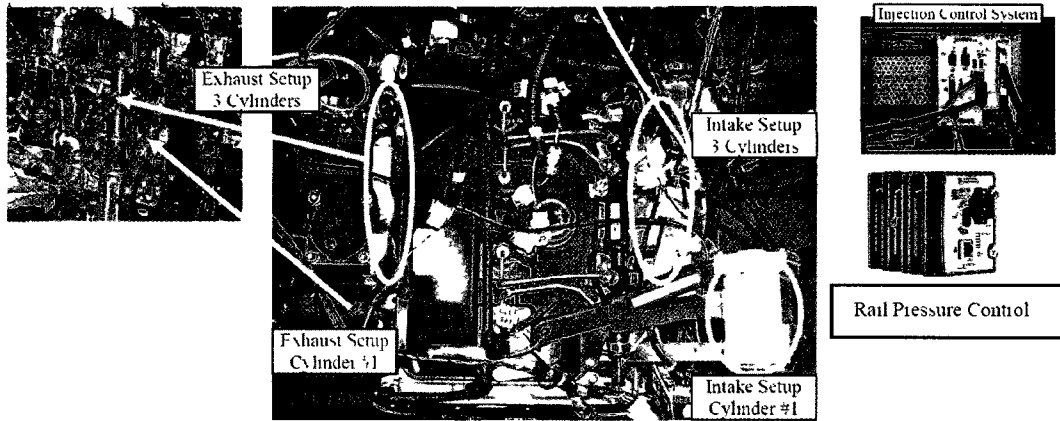
Figure 5-1: Hardware modifications for conversion to a single-cylinder research engine for the EPC experiments.
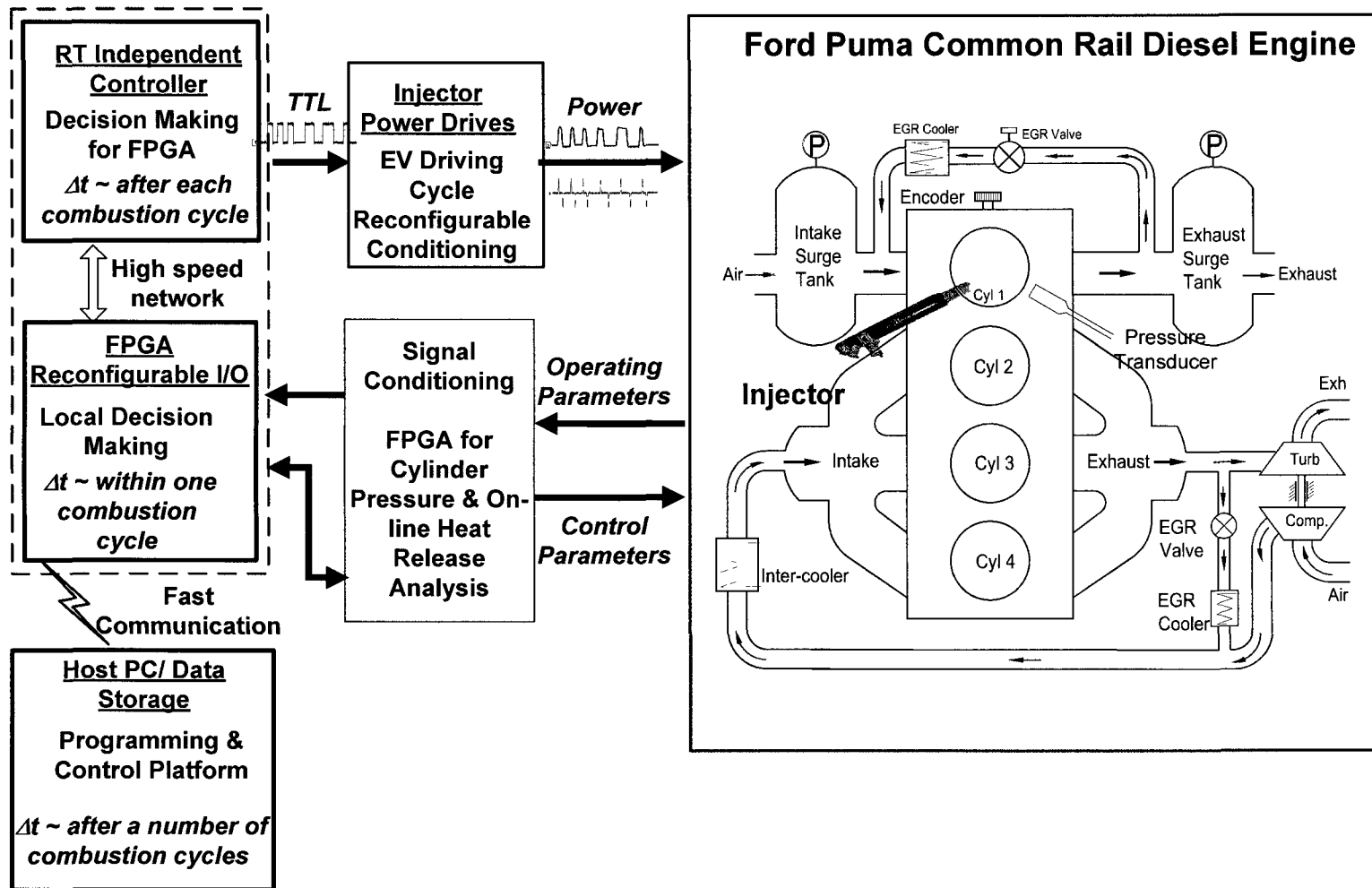
Figure 5-2: Implementation of enhanced premixed combustion strategies.

5.2 Post-processing of In-cylinder Pressure

The in-cylinder pressure was acquired using a glow-plug mounted AVL piezo-electric pressure transducer. The acquired voltage signal was amplified using a Kistler charge amplifier (Model No.5010B), which converted the pressure data to a 0~10 V signal that was acquired by the data-acquisition system. A general-purpose PC-based high-speed data acquisition card (Data-acquisition card Model No.: 6023E) was used for acquiring the cylinder pressure data. The cylinder pressure data acquisition was triggered by the TDC signal generated by the encoder that acted as an external trigger. The 0.1°CA signal produced by the encoder acted as the external clock and the cylinder pressure data was acquired for every 0.1°CA. The block diagram for the data-acquisition of the cylinder pressure is shown in Figure 5-3.

Cylinder pressure data was logged for 200 consecutive cycles at each of the operating conditions. The number of consecutive cycles to be used for averaging was found by considering the variability inherent in the data and the accuracy required. To ensure the confidence level of 99.9% that the sample mean was within 3% of population mean, the sample average was based on 200 cycles [51]. The rate of heat-release versus crank angle was evaluated based on first law of thermodynamics.
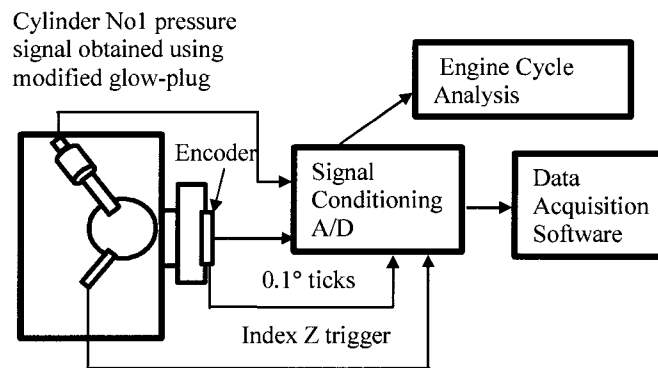
Figure 5-3: System layout showing cylinder pressure data-acquisition.

Following parameters were evaluated from the obtained cylinder pressure data:

- Pmax and the °CA corresponding to Pmax for each cycle

- Rate of change of pressure versus °CA for each cycle

- IMEP for each cycle

- Work done for each cycle

- Rate of heat-released versus °CA for each cycle

- Heat-released versus °CA for each cycle

The net heat-release rate was calculated using the simplified equation derived based on the first law of thermodynamics [4].

$$\frac{dQ_{hr}}{d\theta} - \frac{dQ_{ht}}{d\theta} = \frac{dQ_n}{d\theta} = \frac{1}{(\gamma - 1)}\left[\gamma P \frac{dV}{d\theta} + V \frac{dP}{d\theta}\right]$$

where

$dQ_{hr}/d\theta$ =Heat-release rate by combustion,

$dQ_{ht}/d\theta$ =Heat transfer rate to the cylinder wall,

$dQ_n/d\theta$ =Net heat-released,

θ =Instantaneous engine position in crank angle

γ =Ratio of specific heats,

P =Instantaneous cylinder pressure

V =Instantaneous cylinder volume, respectively.

37

In this simplified equation, the heat-transfer, crevice volume effects and composition effects were ignored. The normalized heat-release rate obtained was compared with the results obtained from the comprehensive in-house engine cycle simulation program SAES [52] for start of combustion, and combustion-phasing. The results were in agreement both the methods, therefore for the present work only the simplified heat-release rate equation was used.

5.3   Emission Analyzers

A dual-bank of exhaust analyzer system, one for the exhaust emissions and the other for the intake gas concentrations, was used for the tests. The NOx, UHC, CO, CO_2, O_2, and soot emissions were monitored for the exhaust emissions while only the O_2 and CO_2 emissions were monitored at the intake. The HC analyzer measured the total concentration of hydrocarbons within a gaseous sample on C1 basis. Table 5-2 summarizes the types of emission analyzers used in the laboratory for the present research.

5.4   EGR Ratio

When EGR is applied, the engine intake consists of fresh air and recycled exhaust. The percentage of recycled gases is commonly represented by an EGR ratio, i.e. the mass ratio of recycled gases to the whole engine intake. The fresh air intake contains negligible amounts of CO_2 while the recycled portion carries a substantial amount of CO_2 that increases with EGR flow rate and engine loads. Thus it was decided to use a CO_2 based approach to describe the EGR ratio and was expressed as the ratio of the intake CO_2 concentration to the exhaust CO_2 concentrations.

Table 5-2: List and specification of emission analyzers

Analyzers	Species	Range	Resolution	Manufacturer and Model No.
Non-Dispersive Infra-Red (NDIR)	CO	(0~2000ppm) and (0~5000ppm)	0.1 ppm	CAI Model 300
	O₂	0~25%	0.01%	CAI Model 300 (Intake) CAI Model 602P Digital (Exhaust)
	CO₂	0~2% and 0~8% for intake 0~8% and 0~40% for exhaust	0.01% 0.01%	CAI Model 200 (Intake) CAI Model 602P Digital (Exhaust)
Chemiluminiscence	NO	(0~3000ppm)	0.01 ppm	CAI Model 600-HCLD Digital
Heated Flame Ionization Detector	THC	(0~3000 ppm)	0.01 ppm	CAI Model 300M-HFID
Variable sampling smoke meter	Smoke/Dry Soot	(0~10 FSN)	0.002 FSN	AVL Model 415S

THC: Total Hydrocarbons

FSN: Filter Smoke Number

5.5   Modeling Work

The modeling work in this thesis was used as a tool to assist in the interpretation of the empirical results and to set the boundary condition for the experiments also. The modeling work presented in the thesis can be divided into three sections (Figure 5-4 and Figure 5-5). The first part of the modeling work was used to understand the homogeneity development prior to the combustion process. This was done using a 3-dimensional computational fluid dynamics tool, KIVA (version 3V). KIVA was primarily developed by Los Alamos Laboratories as a tool to study and simulate two and three-dimensional chemically reactive turbulent fluid flow with sprays. KIVA has deforming mesh capability for analysis of geometries with moving boundaries, which makes it suitable for applications such as internal combustion engines where the physical boundaries or the cylinder volume change with time in a fixed manner. Since, KIVA is 3-dimensional software it was able to describe the temporal and spatial variations of temperature, composition, pressure and flow-fields in the combustion chamber. KIVA includes various sub-models such as spray, ignition, combustion, heat-transfer and turbulence to describe various aspects of the engine combustion process. The details of the mass, momentum energy balance and turbulence equation are given in the Appendix. These simulations were performed from the intake valve closing to the exhaust valve opening conditions.

In the second part of modeling, homogeneity was assumed as a known quantity and the effect of air-fuel history modulation was investigated. This was performed using chemical kinetics software CHEMKIN. The CHEMKIN simulations were used to estimate the start of combustion. The start of combustion parameter estimation allowed making important predictions about the performance parameters for the EPC strategies such as rate-of-pressure rise and efficiency. There are six basic steps involved in using CHEMKIN to solve a typical chemical process modeling problem:

1) Preparing the chemistry input file(s)

2) Assemble the thermodynamic and transport databases

40

3) Prepare the Application-specific input data; such as slider-crank mechanism to specify change in volume as a function of time

4) Running the Pre-Processing programs

5) Run the Application

6) Post-process the results

In the third part of the modeling work, both the homogeneity and the heat-release were taken as the known quantities and the effect of characteristics such as combustion phasing, duration and shaping on the engine cycle efficiency were evaluated using synthetic atmospheric engine simulation software (SAES). SAES is an in-house zero-dimensional engine cycle simulation software that was developed by Dr.Zheng [52]. It was primarily used to describe the thermal effects of the combustion rather than the process itself. Therefore, the fuel-burn rate was treated as a-priori and based on the combustion rate the resulting pressure was calculated in accordance with the first-law of thermodynamics. The basic flow-chart for the SAES program is shown in the Appendix.

```
                    ┌──────────────────────┐
                    │ Modeling activities to│
                    │ support EPC strategy  │
                    └──────────────────────┘
          ┌────────────────┼────────────────────┐
          ▼                ▼                    ▼
  ┌──────────────┐  ┌──────────────┐  ┌──────────────────┐
  │ Understanding│  │Cylinder mixture│ │Cylinder mixture of│
  │ homogeneity  │  │    of known   │ │ known homogeneity │
  │              │  │   homogenity  │ │and known combustion│
  └──────────────┘  └──────────────┘  └──────────────────┘
          ▼                ▼                    ▼
  ┌──────────────┐  ┌──────────────┐  ┌──────────────────┐
  │Computational │  │Zero-dimensional│ │ Zero-dimensional │
  │fluid dynamics│  │chemical kinetics│ │engine simulation :│
  │software: KIVA│  │software: CHEMKIN│ │  SAES/GT-Power   │
  └──────────────┘  └──────────────┘  └──────────────────┘
```
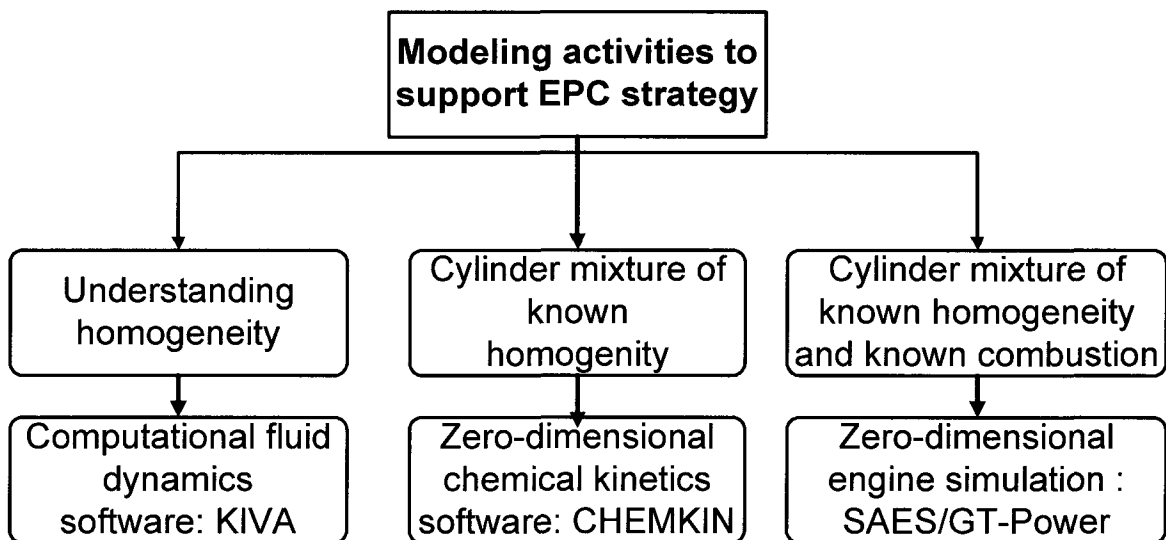
Figure 5-4: List of tools and their application to support EPC combustion strategy.
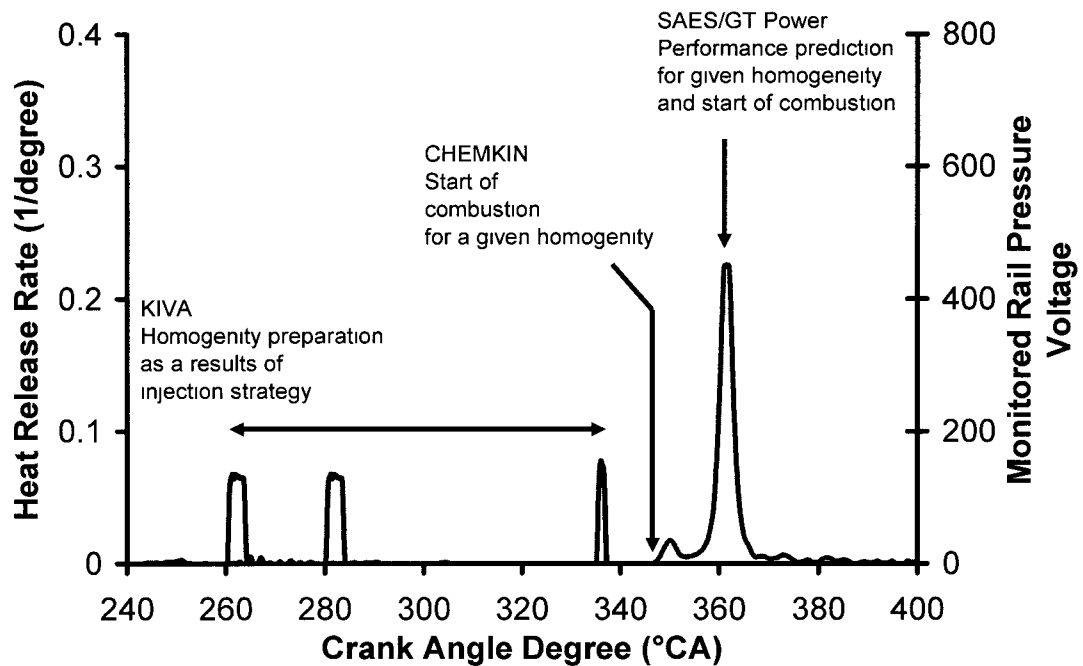
Figure 5-5: Simulation tools and there area of application to support the investigation of EPC combustion strategy.

All the modeling tools namely; KIVA, CHEMKIN and SAES have been developed and validated extensively by other researchers in the past, so the emphasis of was primarily to explain the experimental observations and no efforts were made to incorporate or update any sub-models.

CHAPTER VI

6   RESULTS AND DISCUSSION

6.1   Empirical Work

The objective of EPC combustion was to achieve simultaneous low NOx and low-soot by preparing a lean or a weakened homogenous cylinder charge before the combustion process. As discussed before, the important factors that influence the preparation of this cylinder-charge mixture are the injection characteristics, boost, and EGR. To simplify the cylinder-charge composition modulation, the first experiments were performed with no EGR and boost. In this way the cylinder charge equivalence ratio was modified by only the injection characteristics. Thereafter, experiments considering other factors affecting the EPC combustion were considered and detailed in this chapter.

Table 6-1: Experimental Test Matrix

Experiment	Test Characteristics	Implementation
1	Injection scheduling to modulate homogeneity	Load: 3bar IMEP Injection strategy: Single injection Boundary Conditions: No EGR and boost
2	Injection scheduling to modulate homogeneity with multiple-injection	Load: 3bar IMEP Injection strategy: Multiple-injection strategy Boundary Conditions: No EGR and boost
3	Injection scheduling and EGR to modulate homogeneity	Load: 6~7bar IMEP Injection strategy: Multiple-injection strategy Boundary Conditions: Boost and EGR
4	EGR-enabled EPC	Load: 2.0~8 bar IMEP Injection strategy: Single-injection strategy Boundary Conditions: Boost and EGR
5	EGR-enabled EPC with cylinder pressure-based control	Load: 2.0~9.0 bar IMEP Injection strategy: Single-injection strategy Boundary Conditions: Boost and EGR
6	EPC with split-heat release	Load: 6.0~8.0 bar IMEP Injection strategy: Multiple-injection strategy Boundary Conditions: Boost and EGR

6.1.1 EPC experiments with single injection and no EGR

In this experiment, tests were performed with a single injection strategy with continuous advance in the injection timings. The underlying assumption was that, when the fuel was injected earlier during the compression stroke, the prevailing in-cylinder temperatures would be lower and the fuel would experience a longer ignition delay before the combustion was initiated. This increased ignition delay would then assist in the preparation of a lean homogenous cylinder charge. However, when the commanded start-of-injection (SOI) was advanced from 359°CA to 340°CA, the ignition delay was not substantially affected and little benefits were obtained in reducing NOx (Figure 6-1 and Figure 6-2). The timing advance however resulted in increasing the rate of increase of pressure; therefore it was decided not to advance more than 340°CA in single-shot injection strategy. The tests were performed at two injection pressures, with the assumption that at higher pressures the injection event would finish sooner giving more time for mixture preparation. The soot was the less than 1FSN for all the test points due to low-load and no EGR condition. The observations in this experiment are consistent with other authors such as Shimazaki et al. [38] who observed similar behavior. In their experiments they also observed that for an injection timing of 335~340°CA no NOx reduction was observed and if the injection-timing was advanced there was the onset of knocking. The phenomenon of knocking phenomenon was observed up to 290°CA. Thus it can be seen that it was not possible to prepare a lean-homogenous mixture with a single injection with close-to-TDC start-of-injection timings. Therefore, it was decided to pursue multiple-injection strategy to prepare the lean-homogenous mixture for simultaneous NOx and soot reduction.

Table 6-2: Effect of commanded SOI on ignition-delay

Commanded SOI (°CA)	Start of Combustion (°CA)	Ignition-Delay (°CA)
340	351	11
359	370	11
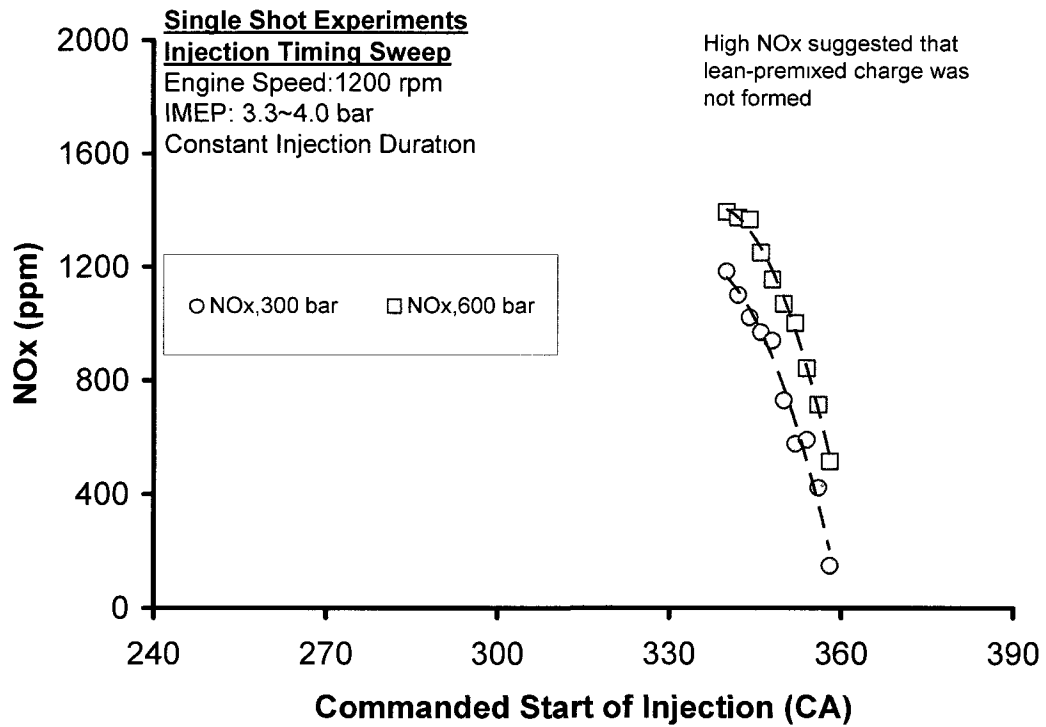
Figure 6-1: Effect of varying the commanded SOI on NOx emissions with a single injection strategy.
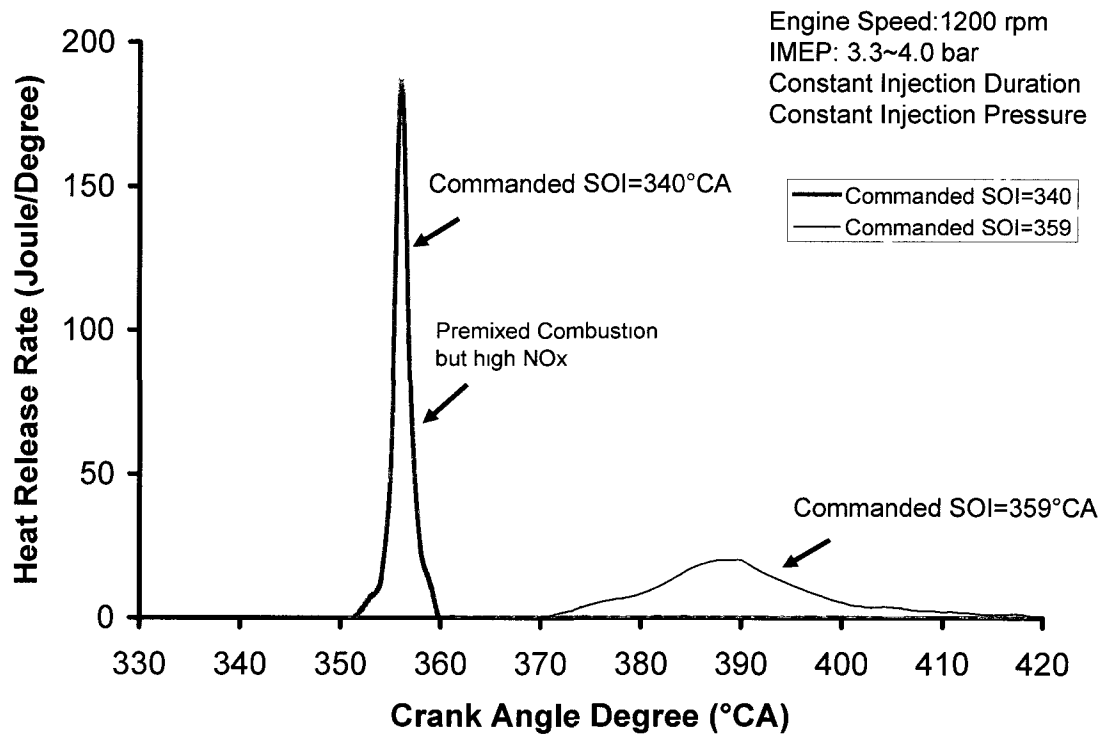
Figure 6-2: Effect of timing advance (conventional timing and no EGR).

6.1.2 EPC with multiple-fuel injection strategy and no EGR

The multiple-injection strategy was implemented very early into the compression stroke to enhance the mixing process and achieve a lean-premixed mixture necessary for simultaneous low-NOx and low-soot. The injection strategy consisted of 7 very early injections starting at 260°CA, with a dwell of 5 degrees and one injection close to TDC, with the rationale that such early injections would assist in the formation of a lean homogenous mixture and the last injection was attempted for combustion phasing control. This injection-strategy was not able to achieve the simultaneous low-NOx and low-soot combustion. The injection strategy was modified primarily for the last injection timing to achieve low-NOx and low-soot combustion and the injection strategy history is shown in Figure 6-3. At point A the last-injection was implemented at 350°CA. Even though a significant part of the fuel was injected very early during the compression stroke, high NOx was observed. It can be seen from the heat-release rate that, for the last injection there was almost no ignition delay which provided little opportunity for the formation of the lean-homogenous charge for the last injection (Figure 6-4). Hence, the last injection was advanced so as to provide extended time for the formation of the lean homogenous mixture. The quantity of the last injection was also reduced to minimize the fraction of fuel injection close to TDC. Both the timing advance and the reduction in the fueling quantity helped to reduce the NOx as can be seen at the point B. Finally, for the point C, all the injections were advanced further into the compression stroke. The first seven injections were spaced 5 degrees apart starting at 240°CA and the last injection was at 330°CA (Figure 6-5). This time the average NOx of around 12 ppm was achieved. At point C if any attempt was made to increase the fueling quantity of the pilot injections, the NOx started to increase again. So, the load levels that could be achieved with a lean-homogenous mixture were limited to around 3bar IMEP without EGR. The soot was the less than 1FSN for all the test points for this group of experiments due to low-load and no EGR condition.
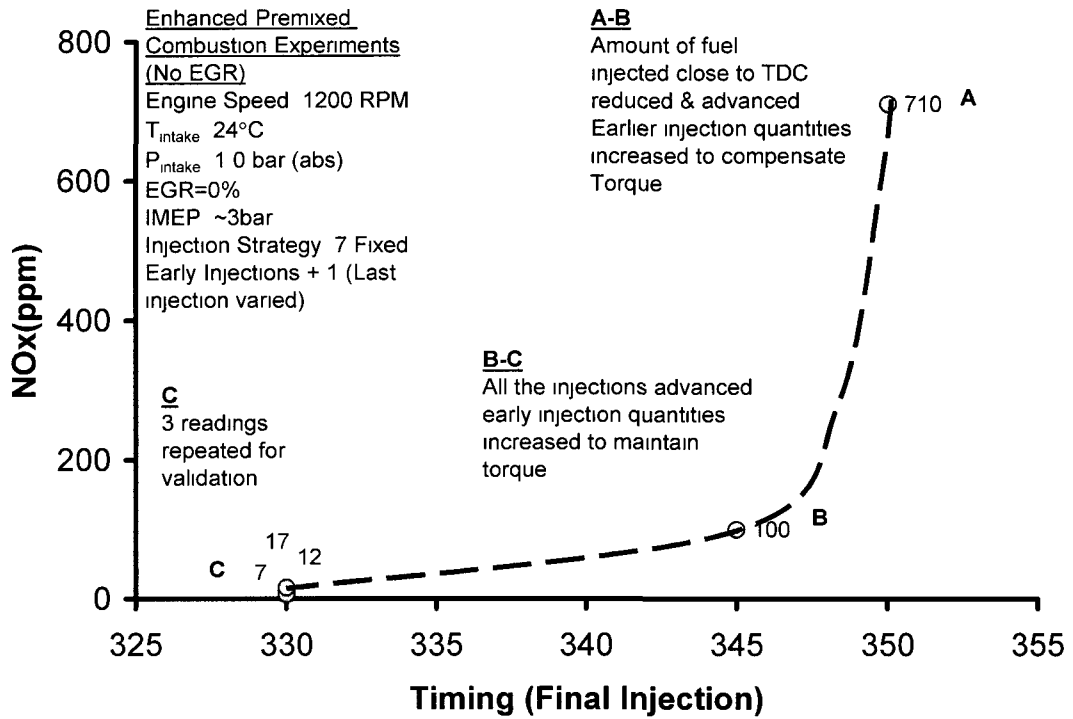
Figure 6-3: Injection timing and quantity selection for lean-homogenous mixture preparation.
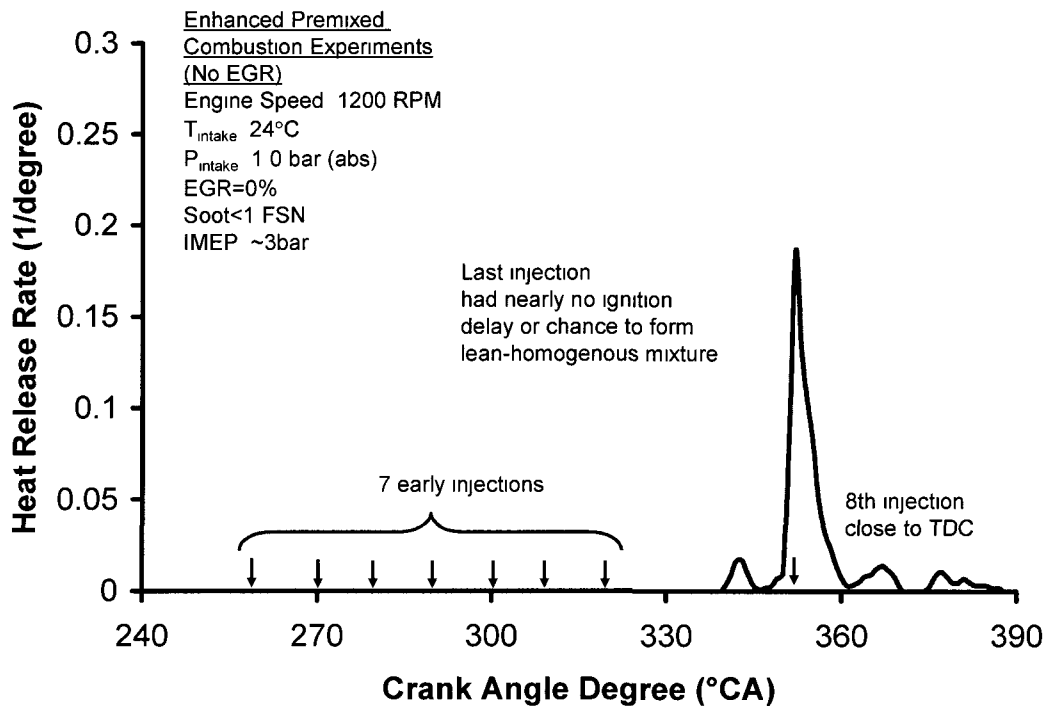
Figure 6-4: Heat-release for point A.
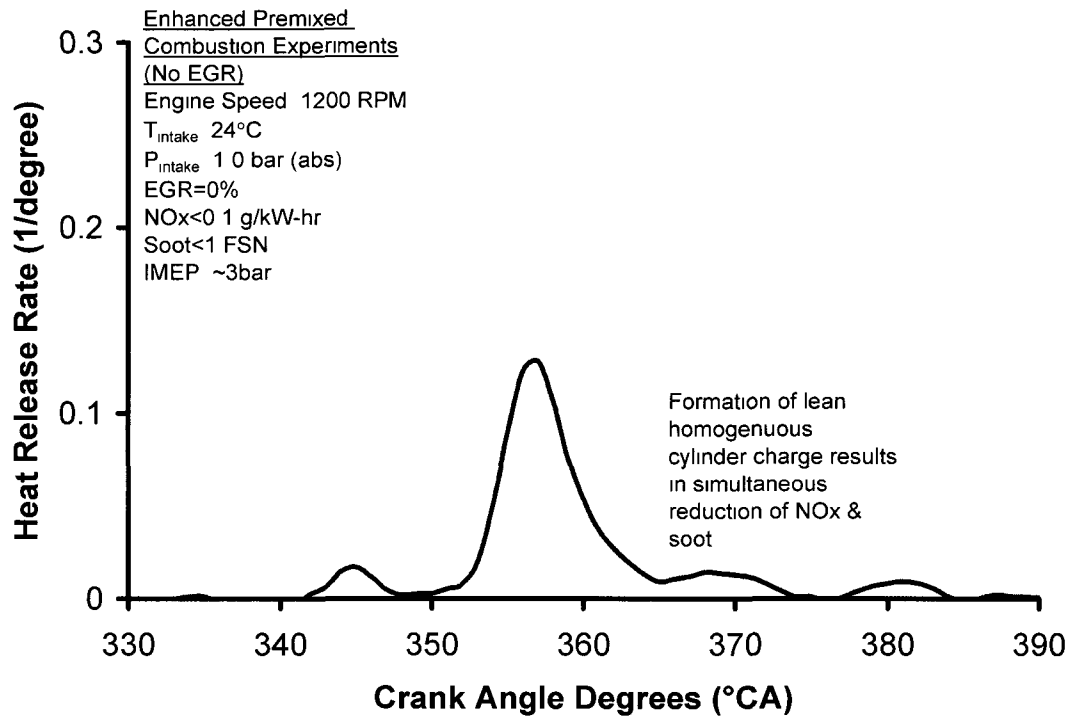
Figure 6-5: Heat-release rate for point C.

6.1.3 EPC at high load with multiple injection strategies and EGR

As mentioned previously, it was possible to implement EPC strategies without EGR only up to a load of 3 bar IMEP. For loads higher than 3 bar IMEP, it was decided to use EGR as an enabler for NOx reduction. As mentioned previously, the use of EGR tends to favor higher soot formation due to reduced oxygen availability. Therefore, an attempt was made to prepare a homogenous mixture and suppress the soot formation in spite of reduced oxygen availability in presence of EGR.

A simplified multiple-injection strategy was implemented with 3 injections (Figure 6-6). The first two injections were again implemented very early during the compression (260°CA, 288°CA) while the third injection was at 335°CA. Initially, a moderate amount of EGR was applied (45%) and it was observed that the fuel underwent spontaneous auto-ignition significantly before TDC. The combustion was initiated at 340°CA thus only a short mixing duration was available for the last injection, thereby resulting in a high-soot of 1.8FSN. However, when the EGR was progressively increased to 55%, the onset of the combustion was postponed. This helped to gain additional time for preparation of the

49

homogenous mixture. The increase of EGR led to two opposing effects on the soot formation; increased sooting tendency due to reduced oxygen availability and increased time for mixture preparation. For the present experiment the soot decreased from 1.8FSN to 1.0 FSN which suggested that the gain in mixture preparation time could compensate for the reduced oxygen availability. An additional benefit was shifting the combustion phasing closer towards the TDC, and this reduced the compression work. This was reflected in the increase in IMEP from 6.6 bar to 7.4 bar IMEP for the same fueling quantity. In addition, the shift in phasing closer towards TDC resulted in a decrease of rate-of-pressure-rise, $(dp/d\theta)_{max}$ from 28 to 20. The increase in EGR also led to a reduction of the oxygen concentration and the higher heat-capacity of the working fluid, thereby reduced the NOx emissions from 1.3 g/kW-hr to 0.1 g/kW-hr. The application of EGR therefore assisted simultaneous reduction of soot and NOx emissions. When the EGR was increased further to 61%, further improvements in the emission and performance characteristics were obtained. The NOx remained close to 0.1 g/kW-hr levels but the soot dropped further to 0.4 FSN. The combustion phasing was postponed further and the peak of heat-release rate was shifted after TDC. The improvement in the combustion phasing reduced the $(dp/d\theta)_{max}$ to 14.3. No change in IMEP was noticed even though the compression work was reduced, this was because when the EGR was increased from 55 to 61% the CO increased from around 500 to 5000 ppm. The increased CO was an indication of incomplete combustion, thus the gain in IMEP due to better combustion phasing was offset by a loss in IMEP due to increase in incomplete combustion.

To decrease the CO emissions it was decided to increase the boost, since increased boost leads to increased oxygen availability. The boost was increased to 75kPa while the EGR ratio was kept constant (Figure 6-7). This resulted in a lower CO, but the combustion phasing was advanced at higher boost. The advancing of the combustion phasing also led to an increase in the rate of increase of pressure. The experiments were also performed at a higher boost of 120kPa but with a same intake oxygen concentration as the baseline boost of 50kPa (Figure 6-8). A higher EGR was needed to reach the same intake oxygen as the baseline case. The use of higher boost helped to attain higher IMEP, while reducing the CO.
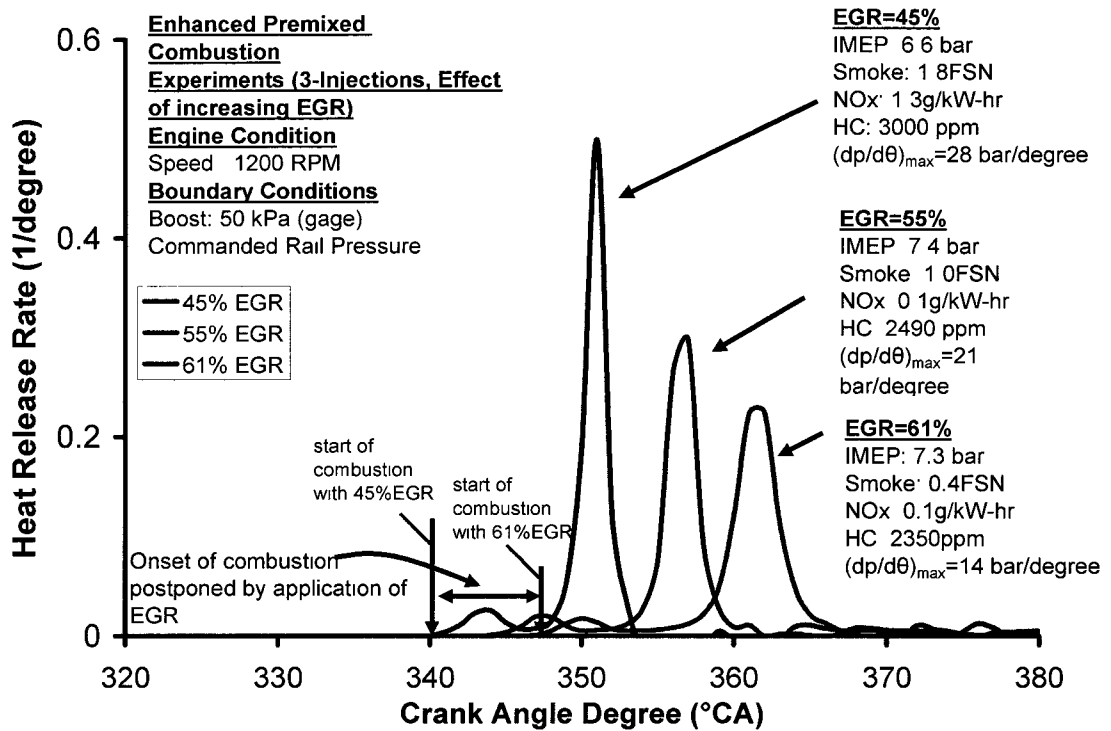
Figure 6-6: Effect of EGR on EPC combustion for a fixed injection strategy.
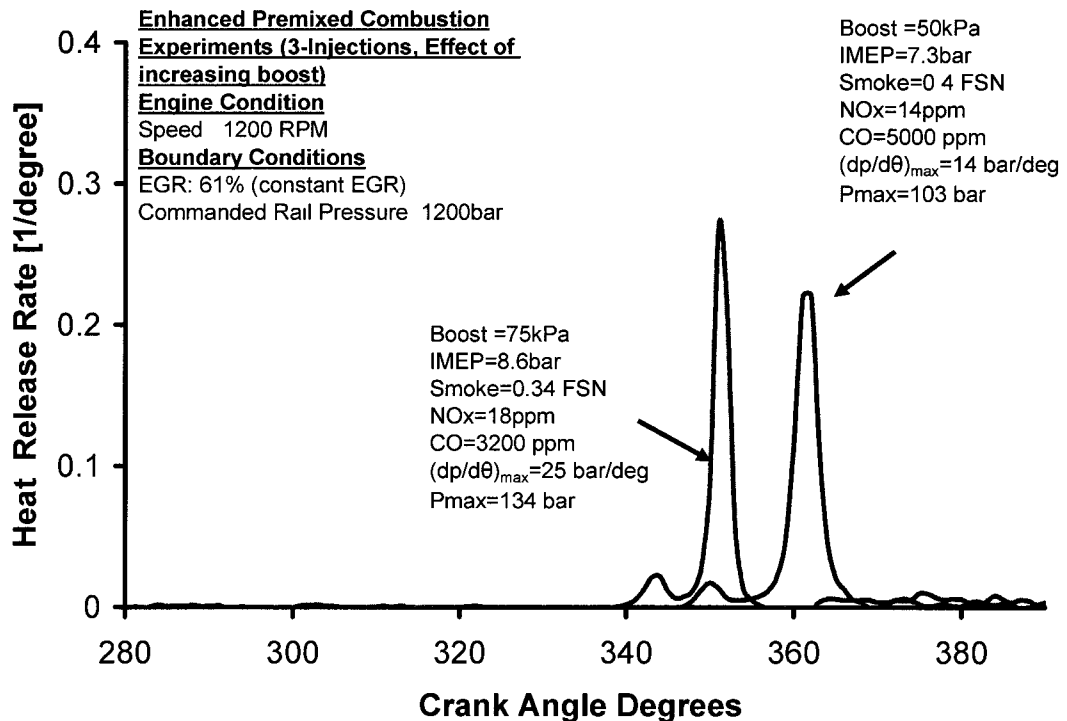
Figure 6-7: Effect of boost on EPC combustion at a constant EGR ratio for a fixed injection strategy.

The use of higher EGR ratio also led to a rate of pressure-rise comparable to the case of 50kPa boost. Therefore, an increase in boost either at constant EGR ratio or at a constant intake oxygen concentration resulted in a decrease in CO; however the increase in boost led to the combustion phasing being advanced from the TDC which had a detrimental effect on the rate-of-pressure rise.
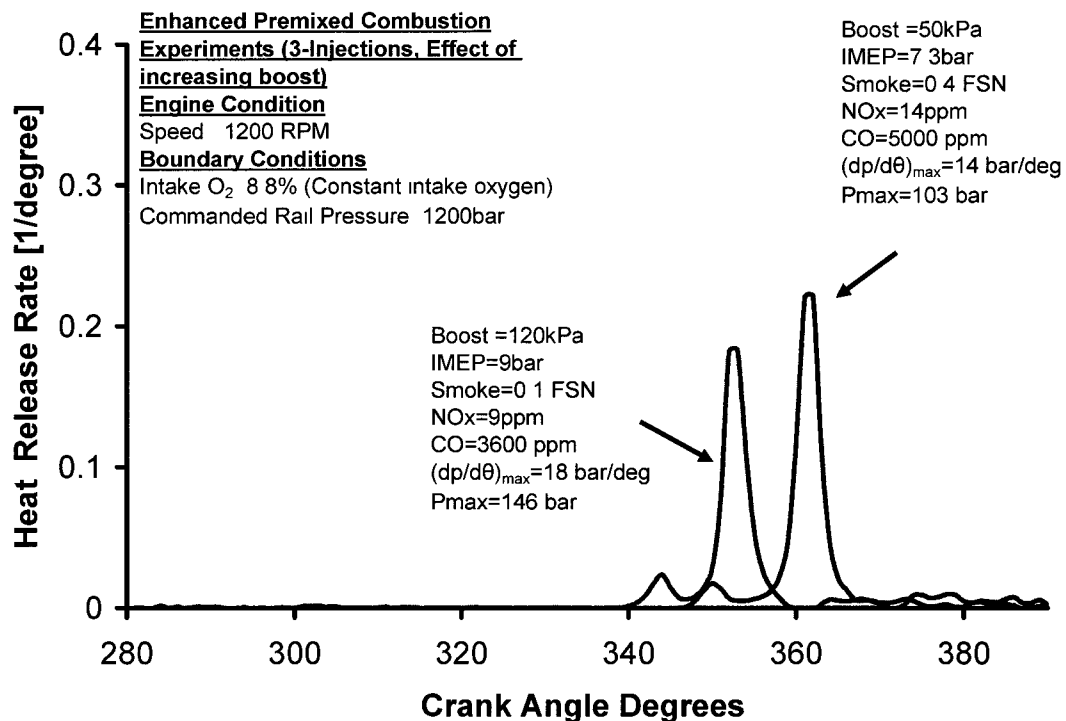
Figure 6-8: Effect of boost on EPC combustion strategy at constant intake oxygen concentration and a fixed injection strategy.

The major characteristic of the multiple early sparse injection strategy was that it was possible to have simultaneous low NOx and low soot but the UHC emissions were very high. To understand the high hydrocarbon issues it was important to understand the properties of diesel fuel. Unlike gasoline, diesel is a hard to vaporize and based on the material safety data sheet for the diesel, the vaporization is initiated only at around 460K and entire vaporization is complete only at 620K. On a crank-angle domain, it means that the fuel vaporization was readily initiated only for injection timings after 280~290°CA. This suggests that the first two injections of the multi-pulse injection strategy would have had a strong propensity to condense because of the prevailing low in-cylinder

temperatures at the time of injection. Another likelihood of UHC is due to the wall-impingement of the early injected fuel. The cylinder-charge density is lower at the time of early injection and favor higher spray penetration. The effect of injection strategy on wall-impingement was investigated numerically using Hiroyasu's model [53]. Hiroyasu et al. performed spray visualization studies and based on their work they proposed empirical equations for spray break-up length, spray-penetration, and spray-angle and drop size distribution. The expression for spray break-up consisted of two parts; one before the time for spray break-up length and the other after the time of spray break-up length.

For $0 < t < t_b$, ,

$$S = 0.39 \left(\frac{2\Delta P}{\rho_l} \right)^{0.5} t$$

for $t > t_b$,

$$S = 2.95 \left(\frac{\Delta P}{\rho_a} \right)^{0.25} (Dt)^{0.5}$$

$$t_b = 28.65 \frac{\rho_l D}{(\rho_a \Delta P)^{0.5}}$$

where,

D   =   nozzle diameter

P_a =   Ambient pressure, MPa

P_i =   Injection pressure, MPa

ΔP =   Difference between injection pressure and ambient pressure, Pa

S   =   Spray-tip penetration, m

53

t	=	Time, seconds
t_b	=	break-up time, seconds
ρ_a	=	Density of air, kg/m^3
ρ_l	=	Density of fuel, kg/m^3

The effect of injection pressure, start of injection timing and boost on spray penetration was numerically investigated as shown in Figure 6-9 ~ Figure 6-11 . It can be seen that the start of injection was the most important factor followed by boost and injection pressure.
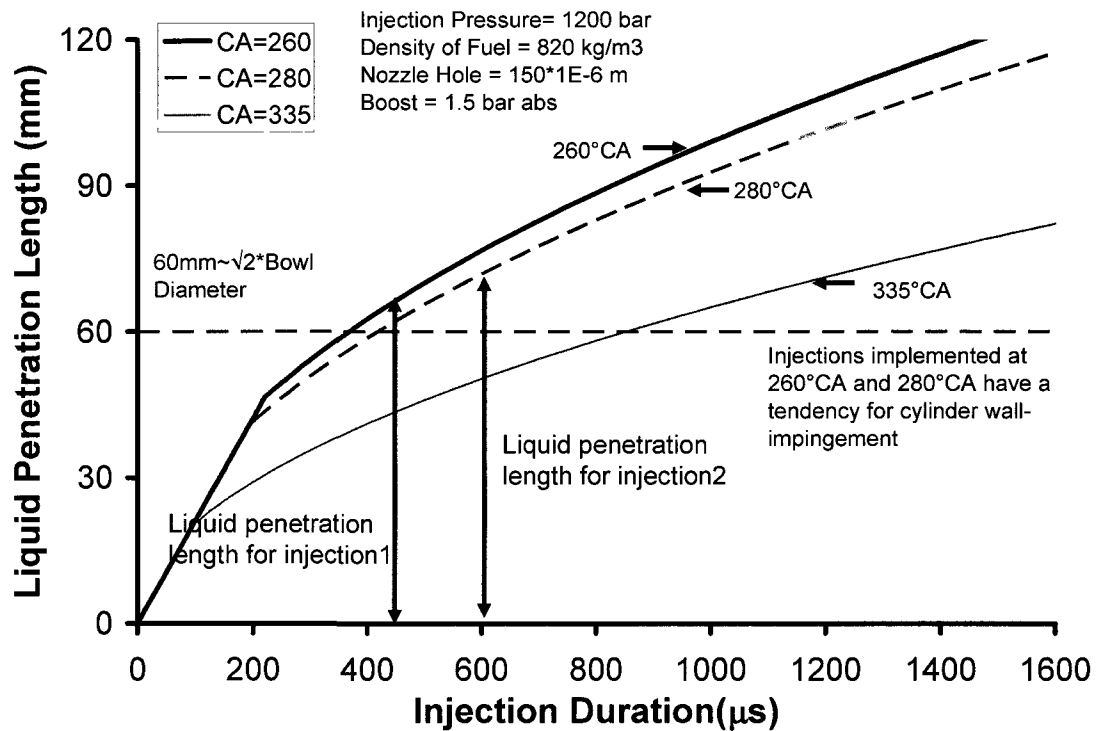
Figure 6-9: Effect of start of injection on liquid penetration length for a fixed injection pressure.
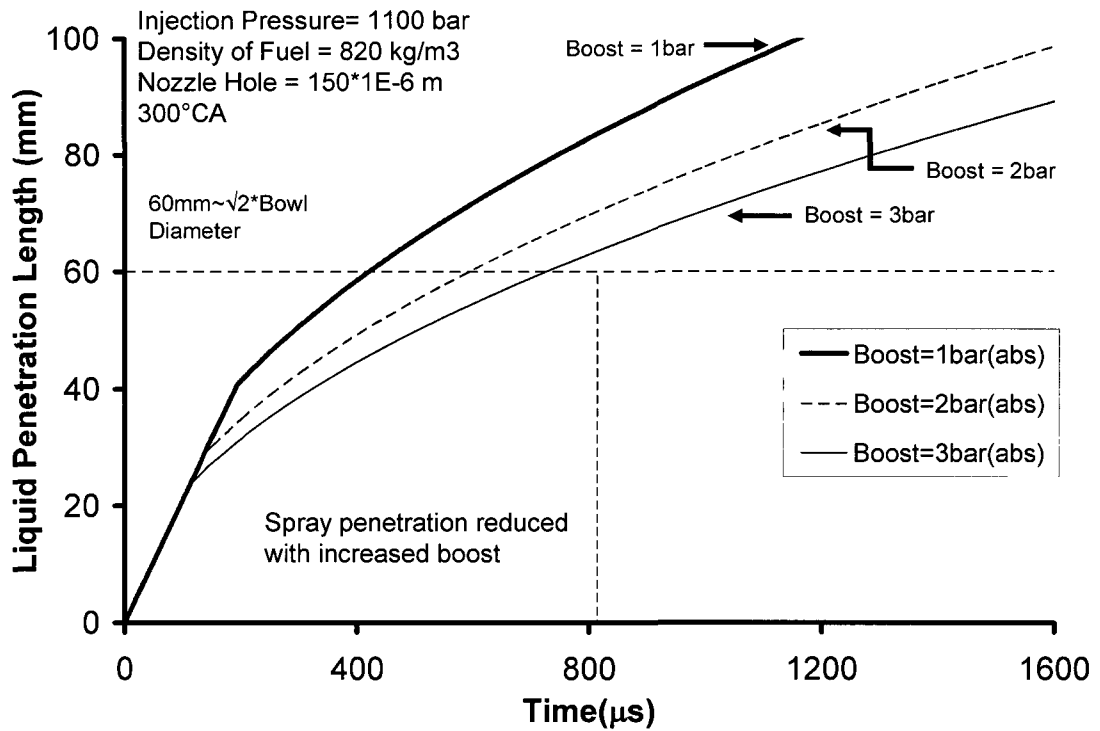
Figure 6-10: Effect of boost on spray penetration for a fixed start of injection.
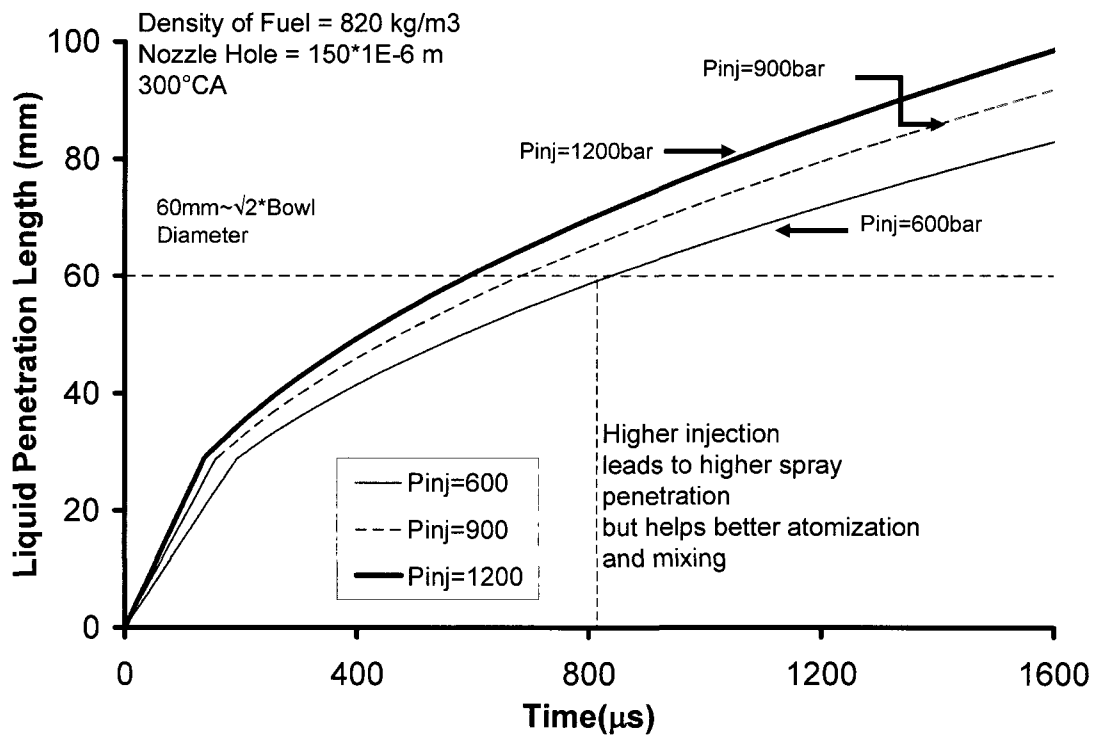
Figure 6-11: Effect of injection pressure on liquid spray penetration length.

The above analysis for the liquid penetration length and the vaporization temperature helped to improvise the injection strategy. Therefore, this time the fuel-injection events were shifted closer to TDC where the in-cylinder temperatures were higher and assisted the fuel vaporization process and the injection quantities were selected in such a way that there was no wall-impingement.

Both the above mentioned corrections in the injection strategy allowed the implementation of EPC combustion with a significant drop in HC emissions (Figure 6-12 and Figure 6-13). A disadvantage of the close-to-TDC injection strategy was that the combustion phasing was advanced for similar levels of EGR and consequently the rate of pressure rise was slightly higher.
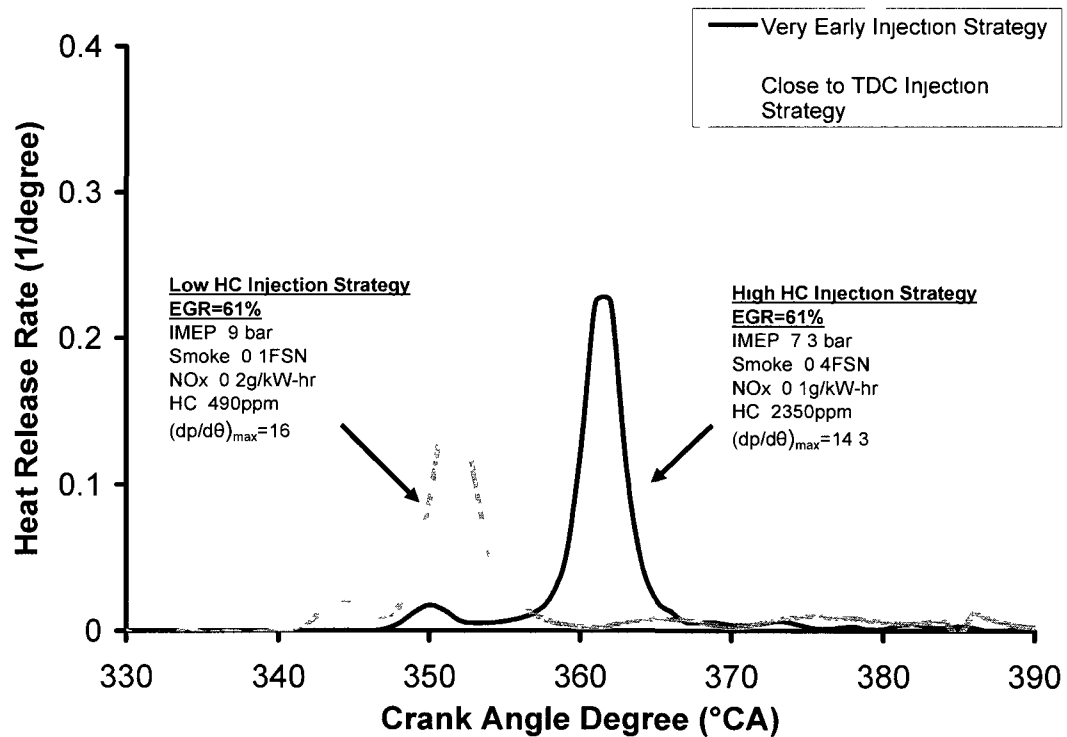
Figure 6-12: Effect of injection strategy on fuel condensation/HC emissions.
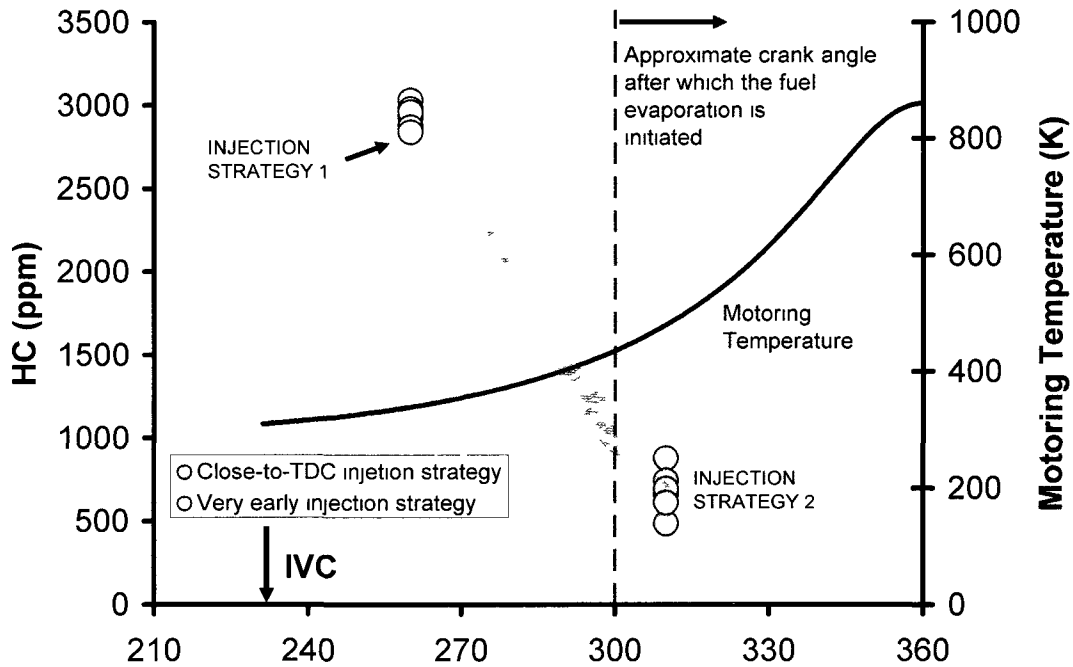
Figure 6-13: Implementation of injection timing guidelines for enhanced premixed.

For the close-to-TDC injection strategy all the injection events were completed before 335°CA and significant reductions were observed in UHC. In the last multiple injection strategy, the injection timings were shifted more closely towards TDC and EGR was progressively increased. The EGR sweep was attempted at three boost-pressures. This was done to see if the hydrocarbon could be reduced further while retaining the low-NOx and low-soot benefits. For this set of experiments a fixed injection scheduling consisting of 2 injections, one at 20°before top dead center (BTDC) and the other at 8°BTDC were considered. The application of EGR at constant boost showed the traditional NOx-PM trade-off (Figure 6-14, Figure 6-15 and Figure 6-16). The increase in boost at a fixed EGR led to a decrease in soot due to increased oxygen availability. However, it was not possible to achieve the simultaneous low NOx and low soot whereas the HC emissions were lower than any of the previous multiple injection strategies discussed. The heat-release rate for a representative case of 100kPa and 51% EGR is shown in Figure 6-17.

57
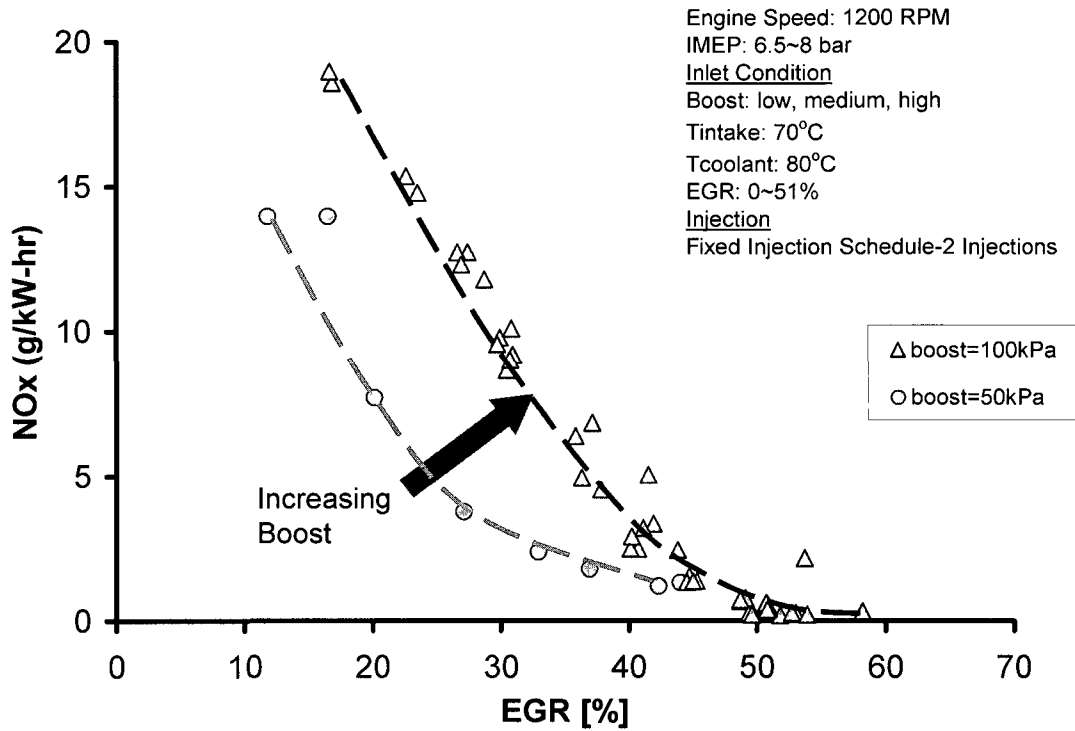
Figure 6-14: Effect of EGR and boost on emission at fixed injection strategy.
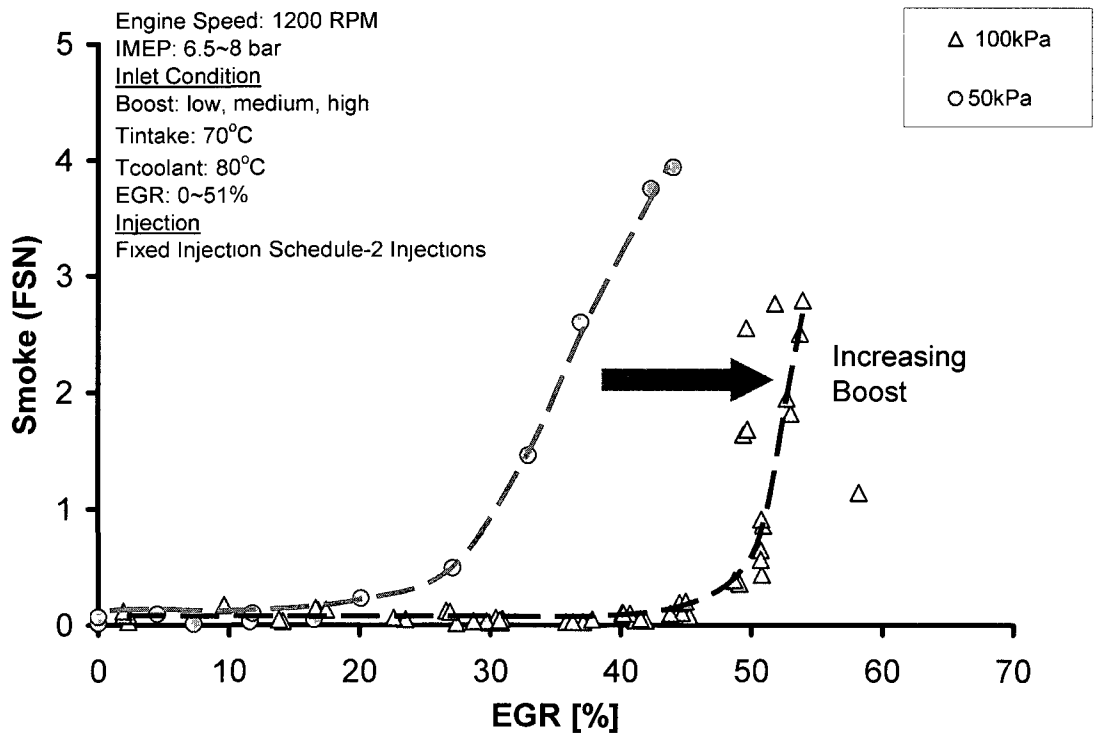
Figure 6-15: Effect of EGR and boost on emission at fixed injection strategy.
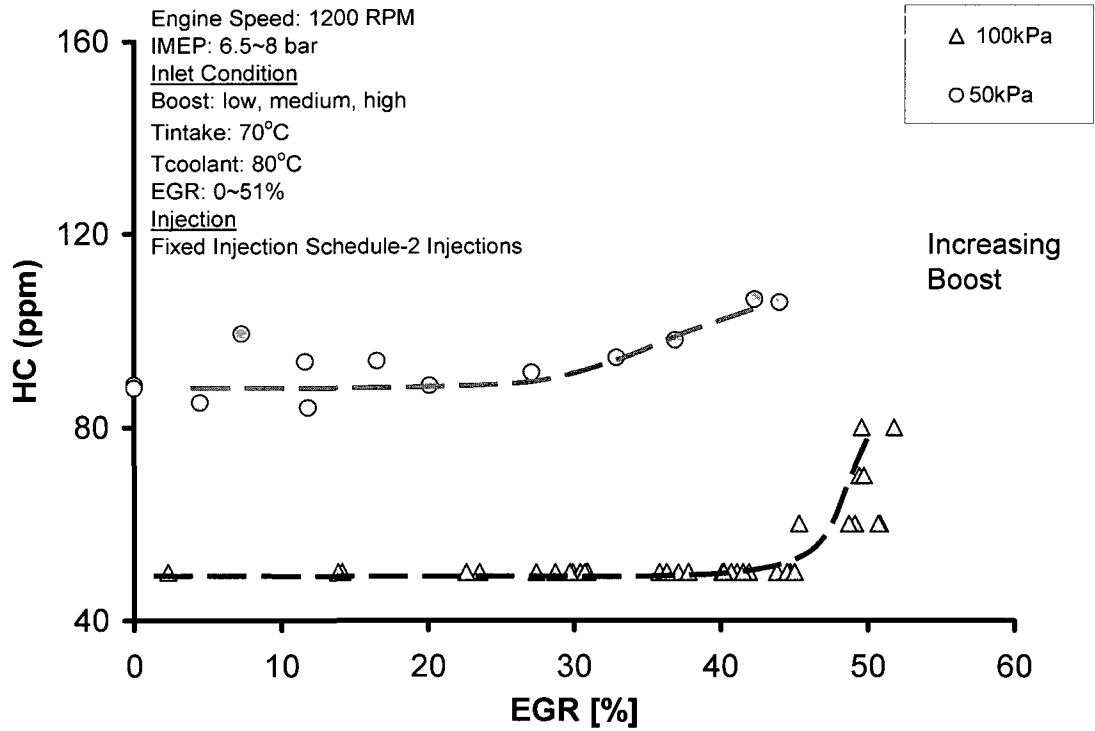
Figure 6-16: Effect of EGR and boost on emission at the fixed-injection strategy.
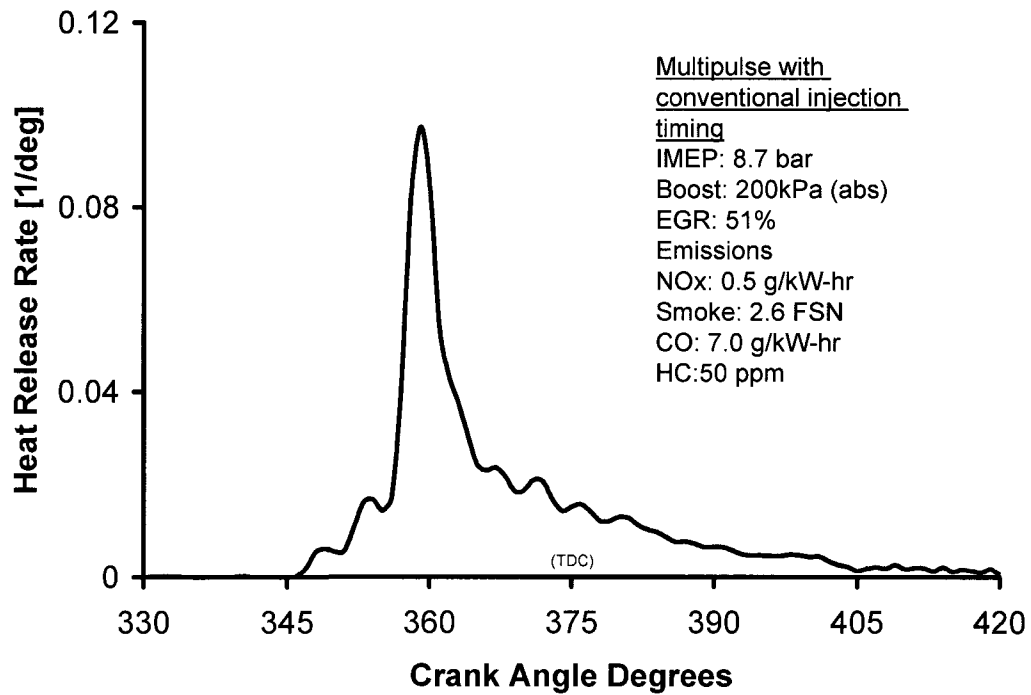
Figure 6-17: Representative heat-release for the case of 2-injections with 100kPa boost and 51% EGR.

From Figure 6-17, it can be seen that the combustion started at 345°CA. So for the first injection at 340°CA an ignition delay of only 5°CA was available for mixture preparation. For the second injection at 352°CA, there was no distinct ignition delay to prepare the homogenous mixture necessary for soot reduction.

Based on the above results it can be seen that the injection strategy had impact on attaining simultaneous low-NOx and low-soot combustion. It was also important to contain the UHC, because UHC is an indicator of incomplete combustion. In order to obtain the simultaneous low-NOx and low-soot, it was necessary to provide sufficient time for mixture preparation. This time was made available by injecting the fuel very early during the compression stroke and having a sufficient ignition delay due to the presence of EGR. Very early injection timings (Figure 6-6) were able to have combustion with low-NOx and low-soot but resulted in high UHC emissions due to fuel-condensation. Therefore, it was necessary to move the injection timings closer towards TDC to assist in the vaporization process. However, there was a limit to which the injection timing could be moved towards the TDC. For injection timings after 340°CA it was not possible to attain the ignition-delay long enough to form a homogenous mixture necessary for simultaneous low-NOx and low-soot. The crank-angle window for injection-timings that were able to achieve simultaneous low-NOx and low-soot are marked in Figure 6-18.
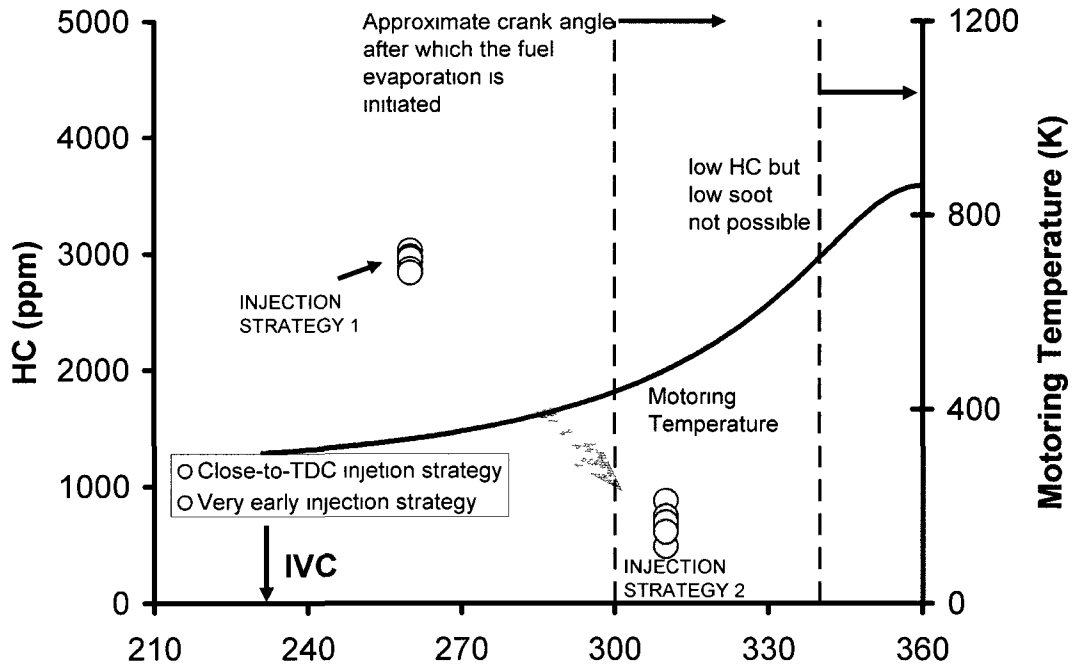
Figure 6-18: Injection timing window that was able to obtain simultaneous low-NOx and low-soot combustion with multi-pulse injection strategies.

The transition from conventional diesel to multi-pulse EPC on the dynamometer has been shown in Figure 6-19. For the EPC combustion shown in this thesis, the transition to the EPC combustion with multi-pulse injection strategy was done from the motoring condition only. If the engine was running in a conventional combustion mode, the engine was brought to idling by the dynamometer, and then the conventional combustion strategy was switched-off before the multi-pulse injection strategy was implemented. As shown in Figure 6-19, at the motoring condition a small amount of fuel was injected very early in the compression stroke. For the injectors considered in the present experiment the minimum stable injection quantity was 200micro-seconds (μs) therefore the injection scheduling consisted of three injections of 200μs. At this stage EGR was immediately engaged to prevent the auto-ignition of the fuel before the TDC. Note, at these conditions too much EGR may extinguish the combustion flame; therefore the amount of EGR needs to be selected with caution. For the present experiments an EGR of 55~60% was used. Once the combustion flame was stabilized for an injection quantity of 200μs, the fueling was gradually increased in small steps, and it was ensured that for each step

adequate amount of EGR was available to prevent the early auto-ignition of fuel early during the compression stroke, For the multi-pulse HCCI injection strategy "multiple-early-dense injection strategy" [44,45] was applied, more details of which can be found in the appendix.
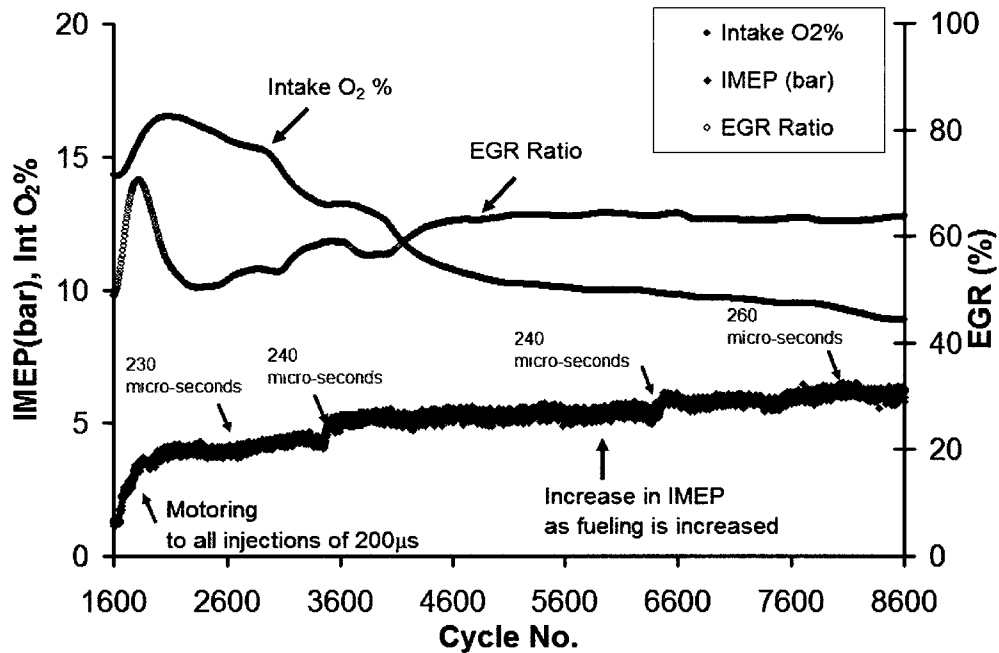
Figure 6-19: Transition from conventional diesel to HCCI combustion mode during the dynamometer tests.

6.1.4 Injection pressure as an enabler for EPC combustion

The use of higher injection pressure at a constant fueling was able to reduce the injection duration and thereby gain the time available for mixing. Single shot experiments were performed at a series of injection pressures at constant IMEP and constant start of combustion. It can be seen that at lower injection pressure the timing had to be advanced substantially to compensate for the longer injection duration (Figure 6-20). Thus, for most of the EPC experiments high injection pressure was used which increased the time available for mixture preparation and also helped in the spray atomization process. However, the use of higher injection pressure resulted in higher accessory work by the engine. The frictional work done was evaluated on an alternate motoring dynamometer for various injection pressures as shown in Figure 6-21.
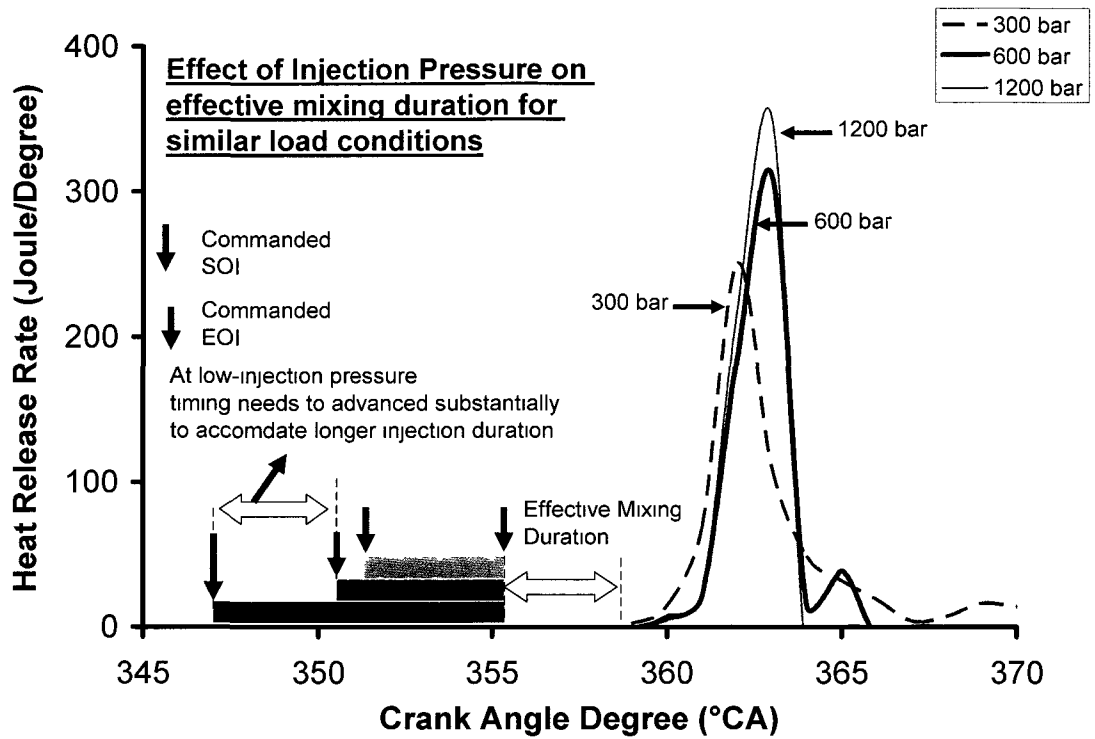
Figure 6-20: Effect of injection pressure on the mixing duration.
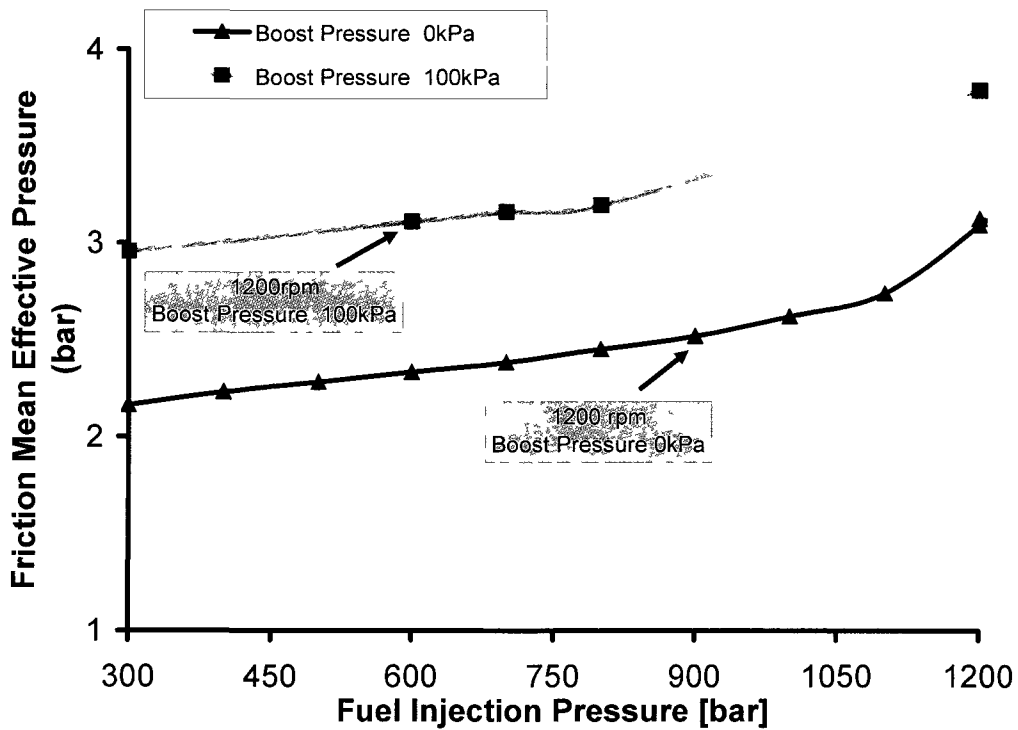
Figure 6-21: Effect of injection-pressure on friction-mean effective pressure determined using a motoring dynamometer.

6.1.5 EGR enabled EPC experiments with single-injection strategy

One drawback of multi-pulse EPC injection strategy in the previous section is the lack of combustion-phasing control directly with injection scheduling. Therefore, as a next step the EPC experiments were performed with a single injection strategy configured close-to-TDC. The use of injection timing close to TDC helped to retain combustion-phasing control by injection-scheduling. As discussed previously during multiple-injection experiments, the increasing use of EGR results in two opposing effects on the soot formation; one was the soot increase due to reduced intake oxygen concentration and second was the increased ignition delay for mixture preparation before the combustion process. An additional effect of the use of EGR is the reduction in the flame temperature, which also helps to shift the combustion towards the low-soot region of the ϕ-T map. Therefore, for the EGR enabled EPC experiment, a single injection was configured close to TDC and the EGR was progressively increased till the combustion approached the low-soot regions due to prolonged ignition delay and lowered flame temperature. The EGR-enabled EPC experiments were first performed for low-load condition with no-boost and low-injection pressure. The load was progressively increased up to 9bar IMEP with appropriate selection of boost, EGR and injection pressure.

6.1.5.1 EGR-enabled EPC experiments at 2.2bar IMEP, low-boost and low-injection pressure

The EGR-enabled EPC experiments were performed at a load of 2.2 bar IMEP. A single-injection strategy was implemented with a commanded SOI of 354°CA. At high EGR-rates the prolonged ignition delay led to a significant departure of combustion phasing from the TDC, therefore the commanded SOI had to be advanced up to 350°CA to maintain the combustion phasing close to TDC. As mentioned above, no boost was implemented and the injection pressure of 430bar was used. The NOx decreased continuously in Figure 6-22 due to dilution, thermal and chemical effects of EGR [54~56]. For this test, a simultaneous low-NOx and low-soot was achieved with an EGR of 60%. Since the experiments were performed at very low-loads even with an implementation of 60% EGR, there was 16% oxygen at the intake (Figure 6-23). As a result there was no substantial increase in soot when high EGR rates were implemented.
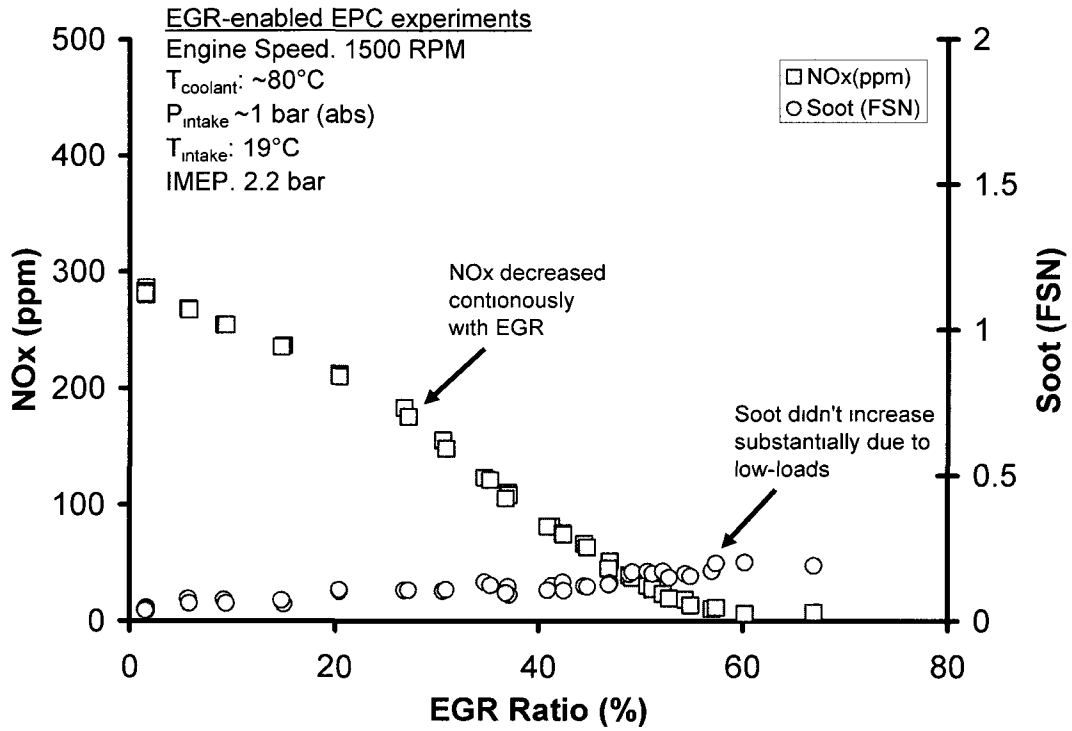
Figure 6-22: EGR-enabled EPC experiments at low-loads.
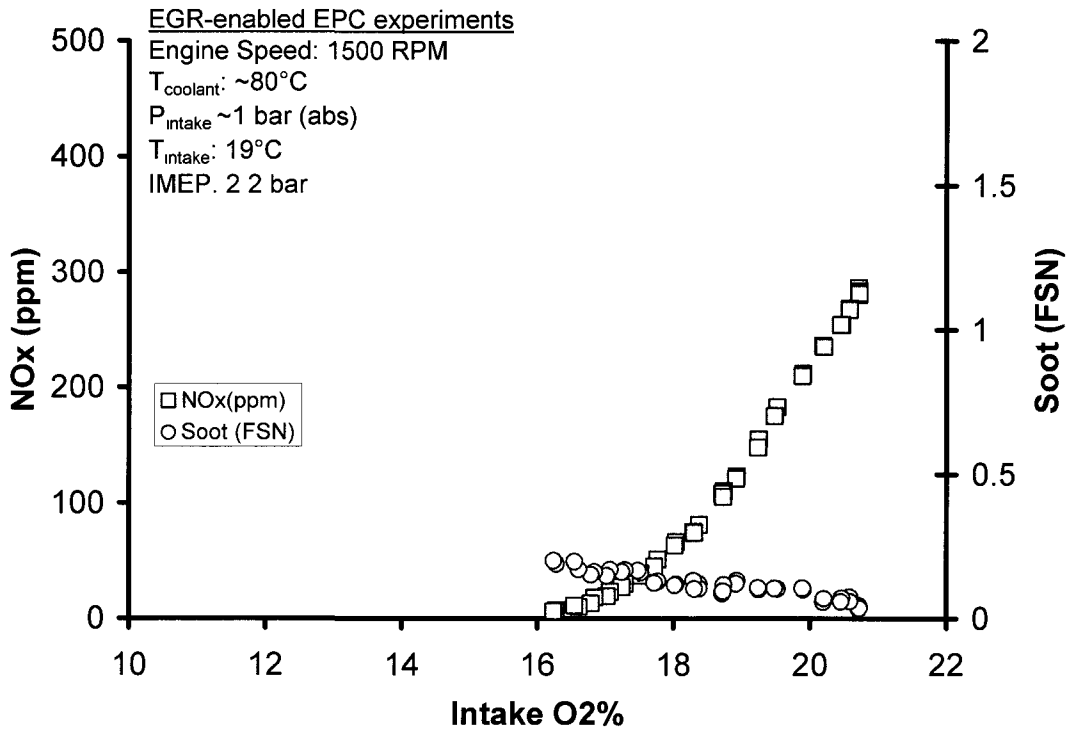
Figure 6-23: EGR-enabled EPC experiments at low-loads.

6.1.5.2 EPC experiments at 4.4bar IMEP with low-boost and low-injection pressure

This time the EPC experiments were performed at a load 4.4bar IMEP with a single injection strategy. The single injection was implemented at a SOI of 356°CA. However, the SOI was continuously adjusted similar to the previous experiments with increasing EGR to maintain the combustion phasing close to TDC. This time the boost was moderately increased to 10kPa while the injection pressure was still kept at 460bar. Under such testing conditions, the NOx-PM trade-off was readily apparent (Figure 6-24). For EGR ratios up to 45% the NOx decreased monotonically. At the same time, the application of EGR led to a rapid decrease in oxygen availability which translated to a substantial increase in soot from the baseline case. Any further increase in EGR had little impact on the NOx emissions; however the soot decreased from its peak value. The segment of the soot versus EGR curve that showed the traditional NOx-PM trade-off is referred to as the Slope-1 of soot formation in this thesis. The mode of combustion where the NOx and the smoke are simultaneously low is considered as the Low-Temperature Combustion variant of the EPC and the segment of soot-EGR curve where the soot is dropping with an increase in the EGR is referred to as Slope-2 of the soot-EGR curve.

Since the intake charge dilution has been identified as a major factor for NOx reduction it was decided to represent the effect of EGR on the intake oxygen concentration basis also (Figure 6-25). According to Figure 6-25, it can be seen that a minimum intake dilution of 14% oxygen was required for low-levels of NOx with EGR enabled EPC. Any decrease in intake oxygen lower than 14% had very little impact on the NOx emissions. Similarly, an oxygen of 10~12% was required for simultaneous low-NOx and low-soot.

The increasing use of EGR compromised the combustion efficiency as indicated by the increased amounts of CO and UHC (Figure 6-26, Figure 6-27). The CO started to climb up rapidly once the 40% EGR rates or 14% intake-oxygen is reached. This EGR window approximately matched the EGR needed for low-NOx. EGR rates in excess of 50% were needed to implement the simultaneous low-NOx, low-soot combustion and for these EGR rates the HC emissions appeared in significant quantity in the exhaust (Figure 6-26 and Figure 6-27).
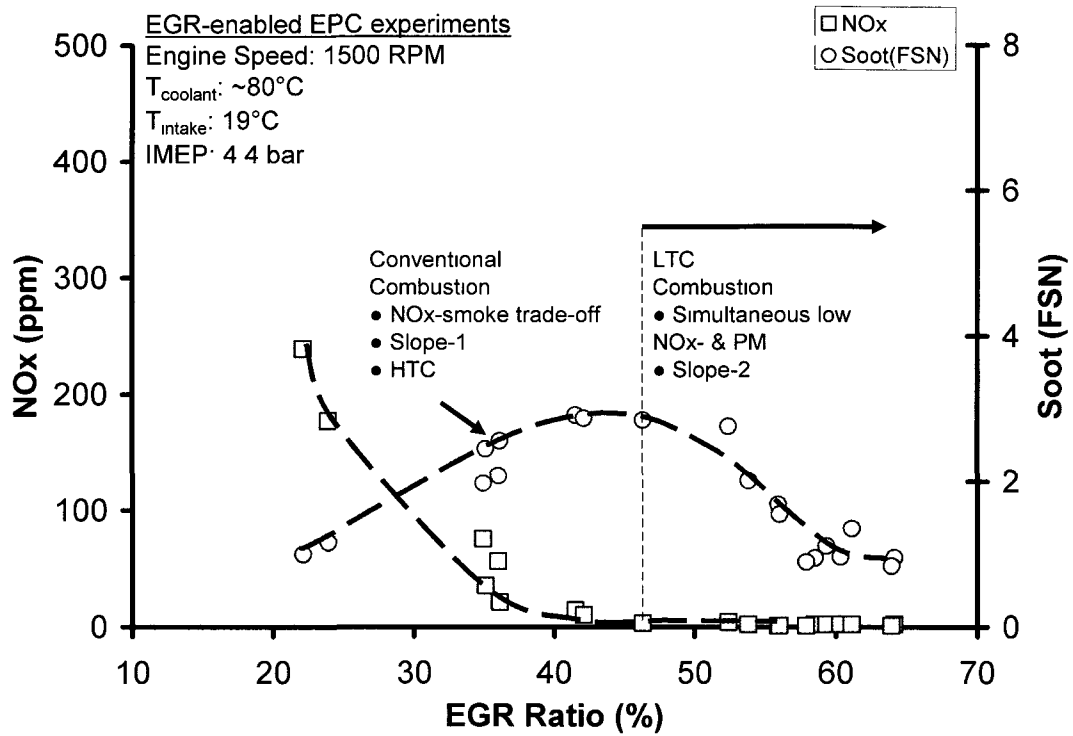
Figure 6-24: Simultaneous reduction of NOx and soot with EGR-enabled EPC combustion using a single injection strategy.
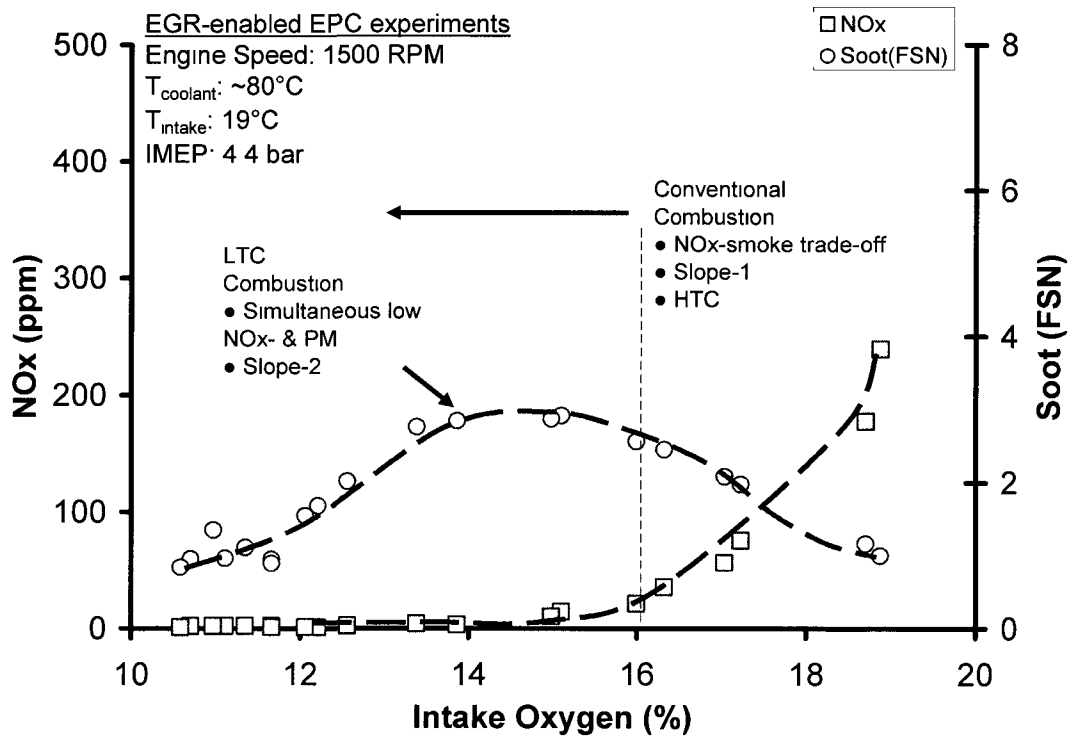
Figure 6-25: Simultaneous reduction of NOx and soot with EGR-enabled EPC.
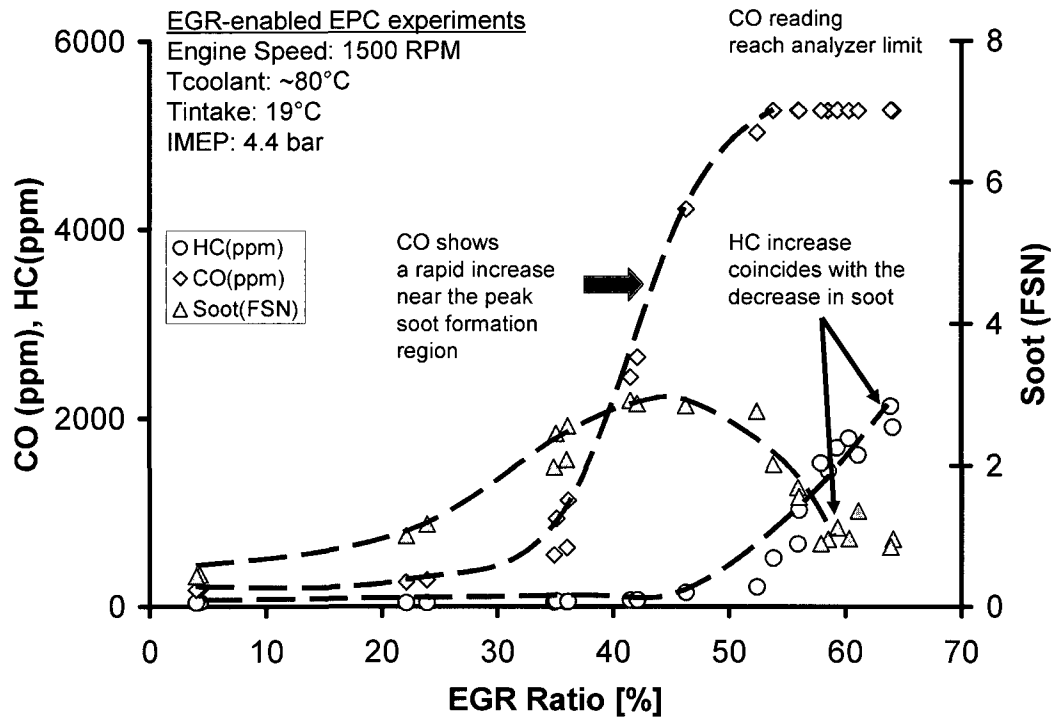
Figure 6-26: Effect of EGR on CO and HC during EGR-enabled EPC.
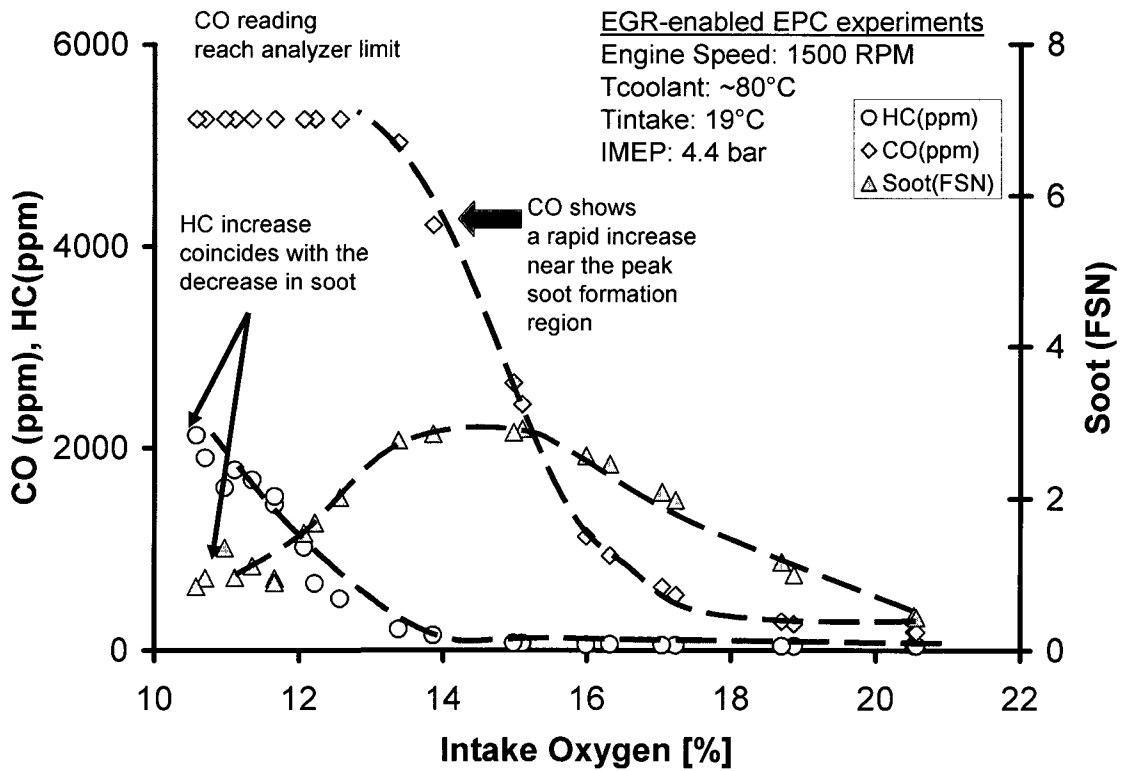
Figure 6-27: Effect of intake-oxygen concentration on CO and HC during EGR-enabled EPC.

68

6.1.5.3 EPC experiments at 5.5 bar IMEP and low injection pressure

This time the load for the EPC experiments was again increased while the boost and the commanded rail pressure were still kept at 15kPa and 500bar respectively. The EGR was again progressively increased till the combustion approached simultaneous low-NOx and low-soot combustion regimes. This time the tests were performed at three different SOI's of 356°CA, 360°CA and 362°CA. Unlike the previous experiments, the SOI was not adjusted when increasing amounts of EGR was applied. The NOx-EGR (Figure 6-28) trend nearly overlapped for all the three injection timings whereas the soot EGR trends were more favorable for the SOI of 360°CA and 362°CA. If the IMEP penalty (Figure 6-29) was also taken into account then the injection timing of 360°CA had a lower IMEP penalty compared to 362°CA. Large amounts of un-burnt hydrocarbon and CO were generated during the combustion in the enhanced premixed regime and as Figure 6-30 shows up to 3% of the input fuel energy was wasted during these combustion modes. The cylinder pressure traces during the EGR sweep for a representative case of 356°CA has been shown in Figure 6-31.
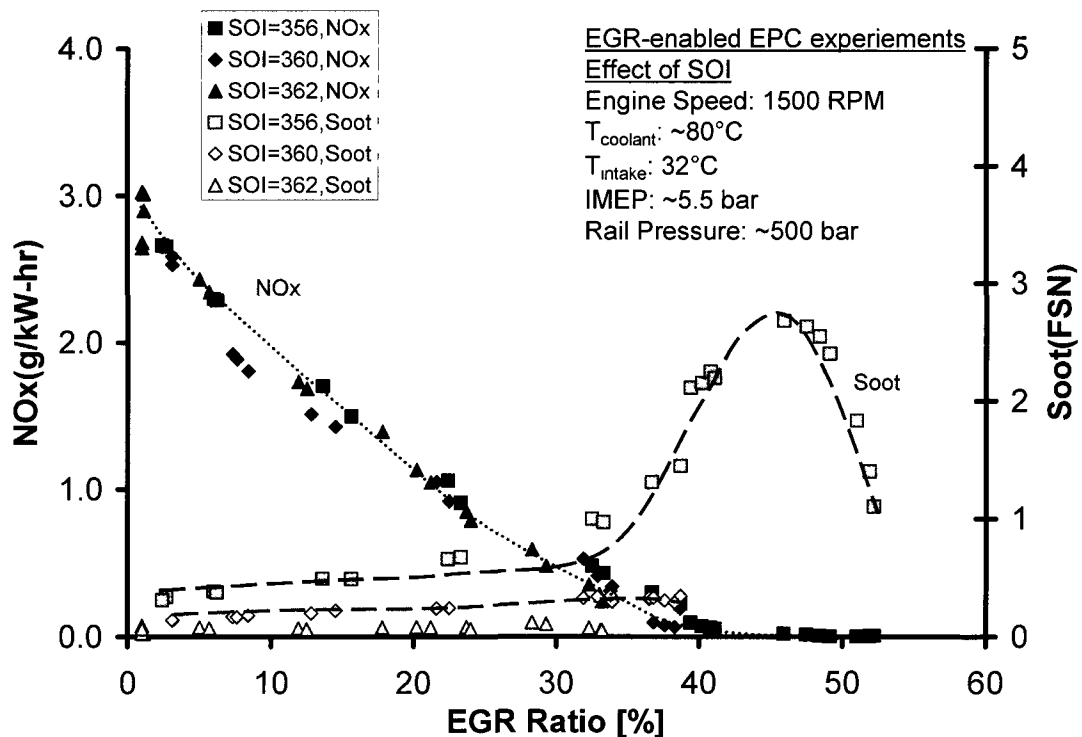
Figure 6-28: Enhanced premixed combustion with EGR prolonged ignition delay.
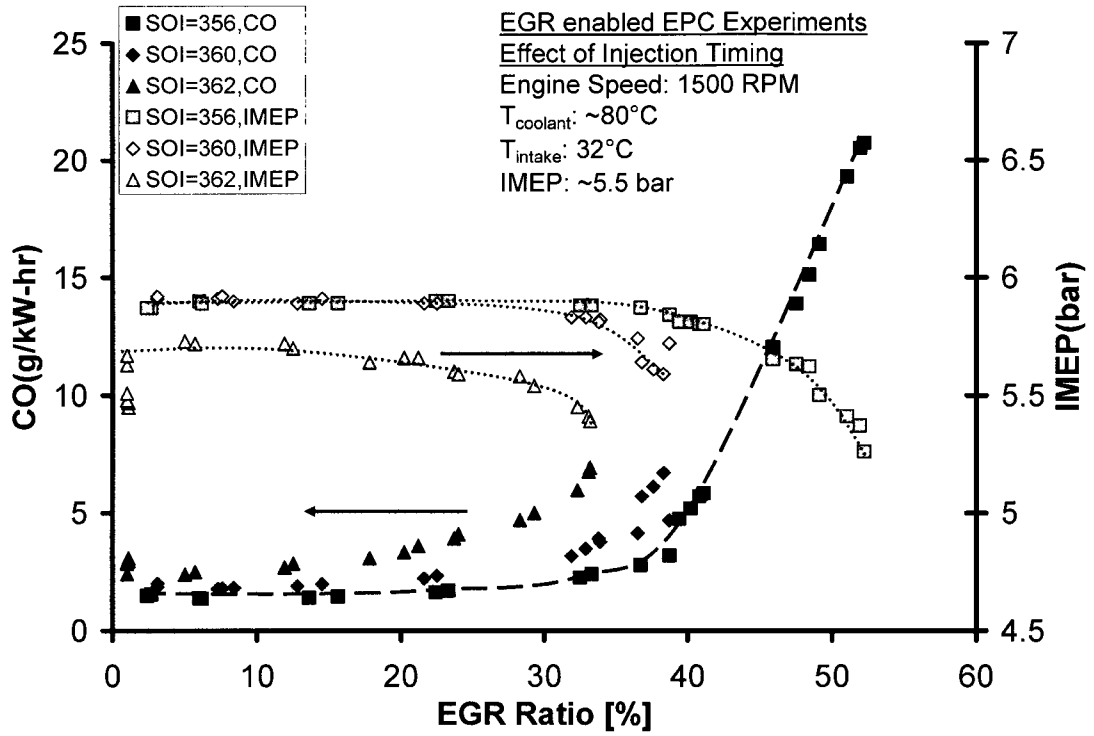
Figure 6-29: IMEP penalty for different injection timing to achieve enhanced premixed combustion.
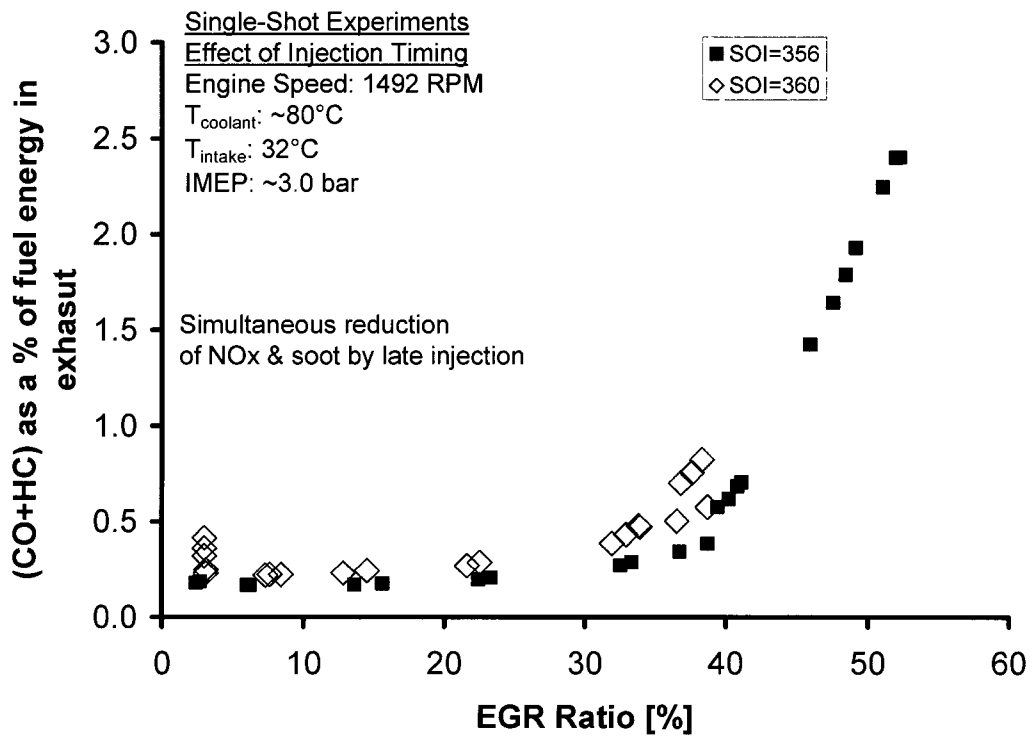
Figure 6-30: Fraction of energy carried by CO and HC in the exhaust.
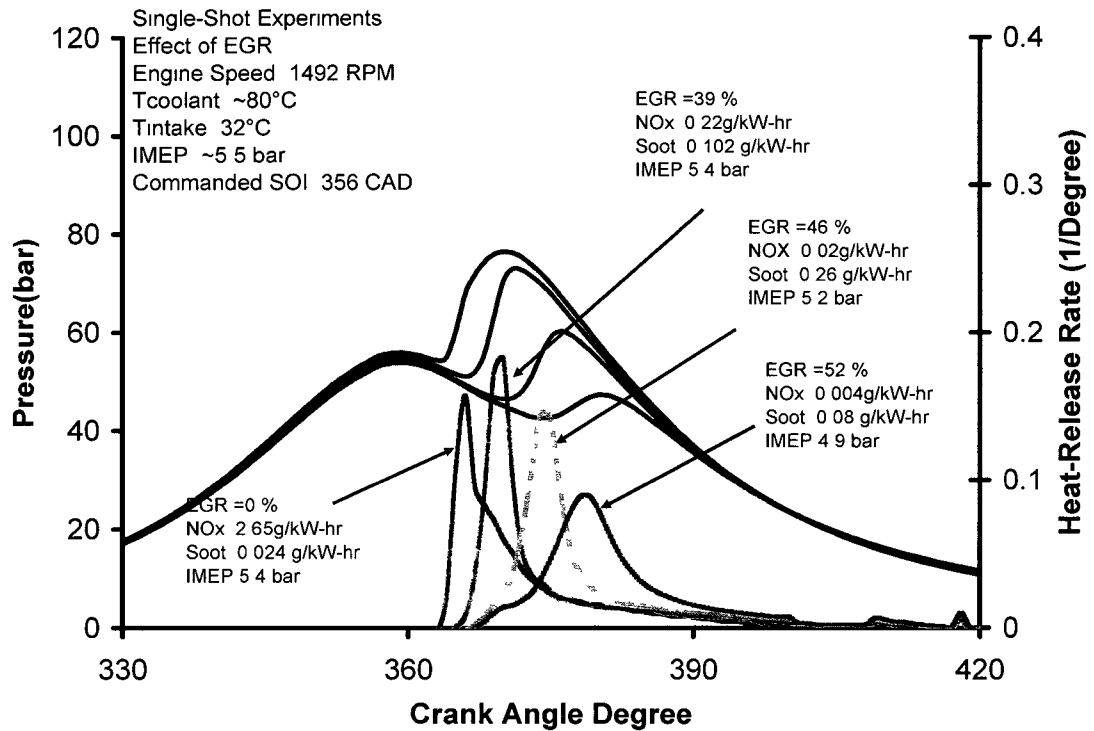
Figure 6-31: Effect of EGR on heat-release rate for a fixed SOI.

6.1.5.4 EPC experiments with high injection pressure and high-boost

This time the load was still kept the same as the previous experiment but both the boost and the injection pressure were raised. The boost was selected as 50kPa and the commanded rail pressure was set to 950bar. For this case experiment, the transition from the Slope-1 to Slope-2 took place at approximately 50% EGR (Figure 6-32). When the load was increased to 8.0bar IMEP at the same boost and injection pressure, the soot continued to increase up to 52% EGR, which suggested that an IMEP of 6.0bar was the load limit for this injection pressure and boost condition (Figure 6-33).
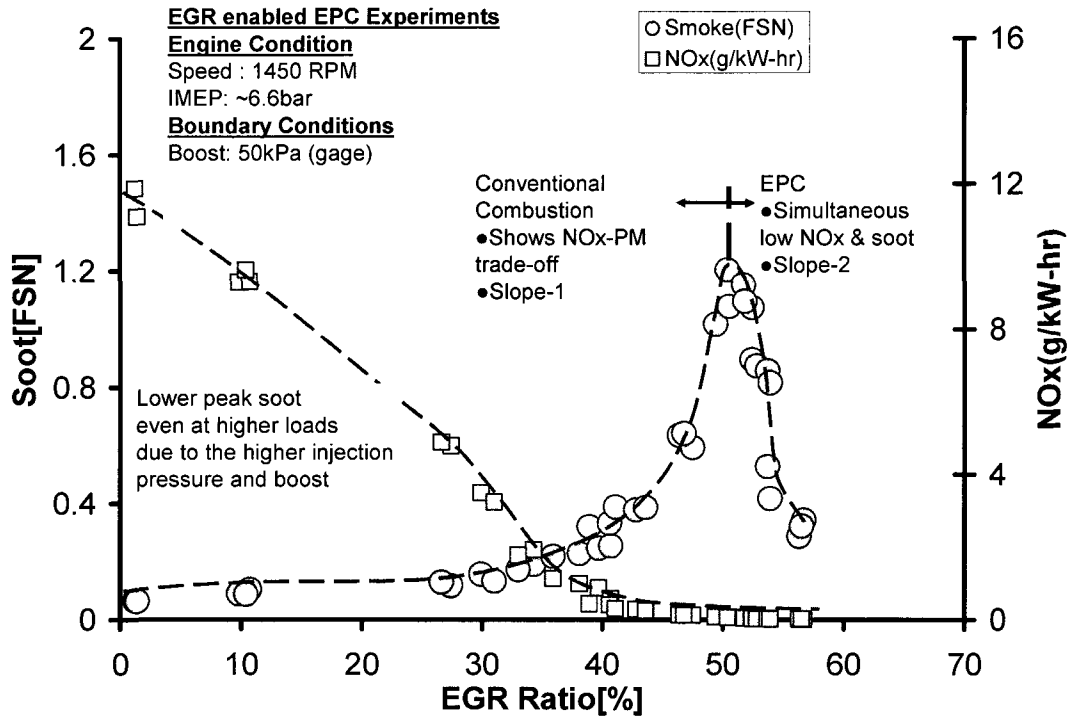
Figure 6-32: EGR-enabled EPC combustion at mid-load conditions with increasing boost and commanded rail pressure.
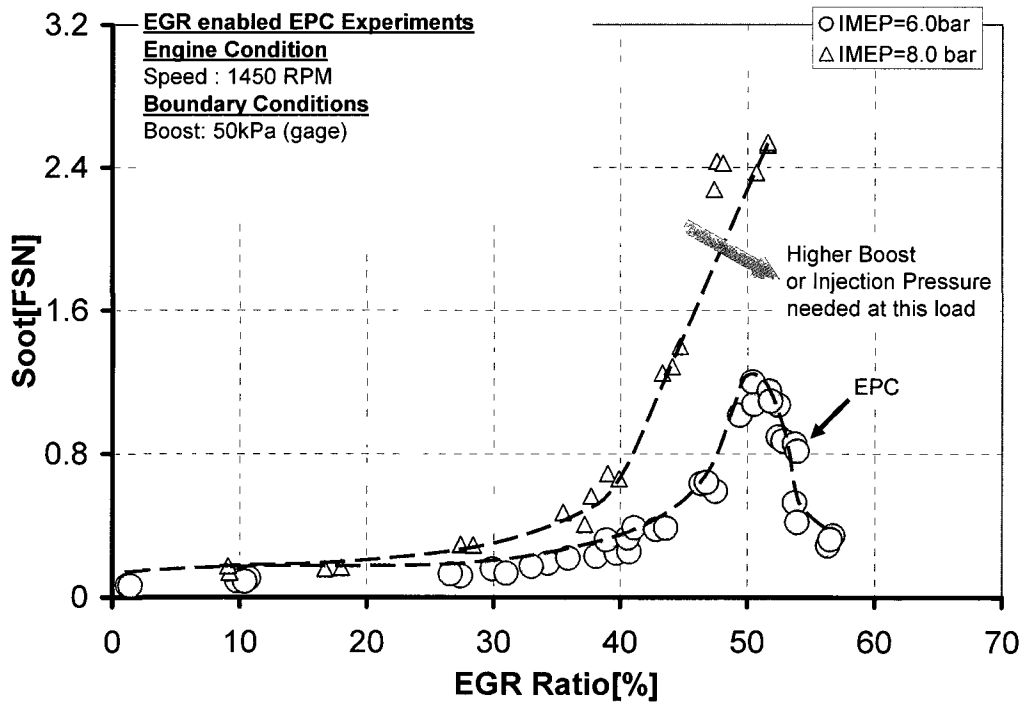
Figure 6-33: Load-limits for a given boost and injection pressure for EGR enabled EPC.

6.1.6 Parametric study during EPC combustion

In this section the above mentioned experiments were grouped together and the effect of load and injection pressure has been investigated on the EPC combustion.

EFFECT OF LOAD

The majority of soot particles originate in the fuel-rich regions of burning diesel jets. As the load was increased, for a fixed boost and injection pressure, there were no additional enablers to assist in the homogenization of the increased amount of fuel. Therefore, there was increased propensity for formation of fuel-rich pockets which resulted in higher soot as the load was increased. The increase in soot with load became more pronounced in the presence of EGR because of the reduction in the oxygen concentration. The effect of increase in load on Slope-1 and Slope-2 of the soot-EGR curve is shown in Figure 6-34 and Figure 6-35. In Figure 6-34, the load is increased moderately from IMEP of 2.2 to 4.5 bar while the injection pressure and the boost was kept constant. At the 4.5 bar test, the peak soot values was 3.0 FSN, while the comparative peak soot at 2.2 bar IMEP was less than 1FSN. However, when the EGR-enabled EPC experiments were implemented at 6.0bar IMEP (Figure 6-35, Figure 6-36) at higher boost (50kPa) and injection pressure (950bar) the peak soot values were contained to less than 1.5FSN. Thus it can be readily seen that the any increase in load needs to be compensated with boost and injection pressure to contain the peak soot in the soot-EGR curve. On an intake oxygen basis, the simultaneous low NOx and low-soot was approached at both 4.4bar and 6.0bar IMEP at 11% oxygen at the intake (Figure 6-37).
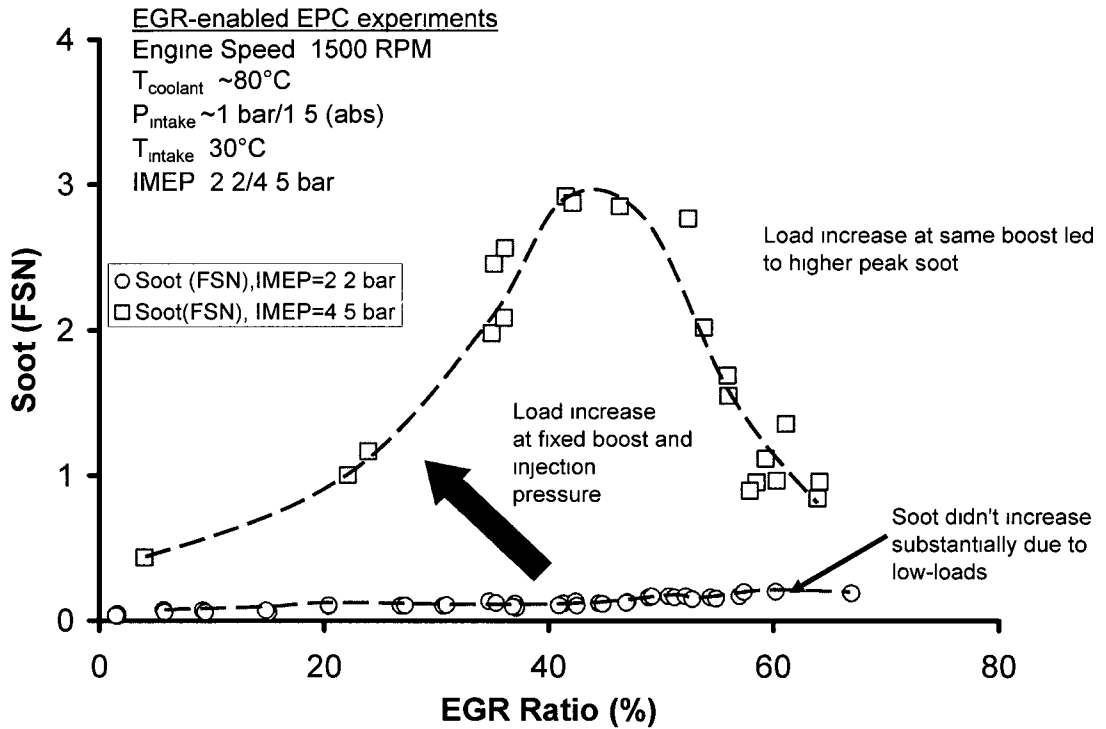
Figure 6-34: Effect of load on Slope-1 and Slope-2 curves of soot formation at fixed boost and injection pressure.
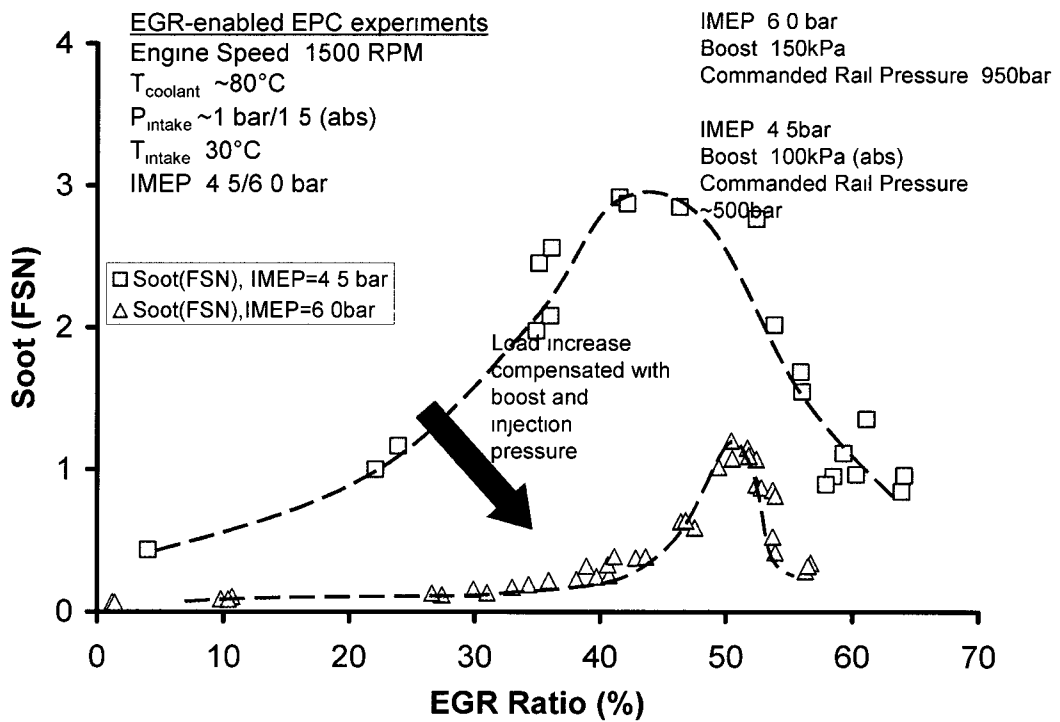
Figure 6-35: Effect of load on Slope-1 and Slope-2 curves of soot formation at increased boost and injection pressure.
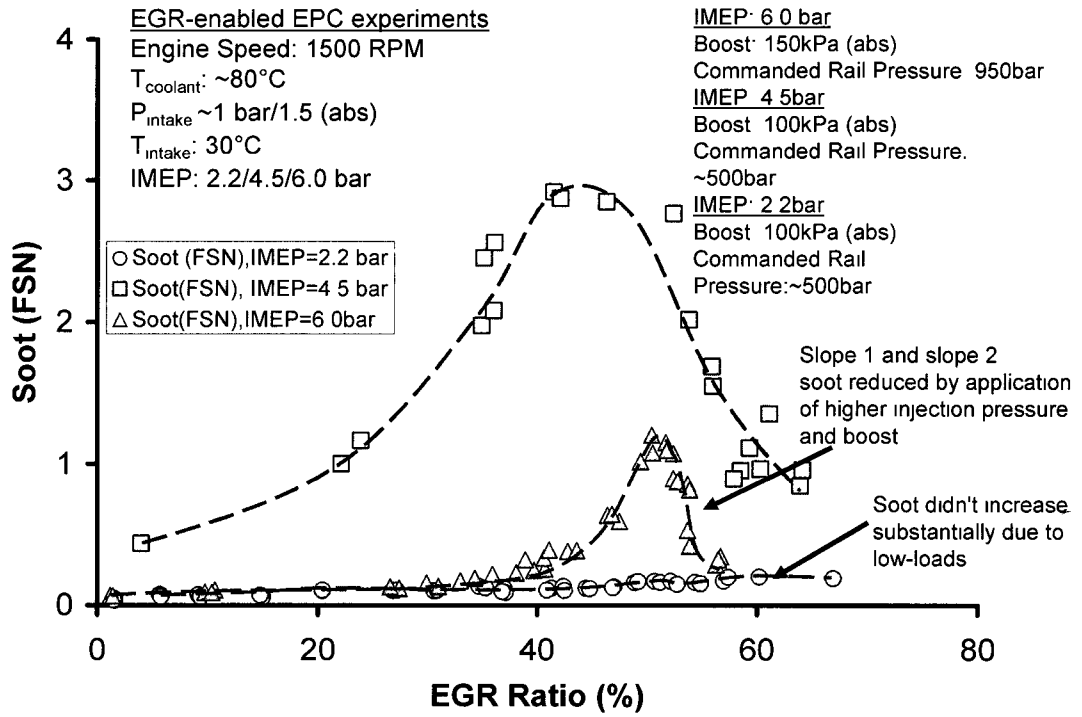
Figure 6-36: Effect of load on Slope-1 and Slope-2 of EPC combustion.
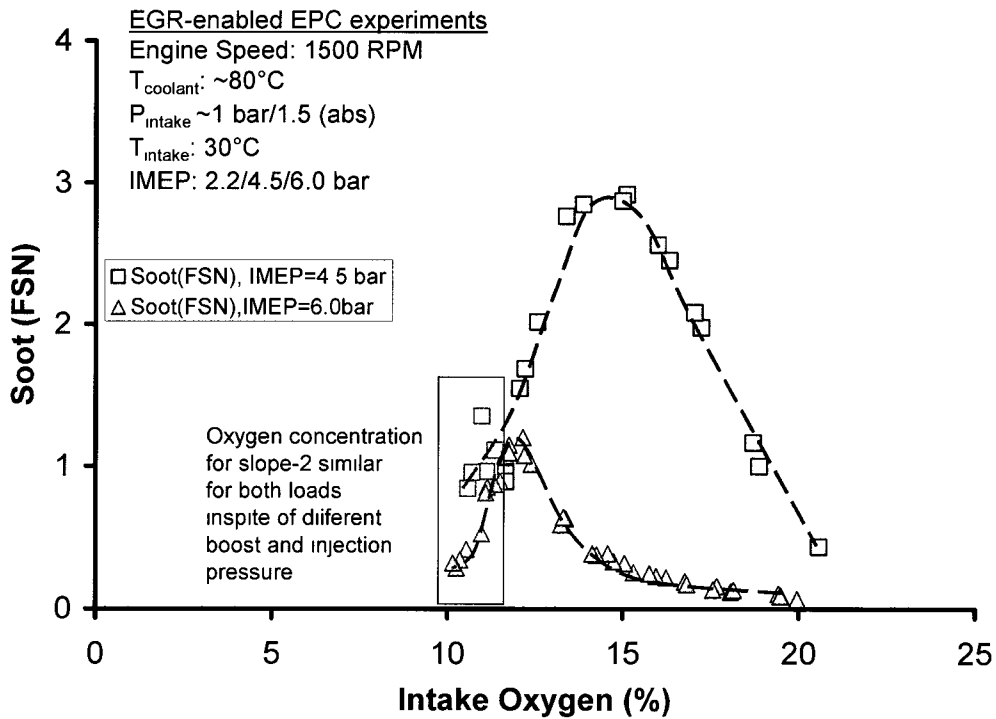
Figure 6-37: Effect of intake oxygen concentration on soot-formation during EGR enabled EPC.

The effect of increased load on NOx formation for the EGR enabled EPC has been examined in Figure 6-38, Figure 6-39 and Figure 6-40. In the addition to the previously discussed EPC experiments test data for 8.0bar IMEP has also been included in the comparison. The tests at the load of 8.0bar IMEP were also performed at a load of 50kPa and a commanded rail pressure of 950bar. It can be seen that a minimum EGR of 50% is required to meet the low NOx levels. Note that the EGR depends also on the load level of engine operation. For instance, an EGR of 50% represents a significant recirculation of exhaust at higher load levels. However, at low-load such as idling, even with 50% EGR sufficient amounts of oxygen may be available at the intake. Therefore, to get a better appreciation all the NOx-EGR curves were translated to NOx-intake oxygen % basis. It can be readily seen that at a given boost of 50kPa the NOx-EGR collapsed to a single line on the NOx-intake oxygen basis (Figure 6-39). A minimum charge dilution of 14% was needed to reach low-levels of NOx. Note that for the experiments at 8.0 bar IMEP it was possible to attain only low-NOx, but the Slope-2 soot could not be attained.
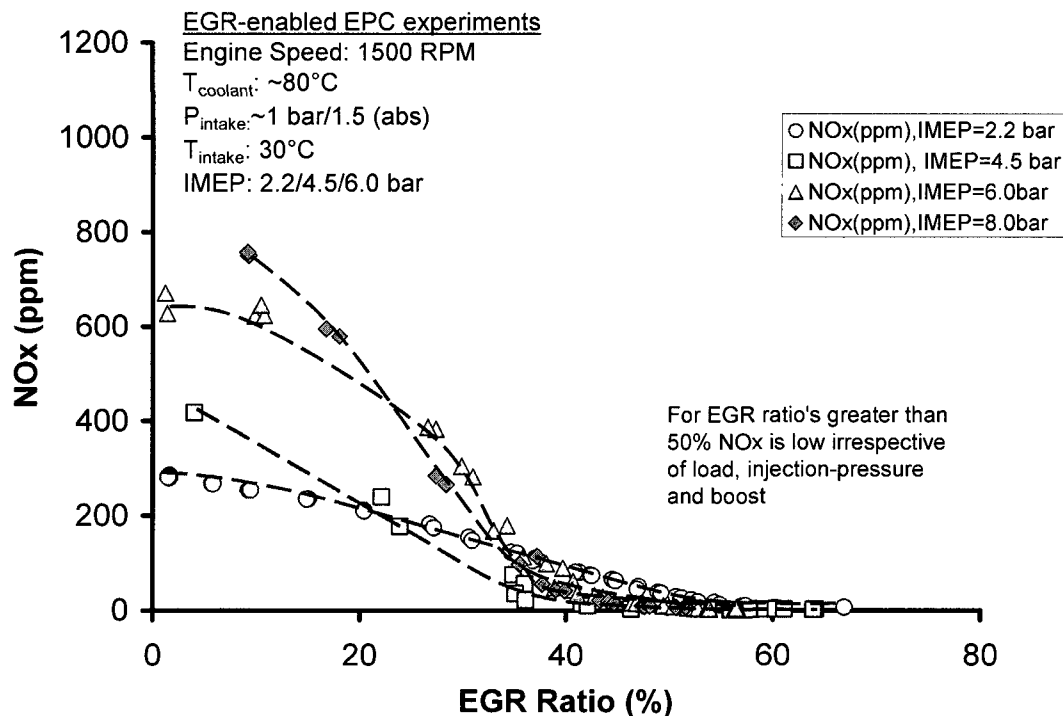
Figure 6-38: Effect of increase in load on NOx during EGR enabled EPC.
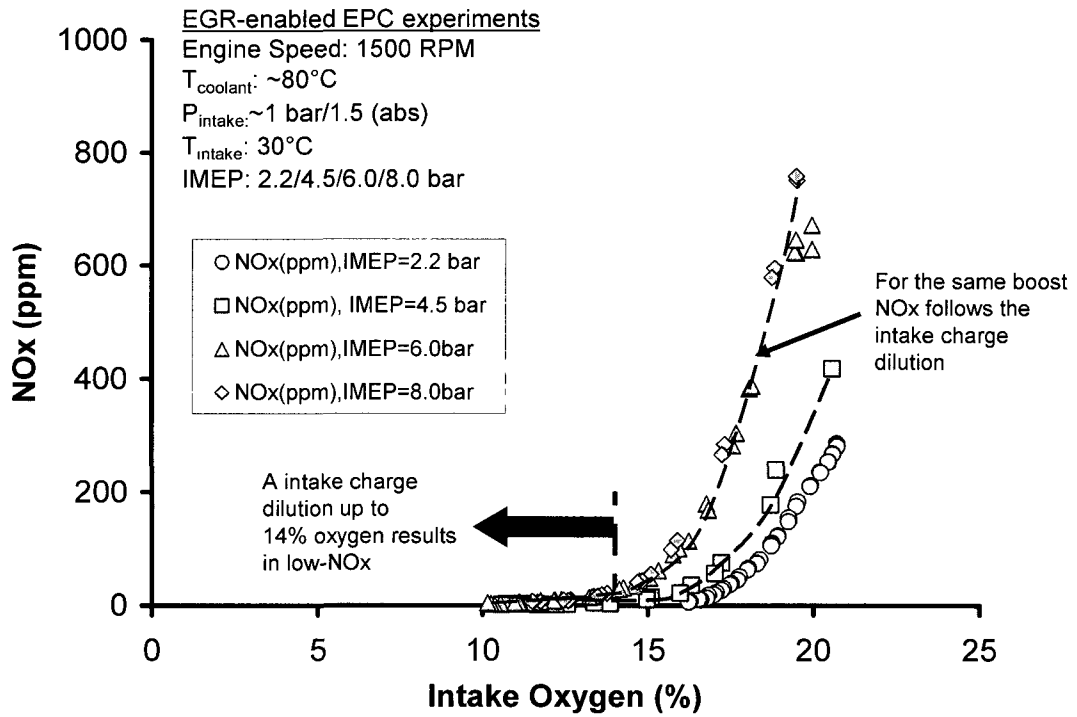
Figure 6-39: Effect of intake oxygen concentration on soot-formation during EGR enabled EPC.
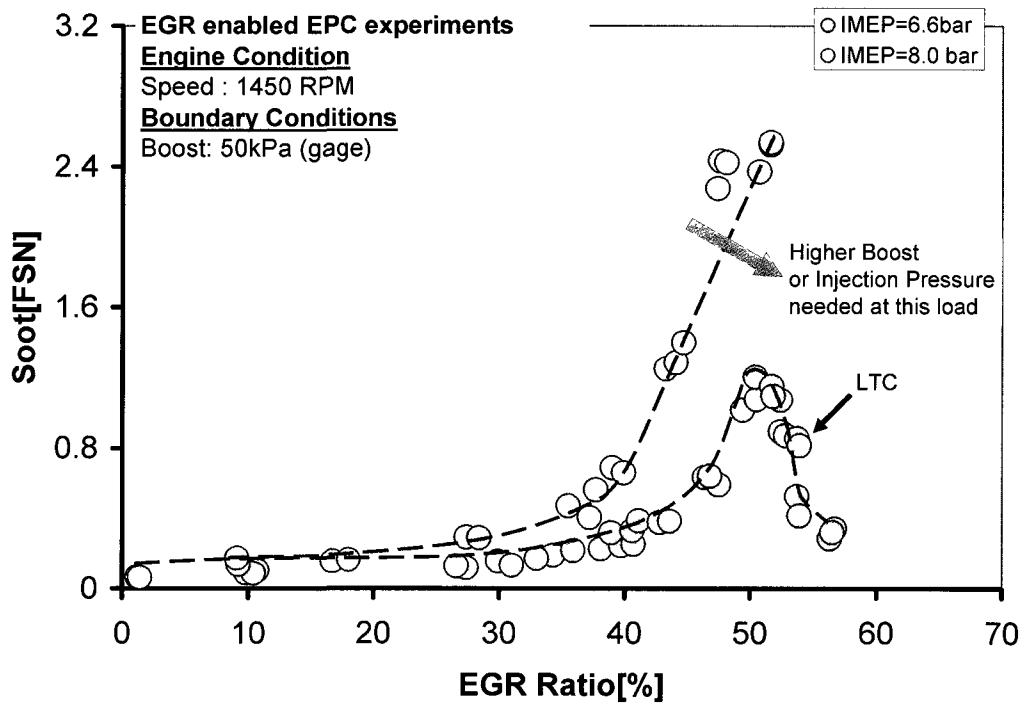
Figure 6-40: EGR-enabled EPC experiments at 8.0 bar IMEP.

EFFECT OF INJECTION PRESSURE

Since, the Slope-2 was not attained at 8.bar IMEP it was decided to revisit the same load condition at higher injection pressure. The soot continued to increase with increasing EGR during the Slope-1 region of the soot-EGR curve. However, it was again not possible to go to the Slope-2 of the EGR-soot curve even with an EGR of 60%. At this level of EGR there was a substantial increase in CO (Figure 6-41). Therefore it was decided not to implement any further increase in EGR to attain EPC combustion at this boost. This time again at higher injection pressure it was not possible to attain the simultaneous low-NOx and low-soot combustion.

Therefore, the EGR enabled EPC was attempted at a higher boost of 100kPa and the higher injection pressure as shown in Figure 6-42. It was possible to obtain simultaneous low-NOx and low-soot combustion this time. Thus it can be seen that even though injection pressure had an effect on containing the peak soot of the soot-EGR curve, it was the boost or the air-fuel ratio that had stronger influence on the attaining low-soot.
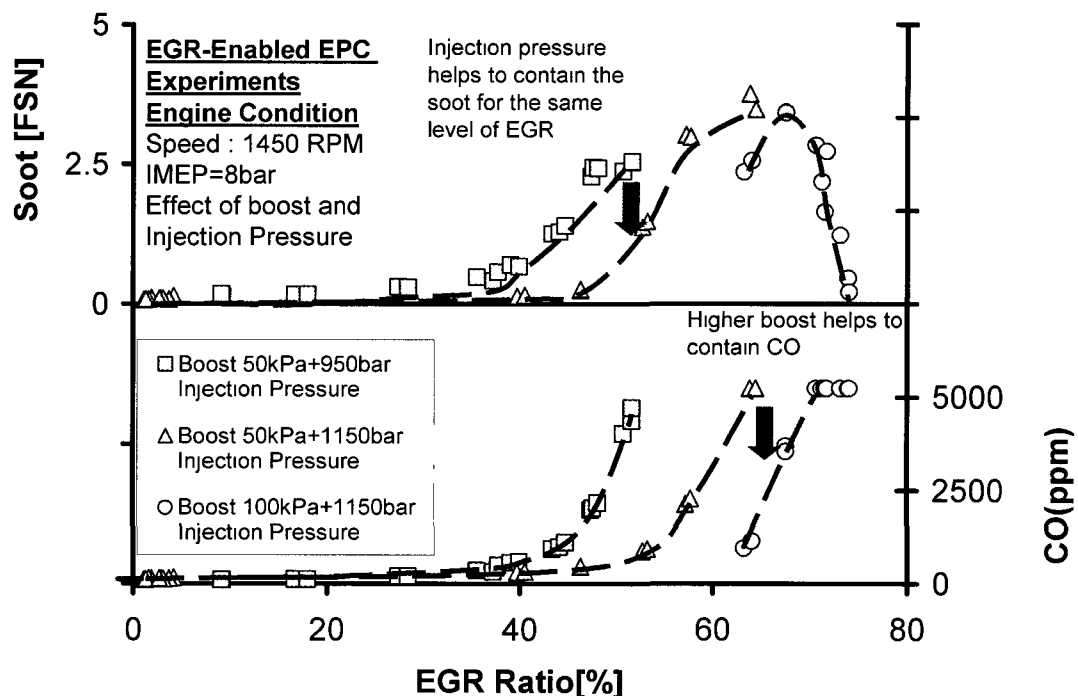
Figure 6-41: Use of higher injection pressure to reduce the peak soot-formation in the Slope-1 region.
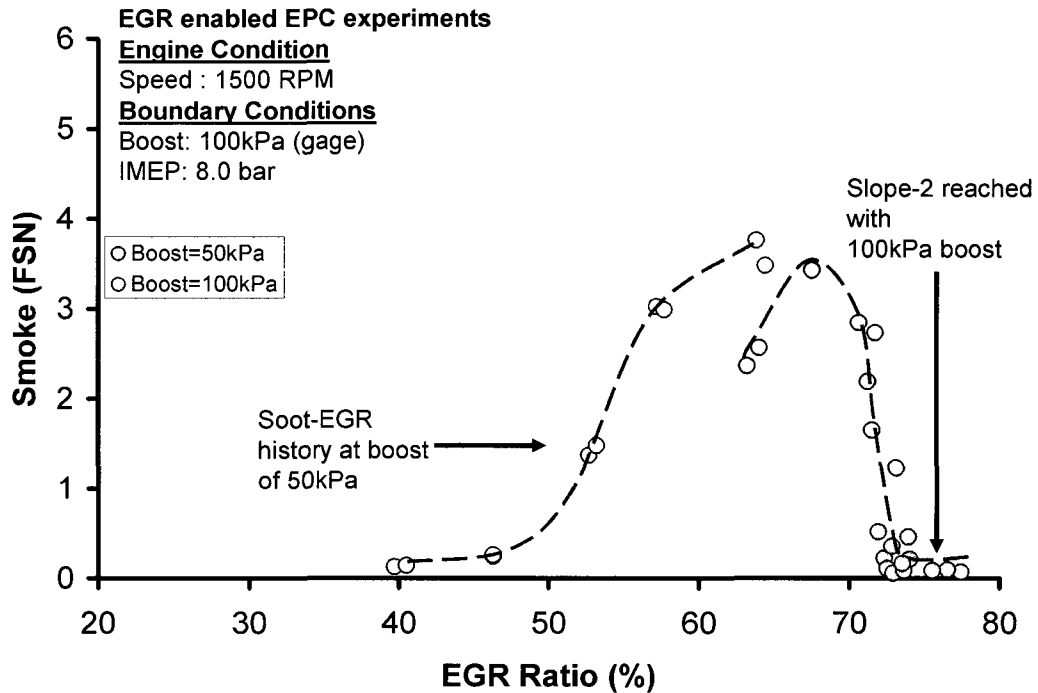
Figure 6-42: Use of higher boost and higher injection pressure to reach EGR enabled EPC.

6.1.7 Limitations of EGR enabled EPC

In the EGR enabled EPC, the prolonged ignition delay was essential to obtain the time necessary for the preparation of the charge mixture with enhanced homogeneity. Prolonging the ignition delay meant that the combustion phasing was always postponed with EGR for a fixed commanded SOI. However, there are two aspects to combustion phasing; a) combustion stability and b) cycle thermal efficiency. As the combustion phasing was retarded from TDC, it progressively entered regions of high cycle-to-cycle to variation, with the combustion flame getting nearly extinguished in the limiting case (Figure 6-43). The relationship between the commanded SOI and the CA-50 is shown in Figure 6-44. It can be readily seen that the combustion phasing has a highly non-linear relationship with the commanded SOI towards retarded injection timings. Similarly, Figure 6-45 and Figure 6-46 show two cases where a change in SOI of 1.5°CA led to a significant change in combustion characteristics. Therefore, it was decided to implement closed-loop on combustion phasing for the next-phase of experiments for EGR enabled EPC.

79
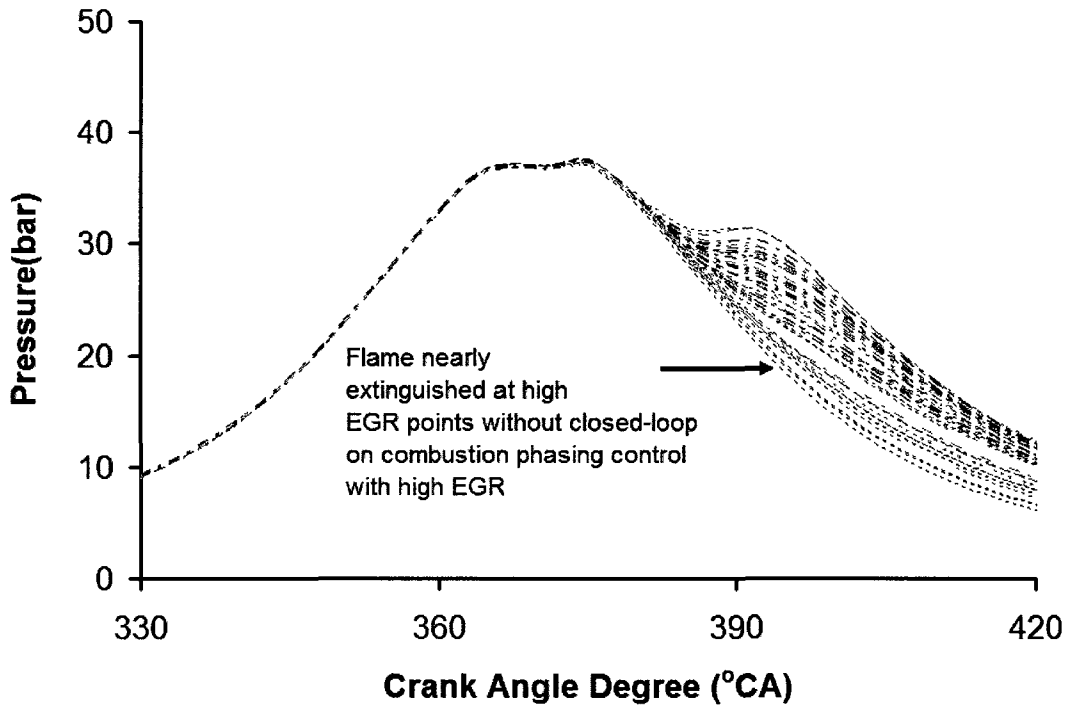
Figure 6-43: Combustion flame nearly died in presence of high-EGR without closed-loop on combustion phasing correction.
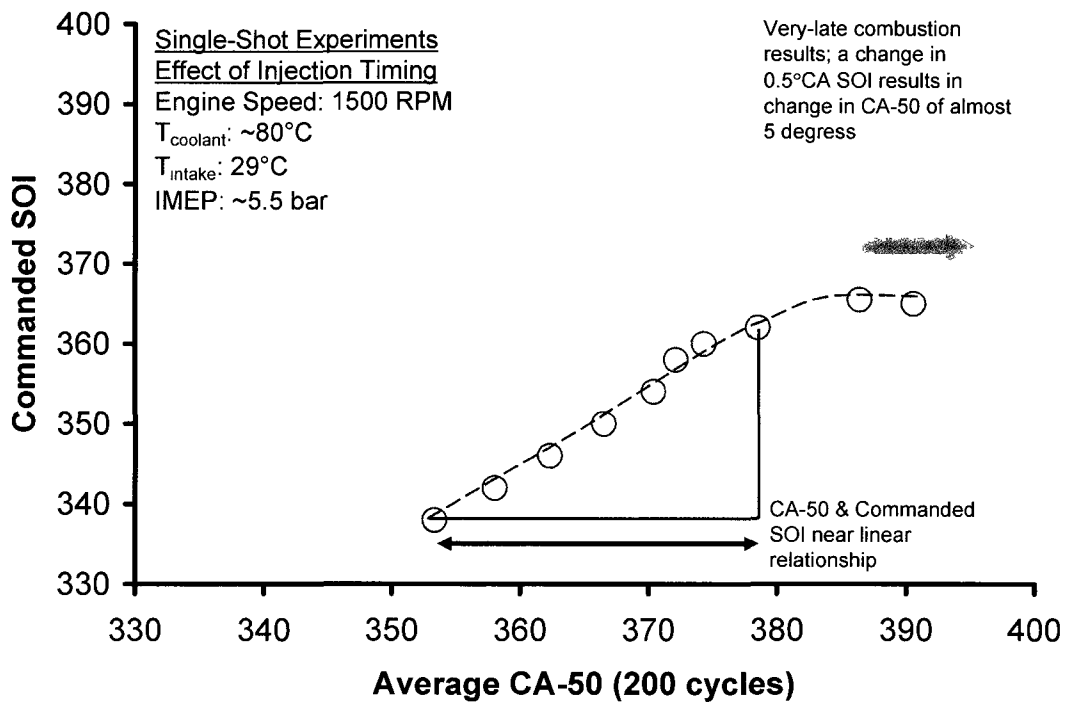
Figure 6-44: Typical relationship between the commanded SOI and the CA-50.
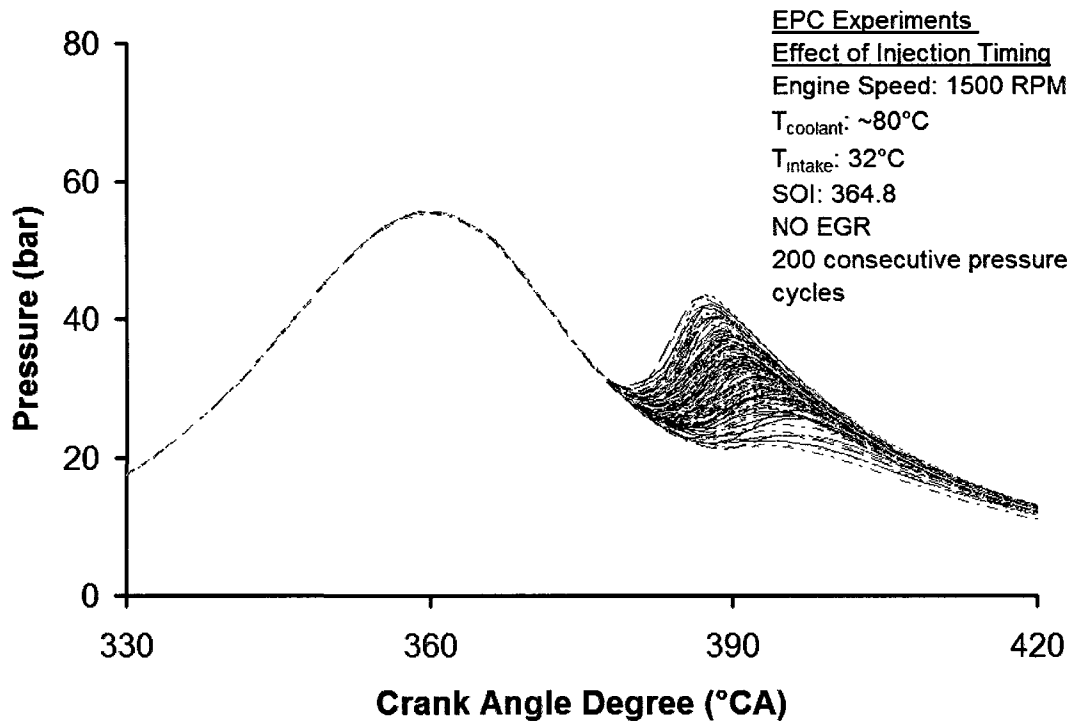
Figure 6-45: 200 consecutive pressure cycles showing the effect of SOI during EPC.
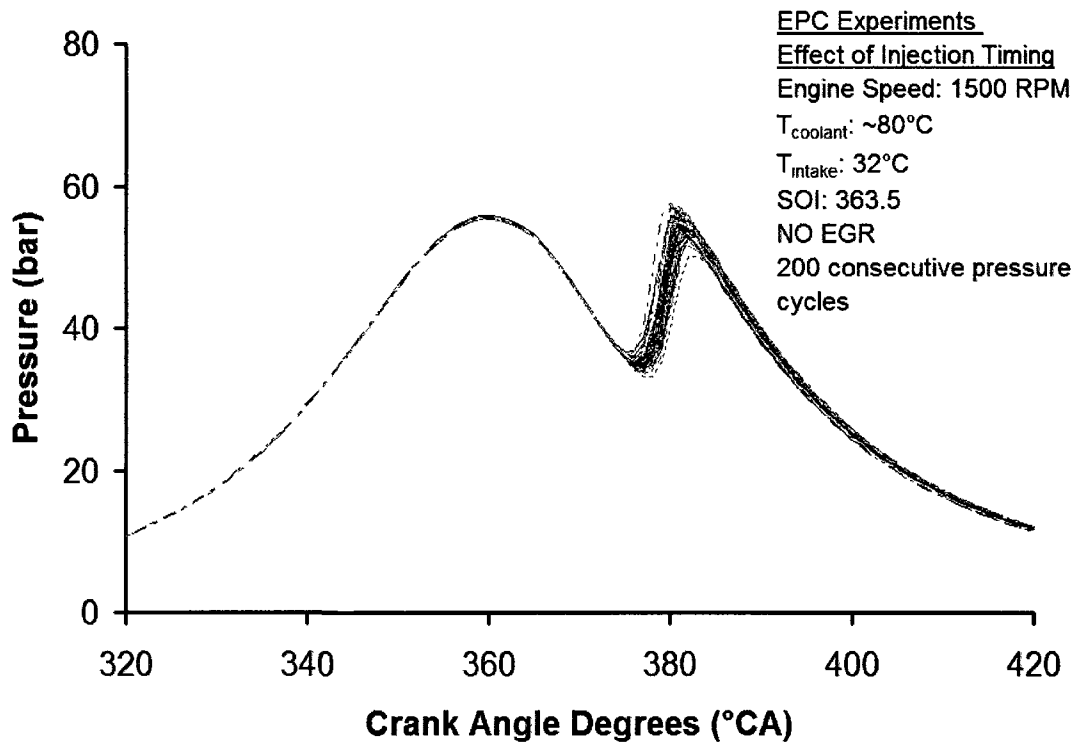
Figure 6-46: 200 consecutive pressure cycles showing the effect of SOI during EPC.

The second limitation of single-shot EPC was that, it could be applied only at low to mid load conditions. A typical commanded injection signal and the actual rate-of-injection for a similar solenoid based common-rail injector that has been provided by a powertrain research company are shown in Figure 6-47. It can be seen that the actual injection duration was longer than the commanded injection duration. This reduces the effective mixing duration which was available for the mixture preparation. At higher loads the ignition delay was typically shortened by the higher temperature of the EGR gas and while the injection duration was prolonged by the greater quantity of fuel injected. The net result was that, it was difficult to complete the injection of the entire fuel prior to the start of combustion, which is one of the necessary conditions for accomplishing premixed combustion. Therefore, for the EGR enabled EPC combustion at higher loads, the fuel delivery strategy needs to be modified by either using a high flow-rate injector or by using multiple injections.
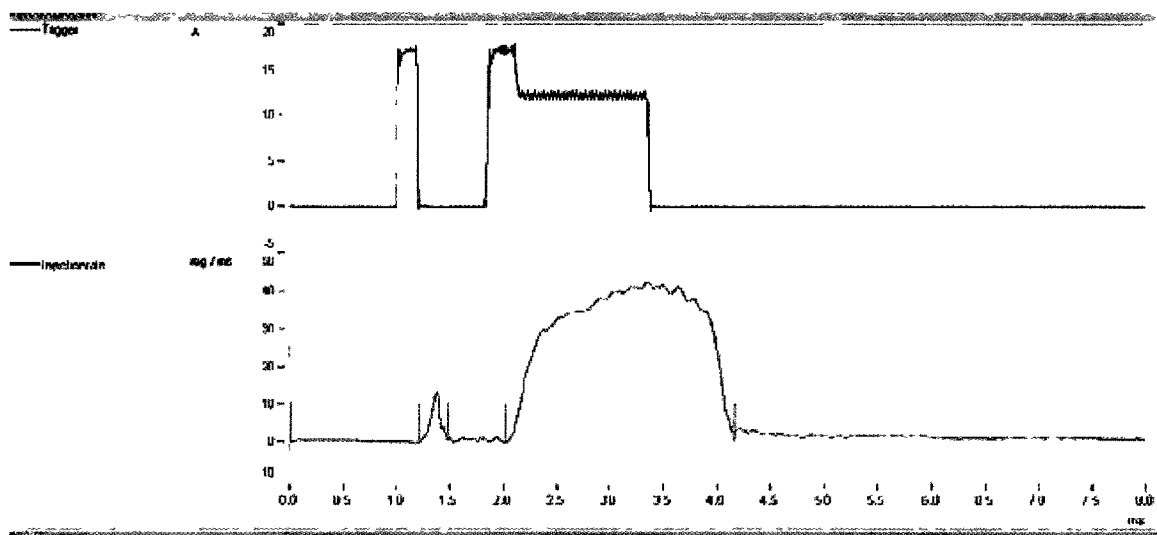
Figure 6-47: Comparison of commanded injection signal and actual injection rate © IAV GmbH [62].

6.2 Adaptive Fuel Injection Control

As shown before, very high amounts of EGR was required to implement EPC combustion, and at these high EGR values very high cycle-to-cycle variation was observed. In the limiting case, the combustion flame nearly got extinguished at very high levels of EGR. Therefore, adaptive fuel-injection techniques were used to anchor the cylinder pressure

82

characteristics in the desired crank angle window and thereby stabilize the engine operation. A cylinder pressure based control algorithm was developed and implemented in these investigations. To facilitate the control, the shape of the heat-release curve was termed as simplex combustion, compounded double hump or complex combustion. The simplex heat-release rate was typically observed when either the injection pressure was high or the fuel preparation was highly premixed. The compounded double hump combustion was commonly observed with split injection, while the complex combustion heat-release rate shape was observed at low-load, with late combustion phasing (Figure 6-48). The crank angle for 50% heat-release, (CA-50%) of a simplex heat-release curve had shown close correlation with the cylinder pressure characteristics, crank angle for maximum rate of increase of pressure, $(\theta_{(dP/d\theta)max})$ (Figure 6-49). It was therefore considered sufficient to approximate the heat-release characteristics with the cylinder pressure characteristics therein. However, the tests also showed that an excessive postponing of the combustion phasing could convert the fast simplex combustion to slower combustion with a wide heat-release shape where the cylinder pressure lost the identifiable features of heat-release. Notwithstanding, for the present experiments the heat-release rate was approximated as the fast-simplex and the implementation of adaptive combustion control was able to largely retain the phasing of combustion and maintain the correlation features between heat-release and cylinder pressure characteristics. Beyond a simplex heat-release shape, the identification of the timing and shape of heat-release and the quality of combustion needs more sophisticated analyses and is being pursued as a new project of study in the lab.
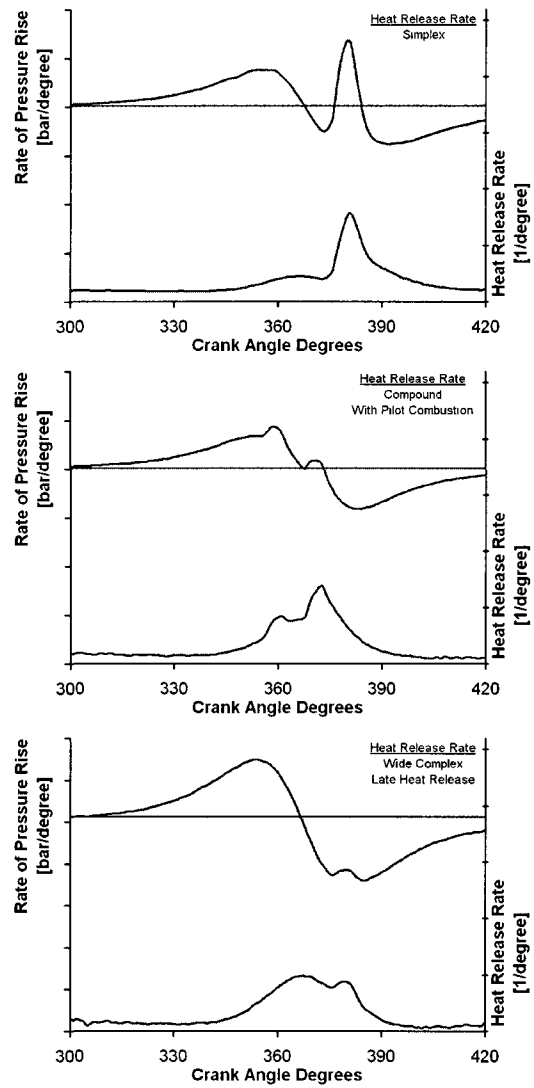
Figure 6-48: Sample heat-release rate characterization based on Ford diesel engine test.
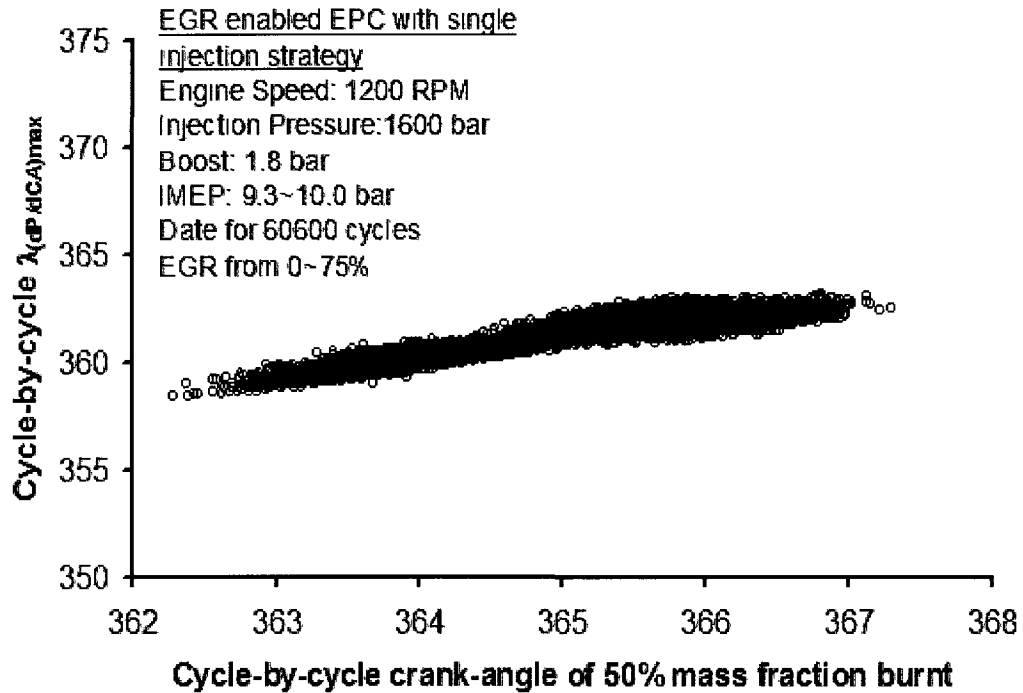
Figure 6-49: Relationship between CA-50% and $\theta_{(dP/d\theta)max}$

The flow chart for the control algorithm is shown in Figure 6-50. In the current control strategy, the actual $(\theta_{(dP/d\theta)max})$ was compared with the set-point value of the $(\theta_{(dP/d\theta)max})$ and if any error was observed, it was corrected by the change in the fuel-injection timing. The injection timing correction can then be implemented in either a fixed compensation or a dynamic compensation mode. In the fixed compensation mode the injection timing correction done in each cycle was constant, however in the dynamic compensation mode the injection timing correction done for each cycle was proportional to the difference between the actual and the commanded $(\theta_{(dP/d\theta)max})$. For the tests described in the thesis, only the dynamic compensation mode was used. Furthermore, two methods of compensation, the fast method and the slow method, were compared were used for the test conditions. The fast and the slow-method refer to the amount of combustion phasing correction done every cycle. In the slow-method a combustion phasing correction of $0.1°CA$ was implemented every cycle while, for the case fast-method, half of the total combustion phasing error was corrected every cycle.
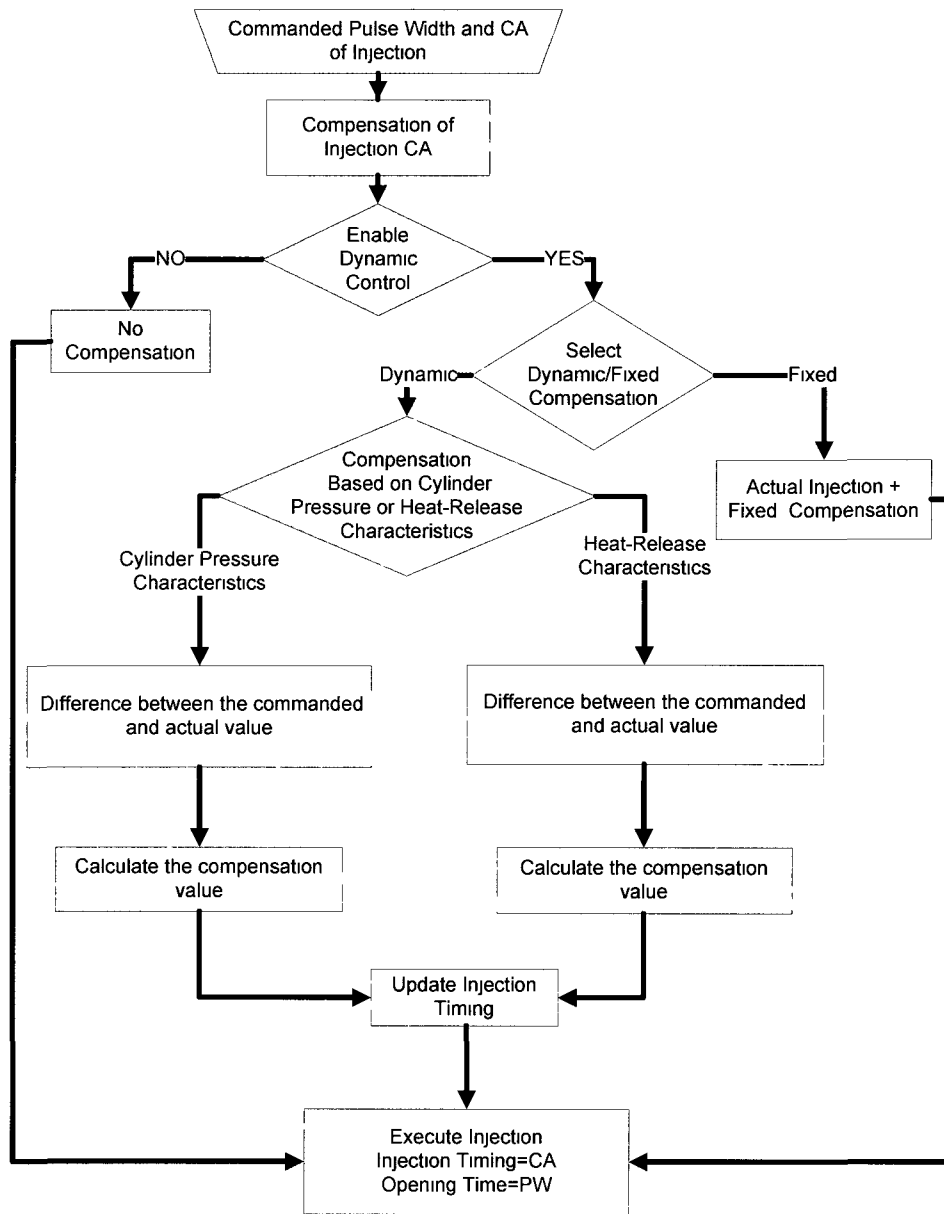
Figure 6-50: The decision-making flowchart for the adaptive control strategies implemented in the tests.

The adaptive fuel injection control tests were categorized into:

- Validation of the adaptive control algorithm

- Step change in EGR at constant boost

- Continuously increasing boost at constant EGR valve position

- Very high EGR condition

- Enhanced premixed combustion with adaptive control

- Transients in enhanced premixed combustion region

6.2.1 Validation of adaptive control algorithm

The first set of tests was performed at a fixed EGR and a fixed boost value and a load of 7.8bar. At this condition, the closed-loop control was turned-on and the combustion synchronization process was compared for both the fast method and the slow method. The results of the slow method and the resulting combustion synchronization with the adaptive control are shown in Figure 6-51 and Figure 6-52. The adaptive fuel injection was turned-on at cycle 0 and the cylinder-pressure based control program was able to synchronize the combustion process so that the crank-angle position of the maximum rate of cylinder pressure increase, represented CA for $(dP/dCA)_{max}$ or $\theta_{(dp/d\theta)max}$, converged to the desired value of 362°CA. A crank-angle resolution of 0.1°CA was used for the decision making part in the FPGA. The similar combustion synchronization with the fast method is shown in Figure 6-53 and Figure 6-54. As the name suggests the fast method was quicker to reach the commanded value of $\theta_{(dp/d\theta)max}$, but it was observed in the later part of the tests that it also resulted in over compensation. For the fast method the adaptive control was engaged only around the 100 cycle mark. A distinct step change can be seen in Figure 6-54 on the y-axis values at around the 100 cycle mark, where the adaptive control was engaged.
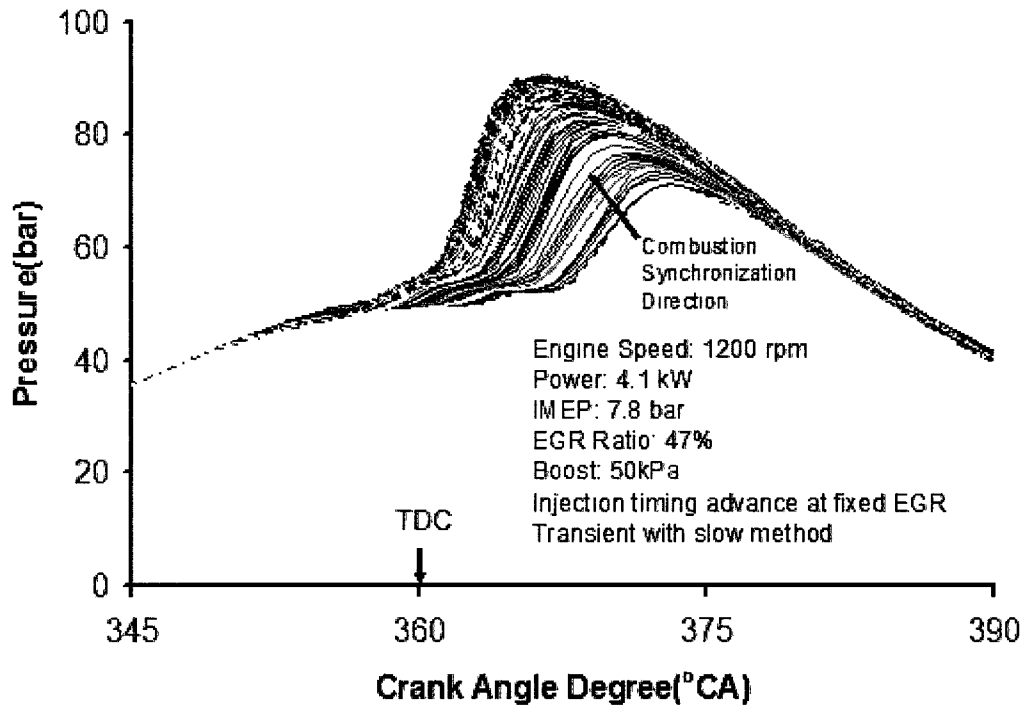
Figure 6-51: The cylinder pressure traces with the adaptive fuel injection control at fixed EGR (slow method).
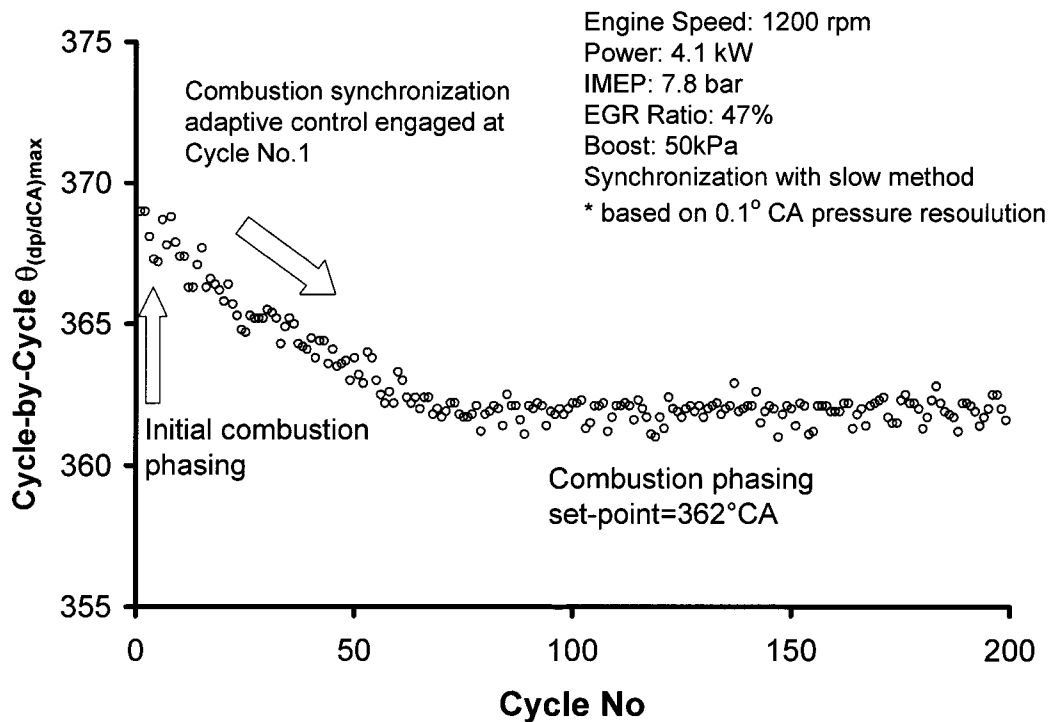
Figure 6-52: The effect of adaptive fuel injection control on transient $\theta_{(dp/d\theta)max}$ synchronization (slow method).
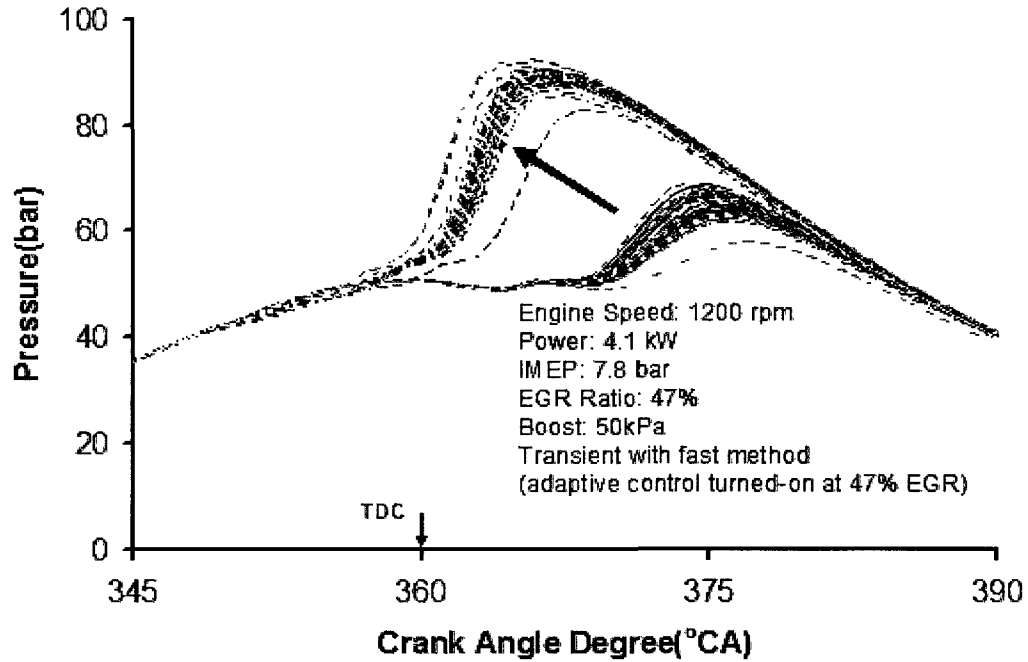
Figure 6-53: The cylinder pressure traces with the adaptive fuel injection control at fixed EGR (fast method).
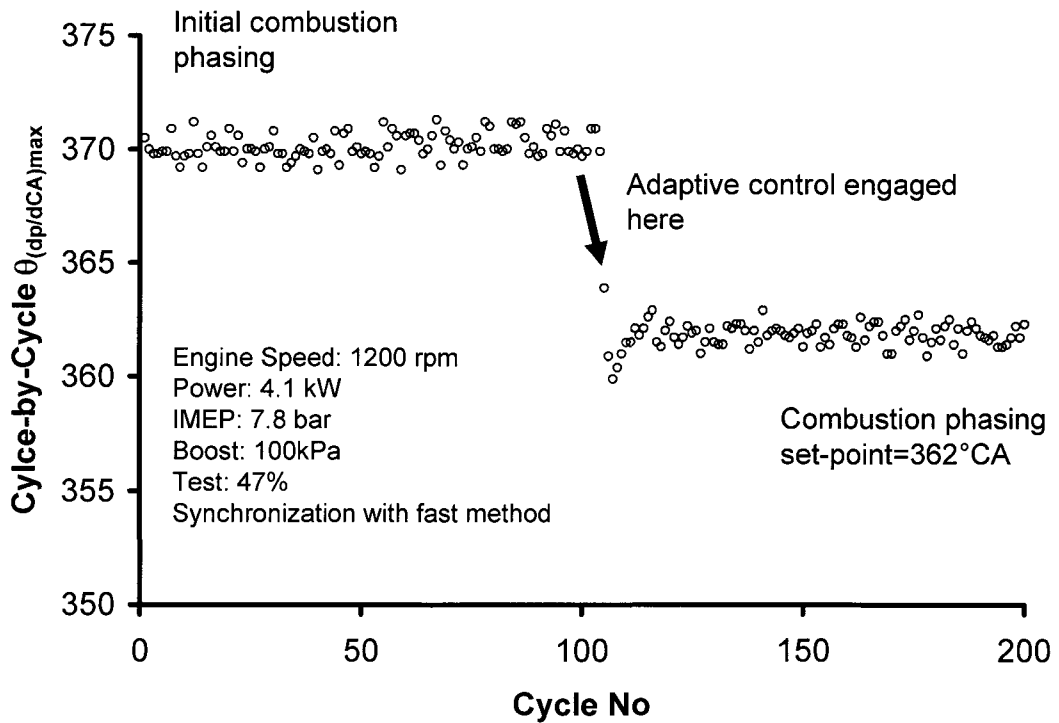
Figure 6-54: The effect of adaptive fuel injection control on transient $\theta_{(dp/d\theta)max}$ synchronization (fast method).

6.2.2 Continuous change in EGR at constant boost

The previous set of experiments showed that the cylinder-pressure based control program could transition the combustion phasing to the desired value at steady-state. The next step was to test the controls program for changes in EGR and boost that may be applied during the EPC experiments. The experiments were performed at a fixed engine speed, with a fixed boost and a load of 7.8bar IMEP. A step in EGR was implemented from 35 to 61% and the response of both the slow and fast adaptive control was documented. The results for the slow method are shown from Figure 6-55 to Figure 6-57. It can be seen that the increasing EGR initially resulted in an increased ignition delay and a retardation of $\theta_{(dp/d\theta)max}$ value. However, the control algorithm was able to advance the start of injection so that the $\theta_{(dp/d\theta)max}$ could be maintained at the desired location. In Figure 6-56 every 5th cycle is plotted instead of all the 200 cycles to show the shifting in the start of injection clearly. The same test was repeated without any adaptive control. The slow adaption method has also been compared to the case of no adaptive control (Figure 6-57). It can be seen that for the case of adaptive control the cycle-to-cycle variation was significantly lower for both $\theta_{(dp/d\theta)max}$ and P_{max}, θ_{Pmax}.
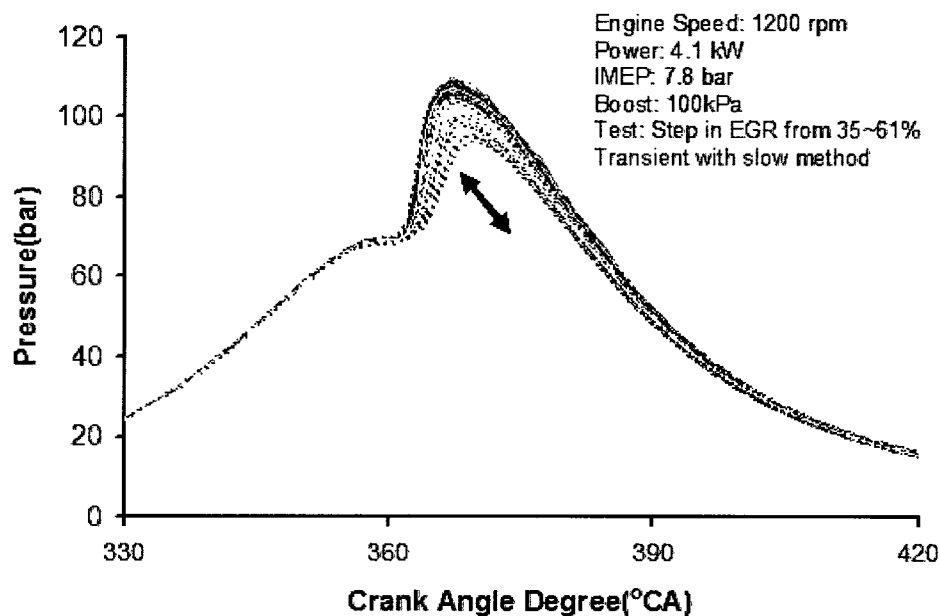
Figure 6-55: Adaptive fuel injection control with continuous change in EGR (slow method).
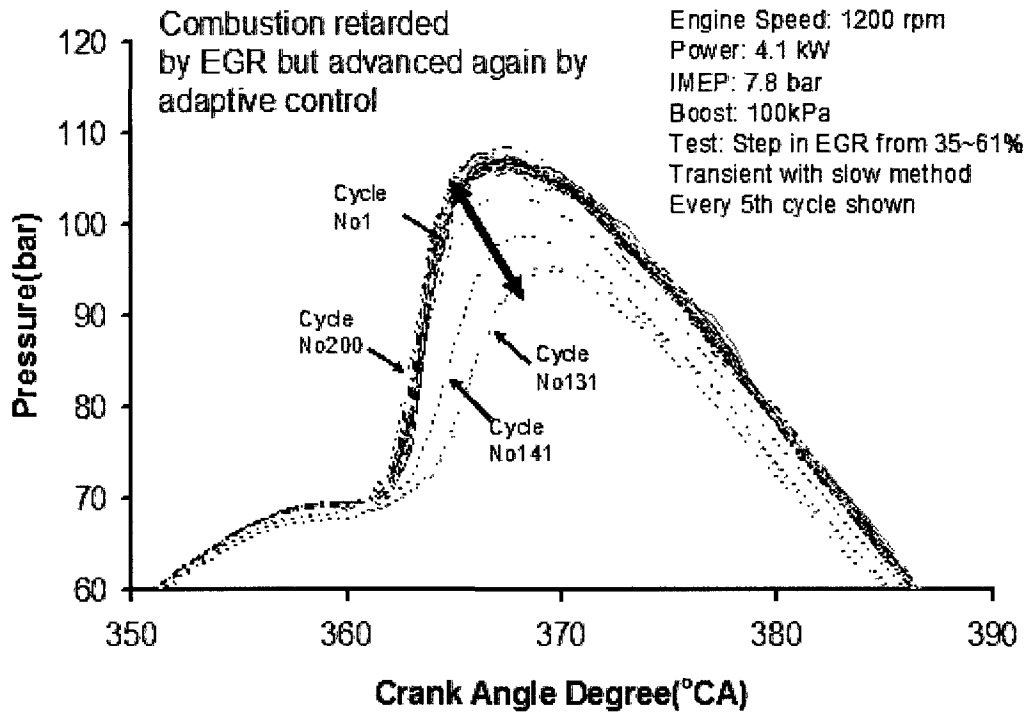
Figure 6-56: Adaptive fuel injection control with continuous change in EGR, every 5th cycle shown (slow method).
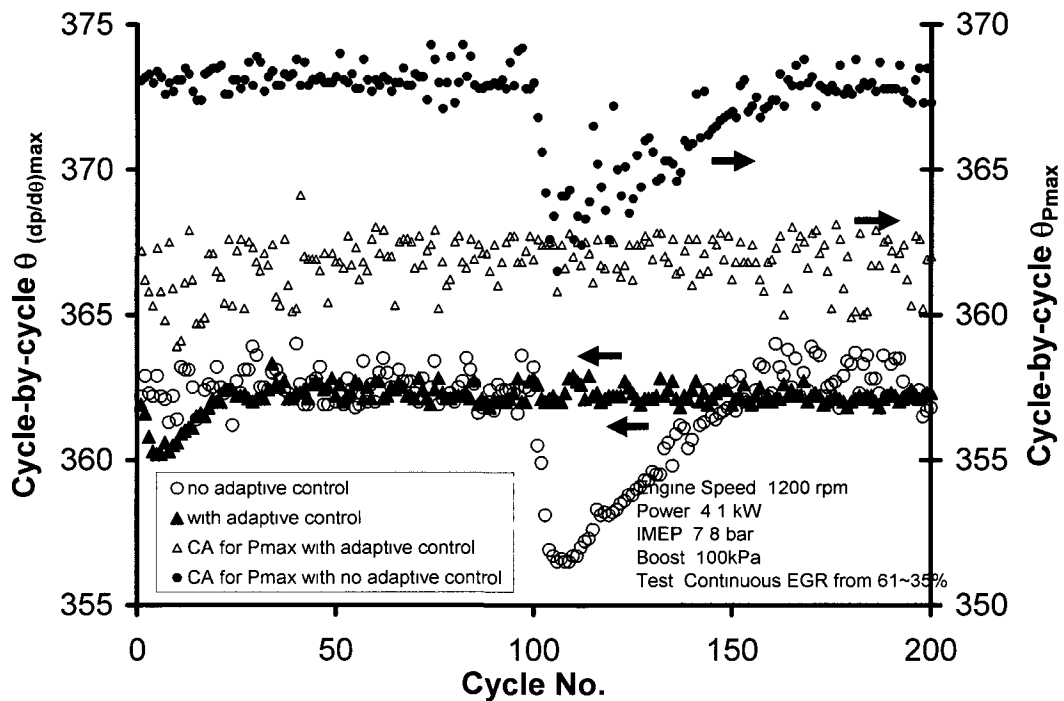
Figure 6-57: The effect of adaptive injection on the transient $\theta_{(dP/d\theta)max}$ with step change in EGR slow method.

6.2.3 Continuous increase in boost at the same EGR valve setting

The experiments were performed at a fixed engine speed, a fixed EGR valve setting, and a single injection of fixed quantity while the boost level was changed from 50 to 100 kPa. Similar tests were also performed where the boost was continuously decreased from 100 to 50kPa. The boost changes were performed with the fast method, the slow method and without any adaptive control (Figure 6-58 to Figure 6-60). The increase in boost, led to a reduction in the ignition delay. This resulted in the advance of the start of combustion without any adaptive fuel injection control. However, in the presence of adaptive control the combustion phasing was kept at the desired value.
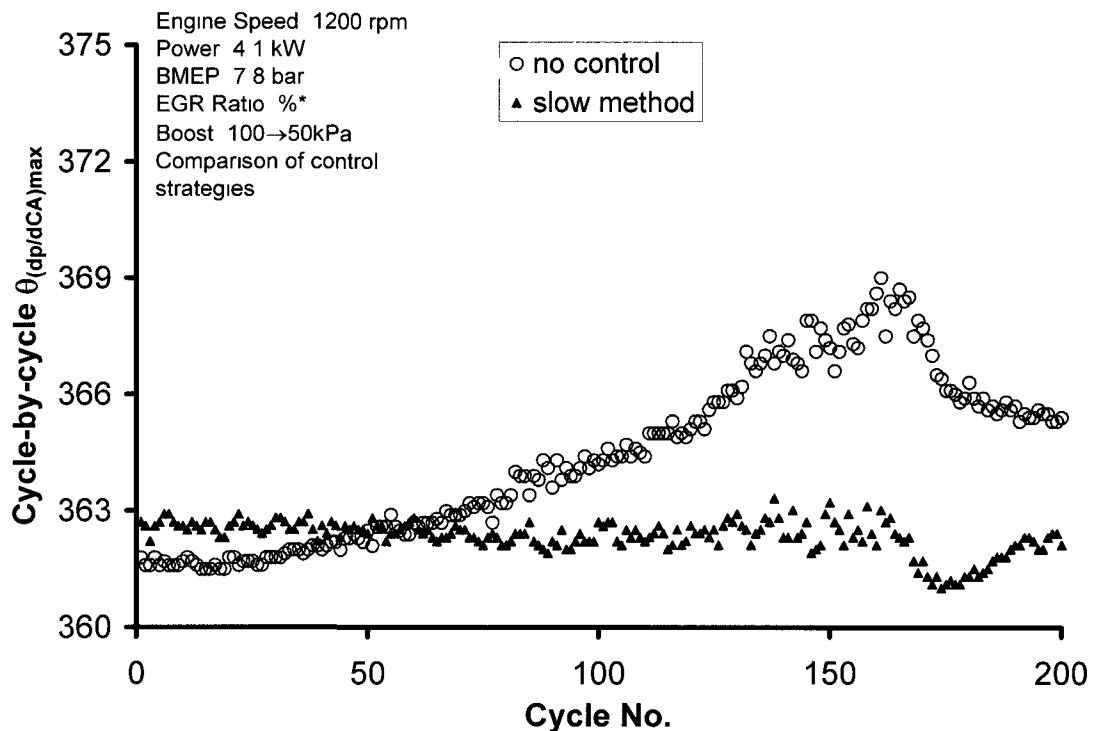
Figure 6-58: The effect of adaptive fuel injection control on the transient $\theta_{(dP/d\theta)max}$ with boost level variations.
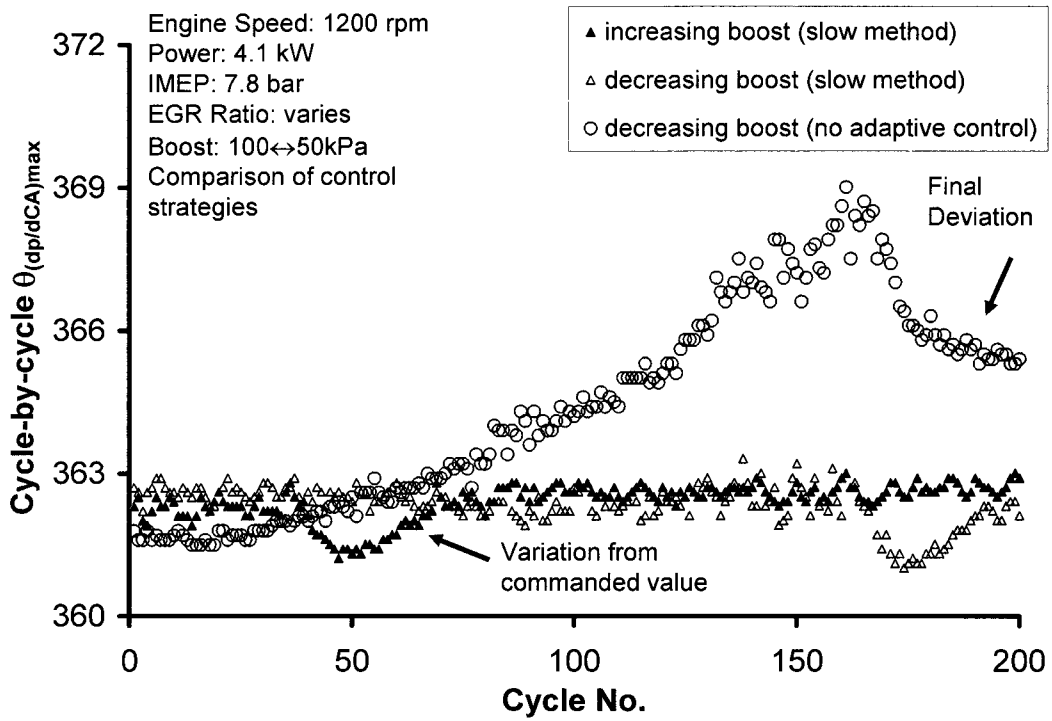
Figure 6-59: The effect of adaptive fuel injection control on the transient $\theta_{(dP/d\theta)max}$ with boost level variations.
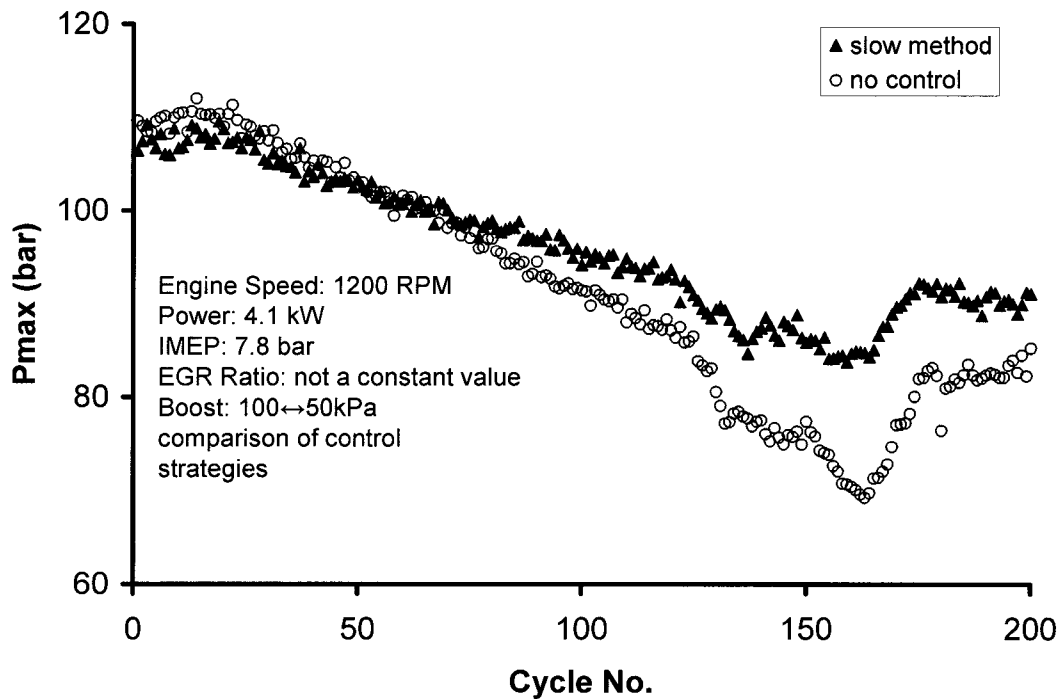
Figure 6-60: The transient Pmax during continuous increase in boost levels.

6.2.4   Very high EGR condition

Once the cylinder-pressure based control algorithm was validated for steady state, EGR and boost change experiments it was decided to implement the cylinder-pressure based control for the EGR enabled EPC experiments. In the EGR enabled EPC experiments were performed with a single injection strategy and the EGR was gradually increased in small steps from 40 to 66%. The comparison of NOx versus EGR with and without adaptive fuel injection control is shown Figure 6-61. The NOx was slightly higher with adaptive control initially, because the SOI was advanced with the closed-loop on combustion phasing. Without the adaptive control, at more than 65% EGR levels, the combustion process showed high cycle-to-cycle variations (Figure 6-62 and Figure 6-63). For some conditions the combustion flame was almost lost (Figure 6-63). For both the test conditions of Figure 6-62 and Figure 6-63, the desired engine operating point was reached with the adaptive fuel injection control turned-on and after a few cycles, the adaptive fuel injection control was turned-off, resulting in high cycle-to-cycle variation. The soot measurements for the tests are also shown in Figure 6-64. The results suggest that the use of adaptive control had no significant influence on the soot for the tests at low-loads.

Speed: 1200RPM
Single Injection: at 353 CA
IMEP: 3.0~3.3 bar (low-load)

□ without adaptive control(low-load)
■ with adaptive control(low-load)

Combustion
unstable at this point without
adaptive control
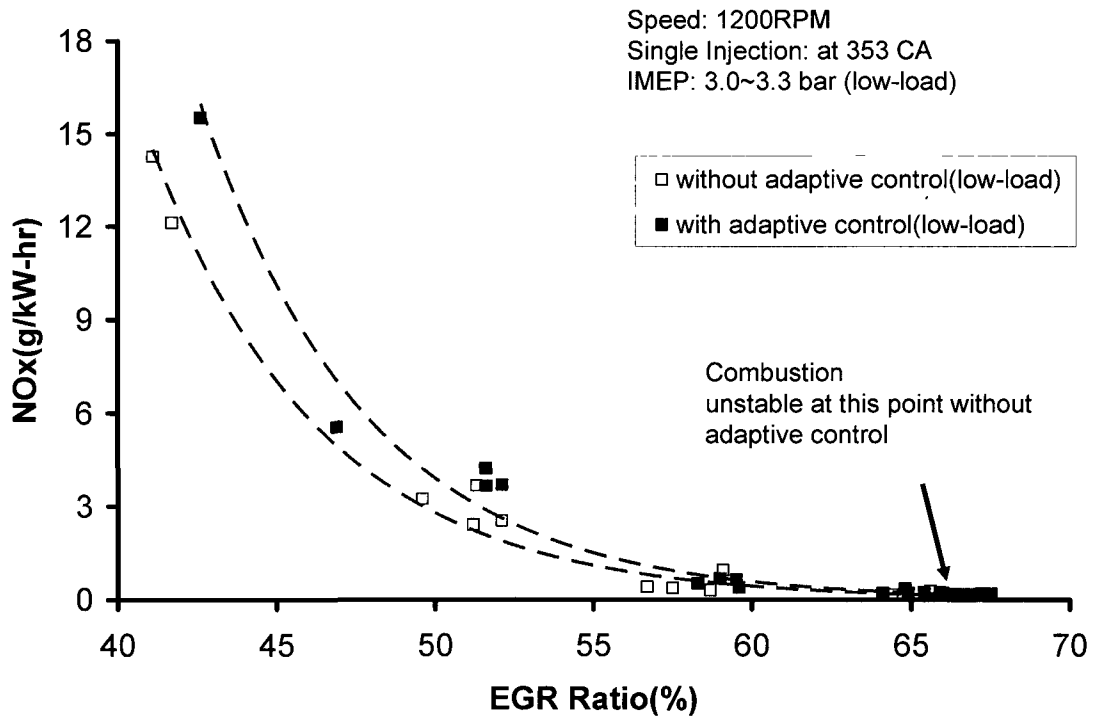
Figure 6-61: NOx reduction by extending EGR limit with the adaptive fuel injection control.

adaptive control being turned-off at high EGR point (Case-1)

< Pmax, with adaptive control

< Pmax, without adaptive control
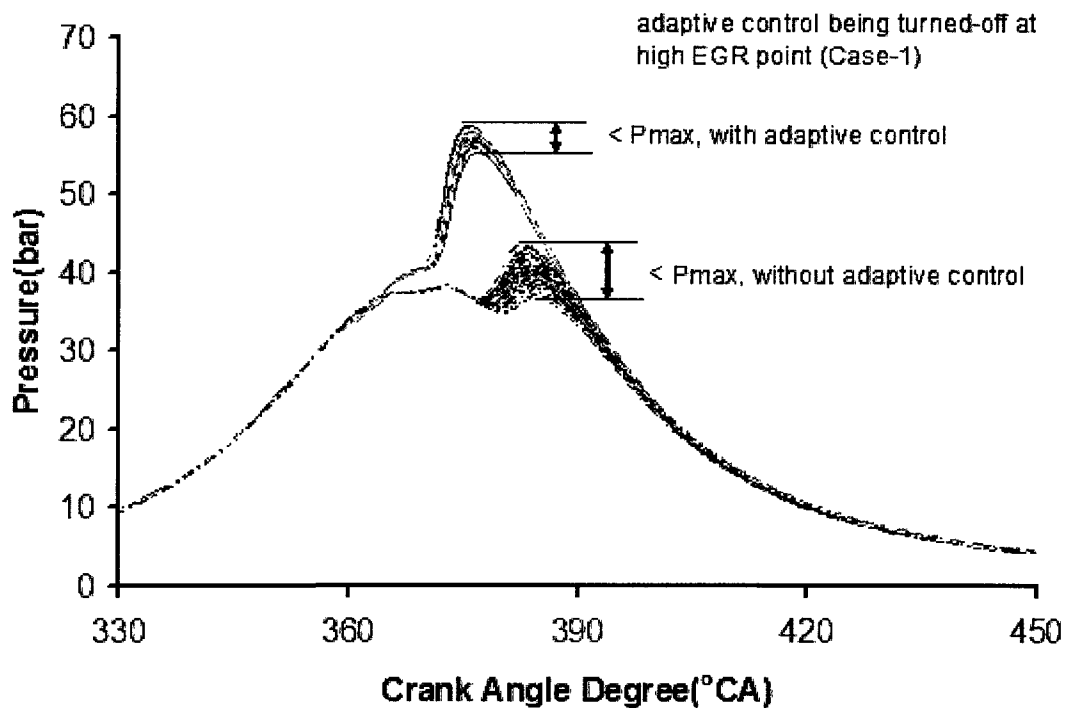
Figure 6-62: The cylinder pressure traces for 200 consecutive cycles with and without adaptive fuel injection control at a heavy EGR ratio.
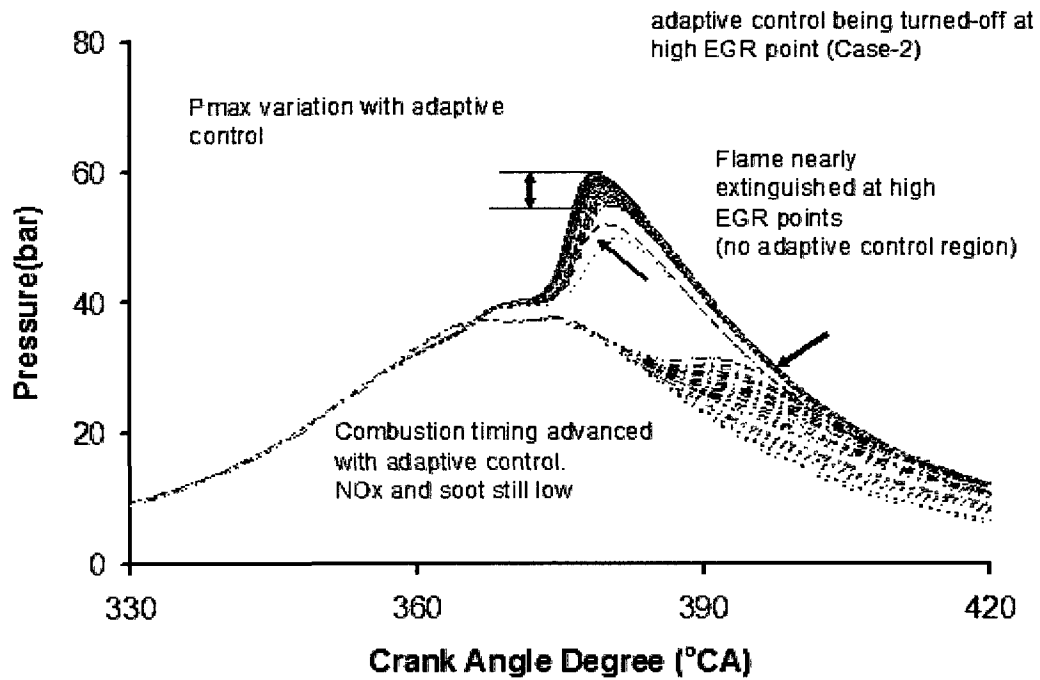
Figure 6-63: The cylinder pressure traces for 200 consecutive cycles with and without adaptive fuel injection control at a heavy EGR ratio.
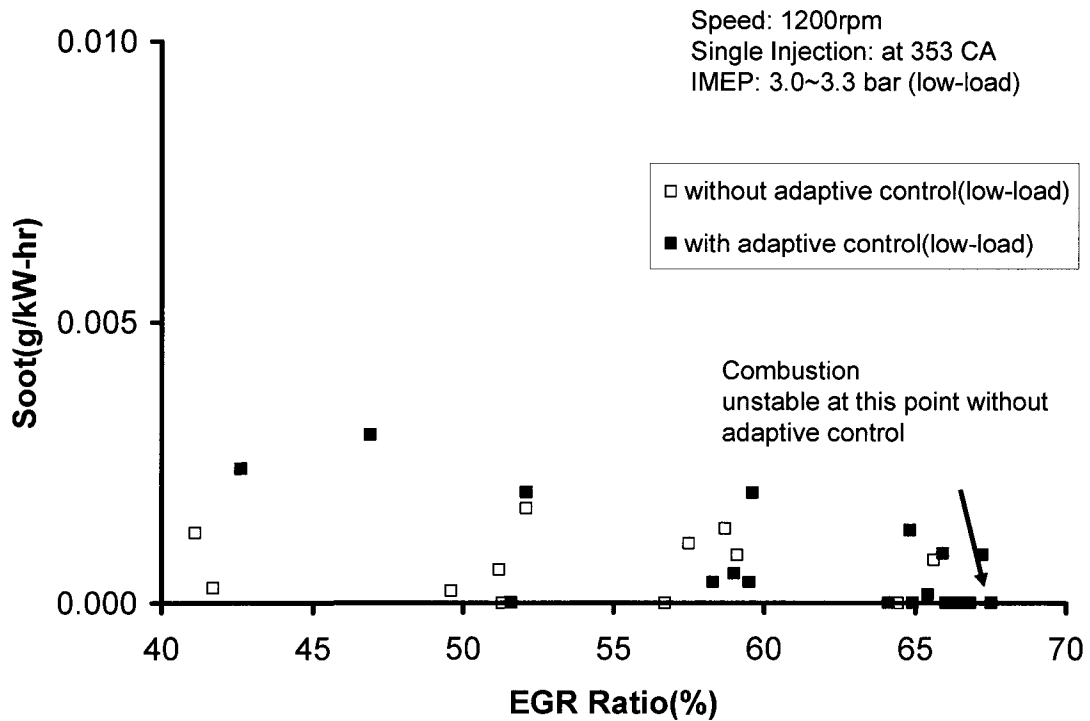
Figure 6-64: The soot comparison for tests with and without adaptive control.

6.2.5 EPC with adaptive control

The EGR enabled EPC was implemented at a high load of 9.0bar IMEP with a boost pressure of 1.8bar (gage) and a single injection at 7°CA BTDC. Note, the SOI of 7°CA BTDC was the initial SOI which was subsequently corrected by the adaptive fuel-injection control in the presence of EGR. The EGR value was again progressively increased till the combustion reached the regions of simultaneous low NOx and soot (Figure 6-65). The entire history of EGR and $\theta_{(dP/d\theta)max}$ during the transition to enhanced premixed combustion mode is shown in Figure 6-65. It can be seen that the adaptive fuel-injection control successfully anchored the combustion phasing within a narrow-band in spite of the increase in EGR-ratio from 0 to 60%. The soot measurements unlike other emission measurements were performed at discrete points and therefore, showed a step-wise pattern. The high levels of EGR was able to reduce the strength of EPC combustion as seen by the decreasing trend of $(dP/dCA)_{max}$. (Figure 6-66)
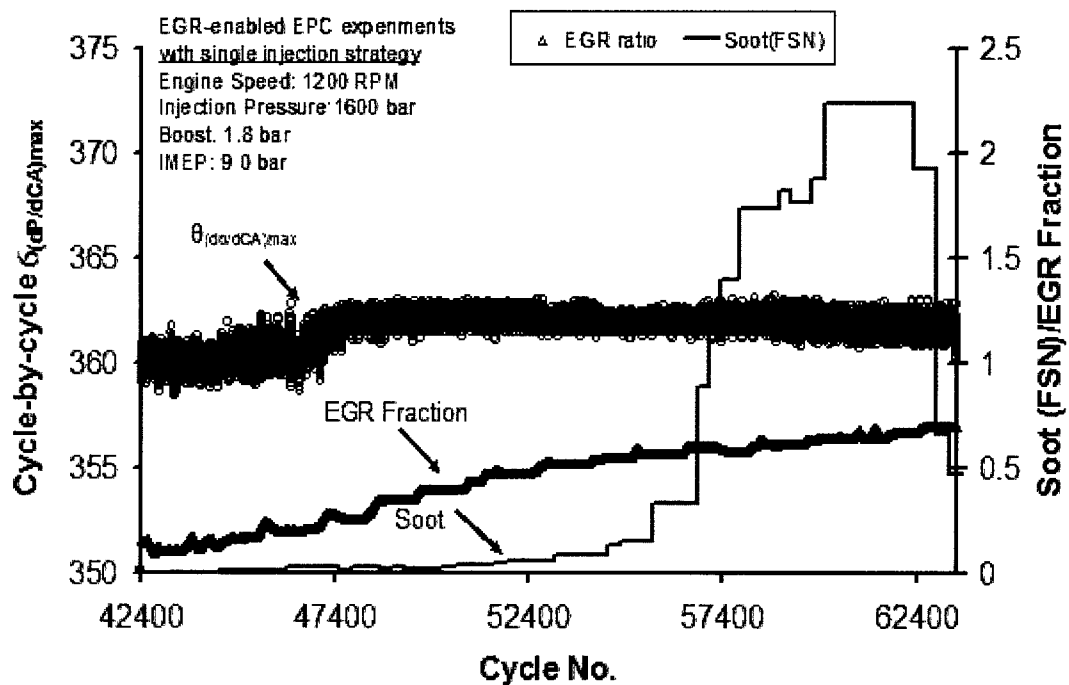
Figure 6-65: The enhanced premixed combustion cycles (NOx) enabled with adaptive control during the dynamometer tests.
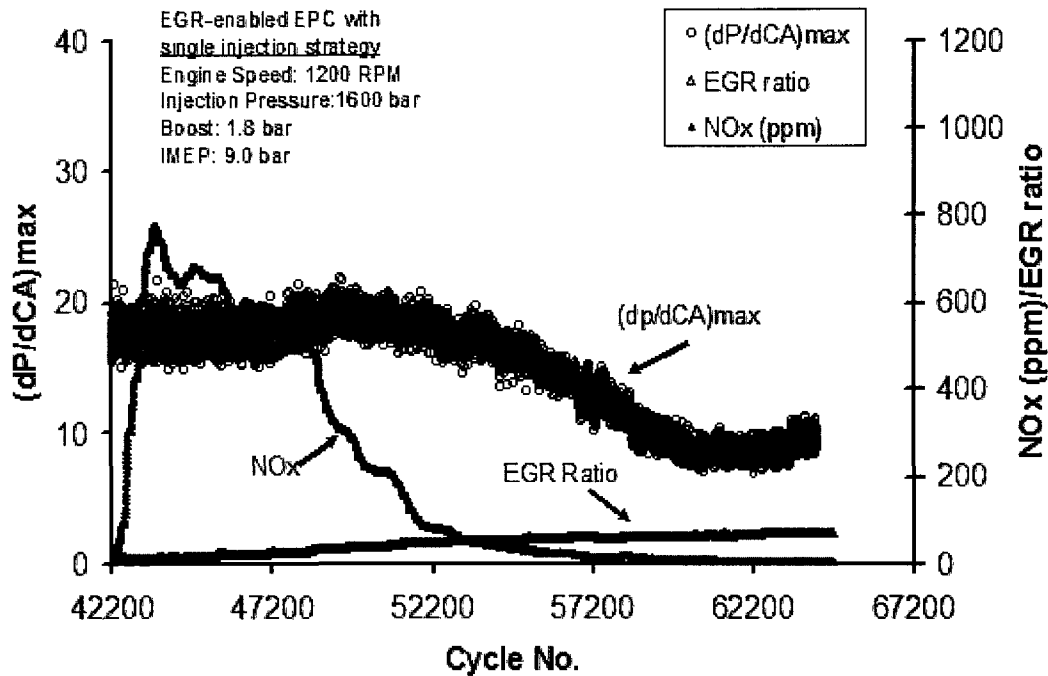
Figure 6-66: The enhanced premixed combustion cycles (soot) enabled with adaptive control during the dynamometer tests.

6.2.6 Transients in enhanced premixed combustion Region

The transient engine operation in the EPC combustion still represents a significant challenge. This is because any change in the engine operating condition has a tremendous impact on the air-fuel ratio which ultimately affects the EPC operating condition. For instance, whenever the fueling is changed in response to a change in the desired power-output, a counteraction in the temperature or local air-fuel ratio history is required to maintain the engine operation in the EPC region. Similarly, a change in the boost pressure during load change results in a change in the ignition delay which needs to be compensated to maintain the combustion within the EPC regime. The compensation to the temperature and air-fuel ratio history during the load and boost transients has been applied here by dynamically adjusting the injection timing and the results obtained during the transient experiments are shown from Figure 6-67 to Figure 6-79.
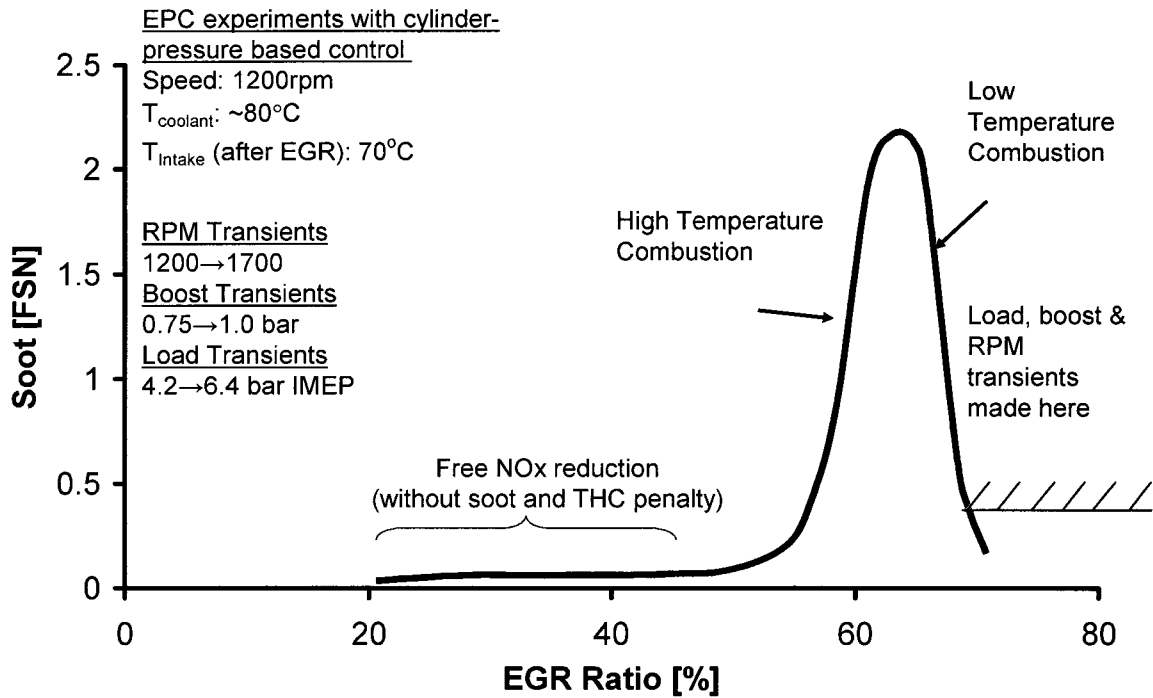
Figure 6-67: Load and boost transient test region.

Load transients (both load increase and decrease) were performed by changing the commanded fuel injection quantity during the engine operation in the enhanced premixed combustion mode (Figure 6-68 to Figure 6-70). The adaptive fuel injection control ensured that the engine combustion continued in the enhanced premixed combustion mode. The emission measurements during the transients showed also no significant increase in any of the measured parameters (Figure 6-71). As stated earlier the soot was measured only at discrete points whereas other emissions were recorded continuously.
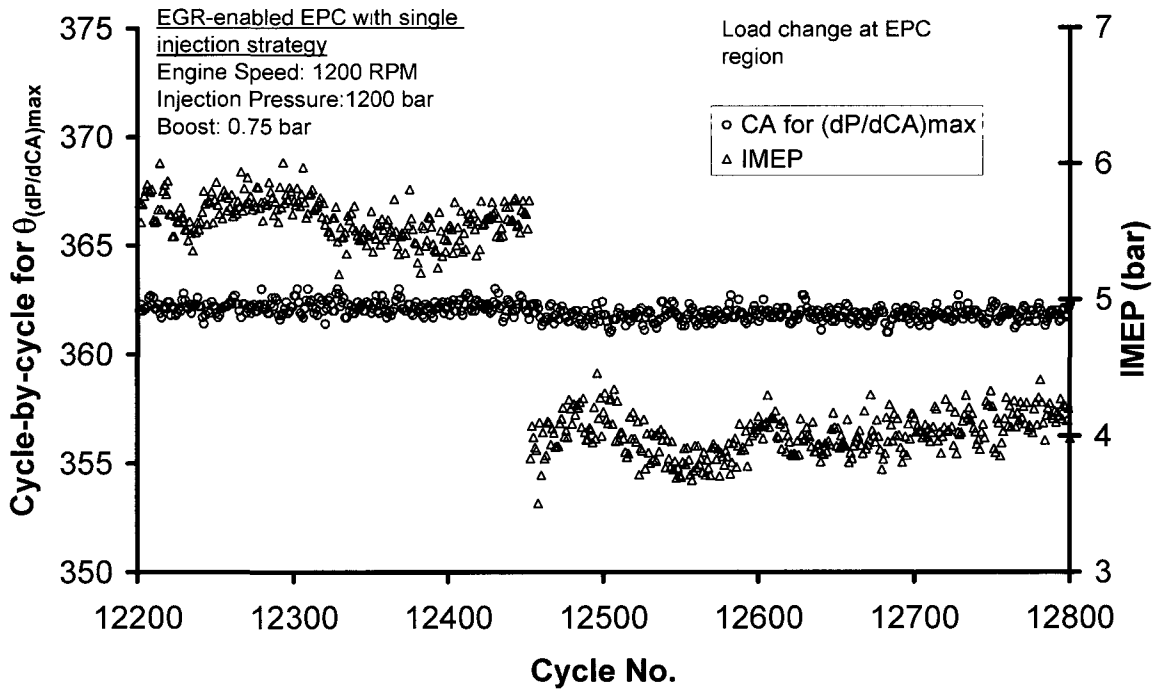
Figure 6-68: Load change in the low-temperature combustion region with adaptive fuel-injection control.
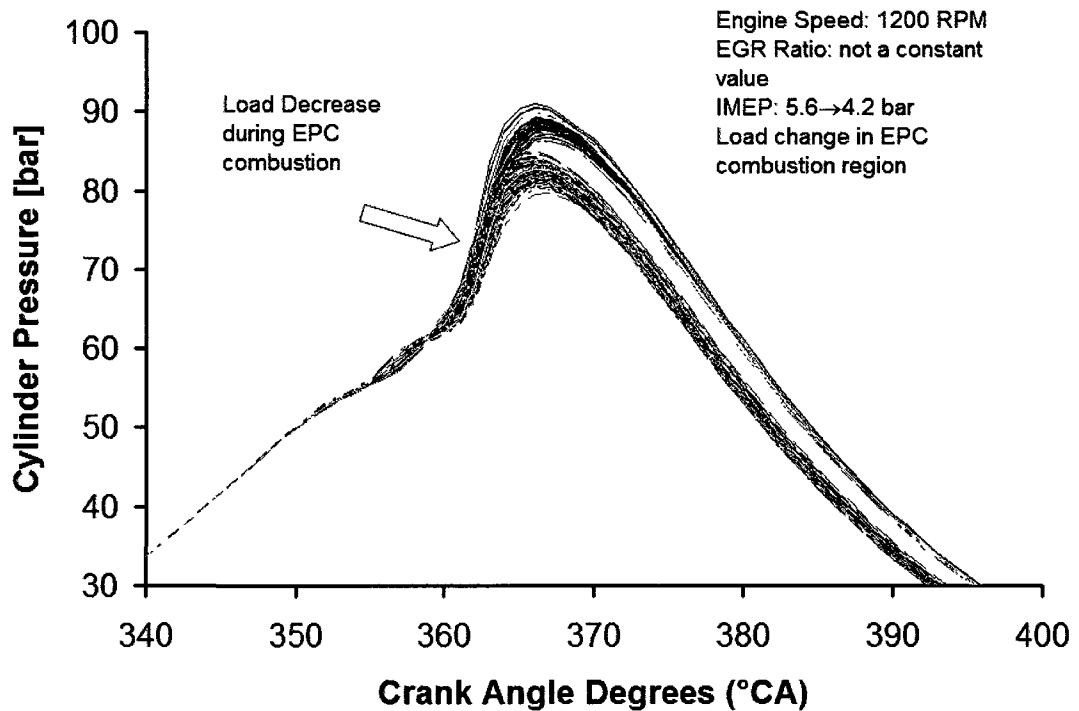
Figure 6-69: Load changes in the low-temperature combustion region with adaptive fuel-injection control.

100
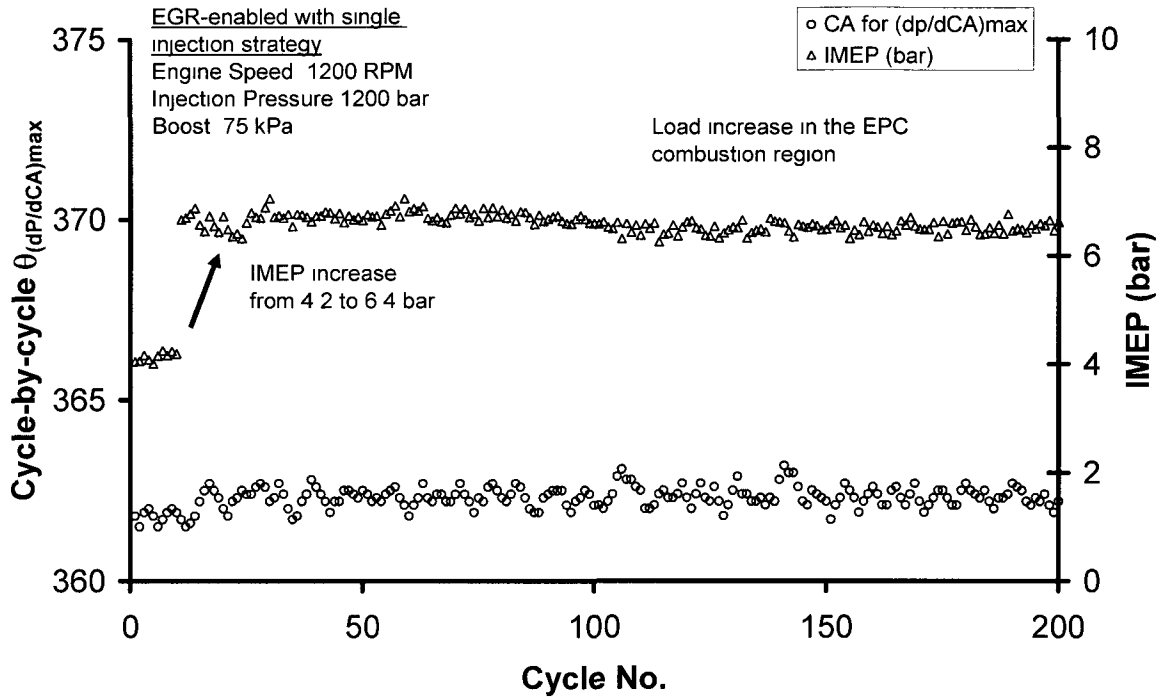
Figure 6-70: Load change in the low-temperature combustion region with adaptive fuel-injection control.
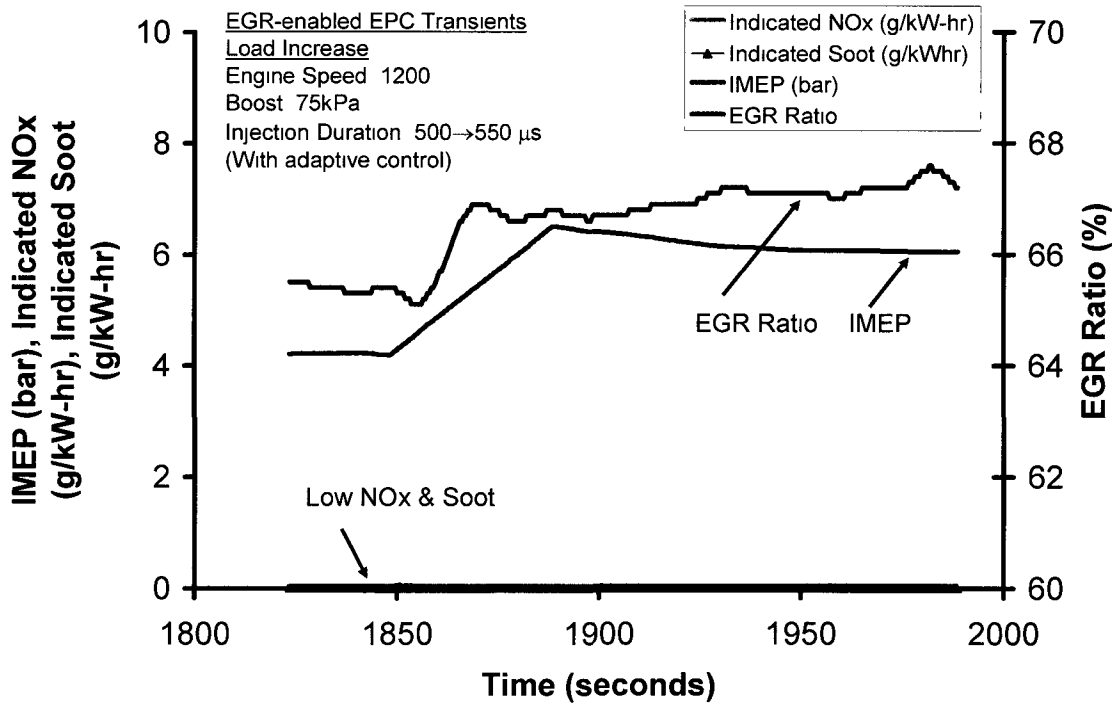
Figure 6-71: Emission measurement history during load transients with adaptive fuel-injection control.

101

Boost transients were performed in the low-temperature combustion mode with adaptive control (Figure 6-72-Figure 6-74). It was observed that during the boost transients the emissions did not increase significantly either with the adaptive control or without the adaptive control. However, the cycle-to-cycle variation was significantly higher without adaptive control (Figure 6-72).
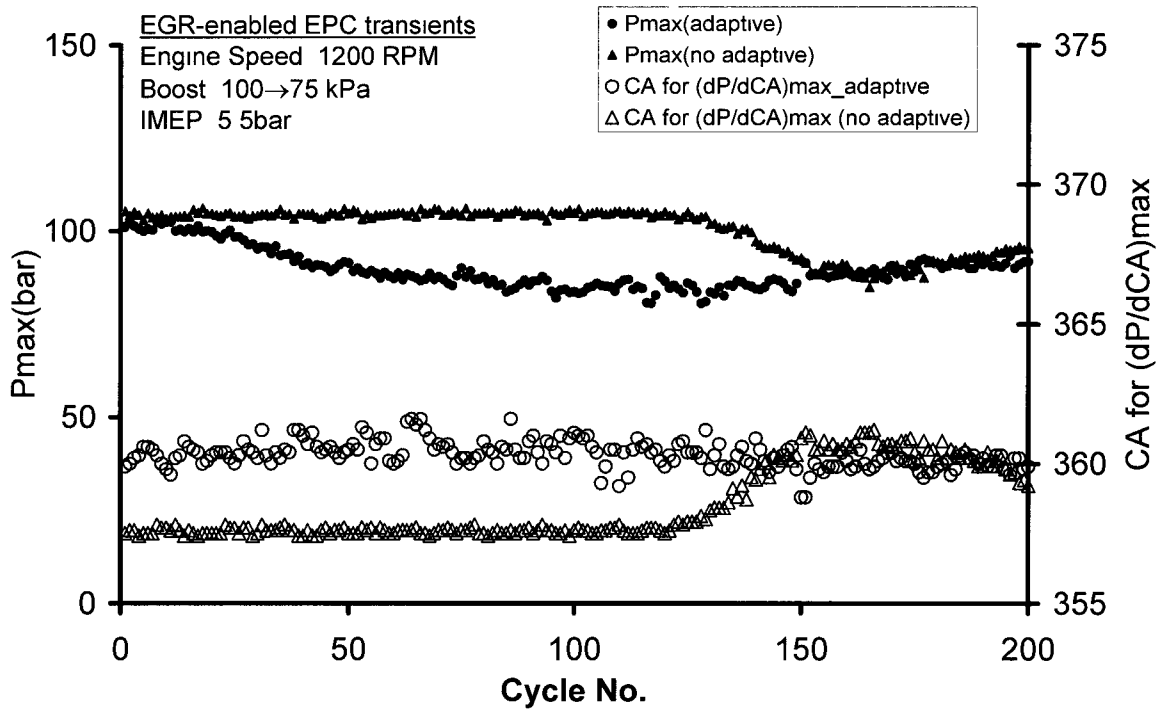
Figure 6-72: Boost transient in low-temperature combustion region with adaptive duel-injection control.
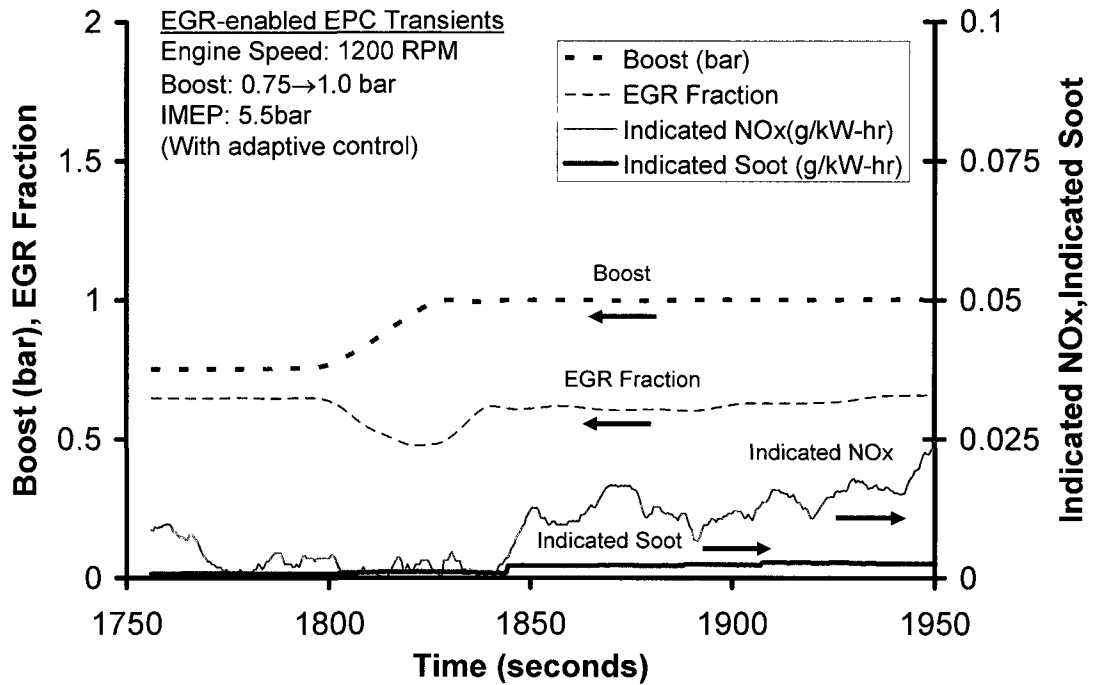
Figure 6-73: Emission transients during boost transients with adaptive fuel-injection control.
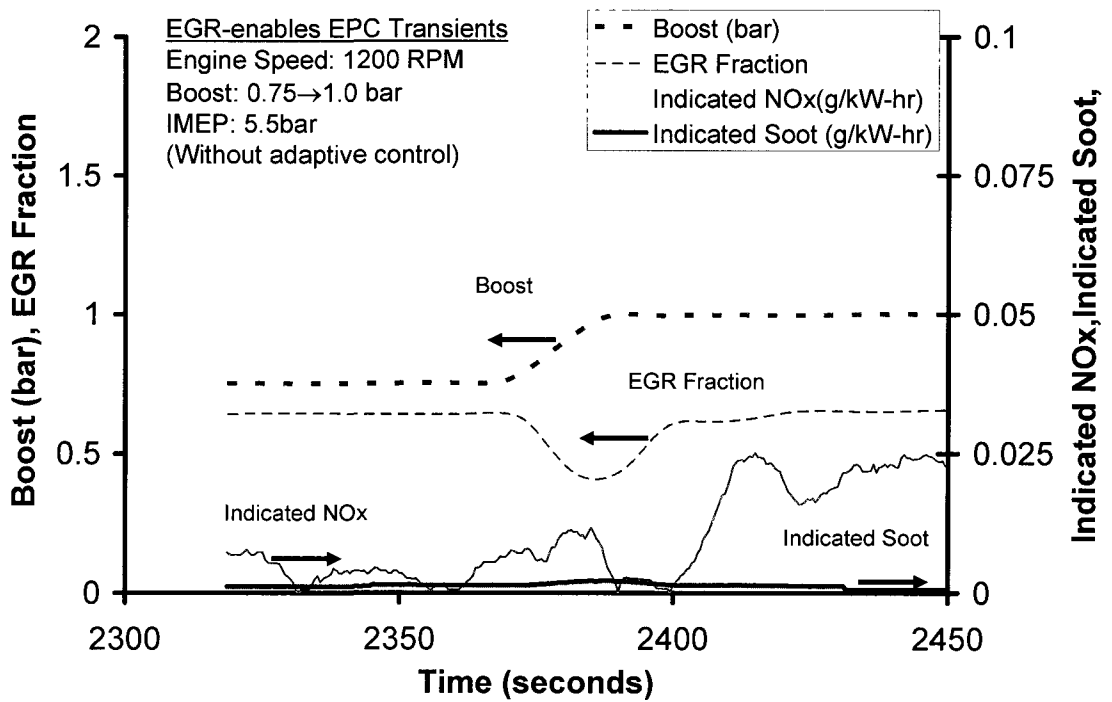
Figure 6-74: Emission response during boost transients without adaptive fuel-injection control.

103

Actual engine transients involve a simultaneous change of multiple parameters. As a representation of multi-parameter transients, tests were performed when both the RPM and the boost were simultaneously varied. The cylinder pressure trends (Figure 6-75) showed that the adaptive fuel-injection control maintained the cylinder pressure characteristics around the desired value. However, the emission trends (Figure 6-76 and Figure 6-77) showed that the NOx emissions increased significantly because of the decrease in exhaust backpressure during transients, which lowered the EGR level.

The next step therefore was to attempt to hold EGR back pressure constant during the transients. In this case the overall EGR value recovered quickly and the engine did not leave the low-temperature combustion region (Figure 6-78 and Figure 6-79). Thus a closed-loop EGR was essential to maintain the emissions in the enhanced premixed combustion mode during the combined RPM-boost transitions.
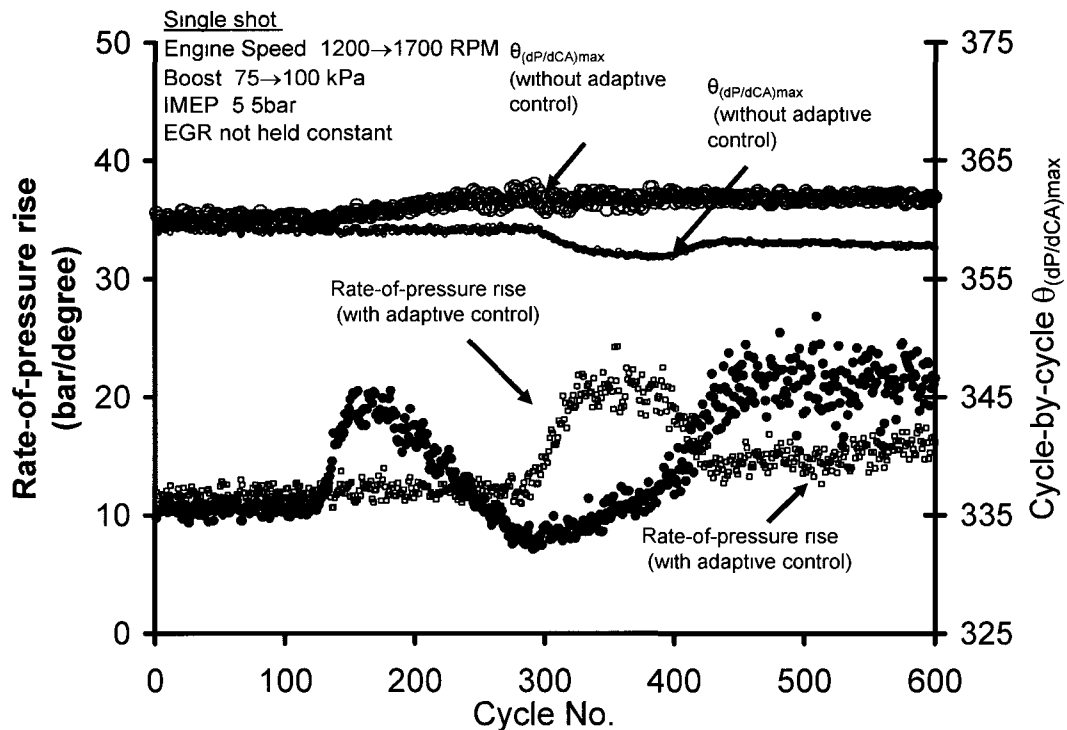
Figure 6-75: Combined effect of boost and RPM change. (EGR not held constant).
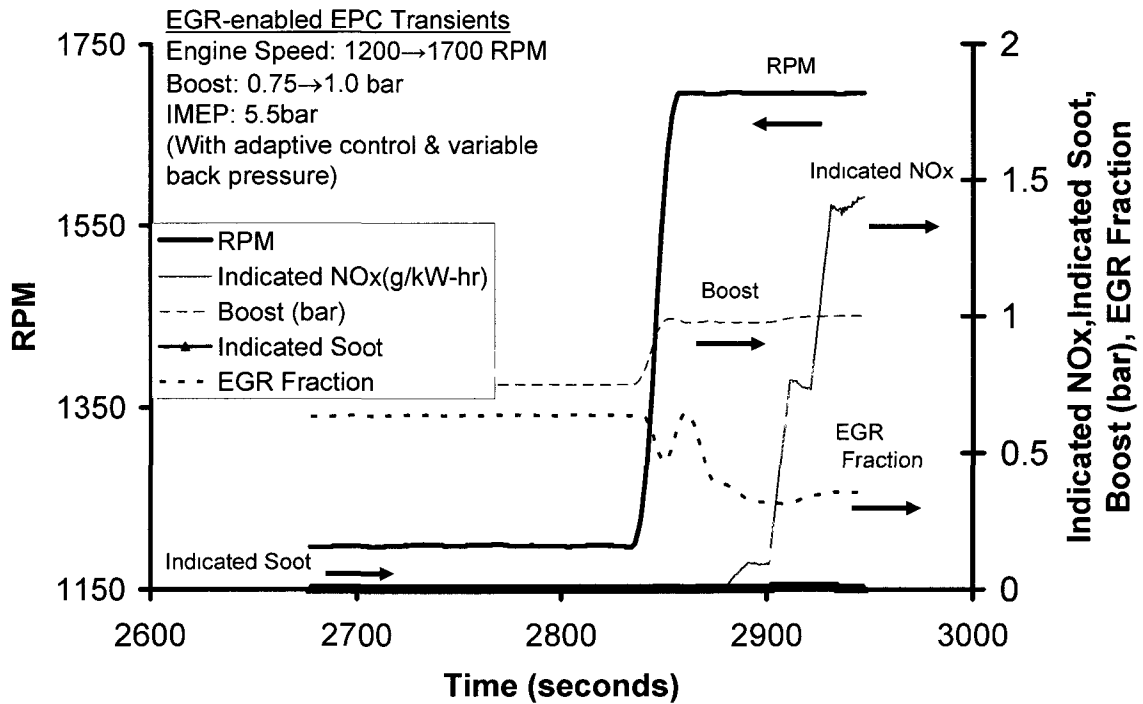
Figure 6-76: Emission response during boost and speed variations with adaptive fuel-injection control (EGR upstream pressure not constant).
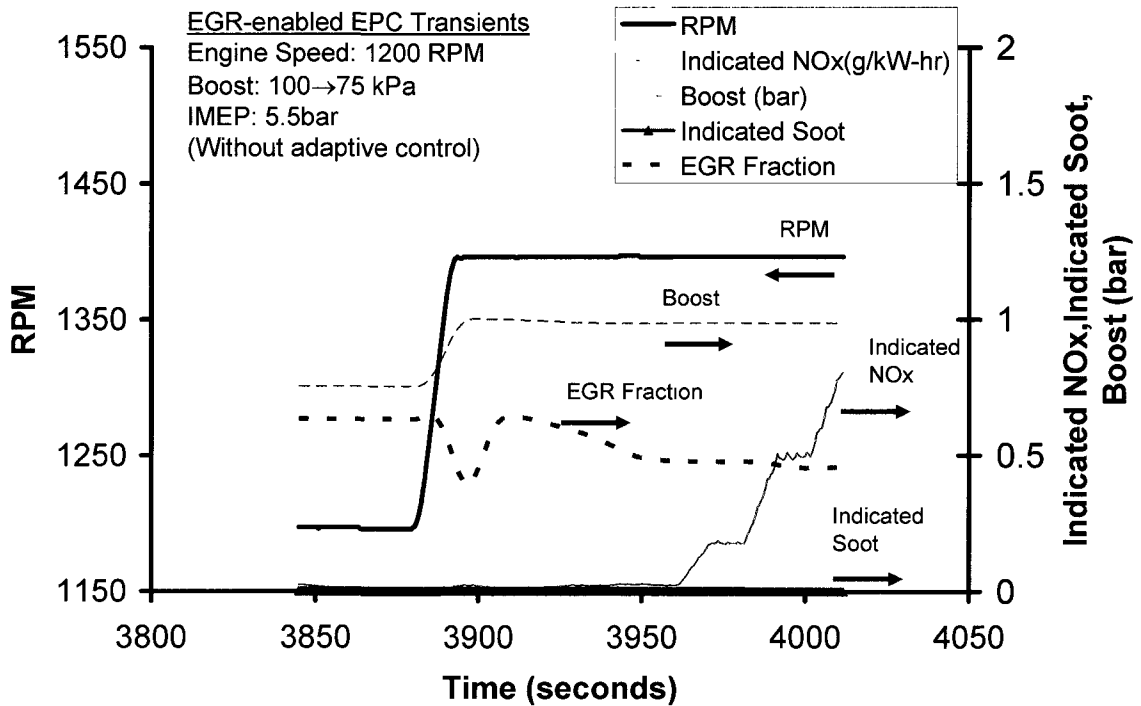
Figure 6-77: Emission response during boost and speed variations without adaptive fuel-injection control. (EGR upstream pressure not constant).

105
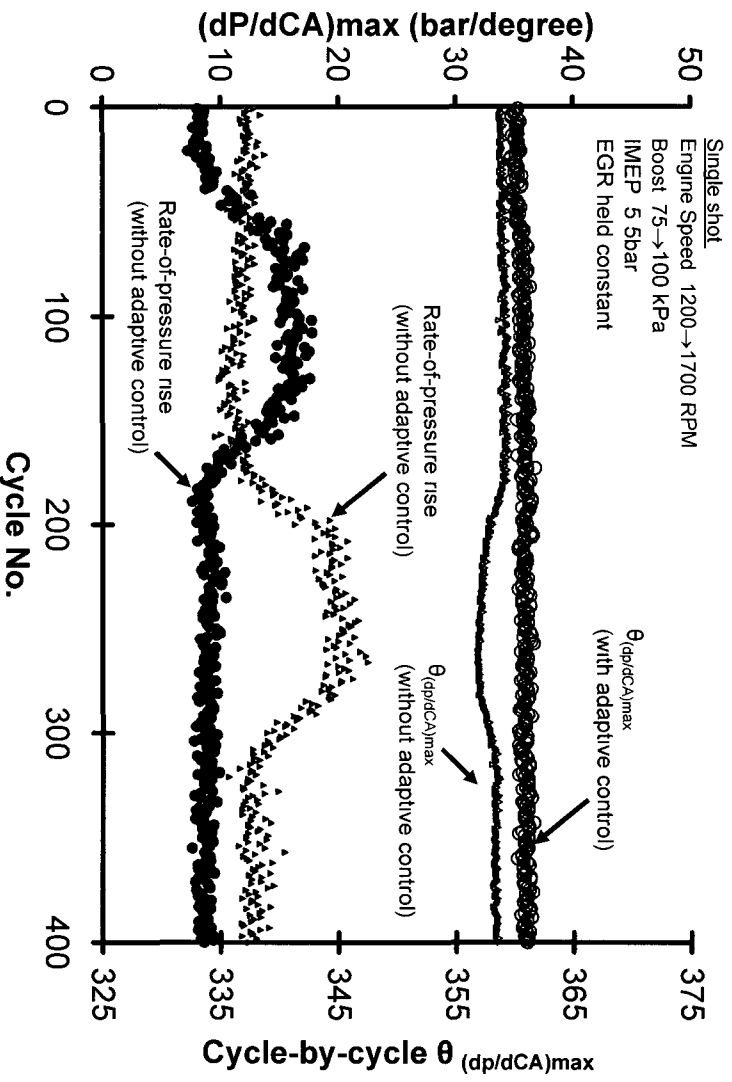
Figure 6-78: Combined effect of boost and RPM change. (EGR held constant).

Single shot
Engine Speed 1200→1700 RPM
Boost 75→100 kPa
IMEP 5 5bar
EGR held constant

Rate-of-pressure rise
(without adaptive control)

Rate-of-pressure rise
(without adaptive control)

$\theta_{(dp/dCA)max}$
(with adaptive control)

$\theta_{(dp/dCA)max}$
(without adaptive control)

(dP/dCA)max (bar/degree)

Cycle No.

Cycle-by-cycle $\theta_{(dp/dCA)max}$
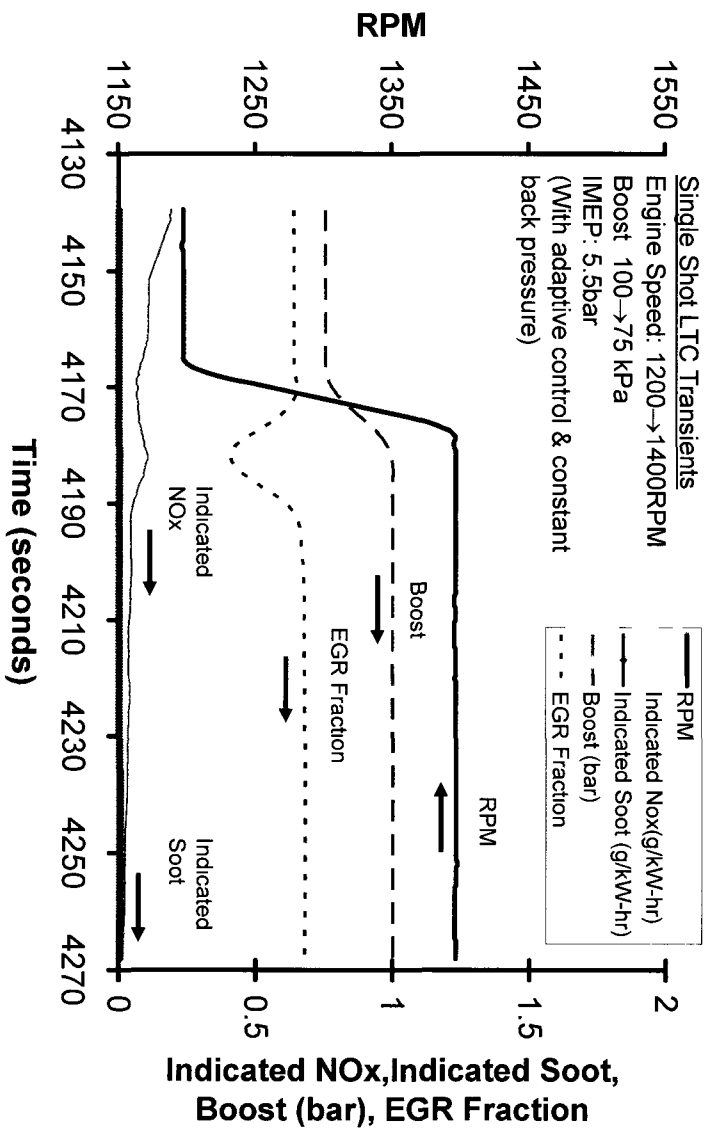
Figure 6-79: Emission response during boost and RPM change. (With adaptive control and EGR back pressure held constant).

Single Shot LTC Transients
Engine Speed: 1200→1400RPM
Boost 100→75 kPa
IMEP: 5.5bar
(With adaptive control & constant back pressure)

RPM

Indicated NOx

Indicated Soot

Boost

EGR Fraction

RPM

—— RPM
——→ Indicated Nox(g/kW-hr)
— — Indicated Soot (g/kW-hr)
— — Boost (bar)
- - - EGR Fraction

Time (seconds)

Indicated NOx,Indicated Soot, Boost (bar), EGR Fraction

106

In this chapter, it has been shown that either a lean-homogenous mixture or a weak-homogenous mixture can be used to achieve simultaneous low-NOx and low-soot combustion. However, the method of using a lean-homogenous mixture for low emissions was applicable only at low-loads. For higher loads, it was found necessary to weaken the cylinder charge with the use of EGR. In the presence of EGR it was possible to implement the low-emission combustion with both single-shot EGR-enabled EPC and multiple-pulse EPC injection strategies. The advantage of the multiple-pulse EPC strategy was that, with this method it was possible to reduce HC as well. However, an important limitation of this method was that the combustion was no longer directly controlled by the injection process and was typically initiated before TDC. The initiation of the combustion before TDC led to an increased cycle work during the compression process. The use of EGR-enabled EPC with a single shot injection strategy for low-emissions was able to retain the coupling between the injection and the combustion process; however this type of combustion suffered from high amounts of HC and CO. Cylinder pressure based control system was also found to be necessary to implement this type combustion. A brief summary of the EPC strategies has been provided in Table 6-3. Since, a considerable amount of data was now available for the EPC combustion, it was decided to compare the efficiency characteristics of the EPC combustion with the conventional combustion and the results are presented in the next chapter.

Table 6-3: Implementation of EPC strategies and their comparative advantages and disadvantages

Mode	Loads	Implementation	NOx and Soot	CO + HC penalty	Phasing penalty	Injection phasing relation
Lean	Low-loads	Single-shot	No	Yes	NO	Yes
Lean	Low-loads	Multiple shots and no EGR	Yes	Moderate	Yes	NO
Weak	Low-mid	Single shot + EGR	Yes	High	Yes	Yes
	Low-mid loads	Single shot + EGR + Cylinder pressure based control	Yes	High	NO	Yes
	Mid-loads	Multiple shots + EGR	Yes	Moderate	Yes	No

CHAPTER VII

7 CYCLE THERMAL EFFICIENCY CHARACTERIZATION FOR EPC

7.1 Efficiency Description

In Chapter-VI, various methods of applying EPC strategies have been discussed to simultaneously reduce NOx and soot emissions. At this stage it was imperative to compare the engine-cycle efficiency for the conventional and the EPC combustion modes. For the case of an internal combustion engine, various efficiency descriptions such as mechanical efficiency, fuel conversion efficiency and combustion efficiency were available in the literature [4,63]. Therefore, as a first step it was essential to understand the description of each of these efficiency terms and then compare the efficiency terms for the conventional and the EPC combustion based on these definitions. To facilitate the understanding of each of the terms, an energy flow diagram was prepared which shows the relative location of each of the efficiency term during the entire fuel conversion process (Figure 7-1).

a) Combustion efficiency: Combustion efficiency was the fraction of the fuel energy that was the released during the combustion process. This term was primarily used to account for the incomplete products of combustion in the exhaust. The typical products of incomplete combustion are CO, HC, soot and very small fraction of hydrogen. For the present research only the CO and HC were considered. The very low soot during the EPC combustion meant that the soot was not a significant factor for energy efficiency considerations. The test data discussed in the literature has shown that the hydrogen production becomes a significant contributor to incomplete combustion only when the engine was running under rich combustion mode [4]. Since, all the EPC experiments had the engine running under lean combustion mode; provision for hydrogen measurement was not included in the research set-up. An additional source of decrease in combustion efficiency was observed to be oil dilution with the fuel condensate. During the EPC combustion experiments it was observed that the engine oil was increased during the engine operations. This is in direct contrast to the convention combustion diesel engine

operation wherein the engine oil level decreases slightly with long running periods. The problem of oil dilution was more pronounced when the injection timings were very advanced as in the case multi-pulse EPC experiments. Similar results have been reported by other authors as well [64]. The problem of combustion efficiency loss due to fuel condensation and subsequent mixing with the oil was accentuated by the fact that the quantity of the fuel lost this way was hard to quantify. More efforts are currently in progress at the Clean Diesel Laboratory to understand and quantify this phenomenon. For the present work the combustion efficiency decrease due to fuel condensation has been highlighted for completeness but no attempt was made to quantify the process.

The combustion efficiency has been traditionally quantified as follows:

$$\eta_c = \frac{H_R(T_A) - H_P(T_A)}{m_f Q_{HV}} \qquad (7.1)$$

where,

$$[H_R(T_A) - H_P(T_A)] = m \left(\sum_{i,reac\tan ts} n_i \Delta h_{f,i}^o - \sum_{i,products} n_i \Delta h_{f,i}^o \right)$$

here

m = mass that passes through the control volume surrounding the engine. It includes both the fuel and the air.

n_i = the number of moles of species i in the reactants or products per unit mass of the working fluid.

$\Delta h_{f,i}^o$ = standard enthalpy of formation of species i at ambient temperature T_A.

$m_f Q_{HV}$ = amount of fuel energy supplied.

An alternative expression for combustion efficiency is given by (7.2). In this expression the chemical energy carried out of the engine by the combustibles is considered as a

representative of the combustion inefficiency [4]. As mentioned before only the combustibles in the form of CO and HC were considered while the chemical energy carried by the soot and hydrogen was ignored.

$$\eta_c = 1 - \frac{\sum_i x_i Q_{HV_i}}{\left[\dot{m}_f / (\dot{m}_a + \dot{m}_f)\right] Q_{HV_f}}$$ (7.2)

where, x_i are the mass fractions of CO and HC respectively. Q_{HV_i} are the lower heating value for these species. The heating value of CO was considered as 10.1 MJ/kg and heating value of HC was considered the same as the diesel fuel and a value of 42.9 MJ/kg was used for the analysis.

b) Fuel conversion efficiency: The fuel conversion efficiency was defined as the ratio of the work produced per cycle to the amount of the fuel energy supplied per cycle that can be released in the combustion process. This efficiency was also called cycle thermal efficiency or the indicated thermal efficiency. Mathematically, this was expressed as shown below:

$$\eta_f = \frac{W_c}{m_f Q_{HV}}$$ (7.3)

where,

m_f = mass of fuel inducted per cycle

$$W_c = \int_0^{720} P dV$$ (7.4)

For the present work only the net IMEP was considered. The difference between the gross IMEP and the net IMEP was not very significant because the exhaust pressure was only a few kilo-Pascal's higher than the intake pressure. In addition, in this thesis the indicated efficiency has been decomposed into phasing efficiency and shaping efficiency as shown later in this chapter.

c) Mechanical efficiency: The ratio of the brake power delivered by the engine to the indicated power was called the mechanical efficiency. Mathematically it was given as

$$\eta_m = \frac{P_b}{P_{ig}} \qquad (7.5)$$

where, P_b = brake power

P_{ig} = indicated power

For the single cylinder research typically mechanical efficiency is not used for analysis, since the several of the accessories such as the coolant, oil and the boost system were not driven directly by the engine.

For the present analysis, a comparison of only indicated thermal efficiency and the combustion efficiency has been presented for the cases of EPC and conventional combustion. The accessory work was kept constant for the comparison points by keeping the coolant and oil temperatures the same. Also the boost was kept the same which ensured that the power consumption of the compressor was similar for test-points considered for efficiency comparison.

Energy-flow diagram for the diesel engine

Input fuel
$m_f LHV$

Combustion Efficiency
(η_{comb})

Total Chemical Heat-Released

Thermodynamic Efficiency
($\eta_{thermal}$)

Gross IMEP

Gas Exchange Efficiency
($\eta_{gas\_exchange}$)

Net IMEP

Mechanical Efficiency
($\eta_{mechanical}$)

BMEP_raw

Mechanical Efficiency_SS
($\eta_{accessories}$)

Net Power (BMEP_net)

Loss Terms

1) Un-burnt Hydrocarbons
(Measured)
2) Carbon-monoxide
(Measured)
3) Fuel condensation resulting in oil dilution
(Quantification difficult indirectly measured by change in quantity of engine oil)

1) Qheat-transfer
2) Qexhaust
3) Phasing Efficiency
4) Shaping Efficiency

1) Pumping work

1) Friction + Accessory work

1) Accessory to drive external device such as compressor

$$\eta_{comb} = 1 - \frac{\sum_i x_i Q_{HV}}{\left[m_f / (m_a + m_f)\right] Q_{HV_f}}$$

$$\eta_{comb} = \frac{H_R(T_A) - H_P(T_A)}{m_f LHV_{fuel}}$$

$$\eta_{Indicated\ gross} = \frac{\int_{180}^{>40} PdV}{m_f (mg/stk) LHV_{fuel}}$$

$$\eta_{Indicated\_net} = \frac{\int_0^{720} PdV}{m_f (mg/stk) LHV_{fuel}}$$

$$\eta_{brake} = \frac{P_{kW\_shaft}}{m_f LHV_{fuel}}$$

Figure 7-1: Energy flow-diagram for a diesel engine based on [63]

113

7.2 Factors Effecting Cycle Thermal Efficiency for EPC Combustion

A comparison of the major emission and the heat-release rate characteristics for the EPC and conventional combustion mode is presented in Figure 7-2. For the conventional combustion, the combustion phasing was configured at phasing window for best-efficiency. This phasing window for best efficiency was experimentally determined for and the same was observed in the modeling results also. For these experiments no emission control measure such as EGR was not applied, which resulted in high combustion efficiency. Thus, a combination of high combustion efficiency and a good phasing ensured that the indicated efficiency was 48%. Also included in this plot are the results of multi-pulse EPC and EGR-enabled EPC experiments. The multi-pulse EPC has slightly lower combustion efficiency which was primarily caused by the large amounts of CO. For the majority of the multi-pulse EPC results the HC was not a significant factor for efficiency reduction because of the implementation of an appropriate selection of injection strategy as detailed in Figure 6-13. However, since the combustion was initiated early during the compression stroke it resulted in a higher amount of compression work that ultimately affected the indicated efficiency. Additionally, since very early injection timings were implemented, oil-dilution by fuel was also observed. For the case of single-shot EGR enabled EPC, the high levels of EGR resulted in a significant drain of the fuel energy to the exhaust in the form of HC and CO. As shown in the figure the combustion efficiency for the EGR enabled EPC had decreased to 96% and an indicated efficiency of only 35% was observed. Thus it can be clearly seen that the major reasons for efficiency penalty for the EPC cycles were: 1) high-levels of high CO and HC 2) off-phasing of combustion event and 3) fuel-condensation.

Figure 7-3 shows the comparison between the typical case of conventional combustion with limited emission control, multi-pulse EPC and EGR-enabled EPC. Instead, of considering single case discretely it was decided to plot the effect of EGR sweep during multiple EPC experiments, conventional combustion and simulation results collectively (Figure 7-3) and it can be seen that the comparison showed that the indicated-efficiency for the EPC cycles was significantly lower than the conventional combustion.
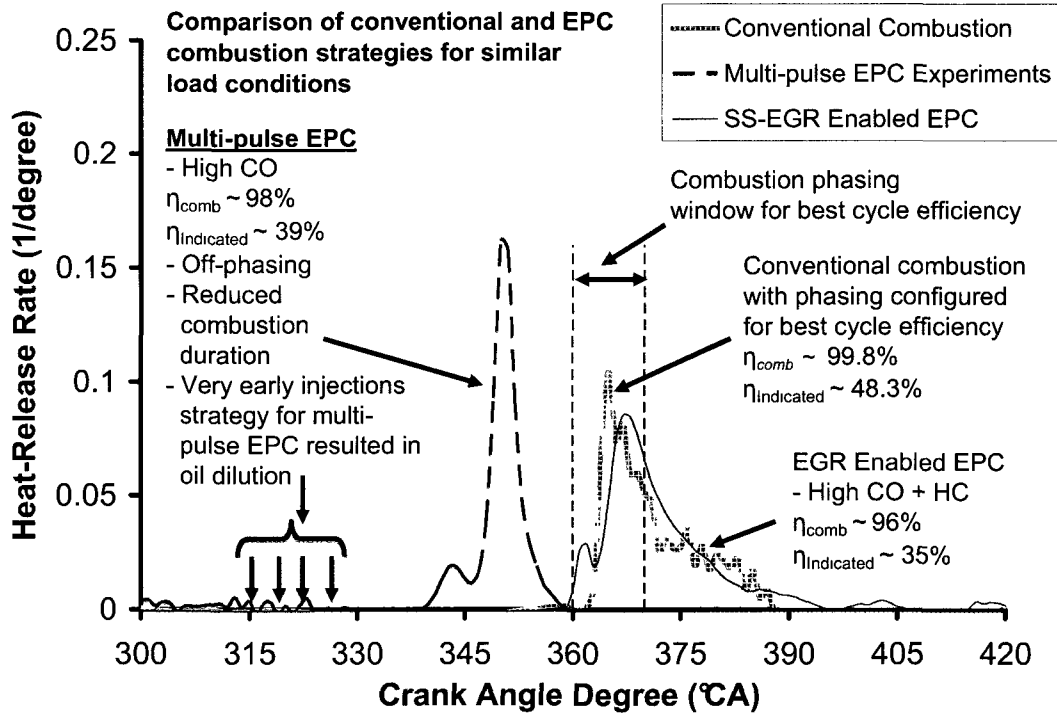
Figure 7-2: Comparison for heat-release rates for EPC and conventional combustion
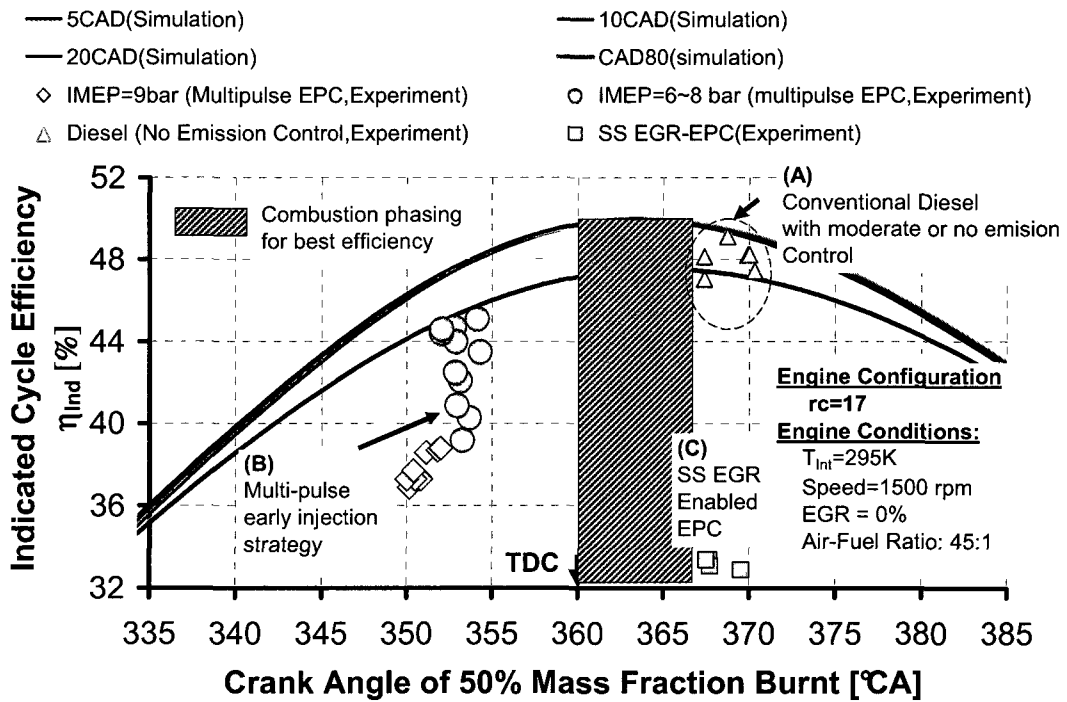
Figure 7-3: Comparison of the fuel-efficiency for different type of EPC combustion strategies with conventional combustion.

Another aspect noticeable on the heat-release rate for the multi-pulse EPC was the reduction in the combustion duration in comparison to the conventional combustion. The reduction in the combustion duration has been noticed by other researchers also and a near-constant volume combustion at TDC has been attributed as a factor that influences thermal efficiency [30,34,63]. Therefore, for the multi-pulse EPC cycles the combustion phasing had a detrimental effect on the cycle efficiency while the shortened combustion duration was supposed to enhance the cycle efficiency.

As a first step the effect of combustion duration and combustion phasing alone was numerically investigated (Figure 7-4 and Figure 7-5) using in-house engine simulation software SAES [52]. The combustion phasing was represented by crank angle for 50% mass-fraction of fuel burnt or CA-50. For the SAES program, a heat-release rate similar to the one observed during the experiments was used as a user input and assuming 100% of the fuel was burnt, the cylinder-pressure was computed for the user specified heat-release rate. A new form of representation that clearly details the effect combustion phasing and duration on cycle thermal efficiency has been given by Yuyu and Zheng [44,45] in the form of contour plots. A similar representation has been adopted in this thesis also (Figure 7-5). It can be seen that the combustion phasing had a strong effect on the indicated efficiency that peaked at a heat-release position of 5~7°CA after TDC. The maximum rate-of-pressure rise $(dp/d\theta)_{max}$ increased as the combustion-phasing or the CA50 advanced and heat-release duration shortened and reached its peak at 10°CA BTDC (Figure 7-6 and Figure 7-7). In general, a short and advanced heat-release rate such as the one shown in Figure 7-2 for multi-pulse EPC suffered not only from lower indicated efficiency but also higher P_{max} and $(dp/d\theta)_{max}$.
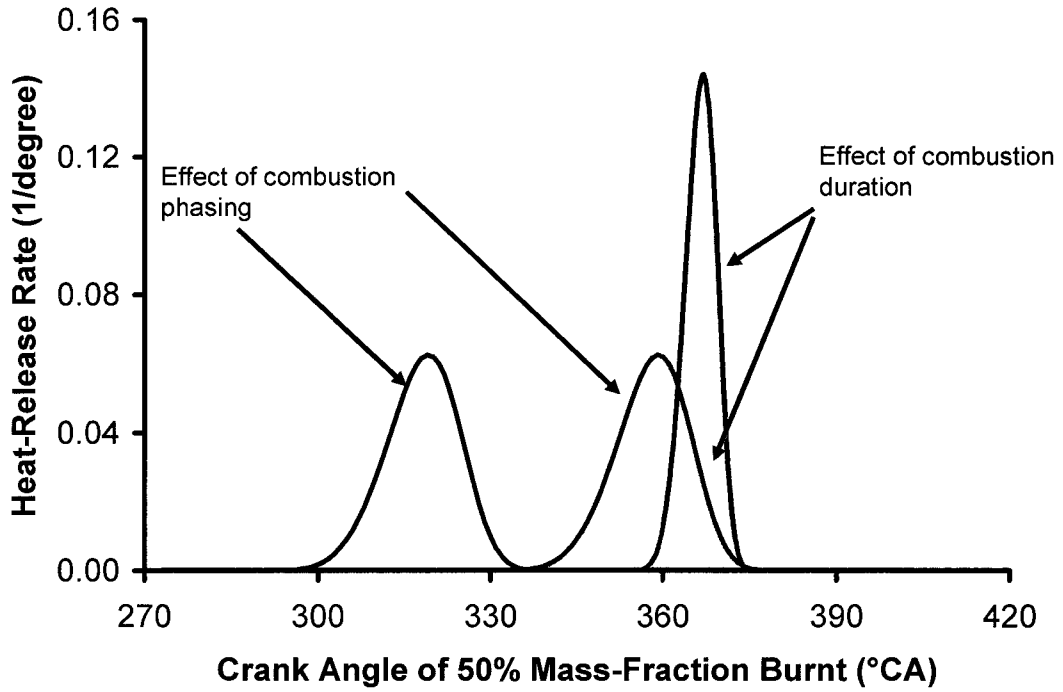
Figure 7-4: Heat-release rates used as input conditions for examining the effect of combustion phasing and duration on cycle thermal efficiency.
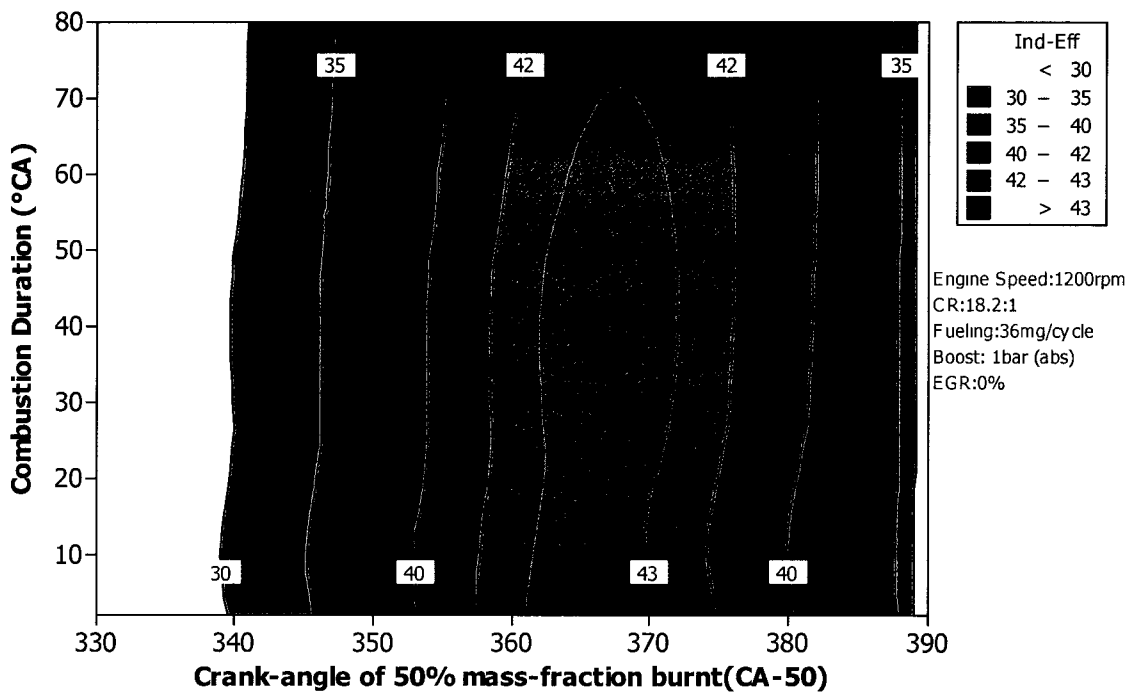
Figure 7-5: Effect of CA50 and combustion duration on η_{ind} at 1200rpm simulated using SAES.
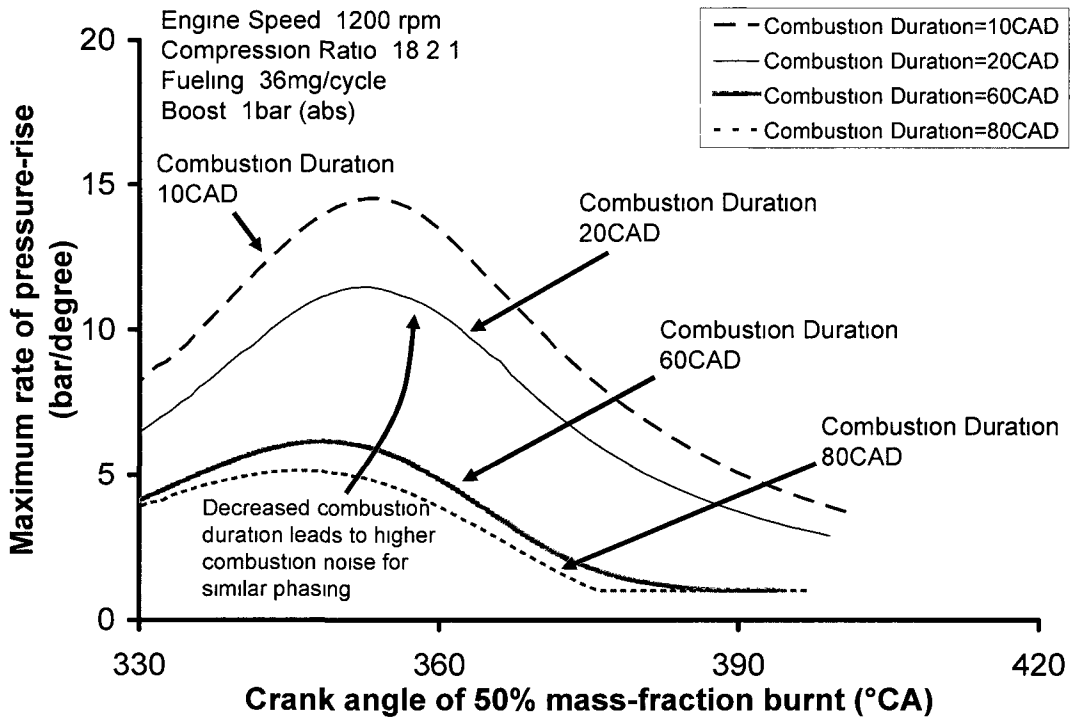
Figure 7-6: Effect of combustion phasing and combustion duration on rate-of-pressure rise simulated using SAES.
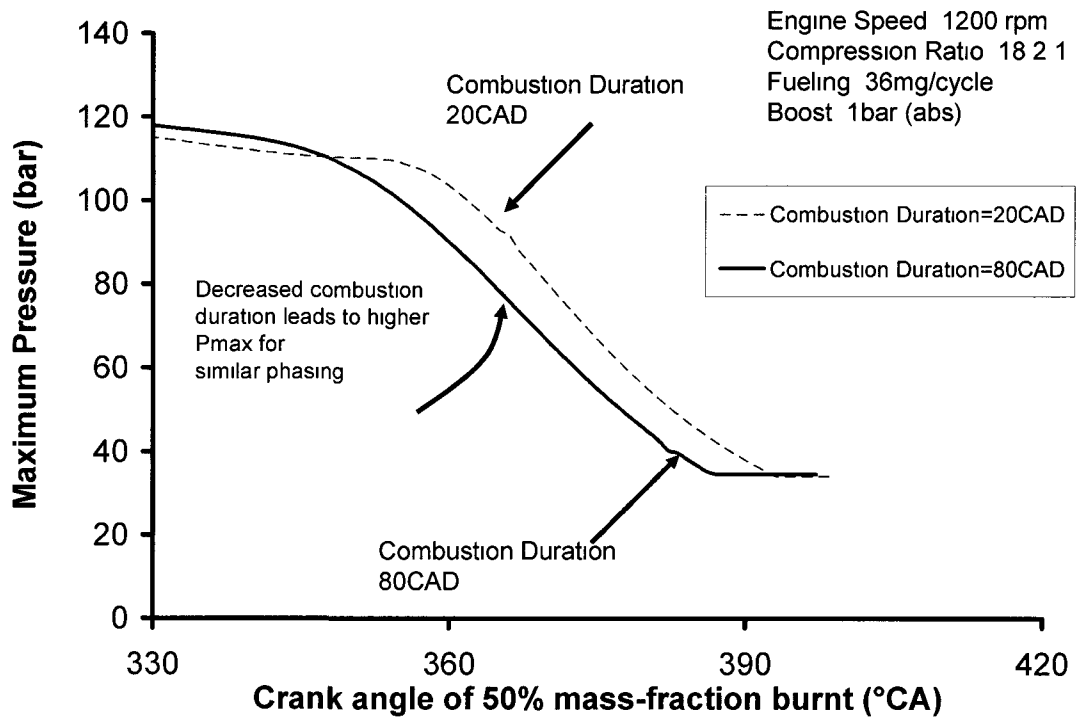
Figure 7-7: Effect of combustion phasing and combustion duration on maximum in-cylinder pressure simulated using SAES.

118

7.3 Equivalence between the Thermal Conversion Efficiency and CO, HC Emissions

In Figure 7-8, a multiple-pulse EPC experiments have been presented at two different levels of EGR. In this experiment, the EGR was increased from 58% to 63% and better combustion phasing was obtained. As per the discussion presented in Section 7.2 a better combustion phasing should have translated into a better indicated thermal efficiency, however no change in work done per cycle or the IMEP was observed. A critical examination of the other emission characteristics revealed that with the higher application of EGR, there was deterioration in the combustion efficiency as reflected by the higher amounts of CO and HC. Thus, the potential benefit in indicated thermal efficiency by the application of EGR was negated by the loss in combustion efficiency. The effect of combustion efficiency on the overall indicated efficiency was analyzed in detail by using the classical approach detailed in the literature and following efficiency terms were used for the analysis [4].

Combustion efficiency (η_c): It was defined as the fraction of the fuel energy that was released in the combustion process and was described by Equation (7.2) shown previously.

Indicated efficiency or the fuel conversion efficiency (η_f): This is the ratio of the work produced per cycle to the amount of the fuel energy per cycle that can be released during the combustion process. This term is typically given by Equation (7.3), an additional expression that was found in the literature was Equation (7.6)

$$\eta_f = \frac{3600}{sfc(g/kW.h)Q_{HV}(MJ/kg)} \tag{7.6}$$

Thermal conversion efficiency (η_t): This term was used to separate out the effects of incomplete combustion and was defined as the ratio of the actual work per cycle to the amount of the fuel chemical energy released in the combustion process. This term was mathematically given by Equation (7.7)

$$\eta_t = \frac{W_c}{\eta_c m_f Q_{HV}}$$ (7.7)

It can be readily seen that all the efficiencies mentioned above are related as follows

$$\eta_f = \eta_c \eta_t$$ (7.8)

As shown in Figure 7-8, for points A and point A' both the points had the same IMEP and a constant fueling per cycle (m_f). Therefore,

$$\eta_{f,A} = \eta_{f,A'}$$

where subscripts A and A' denotes that the data is for points A and A' respectively.

$$\eta_{c,A}\eta_{t,A} = \eta_{c,A'}\eta_{t,A'}$$ (7.9)

$$\frac{\eta_{c,A'}}{\eta_{c,A}} = \frac{\eta_{t,A}}{\eta_{t,A'}}$$ (7.10)

$$1 - \frac{\eta_{c,A'}}{\eta_{c,A}} = 1 - \frac{\eta_{t,A}}{\eta_{t,A'}}$$ (7.11)

$$\frac{\Delta\eta_c}{\eta_{c,A}} = -\frac{\Delta\eta_t}{\eta_{t,A}}$$ (7.12)

$$\Delta\eta_c\% = -\Delta\eta_t\%$$ (7.13)

Thus if there is a 1% increase in η_t, and there is a 1% decrease in η_c then the η_f would remain constant. The values of η_c, η_t and η_f was computed for experimental results shown in Figure 7-8 and the results are shown in Table 7-1. It can be seen that the Equation (7.13) was closely valid for the experimental data as well. Therefore it can be seen that for the experiment the gain indicated efficiency due to the better phasing was nullified by the deterioration in the combustion efficiency.

Table 7-1: Effect of EGR on efficiency distribution for the case of (Figure 7-8)

	m_f (mg/stk)	$\dot{m}_a$ (g/s)	EGR (%)	CO (ppm)	HC (ppm)	IMEP (bar)	η_c (%)	η_t (%)	η_f (%)
A	27.5	6.7	58	1050	206	7.9	99	50.4	49.9
A'	27.5	5.8	63	3728	358	7.9	98	51	50
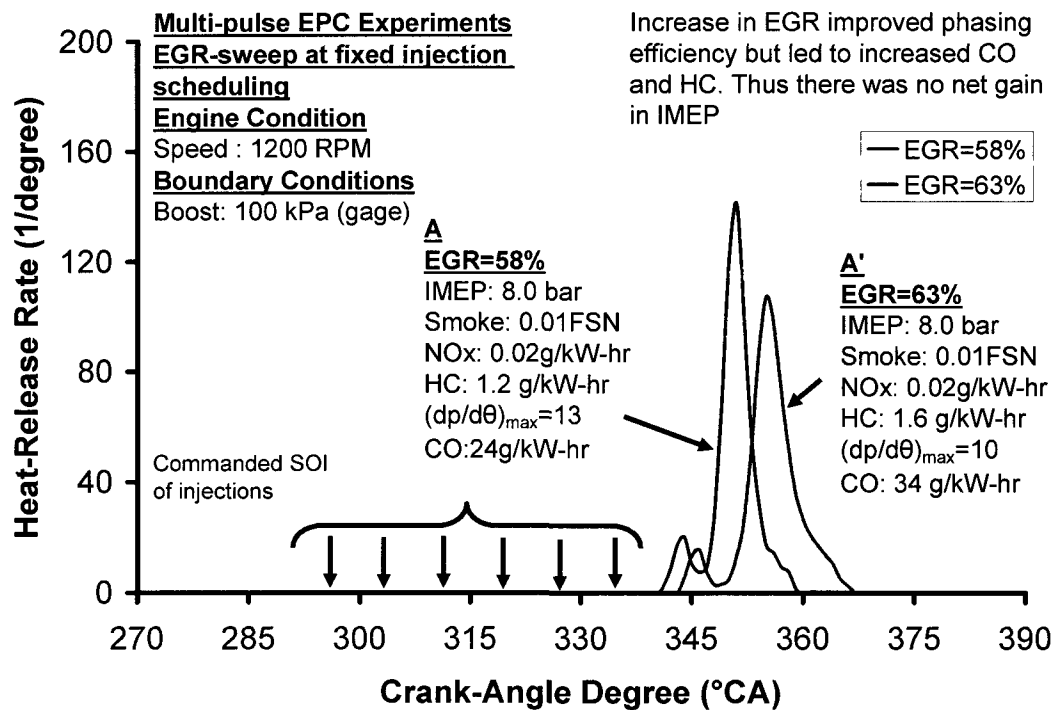
Figure 7-8: Effect of EGR on combustion phasing, CO and HC emissions

A concept of equivalent emission has been proposed wherein the change in indicated thermal efficiency was converted to an equivalent CO or HC emissions. This part was done primarily to decide when to apply the EGR to improve the combustion-phasing. Therefore, if the engine is presently operating with a combustion phasing at A (Figure

7-8) and if we apply EGR to improve the combustion phasing to point A' then this improved indicated phasing efficiency can be converted to an equivalent CO or HC emissions. Thus, if the actual increase in CO was less than the equivalent increase in CO, then at that point it might be beneficial to apply EGR to obtain better combustion phasing and thereby try to attain higher indicated efficiency. For establishing the equivalent CO, Figure 7-5 was used and the change in efficiency with combustion phasing was treated as $\Delta\eta_i$ and then Equation (7.2) and Equation (7.13) were used to estimate the equivalent CO or HC. At the time of estimation it was assumed that all the un-burnt combustibles can be treated either as CO or HC only. From Figure 7-9 it can be seen that seen that a 10°CA departure in combustion phasing from the best phasing was equivalent to a CO of ~9500 ppm or a HC of 4500ppm.
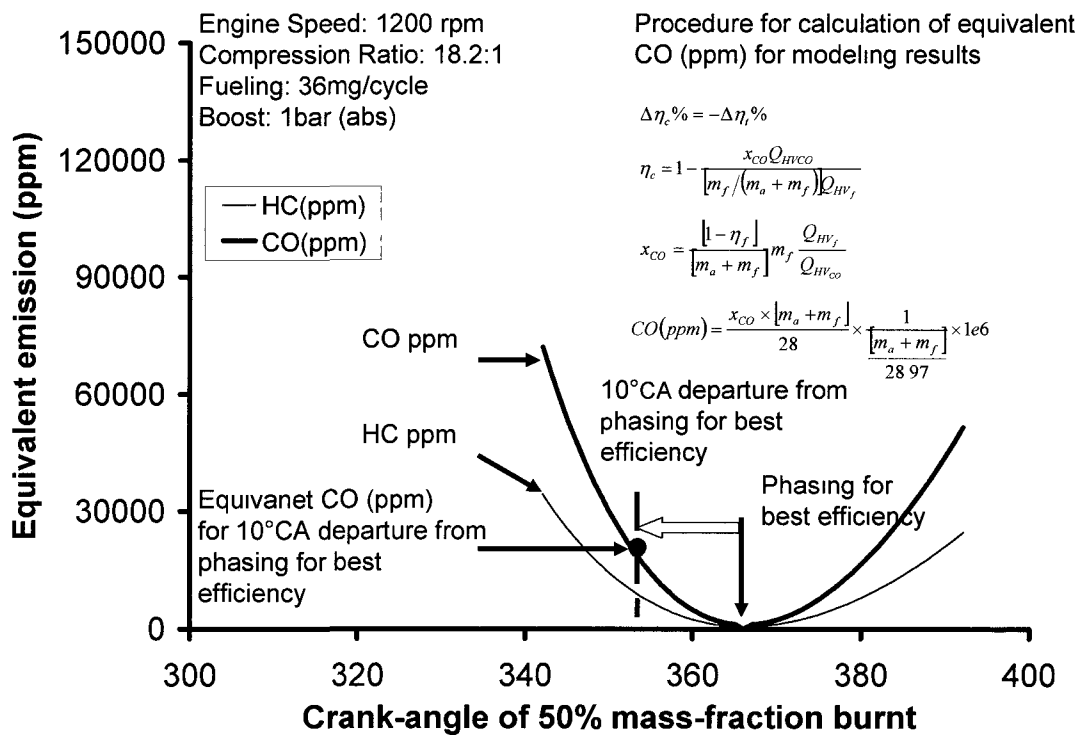
Figure 7-9: Equivalence between efficiency loss due to emissions and combustion phasing.

To evaluate the relative contribution of each of major factors affecting the cycle efficiency a new-methodology has been proposed. In this approach an effort was made to account for the major factors effecting cycle thermal efficiency directly into a single

equation. Furthermore, the thermal efficiency term was decomposed into shaping and phasing efficiency so that the indicated efficiency would have terms to account for the changes in heat-release rate profiles directly. Therefore, an attempt was made to develop an equation that considered explicitly the terms for combustion efficiency and heat-release rate characteristics. The procedure to develop the equation is shown below.

For the fuel injected into the engine cylinder $\dot{m}_f$ [g/s], the majority of the fuel normally completes combustion $\dot{m}_b$ [g/s], while a small portion of fuel, i.e. the fuel loss $\dot{m}_l = \left(\dot{m}_f - \dot{m}_b \right)$, fails to release energy or to release energy fully in the cylinder. The combustion or burning efficiency is thus defined as:

$$\chi_b = \frac{\dot{m}_b}{\dot{m}_f} \tag{7.14}$$

Modern HTC diesel engines may have a burning efficiency exceeding 99.5%. However, as strict in-cylinder NOx control techniques were implemented by techniques such as the EGR, the flame temperature reduces and the exhaust HC and CO rise. The fuel energy loss $\dot{m}_l$ was evaluated herein, with the exhaust HC counted to have the same LHV and hydrogen/carbon ratio as diesel fuel; the LHV of CO is counted as (10.1/42.9) of diesel. The energy content of the soot in the exhaust has been ignored.

Next the term of phasing efficiency was introduced to account for the departure in combustion-phasing for the phasing for best-efficiency. This was primarily helpful to explain combustion such as the multi-pulse EPC which had a tendency to ignite before TDC. The effect of the heat-release phasing was given by χ_p, and was defined as the ratio of the actual indicated cycle thermal efficiency to maximum efficiency obtained for the same heat-release rate at the phasing for the best efficiency. The phasing efficiency was evaluated using Equation (7.15)

$$\chi_p = \frac{\eta}{\eta_{p\max}} \tag{7.15}$$

In the above equation, η is the actual cycle thermal efficiency when the phase of heat-release is off set from the timing of maximum efficiency $\eta_{p\max}$, while the heat-release for both η and $\eta_{p\max}$ are fixed to the same shape. According to previous modeling analyses, a combustion-phasing of approximately 5°CA ATDC provided phasing for best efficiency irrespective of a variety of engine operating parameters [44,45]. In practical engine operations, the phasing efficiency may vary from 90~100% when the CA50 retards from 12°CA BTDC to 5°CA ATDC.

The effect of the heat-release shaping on the efficiency was given by χ_s, which was defined as the ratio of actual cycle thermal efficiency with the when the shape and duration of the heat-release differs from those from those of the maximum efficiency to the maximum efficiency, while the phasing for both the cases was affixed to the peak thermal efficiency. This was evaluated using Equation (7.16) shown below:

$$\chi_s = \frac{\eta_s}{\eta_{s\max}} \tag{7.16}$$

In the above equation, η_s is the actual cycle thermal efficiency when the shape and duration of heat-release differs from those of maximum efficiency $\eta_{s\max}$, while the phasing of heat-release as mentioned before was affixed to the peak thermal efficiency. In practice, the shaping efficiency may vary from 96~100% when the apparent heat-release duration shortens from 60°CA to 5°CA for a simplex shape of heat-release; or vary from 98~100% when the shape of heat-release swaps among simplex, double hump, and complex [44,45]

The value of χ_b, χ_p and χ_s all have proportional relationship with the engine cycle efficiency. In order to evaluate the impacts of the burning, phasing, and shaping efficiencies systematically, an overall combustion coefficient was defined:

$$\chi_c = \chi_b \cdot \chi_p \cdot \chi_s$$

An EGR enabled EPC experiment is taken as a representative case to evaluate the effect of the above mentioned efficiency terms. The EPC combustion was implemented with a single-shot injection strategy (close to TDC) with EGR. The tests were performed at an IMEP of 8.2bar. The boost pressure was selected as 100kPa and the commanded rail-pressure was 1200bar. The EGR was gradually increased till the combustion showed the simultaneous low-NOx and low-soot characteristics (Figure 7-10).

Under such testing conditions, an insignificant amount of soot was formed for EGR less than 40% and after 40% EGR the soot production increased rapidly reaching its peak value near 60% EGR. The NOx decreased continuously with EGR. After 55% EGR the NOx was very low and was not influenced by further increase in EGR. The IMEP penalty incurred with the heavy uses of EGR when a single-shot injection strategy was applied to achieve EPC is shown in Figure 7-11. The IMEP decreased from approximately 8.2bar to 6.5bar.
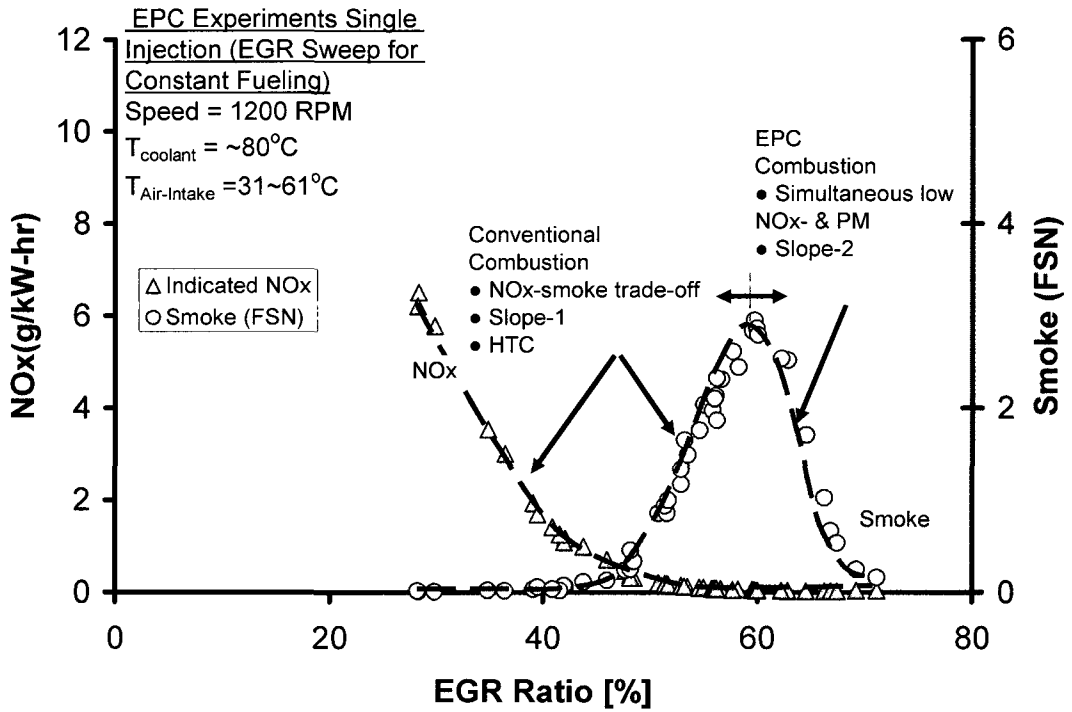
Figure 7-10: EGR enabled EPC with a single-shot combustion.
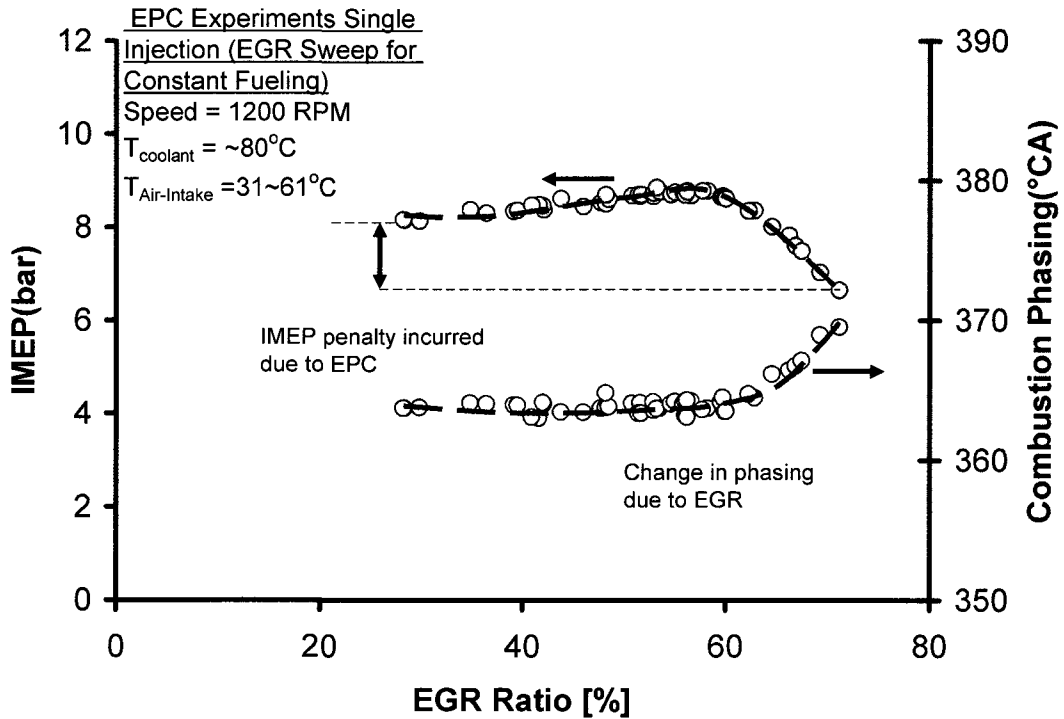
Figure 7-11: IMEP penalty incurred due to EGR enabled EPC with fuel injection timing adjusted to peak IMEP.

The effects of EGR on combustion phasing, combustion duration and combustion in-efficiency are shown in Figure 7-12 and Figure 7-13. The increases in EGR widened the combustion duration from 30°CA to 40°CA. Concurrently, the combustion phasing was postponed from a CA-50 of 364°CA to 369°CA. To partially counter the fuel efficiency reduction, the commanded start of injection (SOI) had to be advanced from around 354°CA to 350°CA to avoid the engine operation in the regions of high cycle-to-cycle variation. The affect of EGR on combustion efficiency in terms of increased CO and HC is shown in Figure 7-13. Although the exhaust CO increased substantially as EGR increased to above 40%, the abrupt increase in exhaust HC did not occur until the in-cylinder combustion entered the regions of EPC, referring to Figure 7-13. In addition, the indicated CO was converted to effective CO which was obtained by multiplying (10.1/42.9) to the indicated CO in g/kW-hr. Figure 7-14 shows the differences in heat-release characteristics for the conventional and EPC combustion. For the EPC combustion, the combustion phasing was postponed from 364°CA to 369°CA, the combustion duration increased from 30°CA to 36°CA and the combustion efficiency dropped to 96.4% due to high CO and un-burnt HC. In the following paragraphs the effect of each of the factors (phasing, duration/shaping and combustion efficiency) was evaluated using in-house engine cycle simulation software SAES [52].
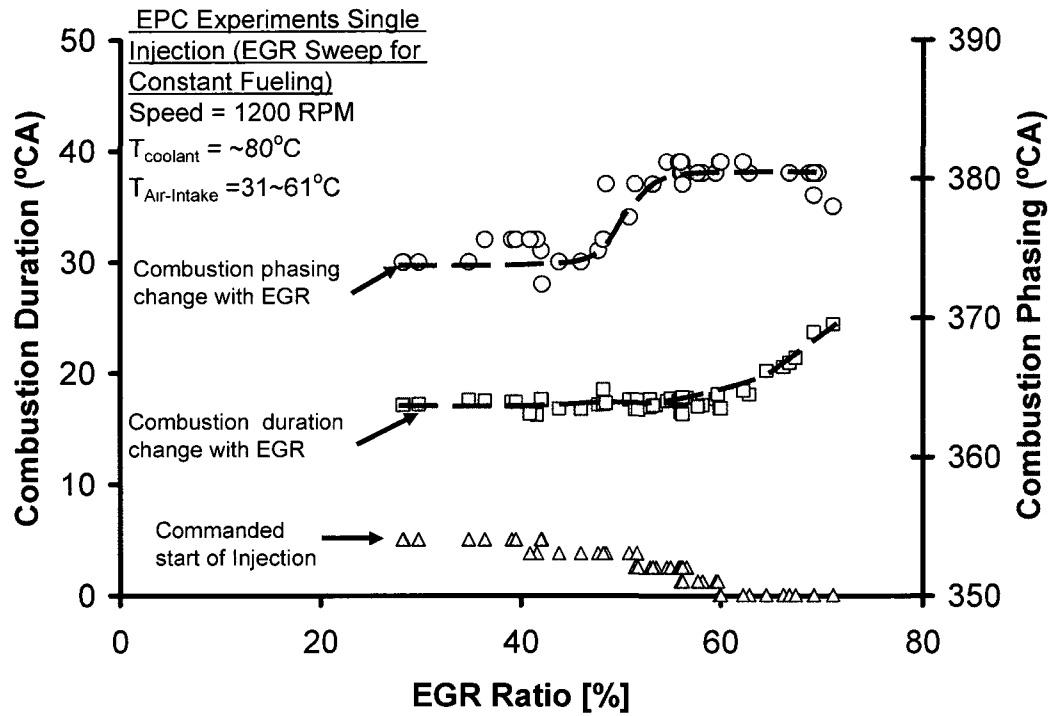
Figure 7-12: Effect of EGR on combustion phasing and duration during the implementation of EPC.
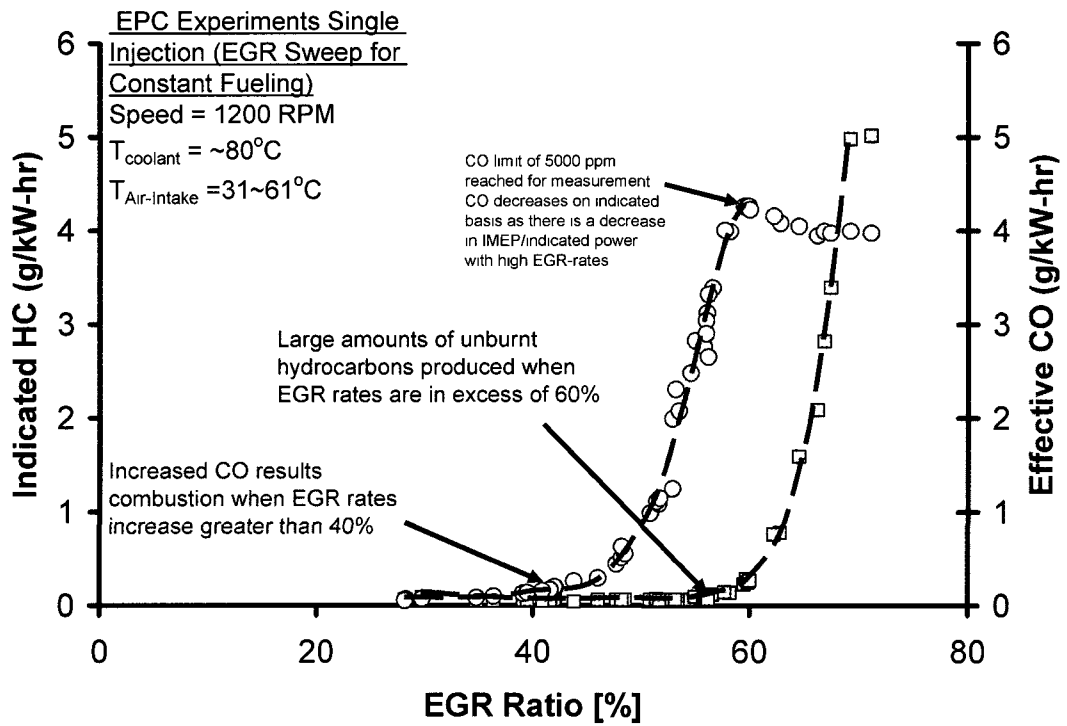
Figure 7-13: Effect of EGR on CO and HC during EPC enabling.
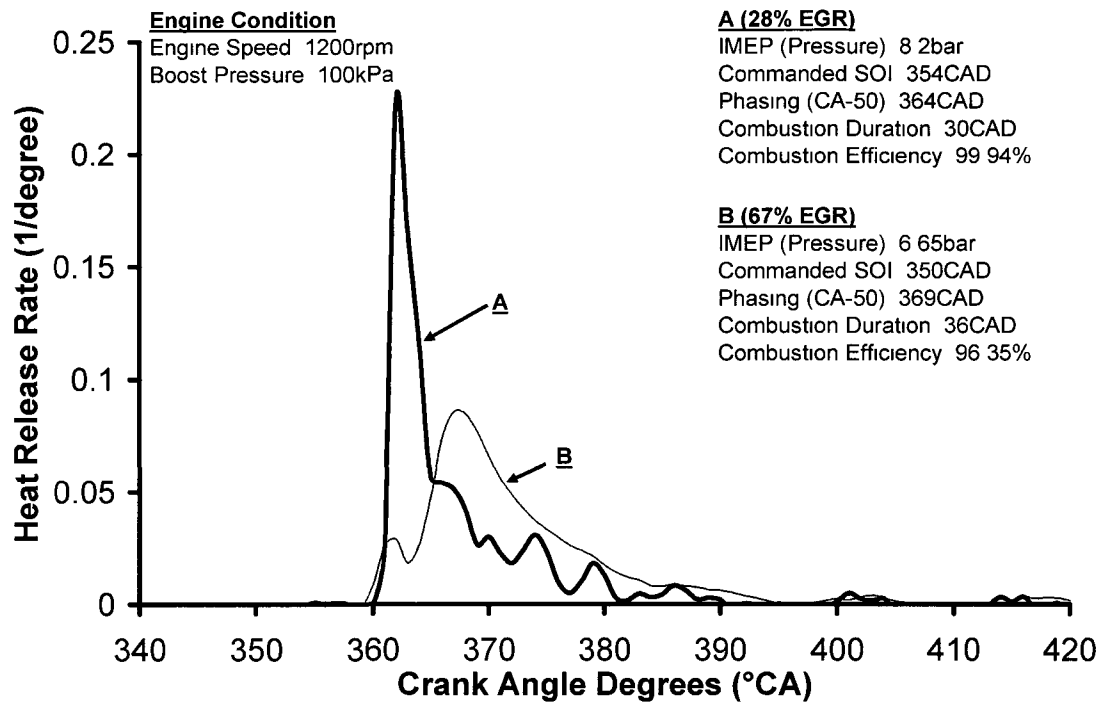
Figure 7-14: Heat-release rate characteristics for the conventional and EPC heat-release rate.

Effect of combustion phasing: Engine cycle simulations were performed in which the conventional heat-release rate was specified as an input and the IMEP was evaluated at the combustion phasing of 364°CA and 369°CA was evaluated. From the simulations it can be seen that because of the change in combustion phasing, an IMEP penalty of only 0.1bar was incurred (Figure 7-15). In a simplified way phasing efficiency for EPC was calculated as $\chi_p = \dfrac{8.1}{8.2} \sim 0.99$.

Effect of combustion shaping and duration: For this simulation run, the cycle simulations were performed once with the conventional heat-release rate as the input and the next time with the EPC heat-release rate was used as the input. For both the simulations the intake-charge composition was kept constant at 28% EGR, and the combustion-efficiency of 99.94% was assumed. This ensured that the cycle thermal efficiency was affected only by change in shaping and combustion duration. The simulations results suggested that with an EPC heat-release-shape incurred very little IMEP penalty (Figure 7-16). In a

simplified way shaping efficiency for EPC combustion was calculated as

$$\chi_s = \frac{8.1}{8.2} \sim 0.99$$

Effect of combustion efficiency: For estimating the effect of combustion efficiency with EPC heat-release rates, experimental results were used. Based on the two previous simulation results (Figure 7-14 and Figure 7-15) and the experimental results (Figure 7-14) it can be concluded that the IMEP change from 8.1bar to 6.5bar was largely due to combustion inefficiency. In a simplified way burning efficiency for EPC combustion was calculated as $\chi_b = \frac{6.5}{8.2} \sim 0.8$. Finally, the efforts were made to improve the efficiency of the EPC cycles (Figure 7-17). For the present case only combustion phase penalty was found to be recoverable. When the combustion phasing was brought back to 365°CA the IMEP increased to 6.7bar. Methods to improve the burning efficiency are shown later in the thesis.
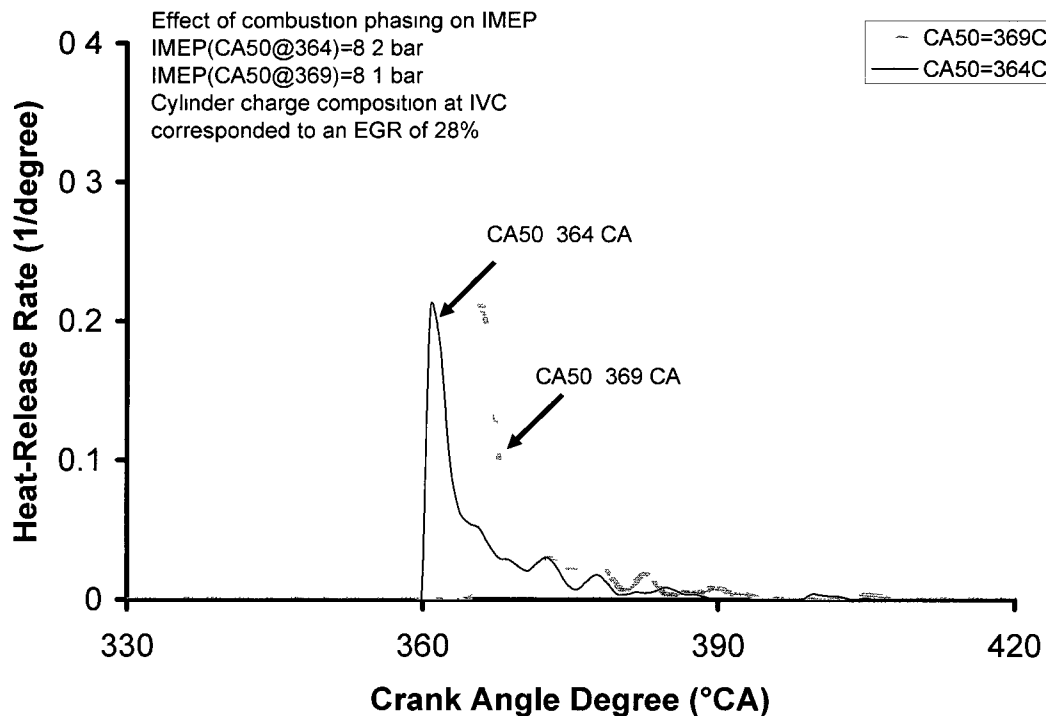
Figure 7-15: Effect of combustion-phasing on IMEP for analyzing the cycle inefficiencies of Figure 7-14.
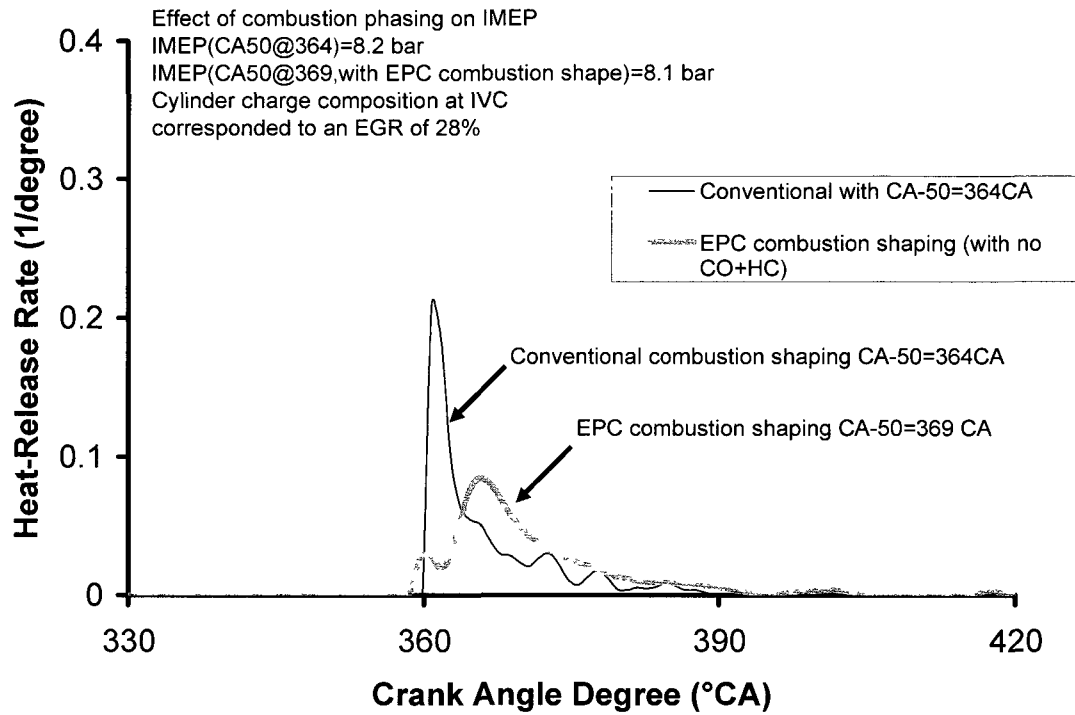
Figure 7-16: Effect of combustion shaping on IMEP for analyzing the cycle inefficiencies of Figure 7-14.
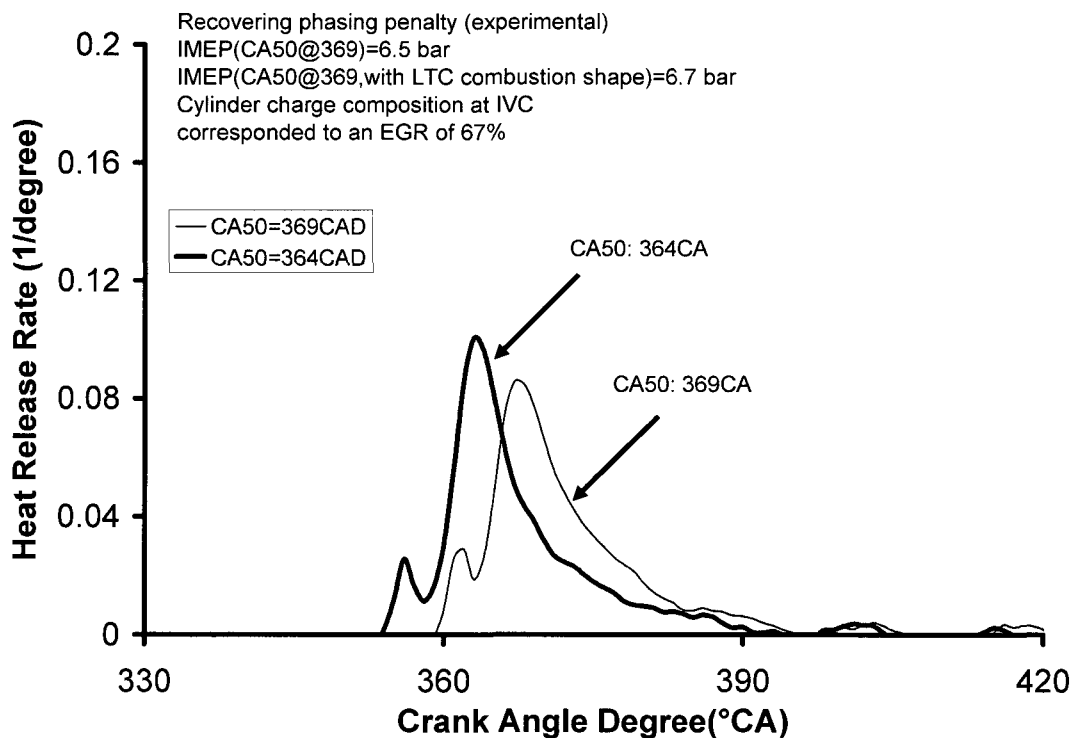
Figure 7-17: EPC cycle efficiency improvement by combustion phasing optimization.

CHAPTER VIII

8 ANALYSIS OF MODELING RESULTS

8.1 CHEMKIN Simulation for Deciding EPC Boundary Conditions

The combustion of a lean homogeneous air/fuel mixture in the cylinder of a diesel engine has shown to result in simultaneous low-NOx and low-soot emissions. This type of combustion has been called by different names such as HCCI, or ATAC or multi-pulse EPC type of combustion. A major disadvantage of this type of combustion was the lack of combustion phasing control directly by fuel-injection scheduling. The combustion-phasing control was governed by the chemical kinetics and was implemented indirectly by modulating the in-cylinder temperature history or in-cylinder equivalence ratio history. Also shortened combustion duration resulted in a rapid in-cylinder pressure rise. The problem of rapid pressure-rise was accentuated, if the combustion is initiated before TDC.

In this section, as a first-step a comparison was made between the experimental start-of-combustion and a purely chemical-kinetics based combustion-phasing prediction using CHEMKIN-III. The CHEMKIN simulations treat the in-cylinder charge as a single-zone model with uniform composition and thermodynamic properties. This type of a single zone analysis has shown to predict the start of combustion with reasonable accuracy and has been used extensively in parametric studies to understand the effects of boundary conditions such as EGR, compression ratio, equivalence ratio by other researchers also [64,66,67]. Since all the cylinder charge ignites nearly instantaneously at the ignition temperature, the single zone model under-predicts the burn duration, and over-predicts peak cylinder pressure, the rate-of change of pressure and NOx emissions. The comparison of combustion-phasing prediction based on chemical kinetics for the low-load and high-load multi-pulse EPC strategies are shown in Figure 8-1 and Figure 8-2. The combustion phasing guidelines have been presented in this section for the EPC combustion based on the chemical-kinetics software CHEMKIN-III.
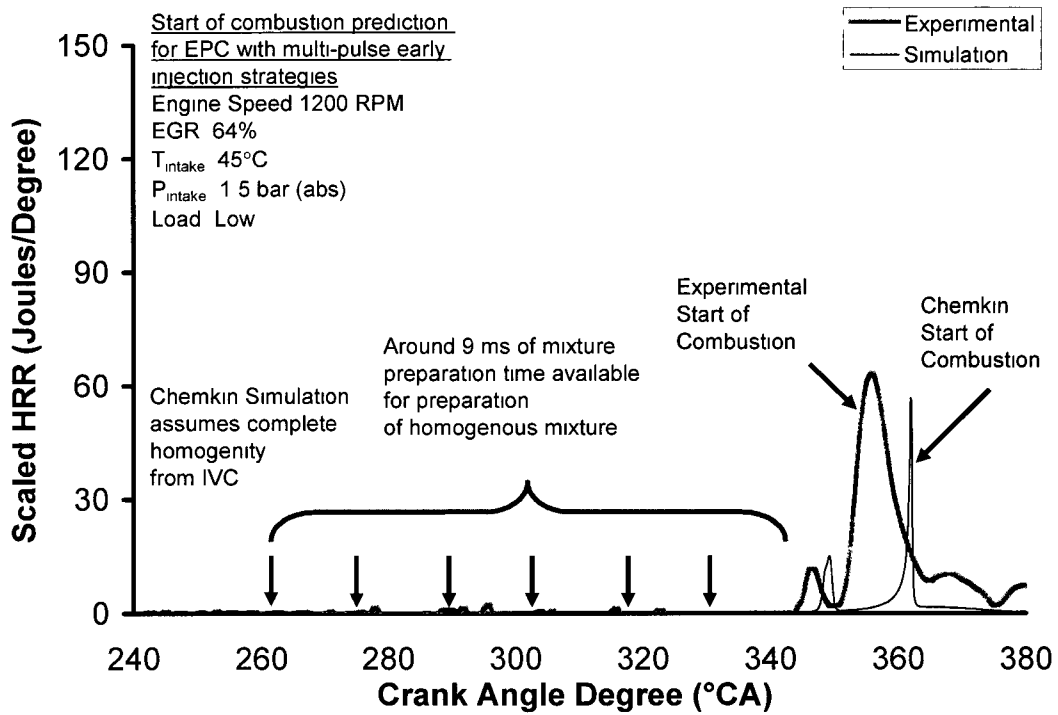
Figure 8-1: Comparison of experimental and chemical kinetics based combustion phasing predictions for EPC combustion with multiple-early injections at low load.
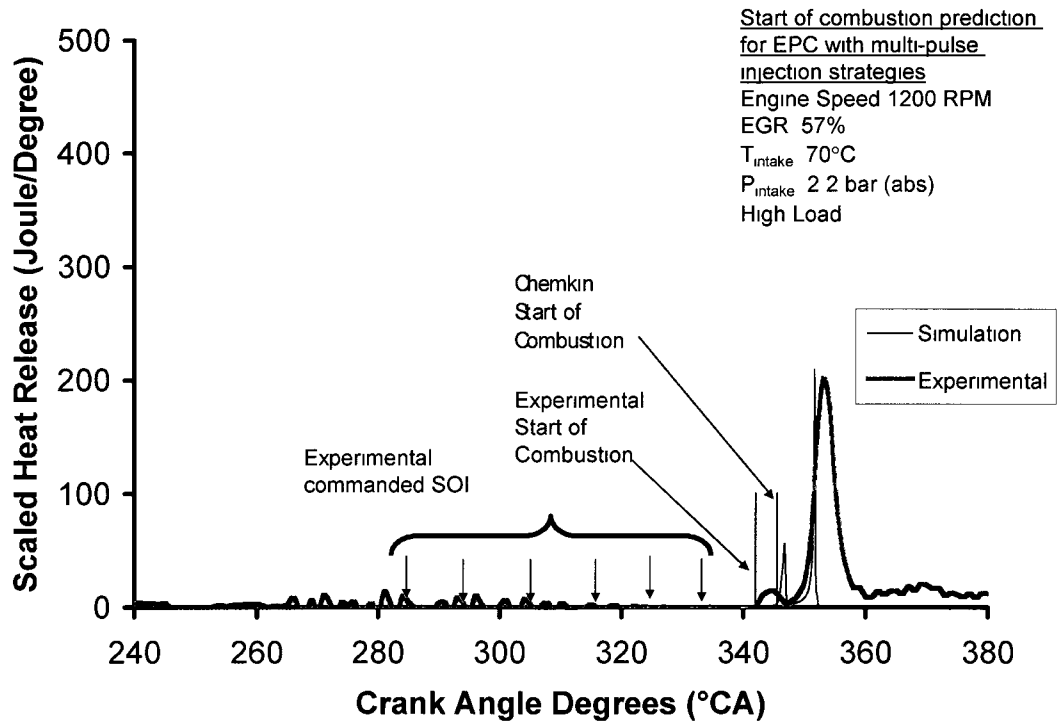
Figure 8-2: Comparison of experimental and chemical kinetics based combustion phasing predictions for EPC combustion with multiple-early injections at high load.

It can be seen that at both low-loads and high-loads, a purely chemical kinetics based combustion phasing combustion prediction show acceptable comparison with the experimental results. Note that these combustion predictions are valid only for EPC combustion with multi-pulse early injections where a homogenous cylinder charge was prepared before the combustion process. Both the EPC experimental results at low-load and the high-loads EPC showed very low soot suggesting that the cylinder-charge mixture was close to homogenous conditions before the combustion was initiated.

Thus it can be seen that the combustion-phasing for the multi-pulse EPC could be estimated by a purely kinetics based model. The two main inputs to the kinetics model were the temperature and the charge composition at the intake valve close (IVC). From an engine perspective the chemical composition at the IVC was decided by the boost and the EGR modulation for that load condition. The temperature at the IVC was decided based on the ambient temperature and the EGR temperature. So for any engine operating condition a desired combustion phasing was decided by the boost, EGR and the intake temperature (Figure 8-3).
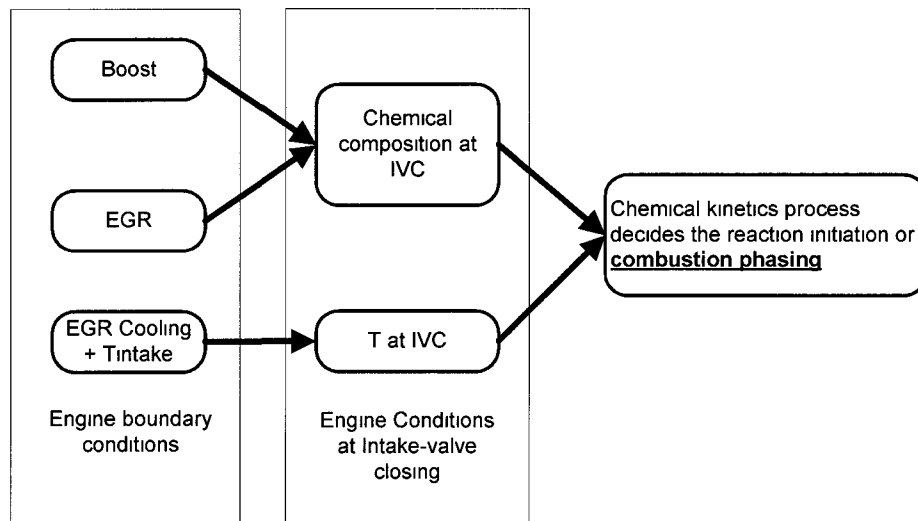
Figure 8-3: Relationship between the engine boundary conditions and the combustion phasing requirements for the multi-pulse EPC combustion strategy.

The boost and the EGR requirements were expressed by using two different air-fuel ratio quantities λ and λ_0. λ represents the actual air-fuel ratio including the effect of EGR

and was calculated as the (mass-of-fresh-air/mass-of-fuel). λ_0 represents the air-fuel if there was no EGR at the same boost. If the quantity of the oxygen coming back with the EGR is ignored, then

$$\lambda_0 = \frac{\lambda}{(1 - EGR)}$$

An advantage of the approach is that λ_0 was related with the boost requirement while the λ, was related to the combined boost and EGR requirement. So as a first step the effect of λ_0 and T_{intake} was investigated on combustion phasing with the assumption of zero EGR (Figure 8-4). From the combustion phasing point of view, this figure suggests that a lower λ_0 has a better combustion phasing.
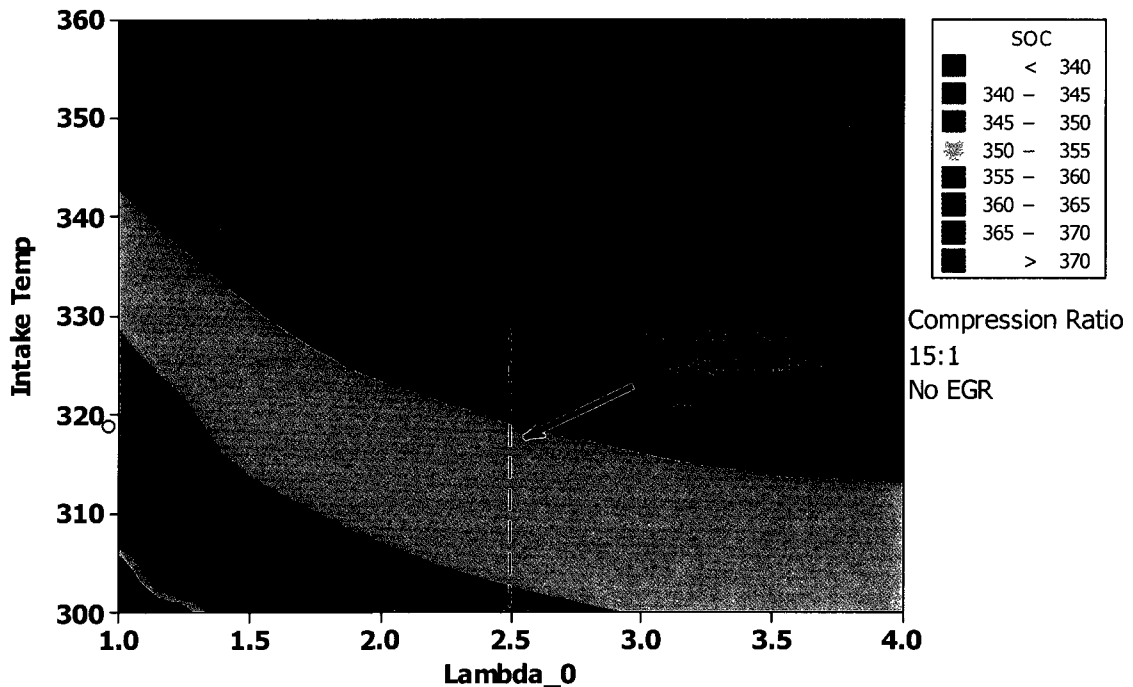
Figure 8-4: Contour plots for the start of combustion as function of overall global equivalence ratio and T_{intake}.

One explanation that has been provided in the literature is that the polytropic-index of compression decreases as we go down in air-fuel ratio [64]. Therefore as the polytropic

index decreases the cylinder charge has to be compressed more to reach the cool-flame initiation temperature (Figure 8-5). However, this observation needs to be considered along with the Figure 3-1, which requires that a minimum homogeneity of λ_0 equal to 2.5 ~ 3 to achieve simultaneous low-NOx and low-soot.
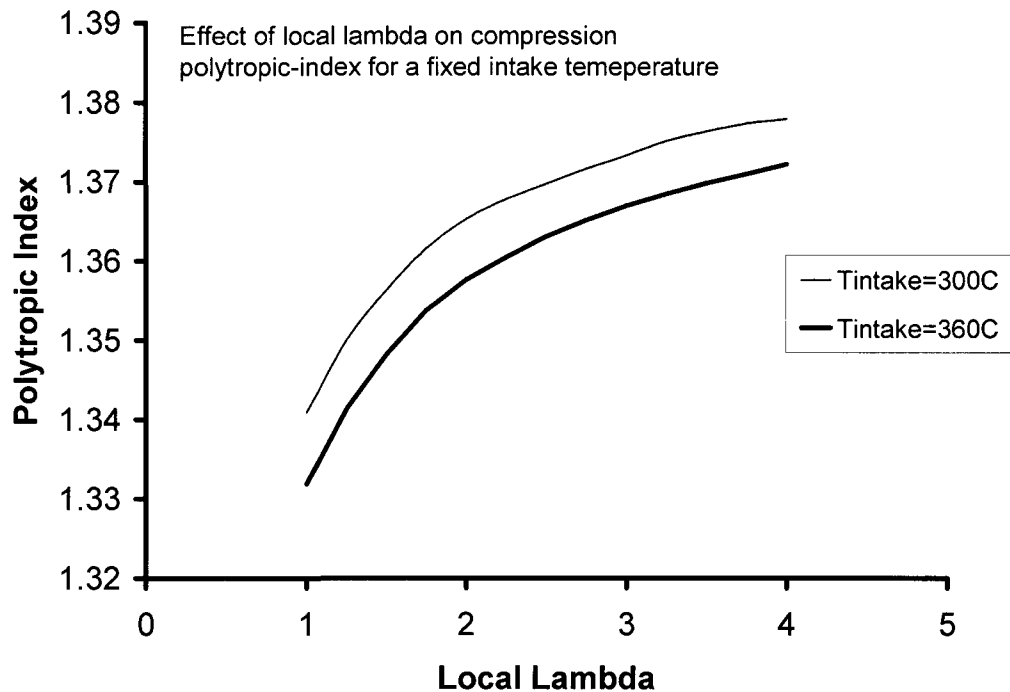
Figure 8-5: Polytropic index as a function of local lambda and intake temperature.

For a λ_0 of 2.5 to 3 the combustion was typically initiated before the TDC as can be seen by the simulations and the experimental results shown earlier (Figure 6-5). Therefore, the effect of EGR as a combustion phasing modulating tool was numerically investigated next. The addition of EGR increases the specific heat and reduces the γ of the mixture, and these effects tend to delay the combustion process. Figure 8-6 shows clearly that for the combustion phasing close to TDC, large amounts of cooled EGR was required. The simulations have been restricted to 55% EGR since a simultaneously high boost and EGR is still a challenging requirement for the modern diesel engine [22]. A contour plot shown in Figure 8-6 provides the T_{intake} and the EGR values for the desired combustion phasing at a given compression ratio and intake valve closing. It should also be noted that in the

presence of EGR, both the intake temperature and the EGR are coupled. The EGR-intake temperature relationship for the single-shot experiments with increasing EGR at a load of 8bar IMEP is shown in Figure 8-7.
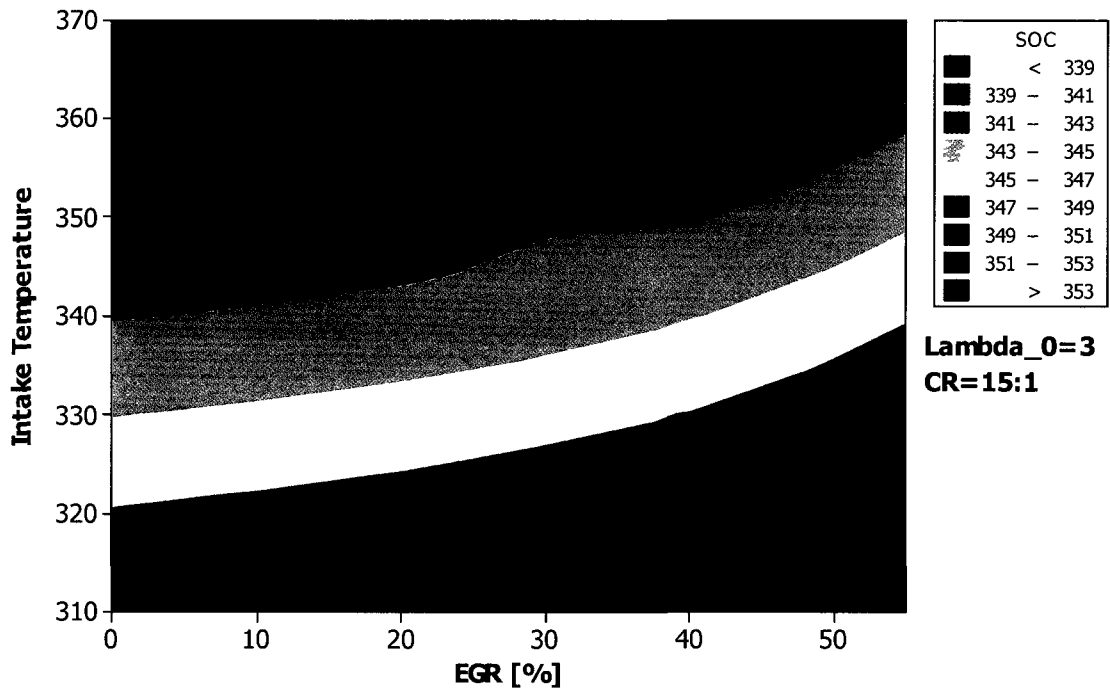
Figure 8-6: Contour plot for SOC as a function of T_{intake} and EGR (CR=15:1).
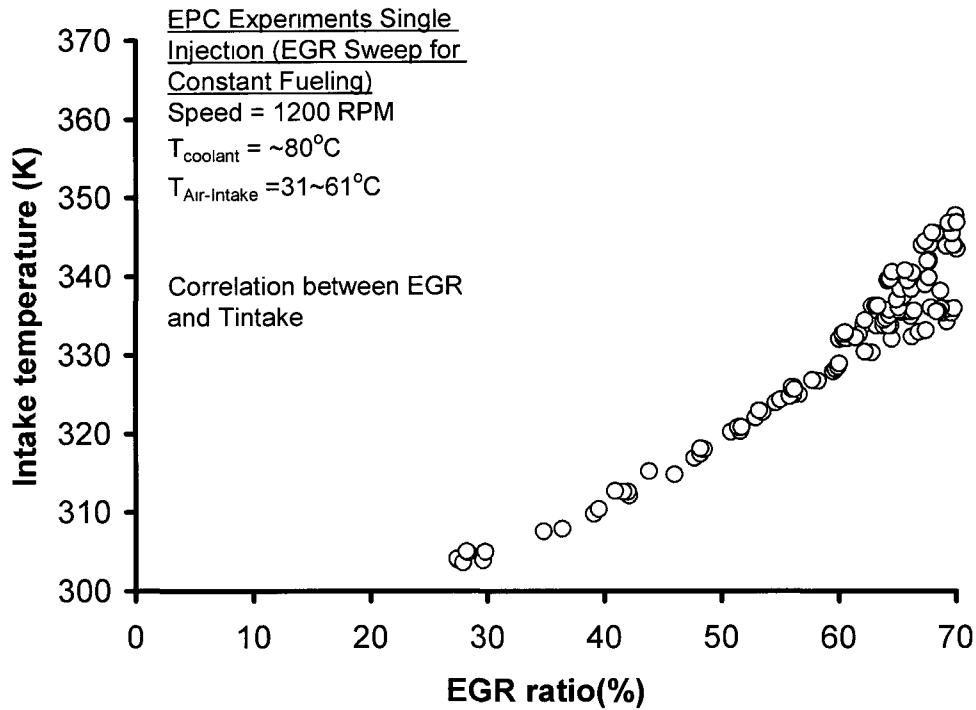
Figure 8-7: Relationship between the intake temperature and the EGR-rates during a typical EGR-sweep.

Therefore, based on the above analysis it was possible to estimate the boundary conditions necessary for the desired combustion phasing. The above guidelines were applied to the case of increasing load at a fixed rpm. This was important, because as the load increased at a fixed combustion phasing the rate-of-pressure increases, which manifests itself in the combustion noise. For a modern diesel engine a maximum-rate of pressure rise greater than 10~12 bar/degree is considered un-acceptable from the point of view of combustion noise. IMEP was considered as a representative of load and simulations were performed at 4, 6, 8, 10 and 12bar IMEP to study the effect of increasing load on combustion noise. For all these cases the equivalence and EGR ratio was kept fixed at λ_0 of 3.0 and 55% respectively.

First CHEMKIN simulations were performed to estimate the start-of-combustion and then this start-of-combustion and a simplified heat-release rate for multi-pulse EPC such as the one shown in Figure 7-4 was used as the input for the SAES simulation. This step helped to combine the advantages of both CHEMKIN and SAES. Now the combustion

phasing was decided by the kinetic process while the pressure was calculated based on an experimental heat-release rate. As the load is increased at a fixed λ_0, both the desired boost and the fueling requirement increase. This increases the maximum cylinder pressure (Pmax) and rate-of-pressure rise $(dp/d\theta)_{max}$ as shown in Figure 8-8, Figure 8-9, and Figure 8-10. It can be seen from Figure 8-10 that at higher loads of 10bar and 12 bar IMEP the maximum rate-of-pressure rise was more than the desired value of 10~12 bar/degree. Therefore, even though the EGR helped to retain the combustion phasing, further temperature modulation was required to limit the maximum rate-of-pressure rise. For this simulation study, temperature modulation by the use of lower compression ratio was then investigated. The start of combustion contours were calculated at new reduced compression ratio of 12 and the same boundary conditions of λ_0 and EGR. The assumption of lower compression ratio helps to postpone the combustion closer towards TDC for the same T_{intake} and EGR as the base compression ratio (Figure 8-11). Postponing the combustion-phasing closer towards the TDC helped to reduce the maximum rate of pressure-rise at high loads (Figure 8-12 and Figure 8-13).

Thus it can be seen that a systematic approach can be adopted to select the boost, EGR ratio and intake temperature for a given load to implement the multi-pulse EPC type of combustion at the desired combustion-phasing. The kinetics simulations were also able to identify the conditions where additional enablers such as variable-valve timing or variable compression ratio may be needed.
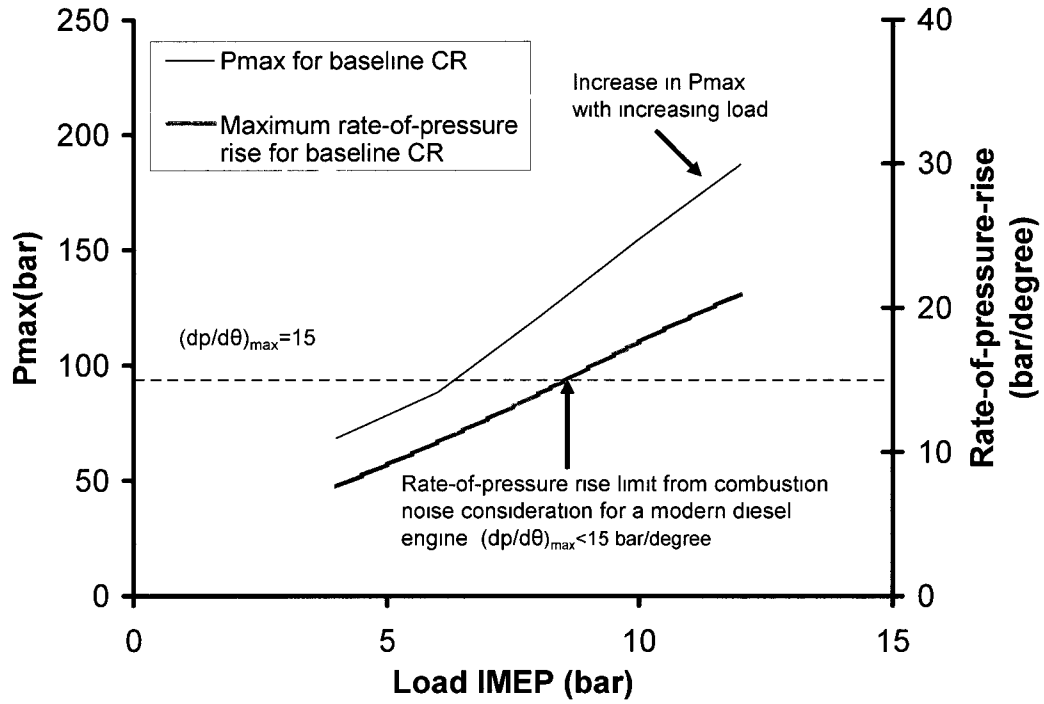
Figure 8-8: Increase in Pmax and maximum rate-of-pressure rise with increasing load for a fixed combustion phasing and fixed EGR.
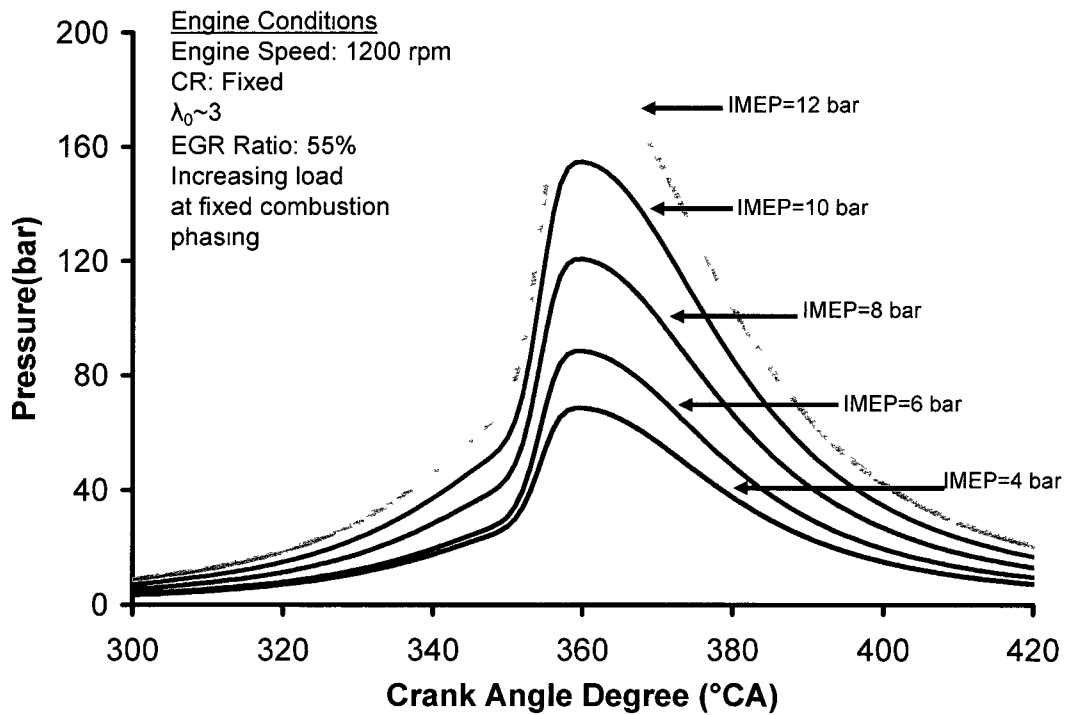
Figure 8-9: Increase in Pmax with increasing load for a fixed combustion phasing and fixed EGR.
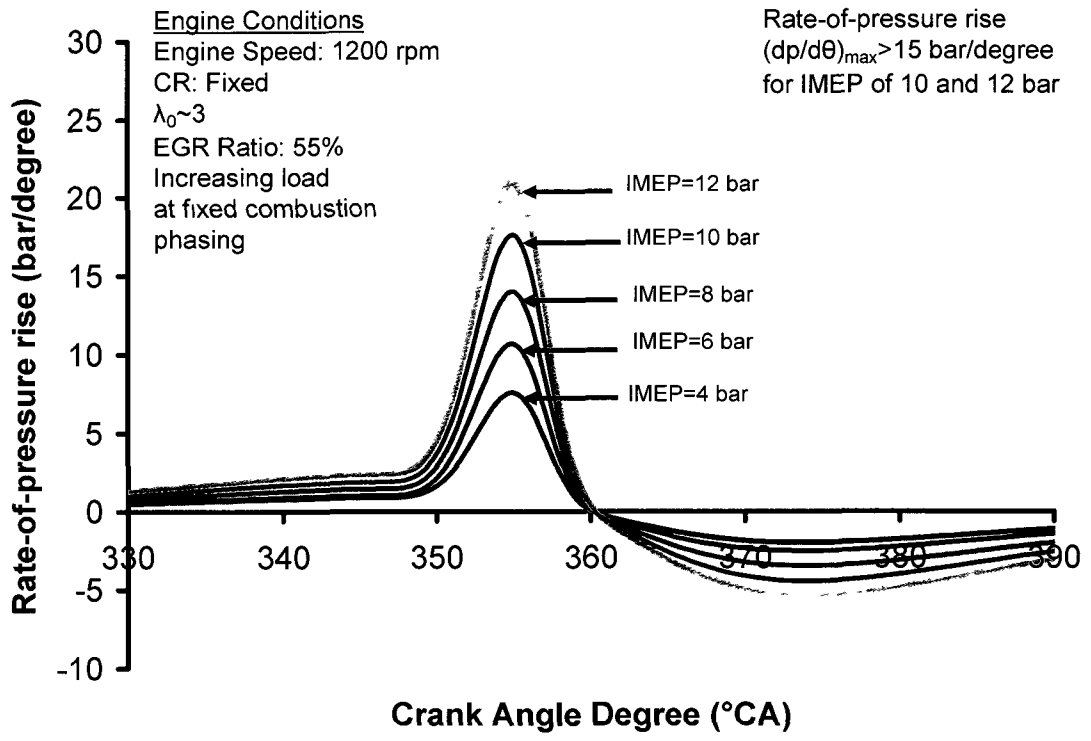
Figure 8-10: Increase in rate-of-increase of pressure with increasing load for a fixed combustion phasing and fixed EGR.
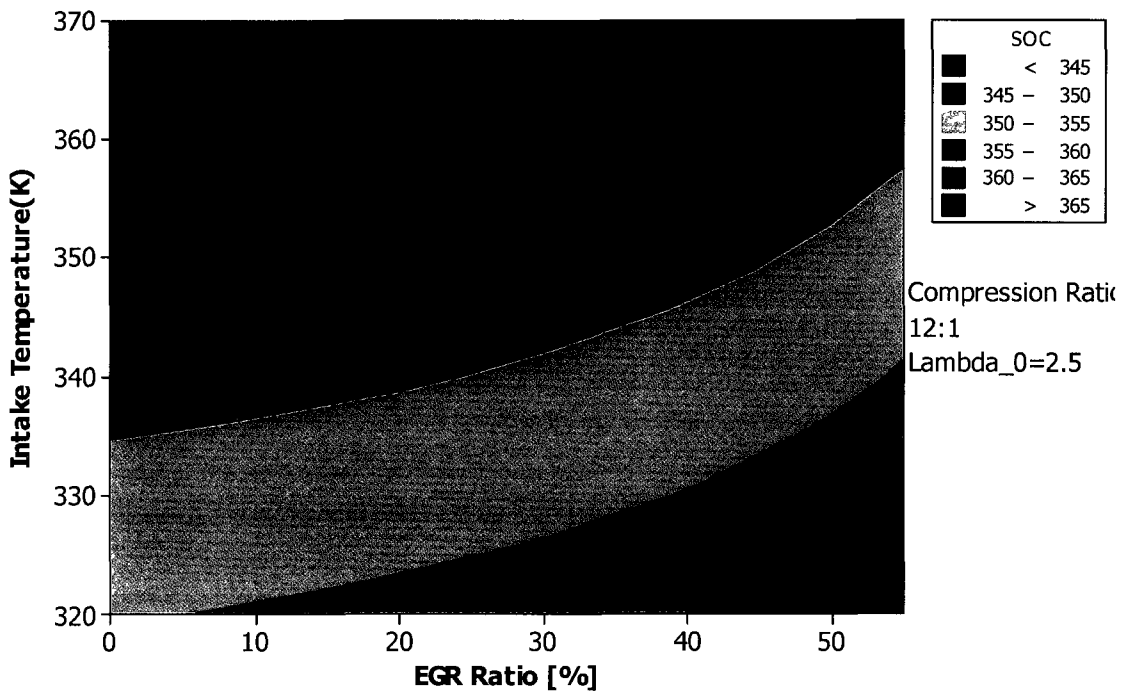
Figure 8-11: Contour plot for SOC as a function of T_{intake} and EGR (CR=12:1).
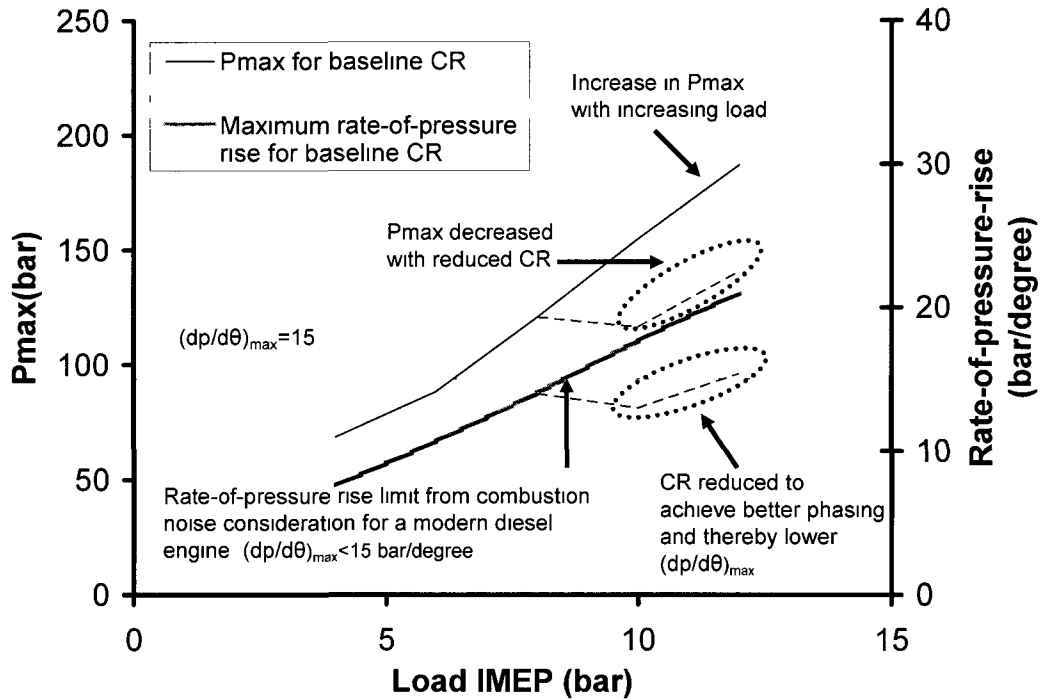
Figure 8-12: Increase in Pmax and maximum rate-of-pressure rise with increasing load for a fixed combustion phasing and fixed EGR.
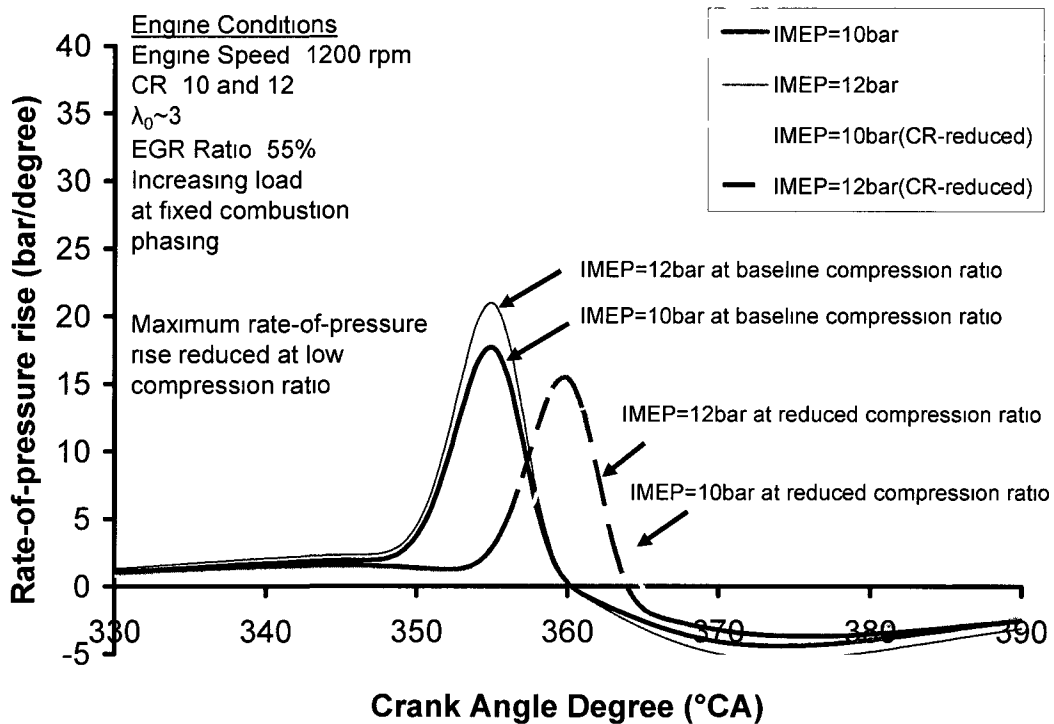
Figure 8-13: Decrease in rate-of-increase of pressure with the lowering in compression ratio.

142

8.2 Simulation Studies for EPC Combustion with EGR Fuel Reforming

Diesel exhaust temperatures normally range from 120°C to 720°C for non-turbocharged systems and 100°C to 600°C for turbocharged systems. The exhaust oxygen concentration usually ranges from about 19% to 4% for naturally aspirated engines and 19% to 7% for turbocharged engines; depending on the load conditions (Figure 8-14). Because of the significant amounts of surplus oxygen in the exhaust, a method was considered here to suppress soot production with the production of reformed gases in the EGR loop. The method also allows using the heat of the exhaust gases. In comparison, exhausts from stoichiometric combustion engines are not suitable for fuel reforming because of the obvious lack of oxygen.
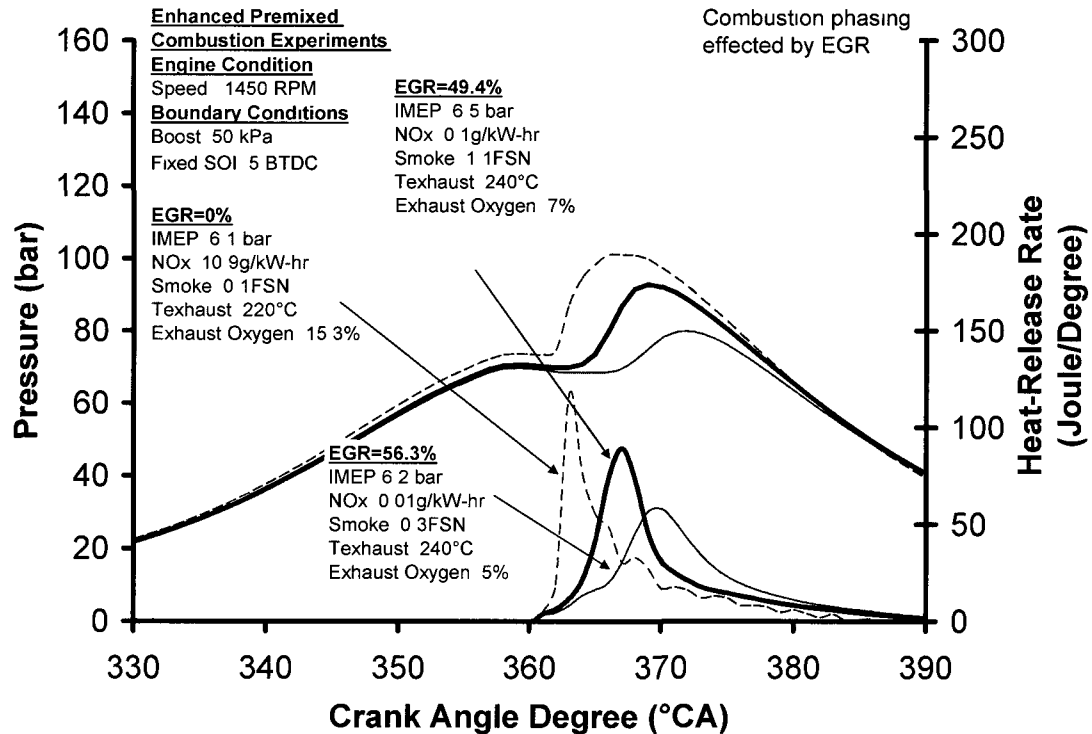
Figure 8-14: Exhaust temperature and exhaust oxygen concentrations during typical EPC running operation.

A schematic of the conceptual EGR reformer is shown in Figure 8-15. The conceptual EGR reformer allows generation of gaseous fuels; hydrogen (H_2) and carbon-monoxide (CO) in the EGR loop with the reforming of a controlled amount of diesel fuel in the

EGR loop. The H_2 and CO produced in the EGR reformer can enhance the in-cylinder premixed combustion and thereby reduce the soot formation.
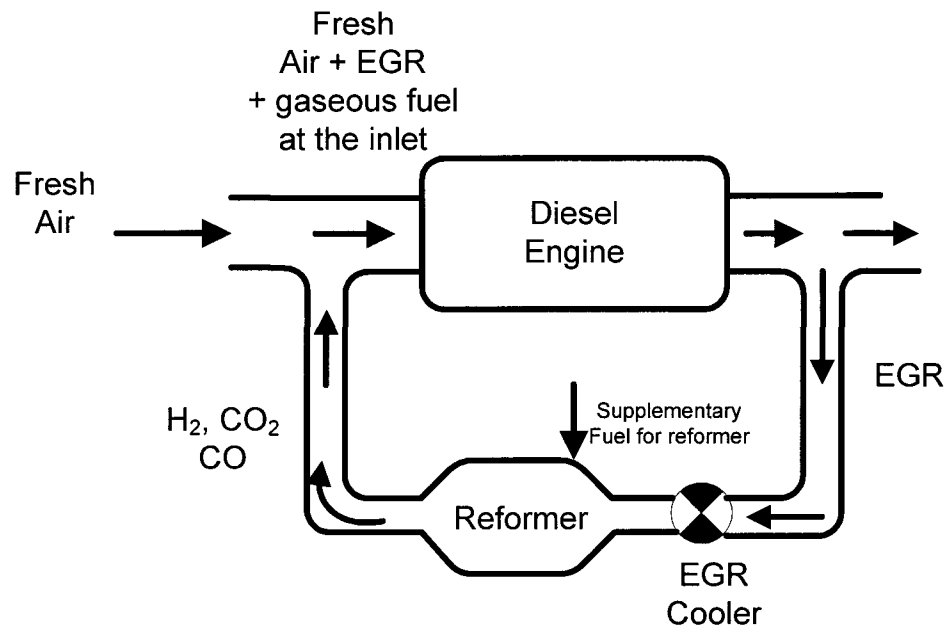
Figure 8-15: Conceptual layout of EGR reformer.

The concept of EGR reformer was investigated numerically by CHEMKIN modeling. Based on this modeling work, the boundary conditions for the operating the EGR reformer were formulated. This concept tries to utilize the heat of the exhaust; therefore an attempt has been made to estimate the reformer efficiency improvement by placing the reformer in the exhaust loop instead of placing it the intake loop.

Determination of boundary conditions: The important boundary conditions that need to be determined for the EGR reformer are the air–fuel ratio, temperature and the pressure of the EGR reformer. The first step was to estimate the hydrogen production as a function of air-fuel ratio, at a fixed temperature and pressure (Figure 8-16). The simulation studies indicated that increasing amounts of hydrogen was produced as the reformer's operating lambda was shifted towards the richer side of stoichiometry in the simulations. For these simulations, n-heptane was used as a representative of diesel fuel and the hydrogen productions estimations are based on equilibrium assumption. The hydrogen production peaked for a lambda of approximately 0.35 and beyond that the hydrogen production

decreased again. The production of other gaseous component CO, also showed a similar increase in production rates as the reformer lambda was shifted towards richer operating regions. The CO production showed an increasing trend up to a lambda of 0.2. Note that it is usually not preferred to run such low lambda values because of the fuel may undergo pyrolysis and result in fouling of the catalyst [68~70]. The sensitivity of hydrogen production towards temperature has been shown in Figure 8-17 and it can be seen that a minimum reformer temperature of 800~900K was needed for hydrogen production. Note that these temperature estimates are based on reactions in the absence of the catalyst; therefore in the presence of the catalyst the reactions temperatures would be significantly lower. Based on these simulations a reformer air-fuel ratio of 0.6 and a reformer temperature of 900K were used for the subsequent analysis.
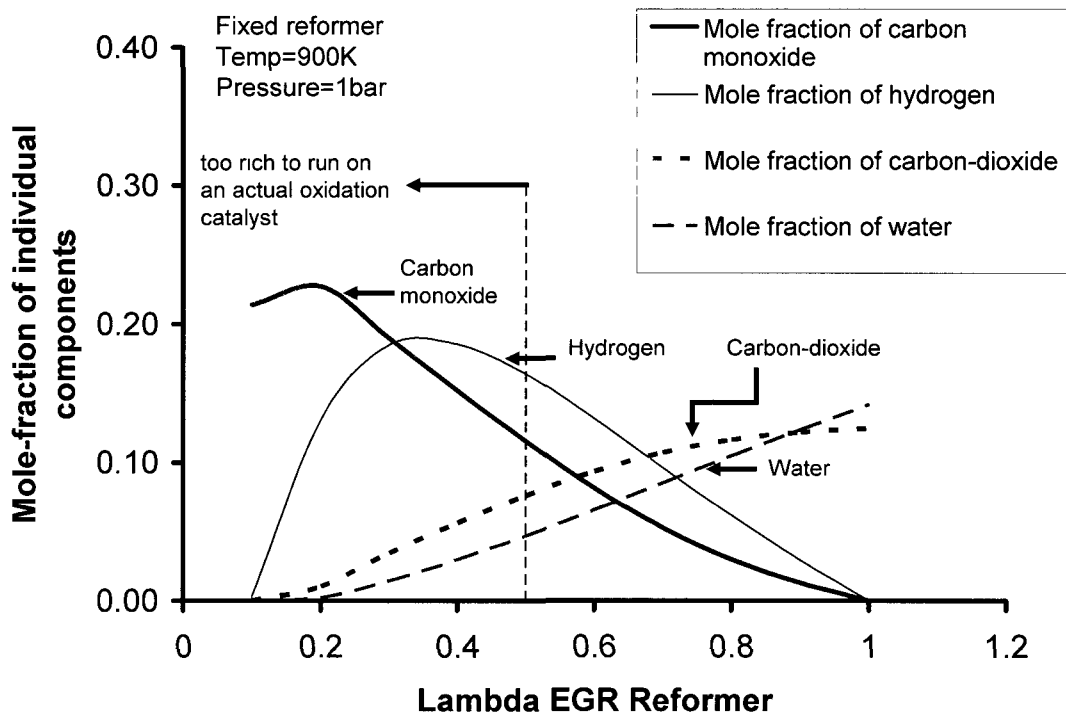
Figure 8-16: Effect of reformer operating lambda on the production of hydrogen and carbon monoxide.
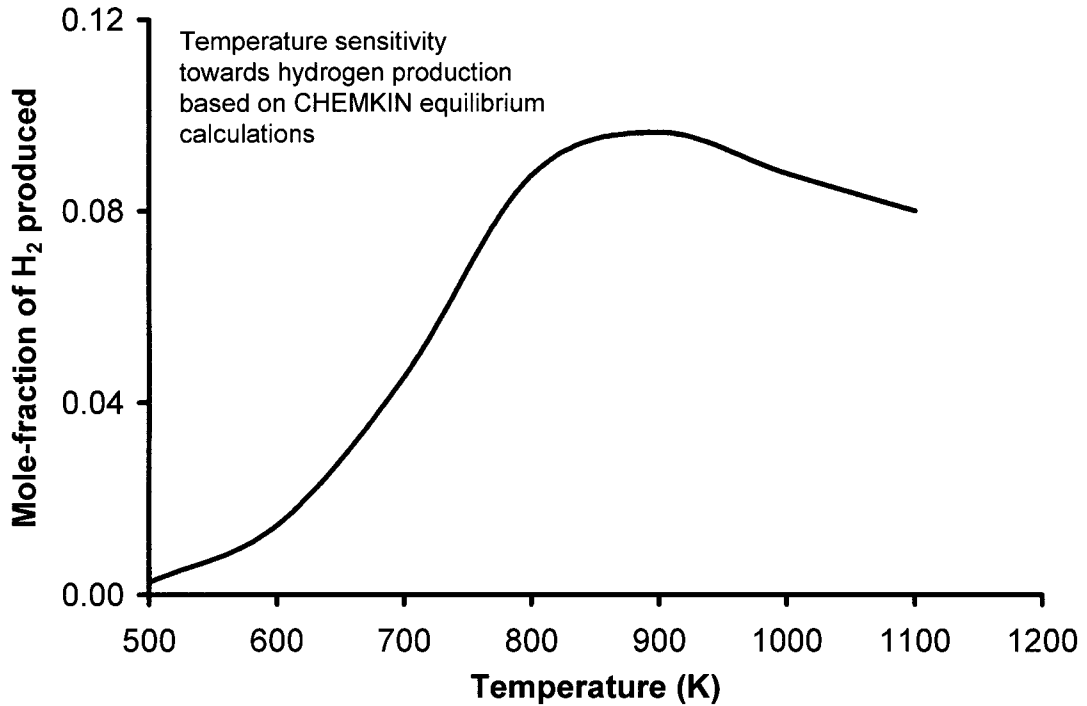
Figure 8-17: Sensitivity of temperature towards hydrogen production.

The next analysis was to estimate the efficiency benefit of using the reformer in the exhaust loop instead of the intake loop, to utilize the heat of the exhaust (Figure 8-18). To facilitate the efficiency analysis for the various operating conditions of the EGR reformer, the concept of adiabatic reformer energy retention efficiency was introduced and was defined as the amount of energy of the gaseous fuel divided by the sum of the energy of the reforming diesel added and the external heating. Therefore, the adiabatic EGR reformer energy retention efficiency was evaluated as,

$$\eta_{reformer} = \frac{\dot{m}_{H_2} LHV_{H_2} + \dot{m}_{CO} LHV_{CO}}{\dot{m}_f LHV_{diesel} + Q_{ext\_heating}}$$

Based on the above definition, by placing the reformer in the exhaust loop, the thermal energy carried in the exhaust gases could be utilized and leads to the reformer efficiency improvements (Table 8-1).

146

Table 8-1: Comparison of reformer efficiency

Reformer Position	Reformer Efficiency		
	1100 K	1200K	1300K
Intake-loop	0.66	0.6	0.58
Exhaust Loop	0.75	0.69	0.66
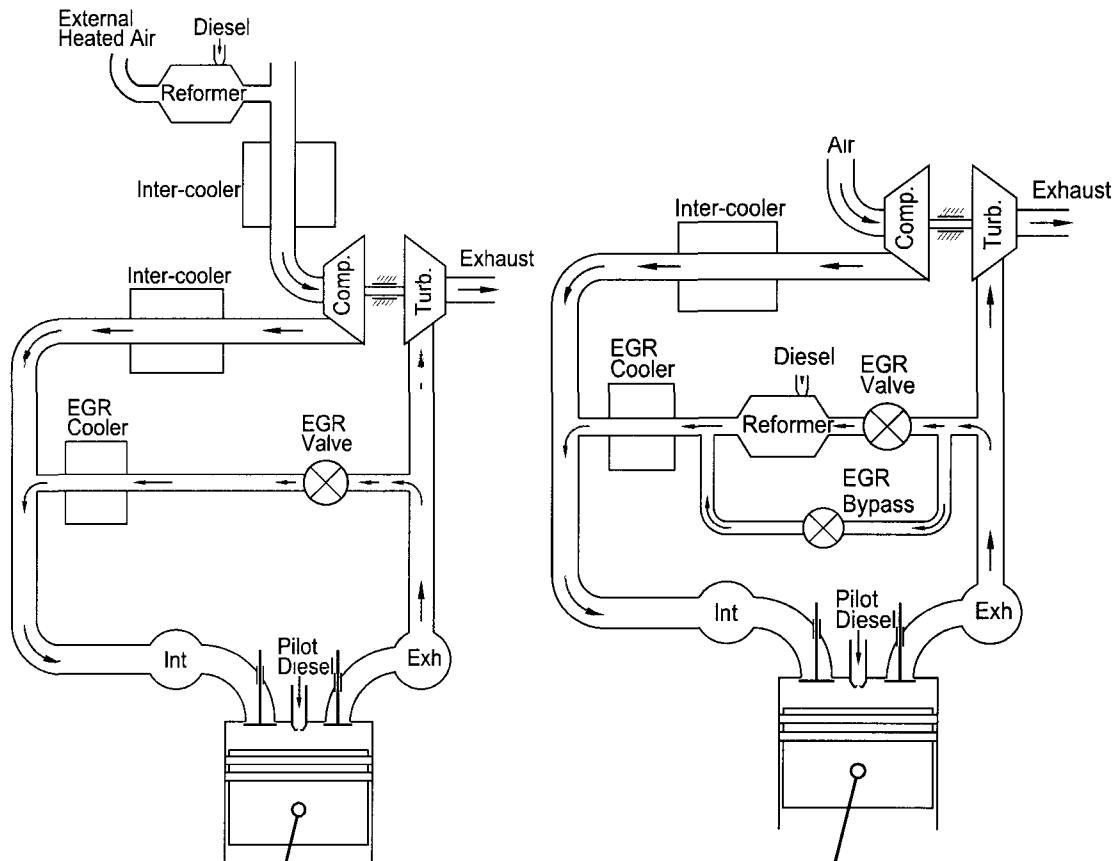
Figure 8-18: Fuel reformer in intake and exhaust loop.

Based on this calculated EGR-reformer efficiency, an overall-energy efficiency analysis was performed for the combined engine and the EGR-reformer system. The use of hydrogen has been reported to improve the brake thermal efficiency due to enhanced rates of combustion. For the present work, assumptions were made based on the results obtained by previous researchers and a linear relationship has been observed between the mass fraction of H_2 used as fuel and the improvement in brake thermal efficiency [71,72].

For the initial analysis the effect of CO has been ignored. Four different cases have been assumed for the simulations:

Case A: No improvement in thermal efficiency of the engine due to H_2 addition

Case B: For every 1% thermal energy contributed from H_2, there is 1% improvement in the thermal efficiency of the engine.

Case C: For every 1% thermal energy contributed from H_2, there is 0.5% improvement in the thermal efficiency of the engine.

Case D: There is a decrease in brake thermal efficiency due to the H_2 addition.

Table 8-2: Assumption values with linear brake thermal efficiency improvement

	Brake thermal efficiency improvement			
Gaseous fuel energy fraction in diesel engine (%)	None A	Aggressive B	Passive C	Decrease D
0	0.41	0.41	0.41	0.41
1	0.41	0.42	0.41	0.40
2	0.41	0.43	0.42	0.39
5	0.41	0.46	0.44	0.36
10	0.41	0.51	0.46	0.31
15	0.41	0.56	0.49	
20	0.41	0.61	0.51	

If $\eta_{original}$ is the original brake thermal efficiency and η_{new} is the new assumed brake thermal efficiency of the engine with H_2 addition, then the efficiency of the EGR reformer system can be written as

$$\eta_{new\_overall} = \frac{\eta_{new} \times \dot{m}_f Q_{LHV\_diesel}}{\left(\dot{m}_{f,reformer} + \dot{m}_{f,engine}\right) Q_{LHV\_diesel}}$$

The overall efficiency based on above equation and Table 8-2 is given in Table 5. For these computations the EGR reformer efficiency of 0.4 was used. It can be seen that a small amount of H_2 (1~2%) can be added without a significant energy penalty if there is little or no change in brake thermal efficiency.

Table 8-3: Calculated overall efficiency accounting for the effect of hydrogen production on the overall brake-thermal efficiency.

	$\eta_{new\_overall}$			
H_2 energy in diesel engine (%)	None A	Aggressive B	Passive C	Decrease D
0	0.41	0.41	0.41	0.38
1	0.40	0.40	0.39	0.35
2	0.40	0.39	0.38	0.28
5	0.38	0.39	0.37	0.20
10	0.36	0.41	0.37	
15	0.33	0.44	0.38	
20	0.32	0.47	0.40	

8.3 Multi-Dimensional Modeling

The three-dimensional KIVA (version KIVA3V) code has been used to understand the combustion process for the conventional and EPC combustion modes. The KIVA code included detailed sub-models to describe each of the important factors influencing the diesel combustion such as the sub-models for atomization, drop distortion, drag, spray break-up, droplet collision, droplet coalescence, drop vaporization and spray/wall interaction. The Shell auto-ignition model was used to model the ignition process. The characteristic-time combustion model was used to model the combustion process. The combustion model included parameters to consider both the laminar and the turbulent part of the combustion process. Furthermore, the Zeldovich mechanism was used for predicting NOx formation, and soot model was based on the work by V. F. Surovikin [73], with the rate constants from Nagle and Strickland-Constable [74]. Tetra-decane was used as the fuel for the simulations, since it has a carbon/hydrogen ratio similar to the experimental fuel. As a first step towards the use of CFD analysis, the experimental data for the conventional combustion was used to validate KIVA results. The experimental fuel-injection parameter, intake-temperature, pressure and composition were used as input for the KIVA model. A comparison of the global quantities namely; pressure and heat-release rate was made for the experimental and the simulation cases. At this stage, some of the model constant had to be calibrated to match the experimental results. The same model-constants were then used for the rest of the analysis. Note; the model constant calibration had to be done separately for the conventional and EPC combustion.

A comparison between the experimental and modeled cylinder pressures and heat-release quantities are shown in Figure 8-19 for the case of conventional combustion. For a conventional combustion a close match in the bulk parameters of pressure and heat-release was observed. However, the present combustion model was insufficient to describe the combustion during the EPC combustion regime. Therefore, the KIVA model was used only to describe the mixing process during for EPC combustion.
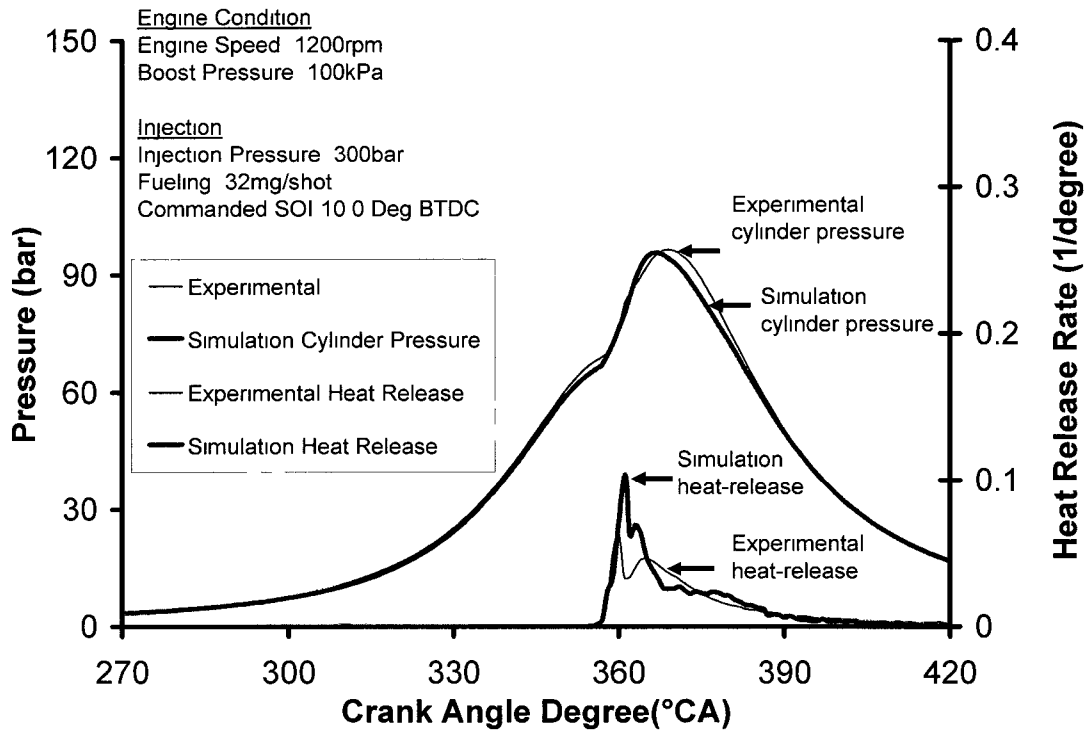
Figure 8-19: Comparison of experimental and simulation cylinder pressure and heat-release rate characteristics.

Mechanism of conventional combustion: An attempt was made to understand the mechanism on conventional combustion by plotting the progress of the combustion on the ϕ-T map and examining the heat-release rate (Figure 8-20~Figure 8-23). As discussed previously, the conventional combustion consists of three major stages; the ignition delay period, the premixed combustion phase and the diffusion combustion phase. ϕ-T map was plotted independently for all the three stages. For the conventional combustion, the in-cylinder bulk temperatures were significantly higher than the initial boiling point of the fuel and therefore the vaporization was readily initiated after the injection. To initiate the combustion process, the fuel has to be within the flammability limits and the temperature should be above the auto-ignition temperature. For the conventional combustion, the in-cylinder temperatures were close to the auto-ignition temperatures, therefore as soon as the fuel-air mixture was mixed to the flammability limits during the ignition delay period the combustion was readily initiated. During the pre-mixed combustion (Figure 8-22), little additional mixing took place, while during the diffusion phase (Figure 8-23) was mixing dominated and wide range of ϕ could be seen on the ϕ-T map.
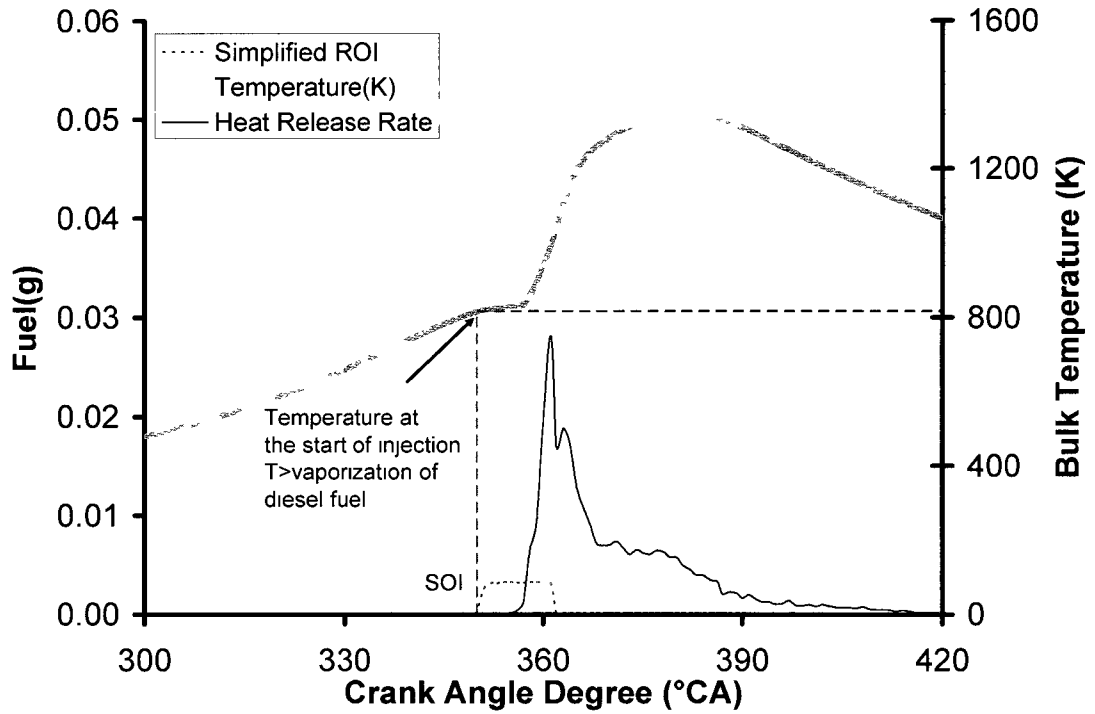
Figure 8-20: The bulk temperature, heat-release rate and modeled rate-of-injection for the conventional combustion.
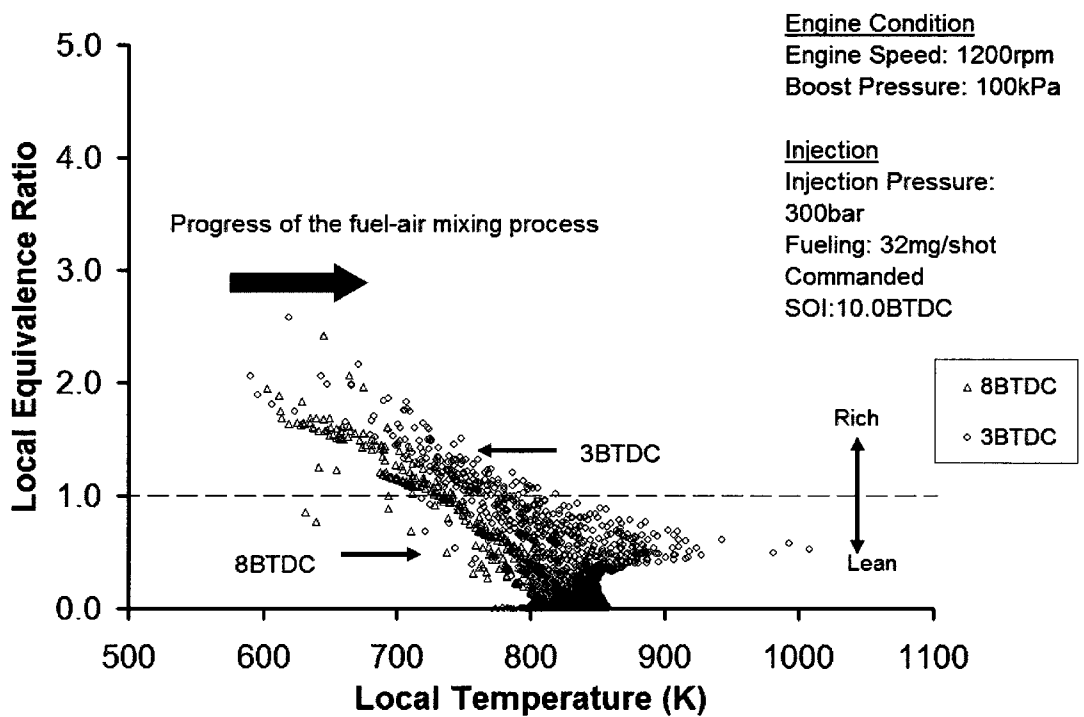
Figure 8-21: Combustion process on the ϕ-T map during the ignition-delay period.
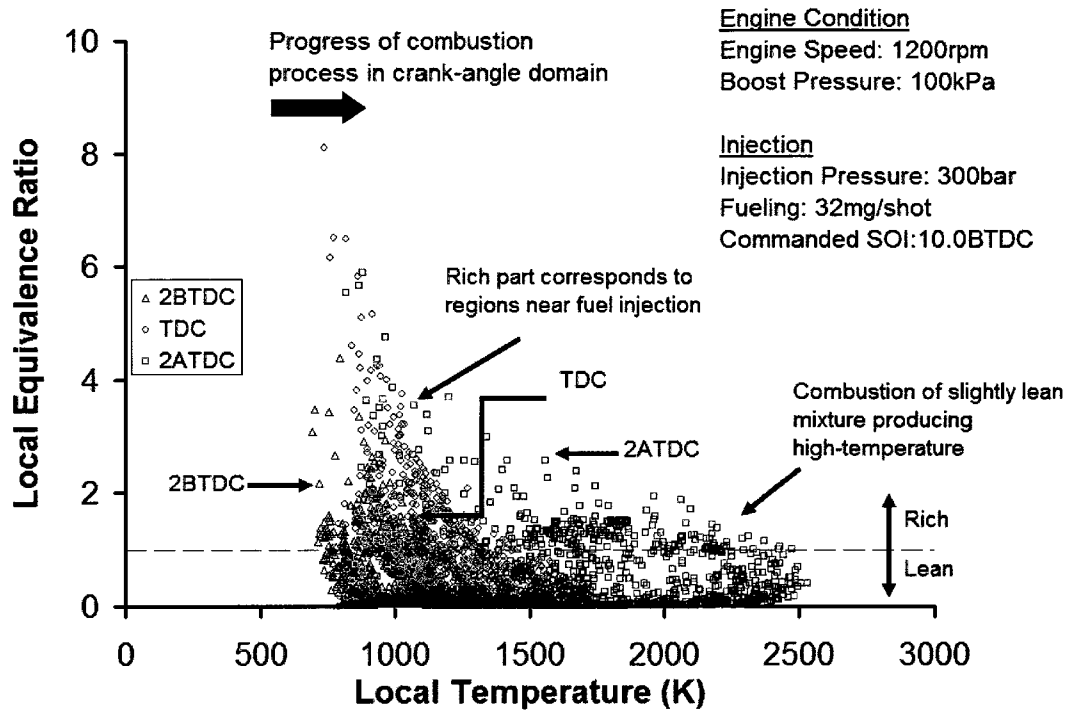
Figure 8-22: Combustion process on the φ-T during the pre-mixed combustion period.
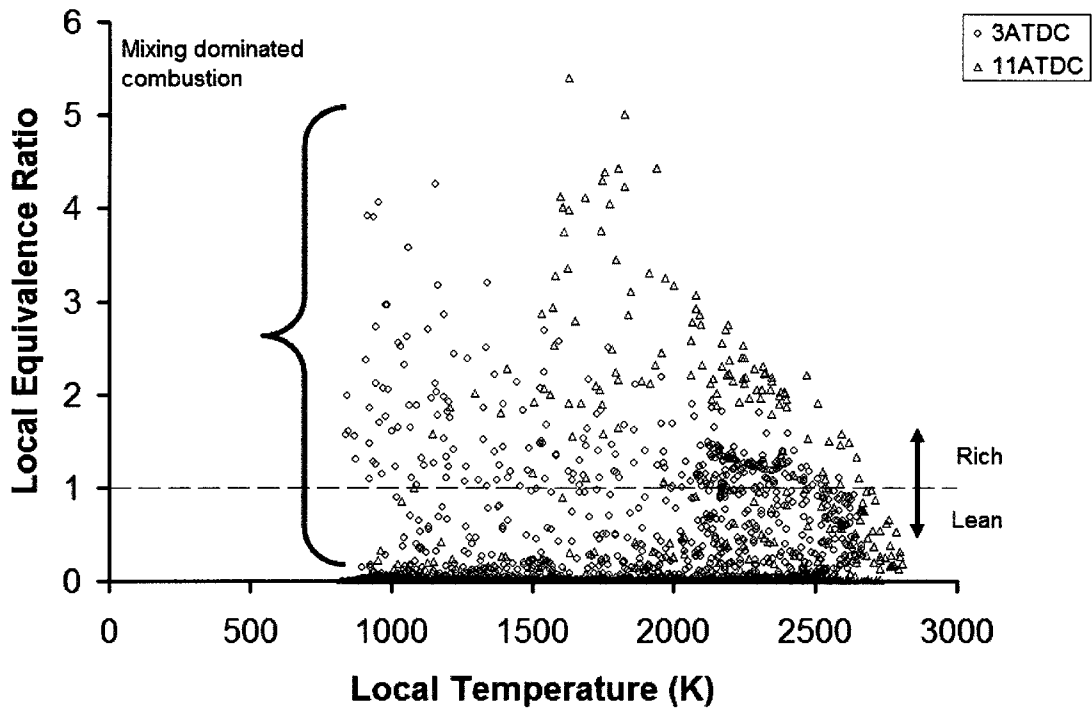
Figure 8-23: Combustion process during the diffusion combustion period.

Enhanced-premixed combustion: For modeling the EPC, the case of a single injection strategy early during the compression process was chosen as the reference. The simulation conditions are as shown below in Table 8-4. For the EPC, the commanded SOI was configured at 38BTDC. At this SOI value, the bulk in-cylinder temperature was lower than the auto-ignition temperature (Figure 8-24). The presence of EGR also had a significant impact on withholding the initiation of the combustion process. Therefore, when the fuel-air mixture reached the flammability limits ($0.6<\phi<1.2$) for the combustion, the temperatures were lower than the auto-ignition value. Thus the combustion process was not initiated and the mixing process continued further in time. This additional time gained helped in the preparation of a weak-homogenous mixture.

The use of KIVA helped to understand the major differences between the conventional combustion and the EPC. As a recap, for the conventional combustion the in-cylinder temperatures are close to the auto-ignition temperatures and as soon as the fuel-air mixture is prepared to the flammability limits the mixture auto-ignites. For the EPC combustion the attainment of auto-ignition temperature lags behind the mixture preparation. Therefore, when the mixture was close to stoichiometric conditions, the temperature was still lower than the auto-ignition temperature. Therefore the mixture dilution continues further and by the time the auto-ignition temperature is attained a lean-homogenous or a weak-homogenous mixture is prepared before the combustion process.

Table 8-4: Simulation conditions for EPC combustion

Engine Speed	1200 rpm
Injection Pressure	1200 bar
SOI	38BTDC
Fuel Injection Quantity	23 mg/stk
Boost	85kPa
EGR	50%
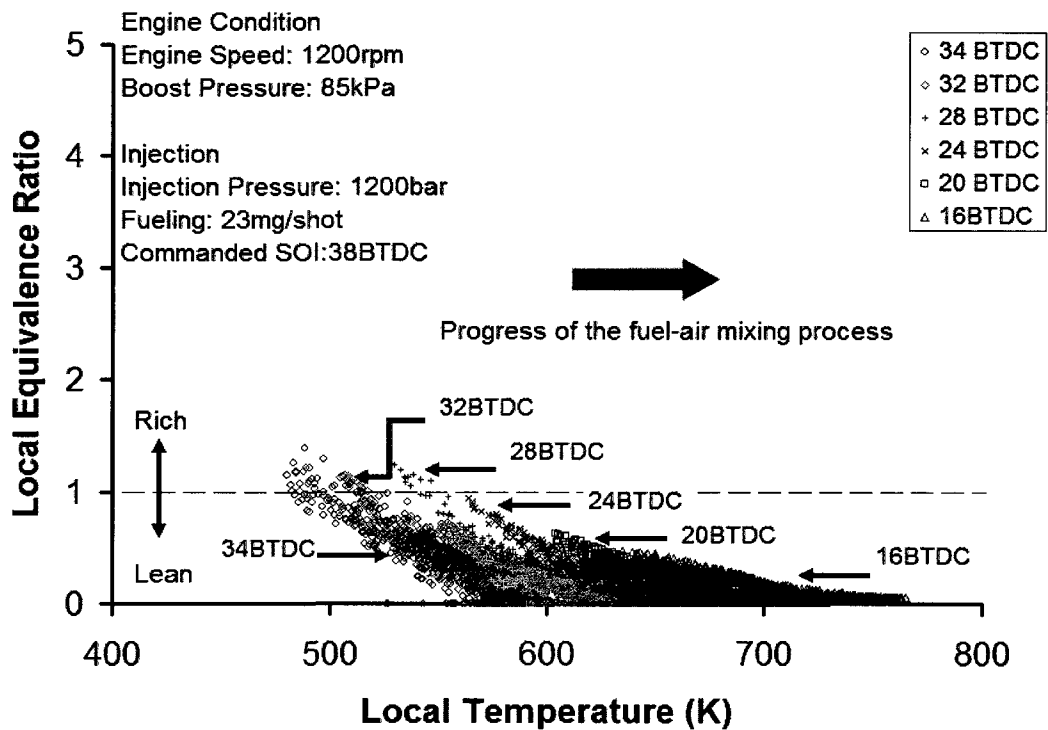
Figure 8-24: Mixing process during the ignition delay period for the EPC combustion.

CHAPTER IX

9 HEAT-RELEASE RATE CHARACTERIZATION

In this chapter, the correlation between the heat-release characteristics and emission/efficiency has been extended to EPC combustion. The influence of heat-release characteristics on emissions for conventional diesel combustion has been investigated extensively in the past and the heat-release characteristics have been correlated with the NOx or the soot production [4, 7, 8]. Figure 9-1 shows the heat-release rate for an engine with a typical mechanical fuel-injection system and no emission control. An examination of the heat-release rate shows a significant portion of the fuel undergoing diffusion dominated combustion resulting in high soot. The injection timing was configured at 17°CA before TDC to obtain the combustion phasing for best efficiency. This advanced combustion phasing resulted in high NOx. The heat-release rate such as the one shown in Figure 9-1 was more common before the advent of stringent emission control measures.
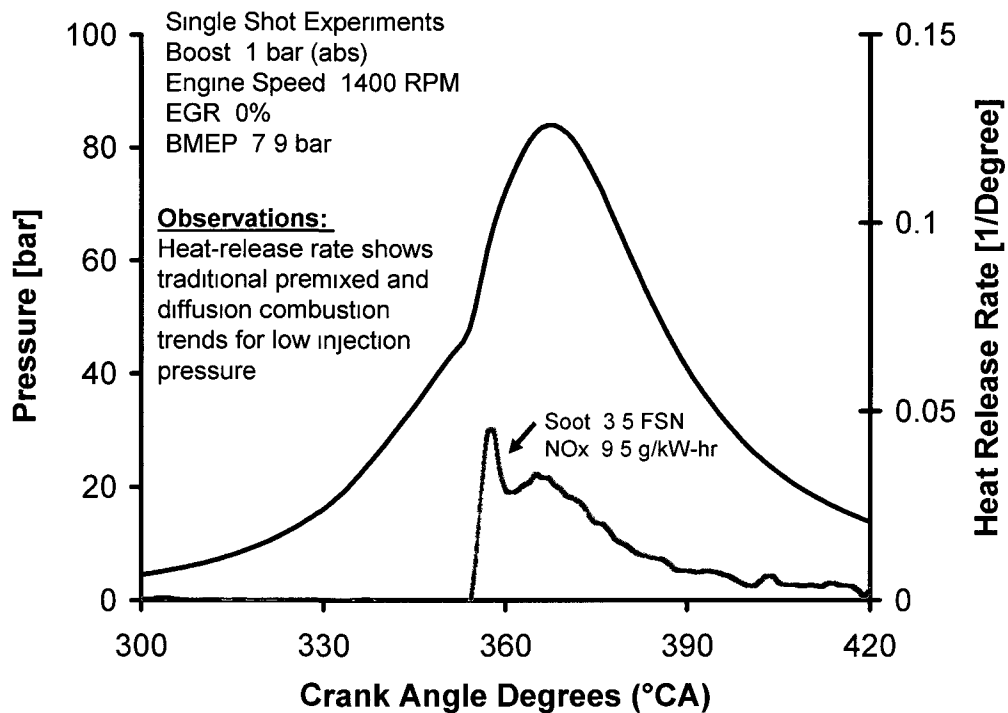
Figure 9-1: Heat-Release rate characteristics for classical diesel combustion without emission control [75].

156

Figure 9-2 shows the heat-release rates with two important NOx emission control techniques; injection timing retard and split injection marked "A" and "B". The additional heat-release rate "C" shows combustion with post-injection for exhaust after–treatment devices.
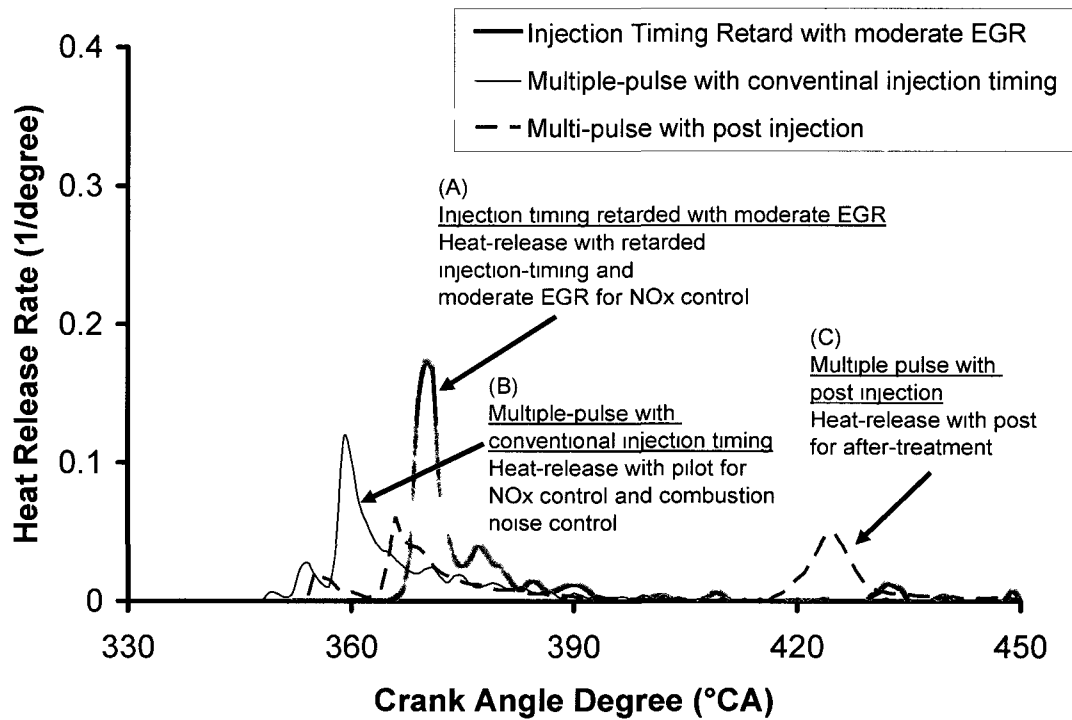
Figure 9-2: Heat-release rates configured for NOx control and post-injection for diesel after-treatment.

This discussion highlights the correlation between the heat-release characteristics and combustion in a modern diesel engine. As mentioned earlier in this chapter, the correlation between the heat-release characteristics and emission/efficiency has been extended to EPC combustion. Based on such an analysis EPC heat-release rate characteristic that meets the following criteria has been produced:

- simultaneous low-NOx and soot emission

- limited increase in carbon-monoxide and hydrocarbon emissions

- retain conventional-diesel cycle efficiency

Once the criteria of heat-release rate necessary for the EPC was established, the transition from the conventional to EPC regimes was performed with the assistance of a simplified heat-release based control.

9.1 Heat-Release Pattern for NOx

The commonly applied techniques for NOx reduction are EGR, injection timing retard and pilot-injection. However, to meet the forthcoming stringent emission norms diesel engine manufacturers are increasingly relying on EGR as the primary in-cylinder NOx control technique [76~77]. The first step was to understand the efficacy of the major techniques; EGR and pilot-injection for NOx reduction. Injection-timing has not been discussed separately as the applicability of this technique has reached its limits. An EGR sweep was performed at a fixed combustion phasing for the case of single injection and 2-injection strategies (Figure 9-3).
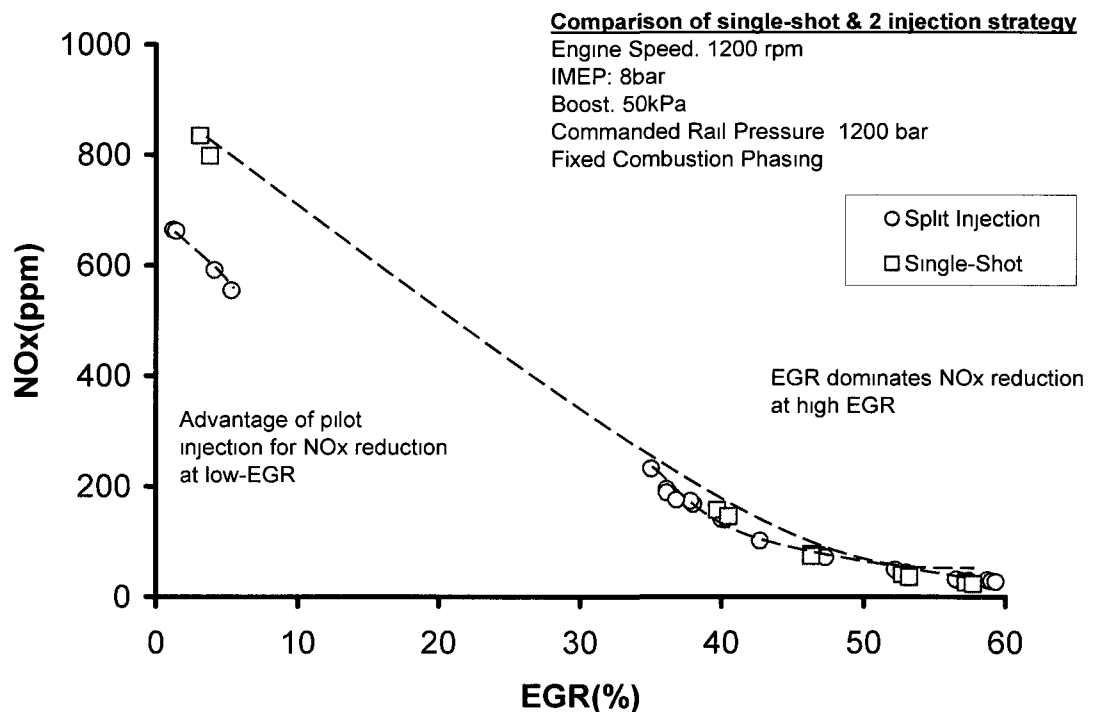
Figure 9-3: Effect of continuously increasing EGR with a fixed combustion phasing for single injection and 2 injection strategies.

At zero EGR, the use of pilot injection reduced NOx in comparison to the single injection strategy; however, after 40% EGR, the NOx was largely decided by EGR (Figure 9-4~Figure 9-6). At very high EGR levels (Figure 9-6) the initiation of the pilot combustion was suppressed and the heat-release rate was similar to the case of single injection. The fixed combustion phasing was achieved by the adaptive fuel-injection control described previously. The corrections were applied only to shifting the main and the pilot-injection with the same dwell when the EGR was changed. Also, the ratio of the pilot to the main injection quantity was kept constant for the entire EGR sweep. The mid-heat-release rate was kept fixed at 5 degrees after TDC. This value was decided based on the experimental and simulation studies which indicated that the indicated-efficiency peaked with CA-50 between 5~7 degrees after TDC when the heat-release duration was less than 40°CA
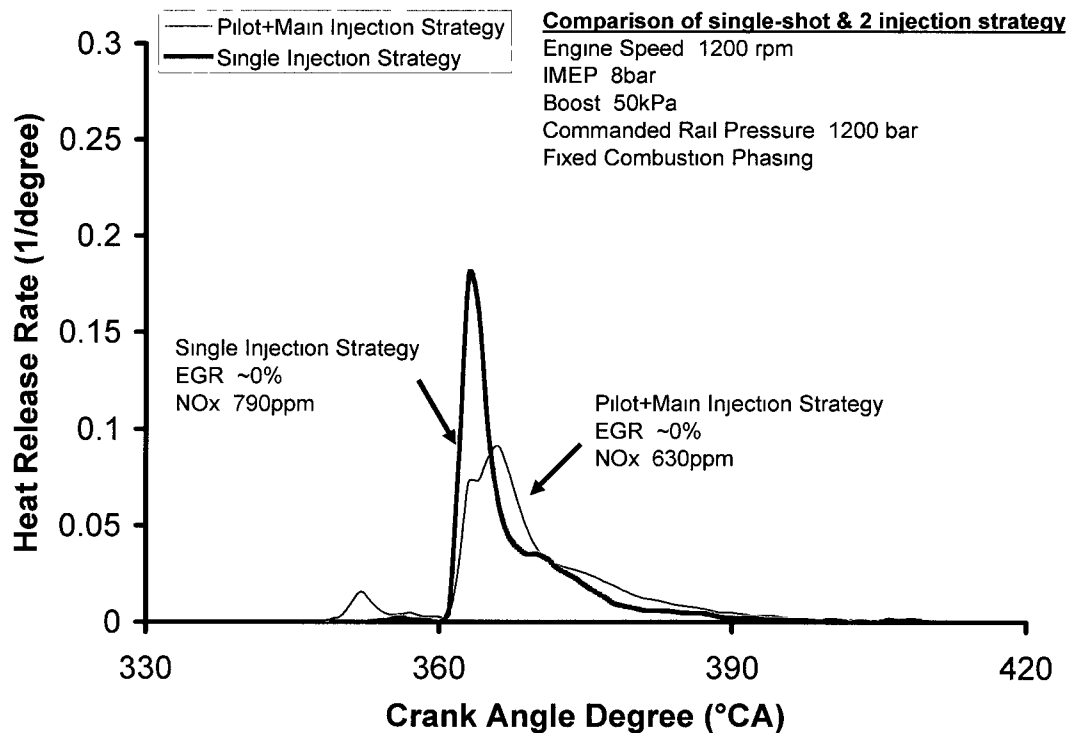
Figure 9-4: NOx reduction by use of pilot injection (very-low EGR).
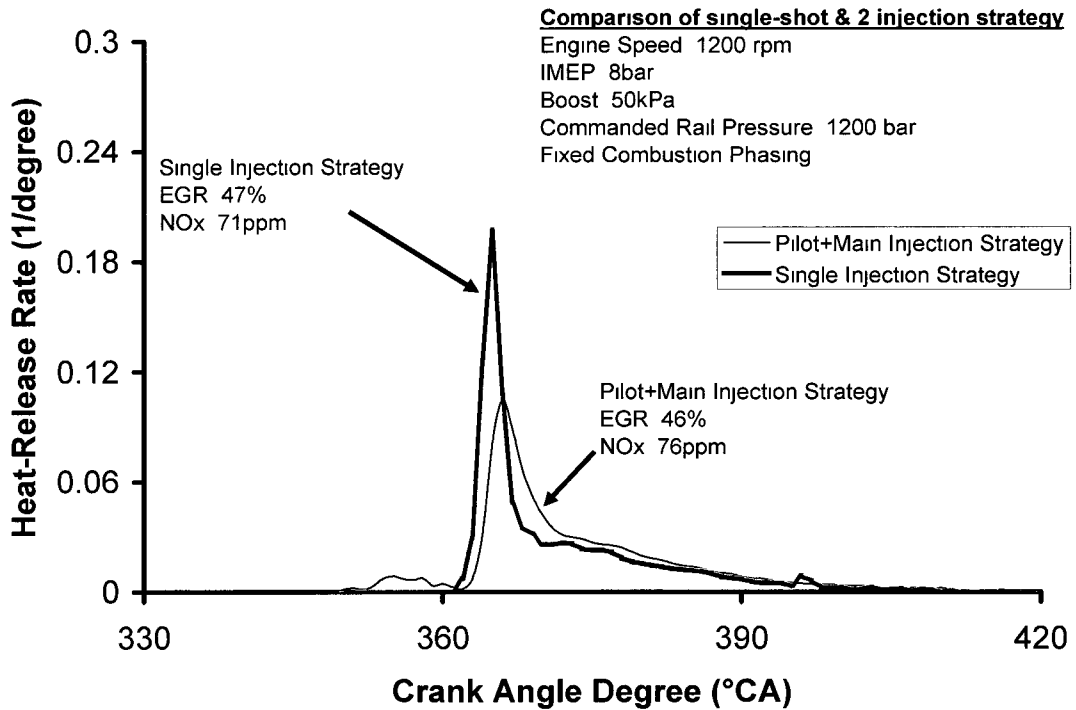
Figure 9-5: Combined effect of EGR and pilot injection for NOx reduction at moderate EGR.
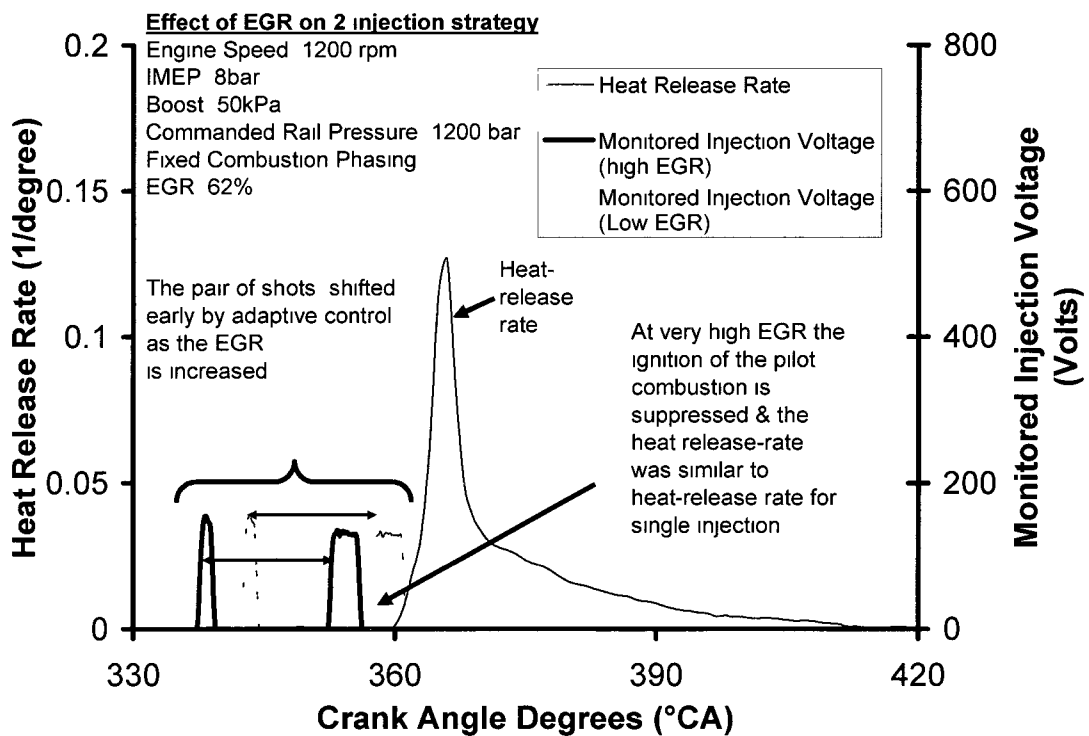
Figure 9-6: Initiation of pilot-combustion suppressed by the use of heavy EGR.

The NOx-EGR behavior was also investigated at other injection pressures and loads for single-injection strategy and it was observed that the NOx decreases monotonically with EGR for all the test conditions (Figure 9-7).
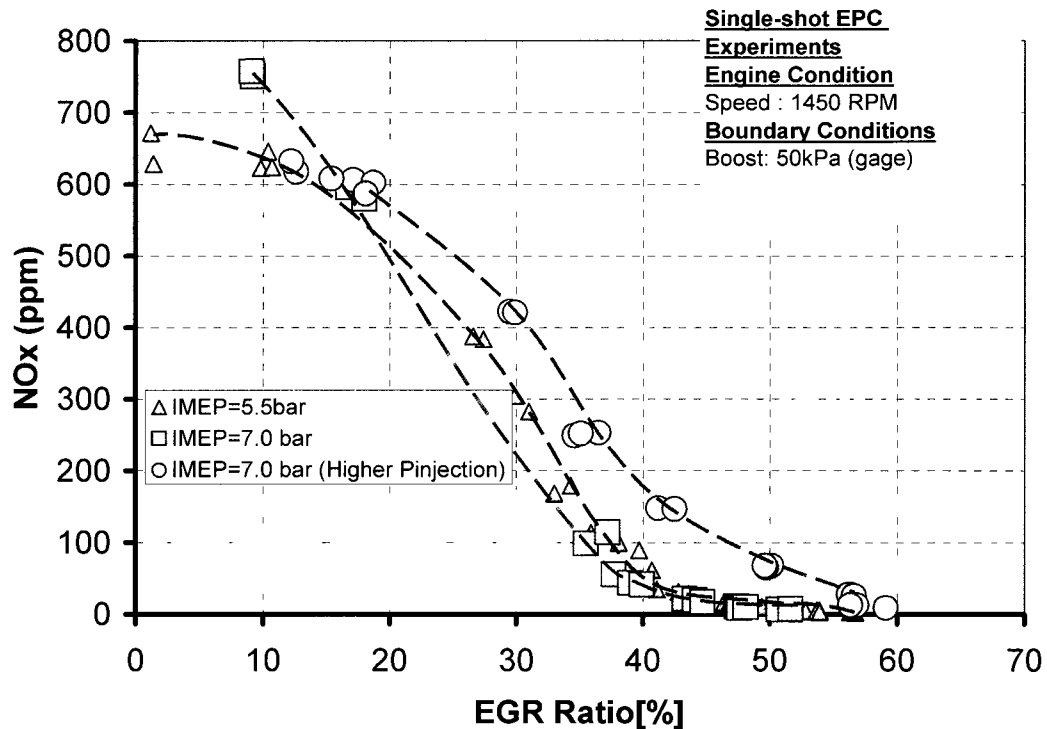
Figure 9-7: Continuous decrease in NOx with increasing EGR.

The experimental data shown in Figure 9-7 for the NOx-EGR curve at different loads converged into a single curve when plotted as a function of intake oxygen, suggesting that the dilution effect was strongest for the present experiment conditions (Figure 9-8). Thus it was observed that for achieving the stringent emission levels the NOx would have a stronger correlation with EGR or intake oxygen % than with the heat-release rate. The NOx and intake charge dilution correlation has been observed by other researchers also [54~56]. The CO formation during EPC was another characteristic that was largely dependent on the EGR/intake oxygen levels. No significant correlation was observed between the heat-release rate pattern and CO formed during EPC.
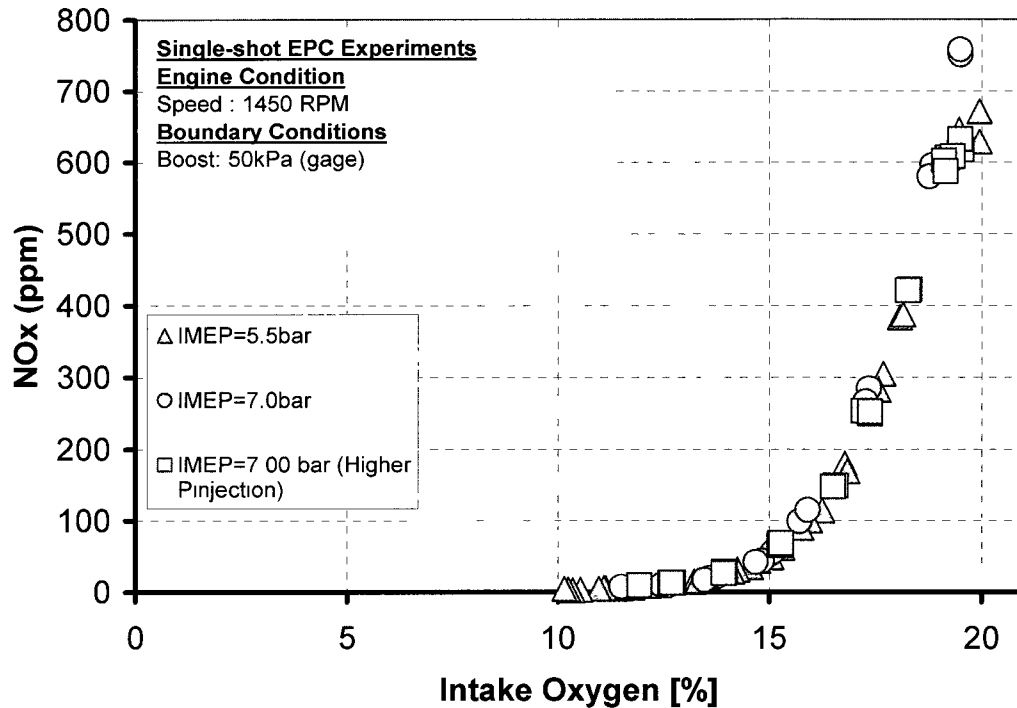
Figure 9-8: NOx as a function of intake oxygen for different load conditions.

9.2 Heat-Release Pattern for Soot

Two approaches have been used to achieve simultaneous low NOx and low soot in presence of EGR. The first approach was the multiple injection strategy with heavy EGR, called multi-pulse-EPC-injection-strategy (Figure 6-6). In this strategy the entire fuel was delivered during the compression stroke in a series of precisely controlled injection pulses. Figure 9-9 again revisits the multi-pulse EPC with three progressively increasing levels of EGR. For 45% EGR, the combustion was initiated immediately after the end of third injection, therefore very little time was available for preparation of the homogenous charge for the third injection, resulting in high soot. When higher amounts of EGR were applied the ignition delay for the third injection was also prolonged providing ample time for mixing for the third injection, thereby resulting in lower soot. Therefore, it can be seen that the injection with the shortest ignition delay had a significant bearing on the soot formation and this ignition delay was called the minimum mixing duration (Figure 9-10). Note that the significance of the last injection would also depend on the fraction of the overall fuel injected.
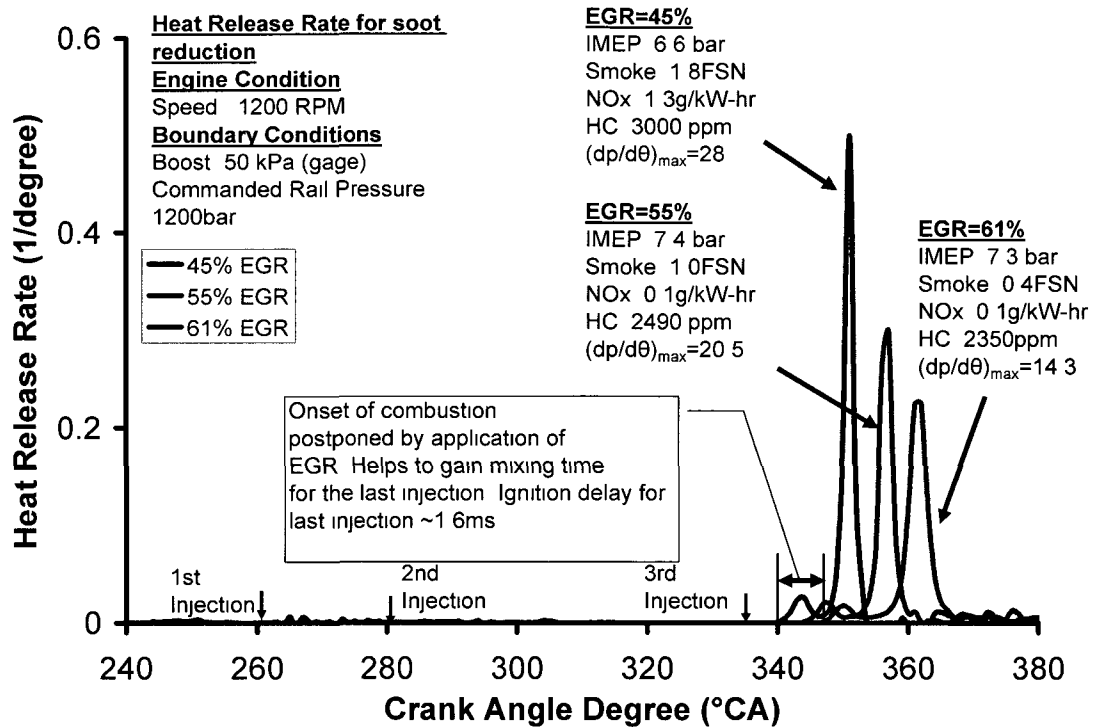
Figure 9-9: Heat-release rate for soot reduction with multiple-injection and application of EGR.
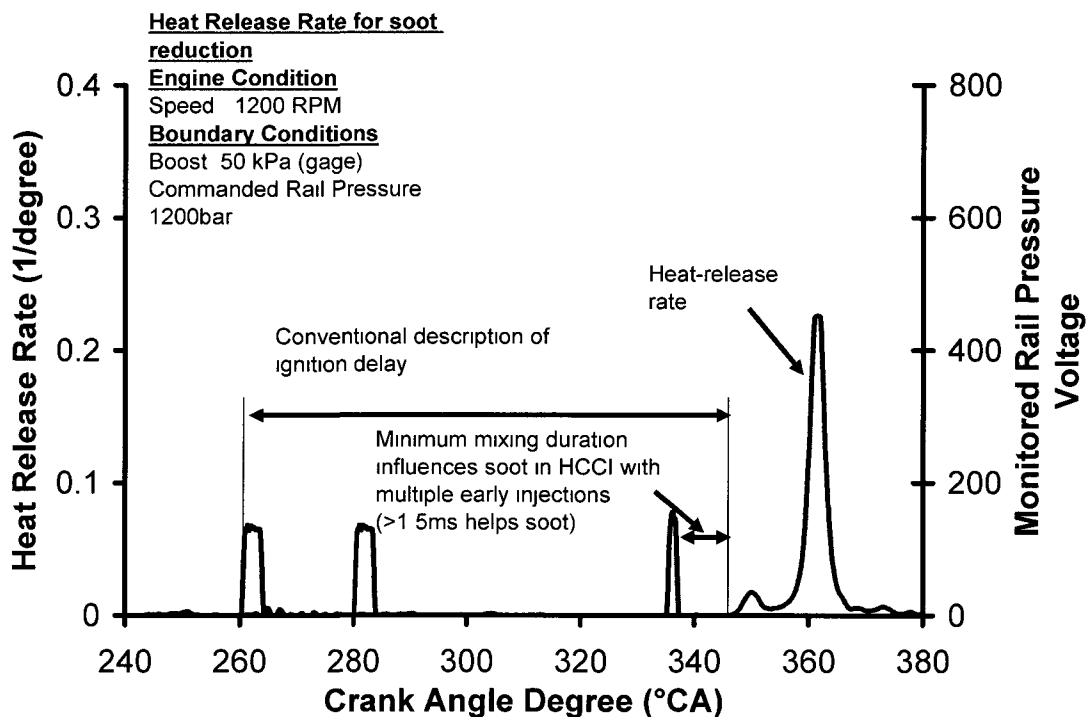
Figure 9-10: Heat-release rate for soot reduction with multiple-injection and EGR.

The second injection strategy employed to reduce smoke (NOx was simultaneously reduced due the use of heavy-EGR) was the single-shot close-to-TDC injection strategy with heavy EGR (Figure 9-11, Figure 9-12). Such an injection strategy was able to reduce soot when the application of EGR prolonged the ignition delay by 50% compared to the case of no EGR or provided an ignition-delay of 1.5 ms [44~45].

The minimum mixing duration for different injection strategies at various loads is shown in Figure 9-13 along with the ignition delay of the single-shot LTC combustion. It can be seen that a heat-release rate with an ignition delay of ~1.5ms for the case of single injection or a minimum-mixing duration of 1.5ms for the case of multiple injection strategy was able to produce low-soot (Figure 9-12).
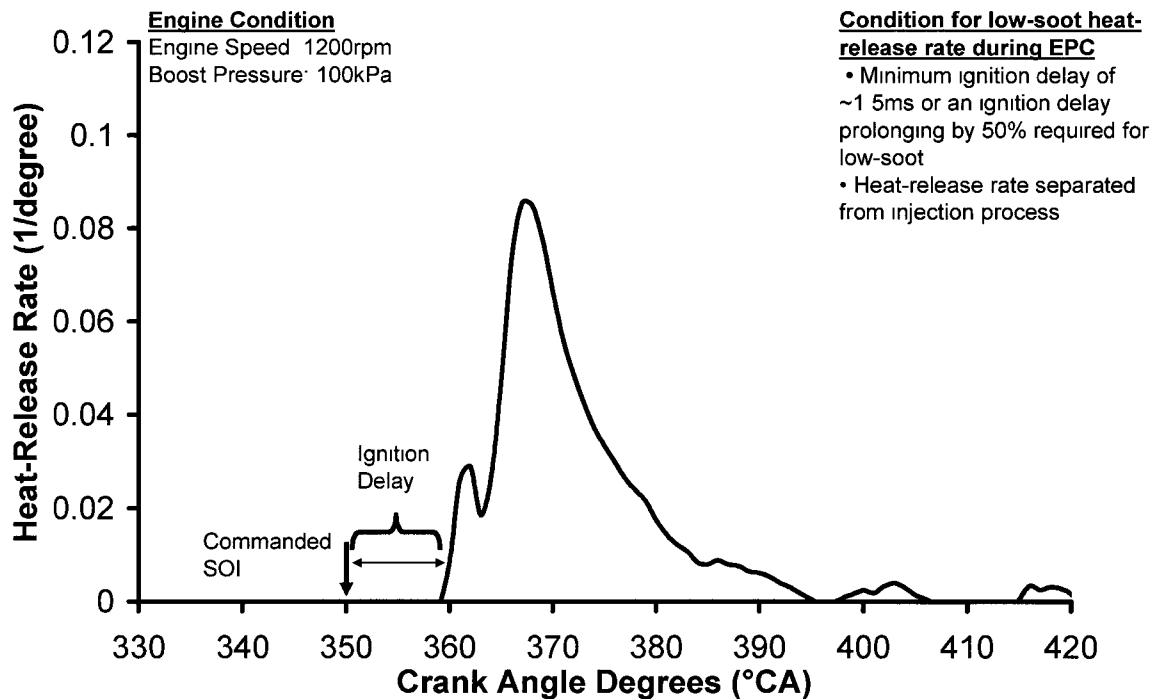
Figure 9-11: Heat-release rate for soot reduction with single-injection and application of heavy-EGR.
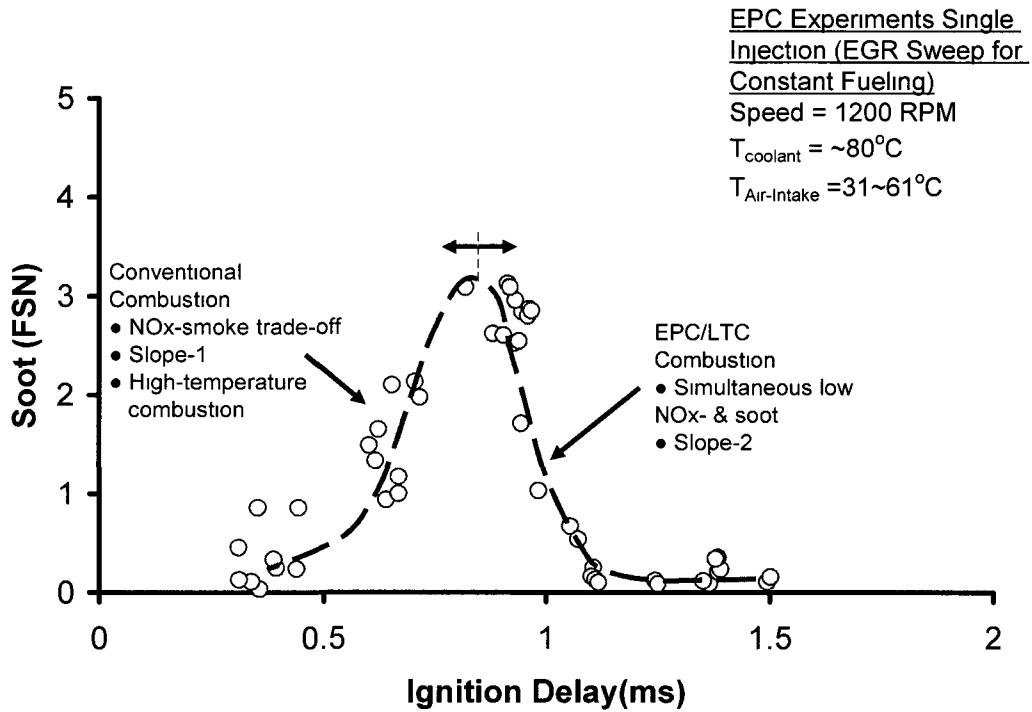
Figure 9-12: Relationship between ignition-delay and smoke for EPC combustion with single-shot injection strategy and a heavy use of EGR.
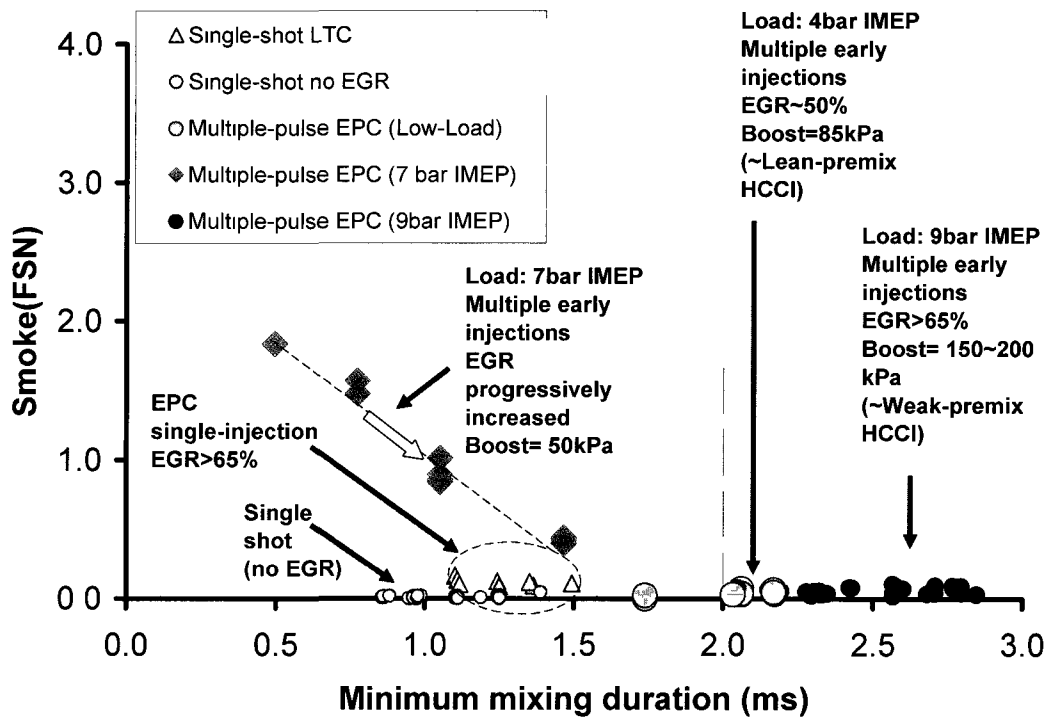
Figure 9-13: The effect of injection strategy on the smoke during EPC.

9.3 Heat-Release Pattern for HC

The heat-release had a stronger relationship with HC for the case of early multiple-pulse injection strategies. For the case of multiple-pulse injection the HC was dependent on the ignition delay process, the injection strategies with longer ignition delay resulted in higher HC (Figure 9-14). The details for "sparse-injection strategy", "dense-injection strategy" used in the Figure 9-14 can be found in the appendix [25, 44, 45, 57].
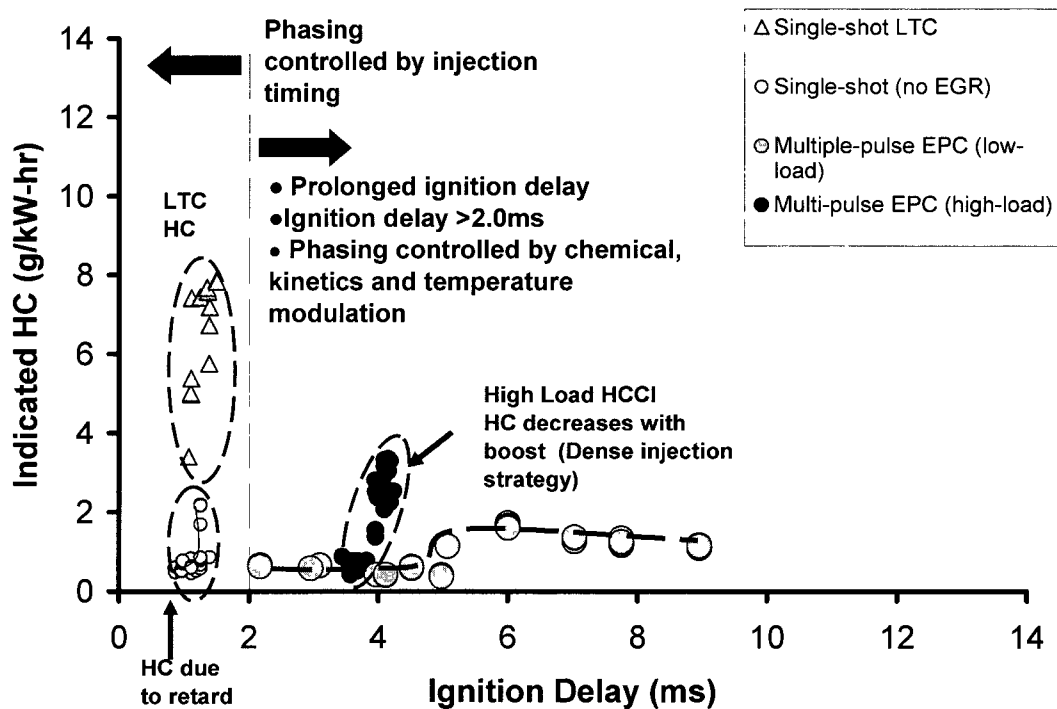
Figure 9-14: Effect of ignition delay on HC for different injection strategies.

9.4 Heat-Release Pattern for Rate-of-Pressure-Rise

As discussed before, the two injection strategies have been used to achieve simultaneous low NOx and soot, namely multi-pulse-HCCI-injection-strategy and single-shot close-to-TDC injection strategy. For single-shot it was possible to implement combustion phasing control directly with injection and it was possible to obtain phasing that meets the emission and performance criteria simultaneously. The limitation of the single-shot EPC is that such a strategy can be applied only at low and mid-load conditions [39, 42, 44, 45, 57]. At higher loads, multi-pulse-HCCI-injection-strategy needs to be applied. However,

for the HCCI-injection strategy the combustion was initiated before TDC, and because of the inherent short combustion-duration the rate-of-pressure rise was high. A typical heat-release rate and rate-of-pressure trace observed at high-load HCCI are shown in Figure 9-15. A high rate-of-pressure-rise is not desired because it leads to high combustion-noise.
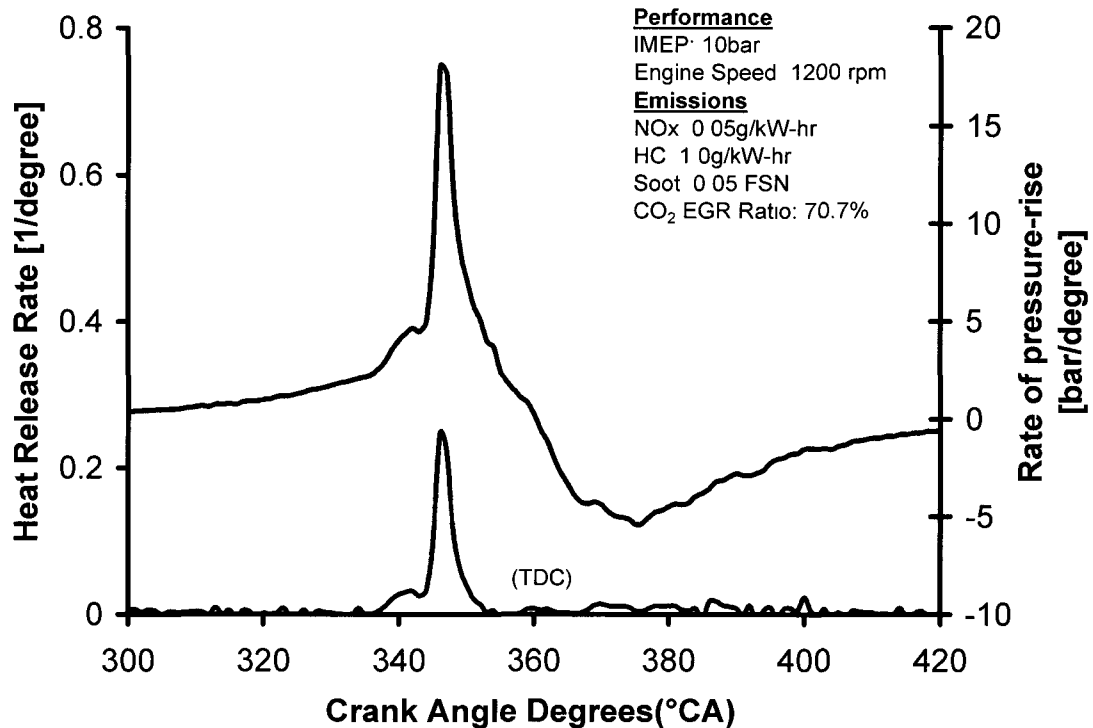
Figure 9-15: Typical heat-release rate and rate of pressure rise curve shown at high loads with multiple-pulse HCCI injection strategy.

To overcome the high-rate-of-pressure rise associated with the multi-pulse-HCCI-injection-strategy, a heat-release rate with split pattern has been experimentally (Figure 9-18) and numerically investigated (Figure 9-16, Figure 9-17, and Figure 9-18). The numerical investigation was performed using in-house engine cycle simulation software [52]. For the simulation two heat-release patterns representative of HCCI type of combustion and split combustion were used as the input and the performance characteristics such as indicated mean effective pressure (IMEP), maximum pressure and maximum rate-of-increase of pressure were evaluated at different combustion durations and combustion phasing events. The results (Figure 9-16, Figure 9-17) show that the implementation of split combustion event may help to reduce combustion noise without

any significant efficiency penalty. The experimental validation at high loads has to be further continued.
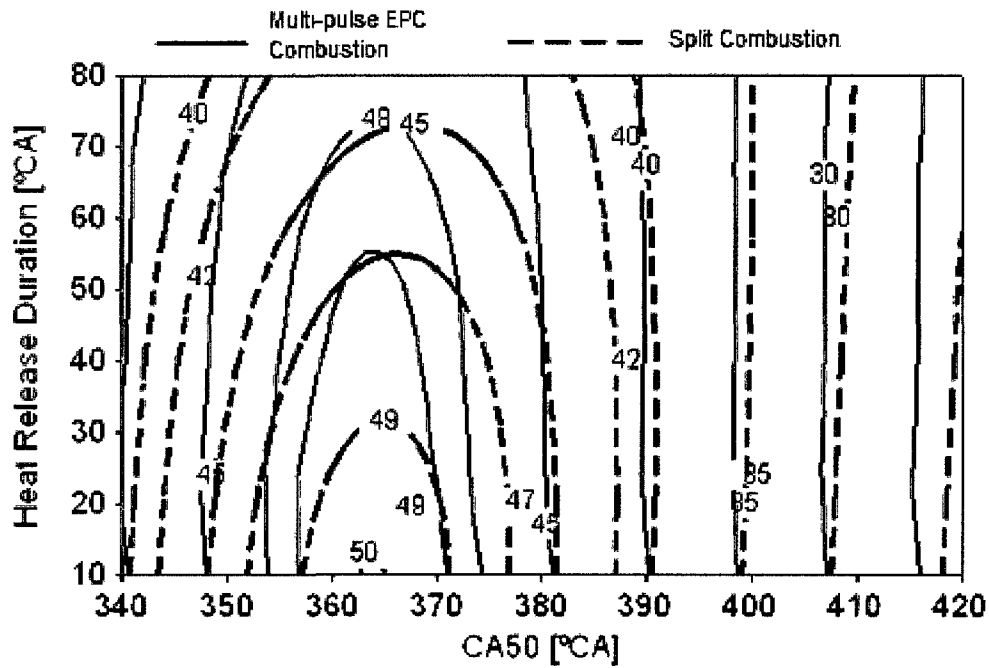
Figure 9-16: Effect of CA50 and combustion duration on η_{ind} and P_{max}, $(dp/d\theta)_{max}$ at 1200rpm, pint=3bar(abs) for single and joint heat-release shapes.
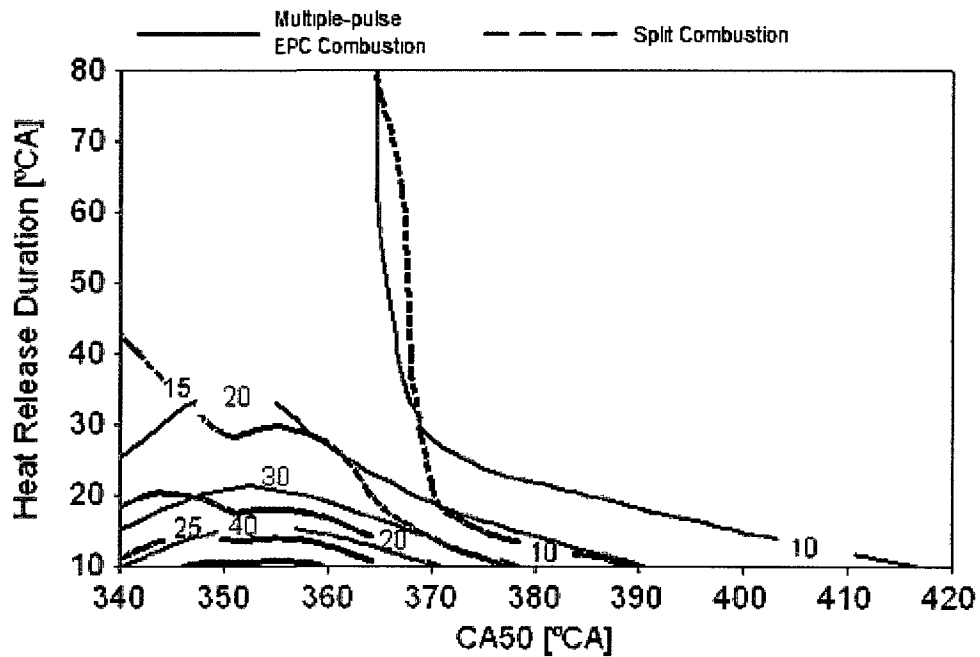
Figure 9-17: $(dp/d\theta)_{max}$ for single hump and joint combustion.
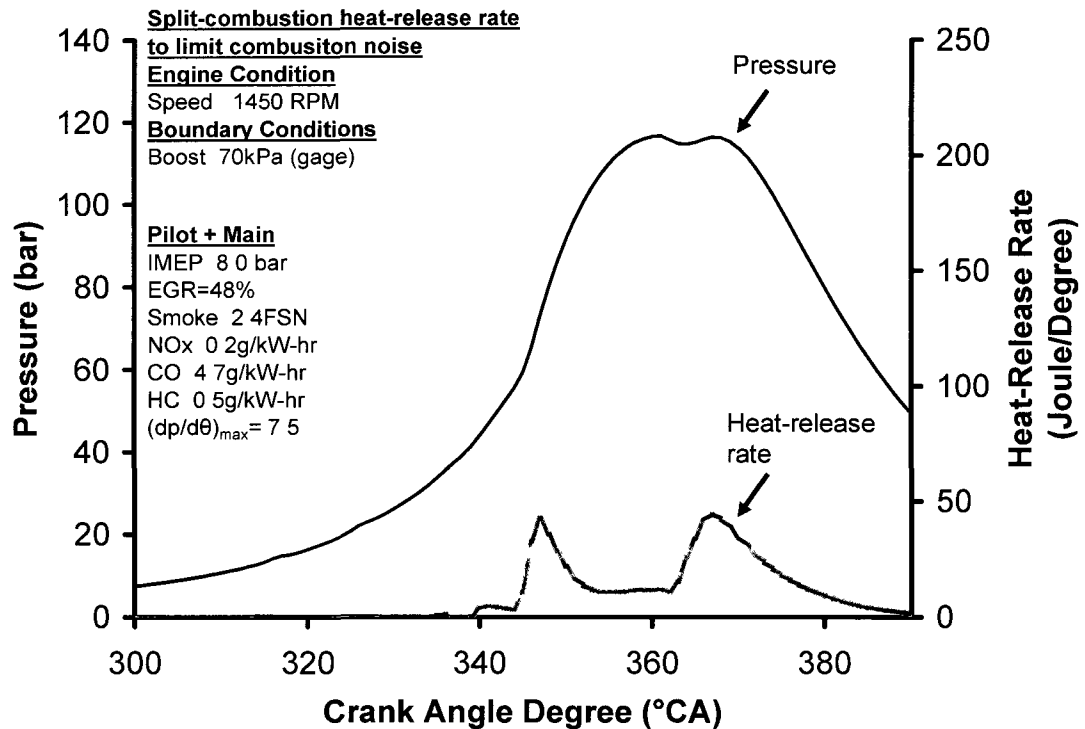
Figure 9-18: Implementation of split combustion heat-release rate to limit rapid pressure rise associated with HCCI type of injection strategy [32].

9.5   Heat-Release Rate, Combustion-Phasing and Fuel Injection Scheduling

The in-cylinder pressure sensor is one of the means to provide real-time data for combustion phasing, which in turn has been identified as one of the major factors that affects the engine cycle thermal efficiency [44, 45]. The block diagram for the conventional diesel combustion phasing control is shown in Figure 9-19. The calculated combustion phasing parameter is compared with the desired combustion phasing characteristics and the resulting error is corrected by the proportional-integral controller. The controller corrects the start of injection of the fuel injection event to achieve the desired combustion phasing. For the medium to high load EPC, large amounts of EGR have been identified as one of the important enablers. When large amounts of EGR is applied, the ignition delay is prolonged due to inhibited mixture-reactivity, therefore to maintain the combustion phasing similar to the case of no EGR the fuel-injection timing has to be advanced. For combustion process with a very long ignition-delay the combustion and the injection processes tend to differ appreciably from conventional combustion.

HRR_feedback
based on pressure diagnostics

HRR_set point

Fuel-subsytem

Injection
Scheduling
(crank-angle basis)

Engine

Useful work
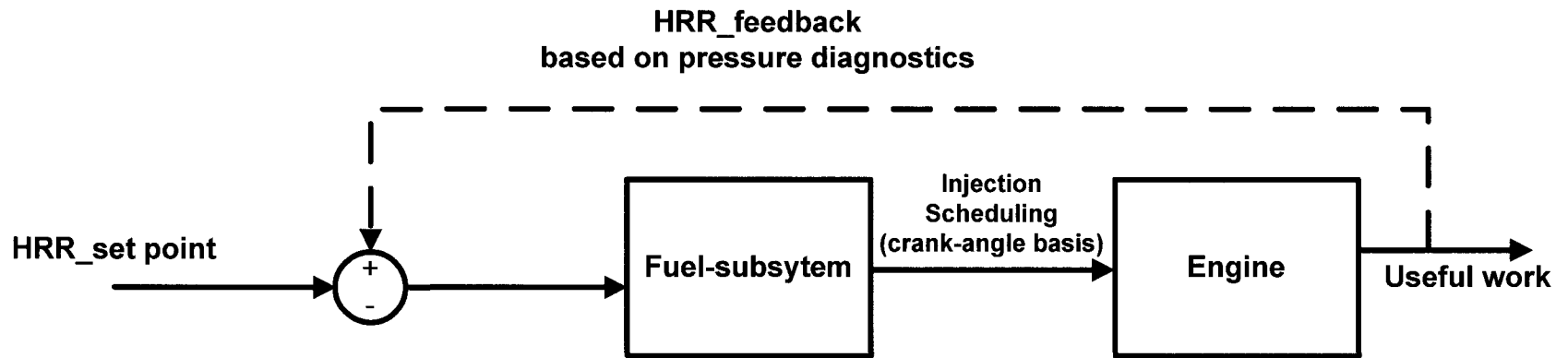
Traditional combustion phasing control where the
injection and the combustion-phasing are coupled

Figure 9-19: Combustion phasing control when the injection and the combustion phasing are coupled.

Therefore, in this section, an attempt has been made to identify the regions where the start-of-injection correction may be applied to obtain the desired heat-release rate. This was considered important because once the injection-timing leaves this region the combustion phasing is controlled by altering mixture reactivity or altering time-temperature history of the mixture. This was done by compiling the test results described earlier in the thesis and performing a few additional tests. At each of the test-points the relationship between the commanded start-of-injection and its relationship with the combustion phasing was observed.

The first case considered was the EGR enabled EPC discussed previously. The case of 8.0bar IMEP with a boost of 100kPa and an injection pressure of 1200bar was selected for the analysis. For this case as the EGR was increased to approach the simultaneous low-NOx and low-soot combustion, the cylinder pressure-based injection control was also implemented manually to keep the combustion phasing at a fixed location. The injection timing correction required with increasing amounts of EGR is shown in Figure 9-20. For these tests, an SOI correction up to 342°CA was required and the relationship between the SOI and the combustion was still retained. Thus the first observation was that up to 342°CA, even in the presence of high EGR the combustion-phasing and injection timing was still coupled.

Next the start of injection timing before 340°CA was investigated for the injection timing versus the combustion phasing correlation. An injection timing sweep was performed from 260°CA to 322°CA (Figure 9-21). Multiple injection strategies were required for early injections to reduce the wall-impingement. In Figure 9-21 based on the timing sweeps, two areas have been marked as regions A and B;

In region-A, the combustion phasing was controlled by chemical kinetics and temperature modulation. In this region, when the injection timing was advanced from 301°CA to 281°CA for the 4-injection strategy, the combustion phasing was shifted towards TDC a couple of degrees. This is in contrast to region-B where the advancing the injection timing led to a advancing in the combustion phasing. Similar, behavior was observed for other injection strategies.

In Figure 9-22, an EGR sweep is included for a fixed injection timing starting at 260°CA and it can be seen that for these early injection timings the sensitivity of combustion phasing towards EGR modulation was more than the sensitivity towards injection timing. The data in Figure 9-22 was converted to an ignition delay basis in Figure 9-23, and it can be seen, for an ignition delay greater than 2milli-seconds (ms) the combustion phasing was affected more by chemical kinetics/temperature modulation and less by injection timing.

In region-B, the combustion phasing followed the same pattern as the injection timing trends.
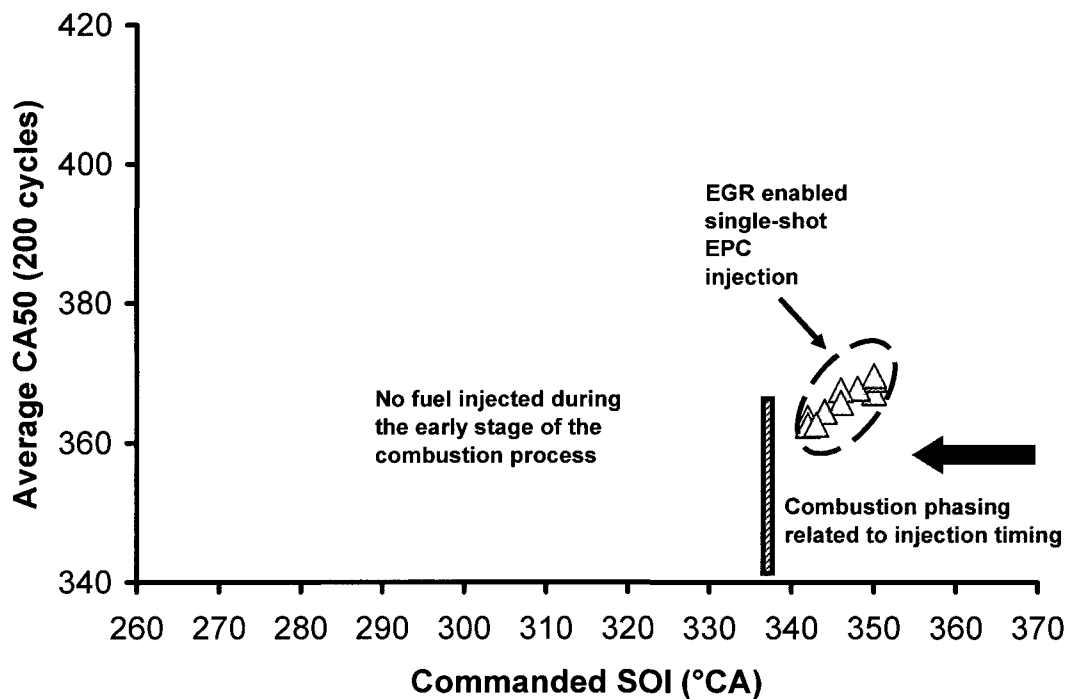
Figure 9-20: Injection timing correction for single-shot EPC combustion.
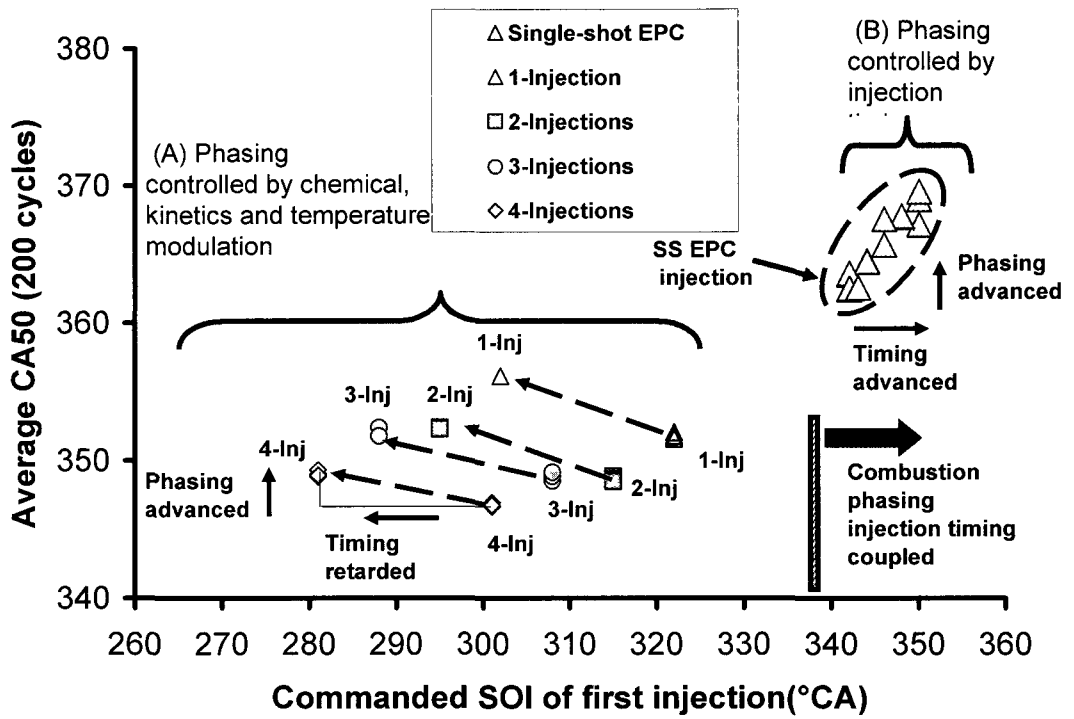
Figure 9-21: Understanding the injection timing and combustion phasing correlation.
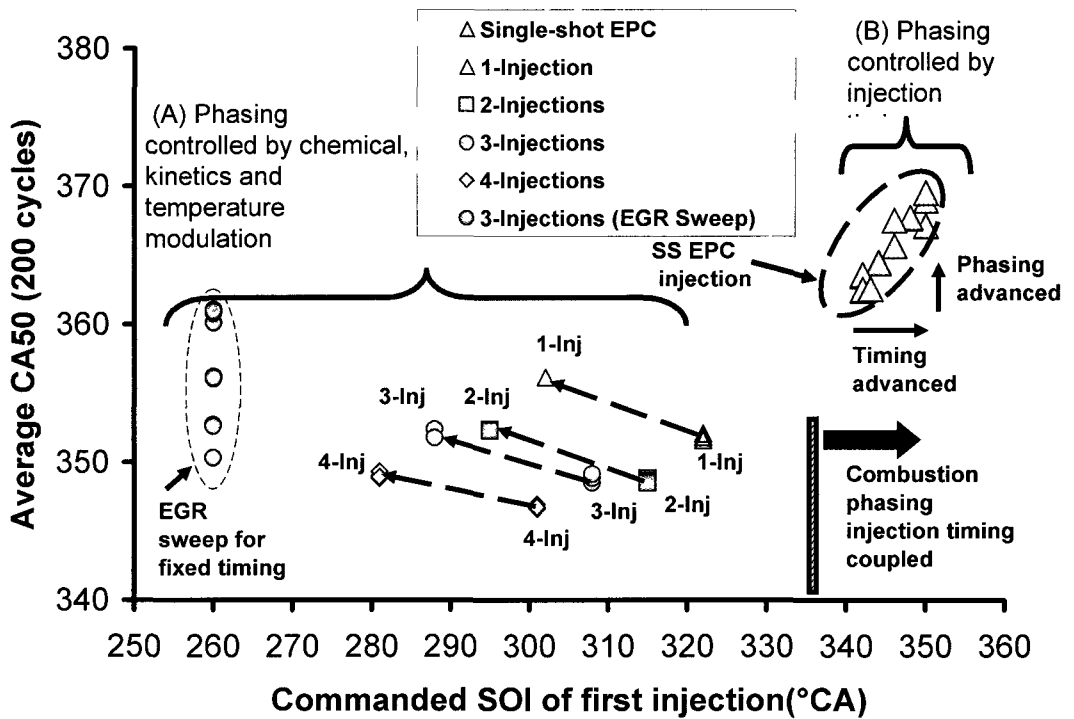
Figure 9-22: Understanding the injection timing and combustion phasing correlation.

173
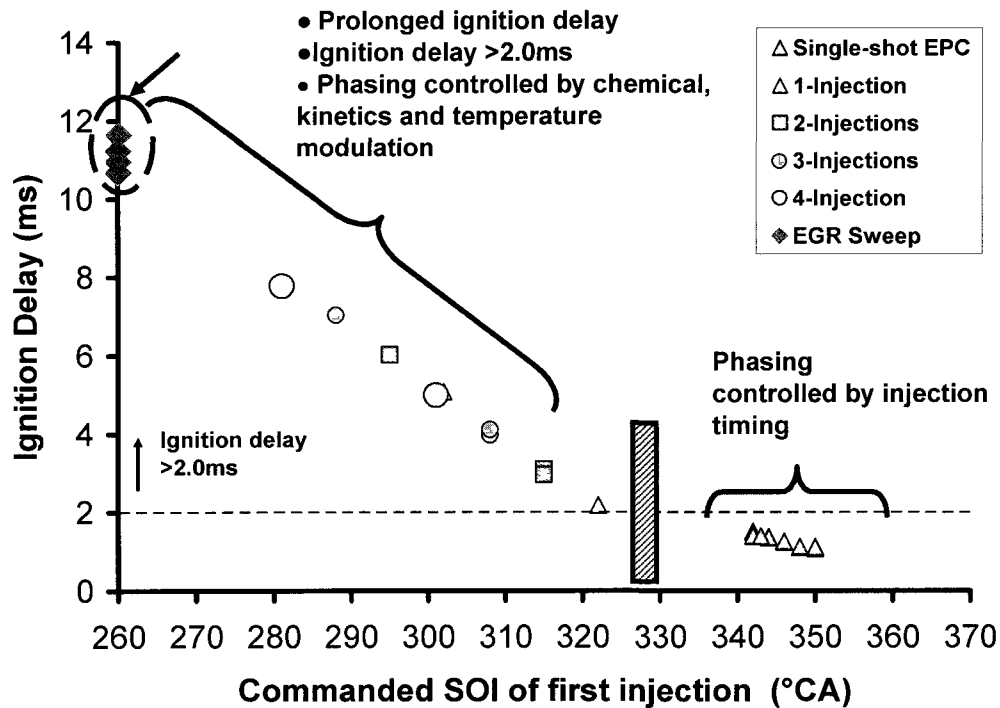
Figure 9-23: Ignition delay correlation with commanded start of injection.

9.6 Heat-Release Rate Pattern for Thermal Efficiency

The empirical results and the engine cycle simulations have indicated that the combustion phasing dominates the maximum attainable fuel efficiency of the engine. Note that the phasing domination cedes to high HC and CO production when the fuel combustion efficiency is severely deteriorated by means such as excessive EGR [44, 45].

9.7 Heat-Release Rate Pattern for CO Post-Oxidation

One of the primary reasons for reduction in efficiency of the LTC compared to the conventional diesel cycle was incomplete combustion. As a result of the incomplete combustion the fuel energy was being wasted as UHC or carbon-monoxide. UHC reduction for the EPC fuel-injection has been discussed earlier by optimizing the injection strategy. In this section injection-strategy modulation was attempted to reduce the CO by post-oxidation. This strategy was called HCCI-plus-late-main-injection strategy. For a conventional multi-pulse EPC injection strategy, all the fuel was injected early during the compression process and the EGR was used to withhold the combustion

174

process and obtain an appropriate combustion phasing. An alternative to this approach was to inject only a part of the fuel; called HCCI Injection Part very early during the compression process and to inject the remainder of the fuel; called late main injection towards the end of the heat-release of the HCCI fuel injection [57]. The logic behind such a strategy was that the first part of the fuel-injected as the HCCI injection would have a prolonged ignition delay and would undergo the simultaneous low-NOx, low-soot and high CO combustion. The late-main-injection event would have a very short ignition delay period and undergo close to conventional combustion and would destroy the CO produced in the due to the incomplete combustion of the HCCI part of fuel injection (Figure 9-24).
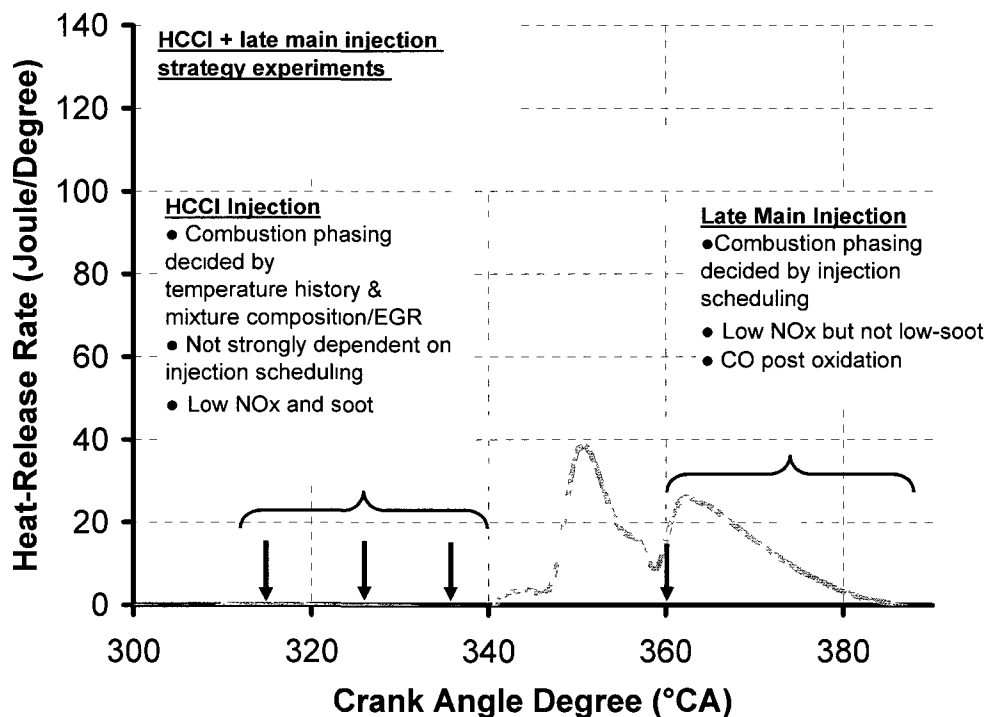
Figure 9-24: Post oxidation of CO by late-injection.

A comparison of the engine operation at HCCI-plus-late-injection strategy (marked A), HCCI-only-injection (marked B) and main-only-injection (marked C) is shown in Figure 9-25. The HCCI-plus-late-injection strategy consisted of injections at 315°CA, 325°CA, 335°CA and 360°CA. For the HCCI-only-injection strategy, the last injection at 360°CA was turned-off while for main-only-injection strategy; the first three injections were

turned-off. The boost was kept constant at 70kPa and the EGR was kept constant at 50% EGR during the entire test. The NOx during the HCCI-with-late-main injection was almost the same as the main-injection-only injection strategy, which indicated that the NOx was not affected by the increase in engine load. This indicated that there may be additional inter-cycle EGR effect due to first stage of heat-release during the HCCI with late main injection strategy. However, during the HCCI with late main injection strategy, the CO was lower than the HCCI only injection. This suggests that the late main injection aids in the oxidation of the CO and thereby improve the combustion efficiency.
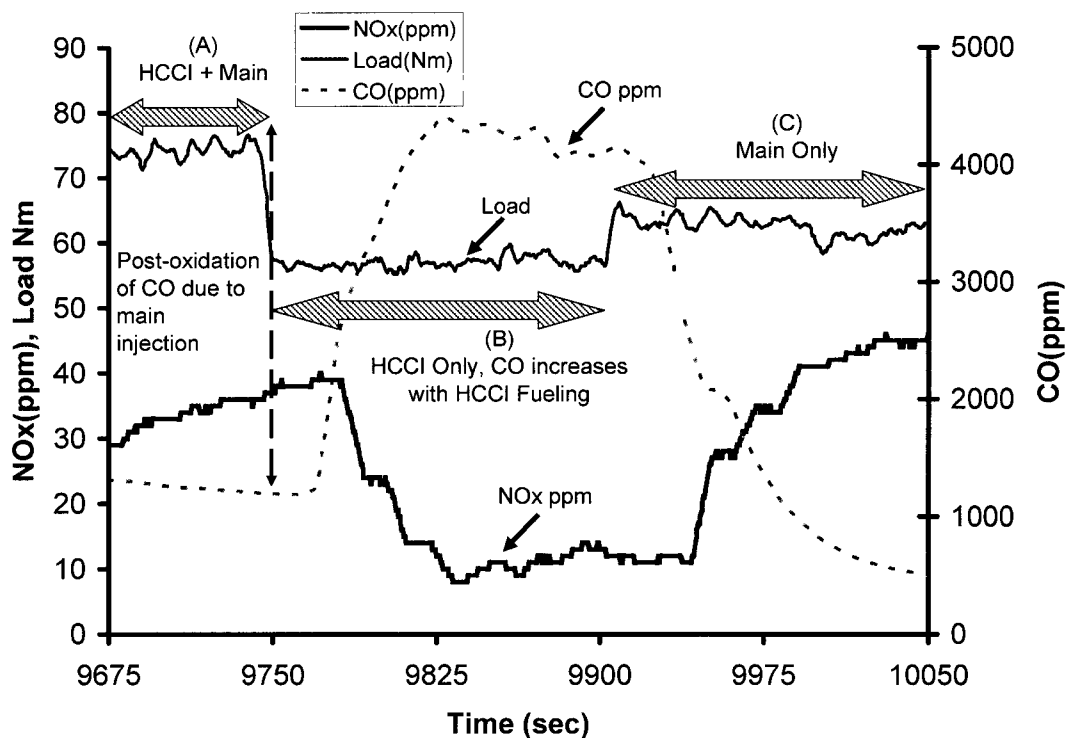
Figure 9-25: Post oxidation of CO by late-injection.

The comparison of the HCCI plus late injection with single shot LTC combustion is shown in Table 9-1. The HCCI plus late injection had a similar NOx as the single-shot LTC NOx but the smoke was significantly high. It may be noted that the LTC was achieved only at around 65% EGR, a simultaneously high EGR and high boost is still considered a challenging requirement for the modern diesel engines [22]. As mentioned before the comparison of the emissions (Table 9-1) shows that the CO for HCCI plus late main injection decreased in comparison to the LTC injection strategy.

Table 9-1: Comparison of HCCI plus late injection strategy with single-shot LTC

	HCCI plus late-injection	LTC (Slope-1)	LTC (Slope-2)
NOx (g/kW-hr)	0.2	0.2	0.2
Soot (FSN)	2.4	0.6	0.3
Effective CO* (g/kW-hr)	1.9	1.7	5.0
EGR [%]	50	60	65
$(dp/d\theta)_{max}$ (bar/degree)	7.5	14	4

* Effective CO=CO(g/kW-hr)X(LHV of CO/LHV of Diesel)

A typical pressure and heat-release diagram for the HCCI plus late injection strategy is shown in (Figure 9-26, Figure 9-27). There were certain disadvantages associated with the HCCI plus late injection strategy also. For the HCCI type of injection strategy, the soot was 0.1 FSN; however, when the HCCI plus late injection strategy was implemented the soot increased to 2.4FSN. This soot was higher than the single-shot soot at this EGR level also. This suggested that the last injection (for the HCCI plus late injection strategy) which was undergoing conventional combustion had difficulty in finding oxygen resulting in high soot. For the given boost and injection pressure it was possible to achieve low NOx and low CO combustion up to a load of 7 bar. Note that a smoke level of FSN~2.5 was considered acceptable with diesel particulate after-treatment for this load level [77]. The difficulty in finding oxygen for the HCCI plus late injection strategy limited the EGR that may be applied (Figure 9-27). For instance when the EGR was increased 48% to 54% the soot increased rapidly from 1.2 FSN to 3.7 FSN. For single-shot enhanced premixed combustion the smoke was significantly lower (Figure 9-28). The reduced ignition delay for the injection at 360°CA (pilot + main) also led to low $(dp/d\theta)_{max}$ or combustion noise.
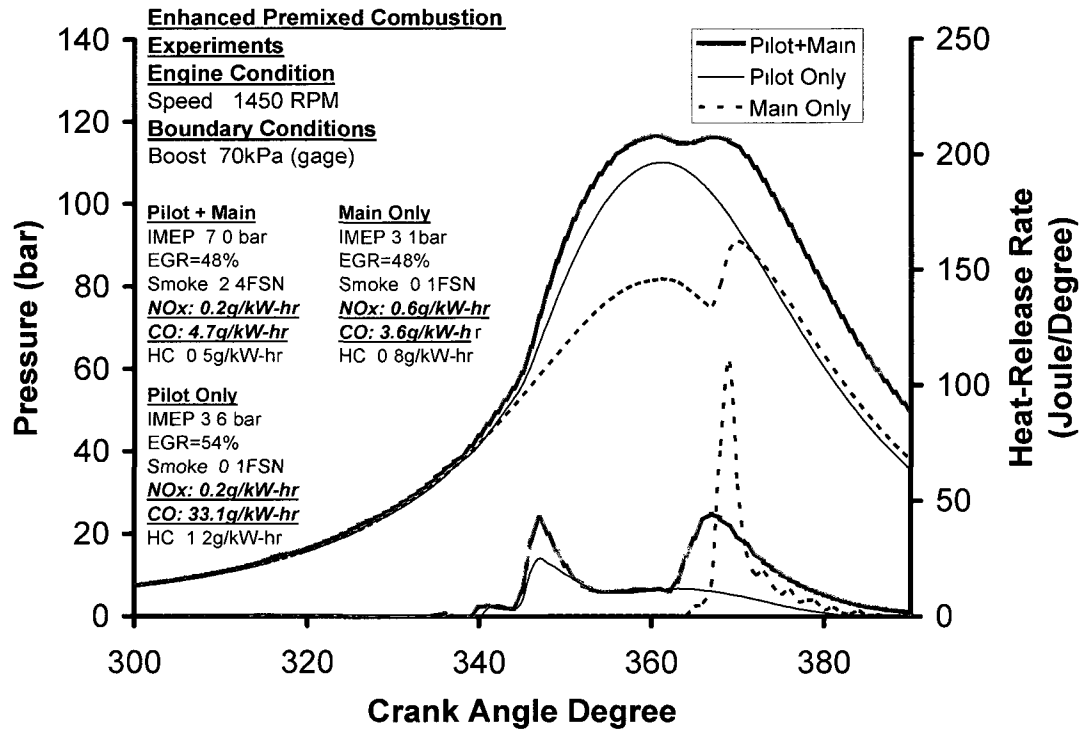
Figure 9-26: Empirical results with HCCI-plus-late-main injection strategy.

Table 9-2: Advantages and disadvantages of HCCI plus late injection strategy

Advantages	Disadvantages
(1)Combustion phasing of second part still controlled by injection timing (2)Lower $(dp/d\theta)_{max}$ (3)Oxidation of CO (4)Lower EGR needed compared to full HCCI for similar NOx	(1)Higher Smoke than HCCI type of combustion. FSN>2.0, DPF needed.
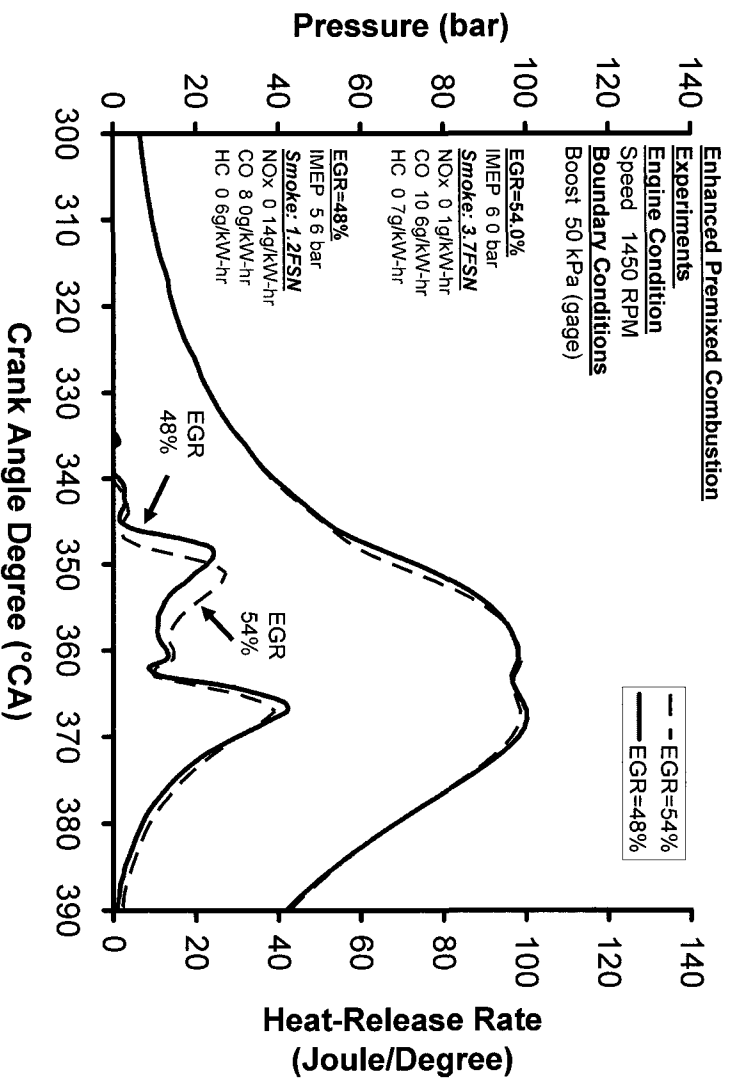
Figure 9-27: Sensitivity towards EGR for enhanced premixed experiments.

Enhanced Premixed Combustion
Experiments
Engine Condition
Speed 1450 RPM
Boundary Conditions
Boost 50 kPa (gage)

EGR=54.0%
IMEP 6.0 bar
Smoke: 3.7FSN
NOx 0.1g/kW-hr
CO 10.6g/kW-hr
HC 0.7g/kW-hr

EGR=48%
IMEP 5.6 bar
Smoke: 1.2FSN
NOx 0.14g/kW-hr
CO 8.0g/kW-hr
HC 0.6g/kW-hr

EGR 48%
EGR 54%

— — EGR=54%
—— EGR=48%

Pressure (bar)
Crank Angle Degree (°CA)
Heat-Release Rate (Joule/Degree)
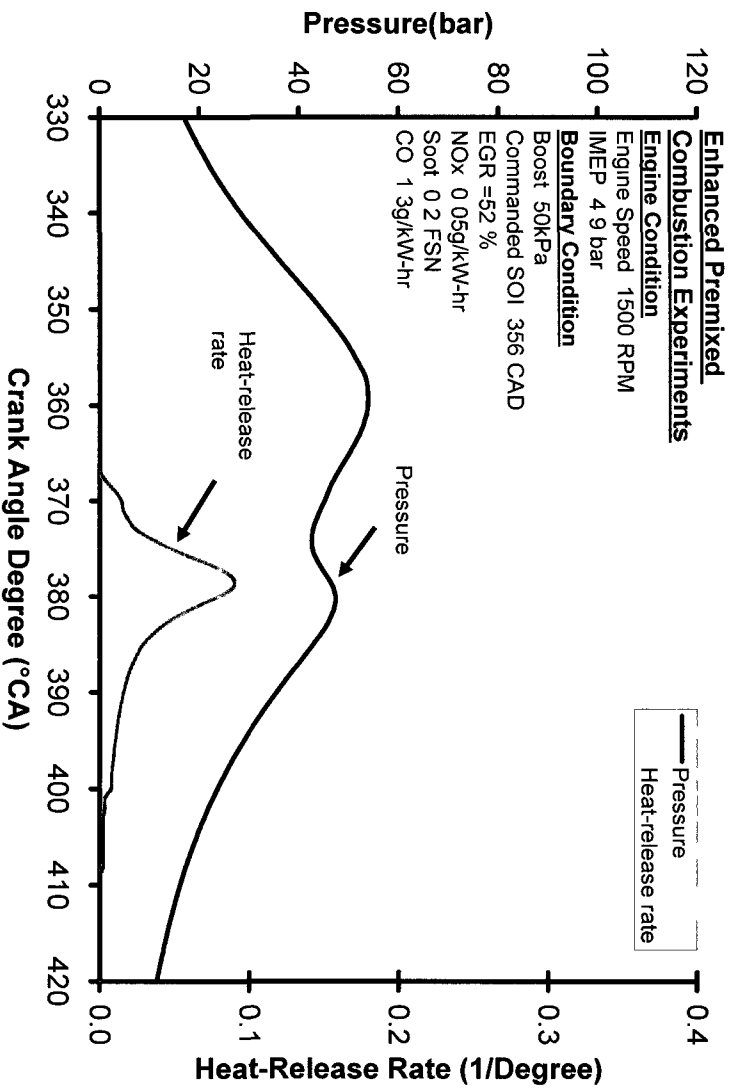
Figure 9-28: Single-shot enhanced premixed combustion with high EGR.

Enhanced Premixed
Combustion Experiments
Engine Condition
Engine Speed 1500 RPM
IMEP 4.9 bar
Boundary Condition
Boost 50kPa
Commanded SOI 356 CAD
EGR =52 %
NOx 0.05g/kW-hr
Soot 0.2 FSN
CO 1.3g/kW-hr

Heat-release rate
Pressure

—— Pressure
—— Heat-release rate

Pressure(bar)
Crank Angle Degree (°CA)
Heat-Release Rate (1/Degree)

179

9.8 Implementation of EPC

In view of the above discussion and the experimental results discussed in earlier chapters, the heat-release rate characteristics that favored EPC combustion are shown in Table 9-3. The NOx during the EPC combustion was primarily dependent on the dilution/EGR level. At high EGR levels, even if the pilot injection was implemented, the pilot combustion was suppressed and the overall combustion was similar to the case of single injection. The NOx reduction without implementation of EGR was possible at low-loads as discussed in Chapter 6. However, at higher loads EGR was an important enabler for NOx reduction. Similarly, a heat-release pattern that had a minimum ignition delay of around 1.5ms for the case of single-shot injection strategy or a minimum mixing duration of 1.5ms helped to reduce soot. At the same time if this ignition delay became too long, large amounts of HC was formed and the coupling between the injection and the combustion phasing was weakened. The combustion phasing, i.e. position of CA50, had a strong effect on the indicated efficiency that peaked at a heat-release position of 5~7°CA after TDC.

Table 9-3: Desired heat-release characteristics.

Emission	Heat-release Pattern
NOx	Not dependent on heat-release characteristics at high EGR. Dilution effect significant.
Soot	a) Required an ignition delay of 1.5ms or ignition-delay prolonging of 50% b) 1.5ms minimum mixing duration for multi-pulse HCCI
HC	Higher HC associated with longer ignition delay
Combustion phasing	Decoupled from injection timing when ignition delay was very long (>2ms)
Cycle thermal efficiency	Combustion phasing is the primary factor, followed by combustion duration. However, both cede to high CO and HC in presence of heavy EGR
Combustion noise control	Partly addressed by split-heat-release rates

The combustion process with the desired ignition-delay and the combustion-phasing was obtained during the EPC combustion by the coordinated efforts of the fuel system and the air system. The significant effect of the air-system on the combustion-phasing during EPC combustion was a significant departure from the conventional combustion where the combustion phasing was directly controlled by the fuel-injection scheduling. The desired heat-release rate characteristic and the required load levels act as the input to both the air and the fuel-system. The outputs from the fuel-injection system were the fuel-injection quantity, and the fuel injection scheduling. The mass air flow-rate and EGR flow-rate are the outputs of the air-system (Figure 9-29). The cylinder pressure-sensor provides the cycle-resolved cylinder pressure data which was processed at the end of the cycle to evaluate the IMEP and combustion phasing. The deviation in the combustion phasing from the desired value was corrected by the fuel-system or the air-system depending on the ignition-delay. If the ignition-delay was lower than the threshold ignition-delay of 2milli-seconds, the deviation of the combustion-phasing from the desired value was adjusted mainly by the injection scheduling. However, if the ignition-delay was larger than the threshold of 2milli-seconds, the combustion-phasing was not strongly coupled with the injection-scheduling and was instead more influenced by the air-fuel ratio history modulation by factors such as EGR.

The torque correction or adjustments were done primarily by adjusting fuel quantity. However, if the air-system cannot navigate the combustion phasing to the phasing for the best-efficiency, the fueling system provides higher-fueling to achieve the given torque or the load-levels. At the present time the IMEP/Torque corrections by the Fuel-system are done manually in response to the IMEP calculated by the pressure-diagnostic routine. The fuel-system however, included closed-loop control on combustion phasing if the ignition delay was shorter than the critical ignition-delay of 2 milli-seconds. For the Air-subsystem all the corrections were done manually to compensate for any change from the desired heat-release characteristics (Table 9-4 and Table 9-5).
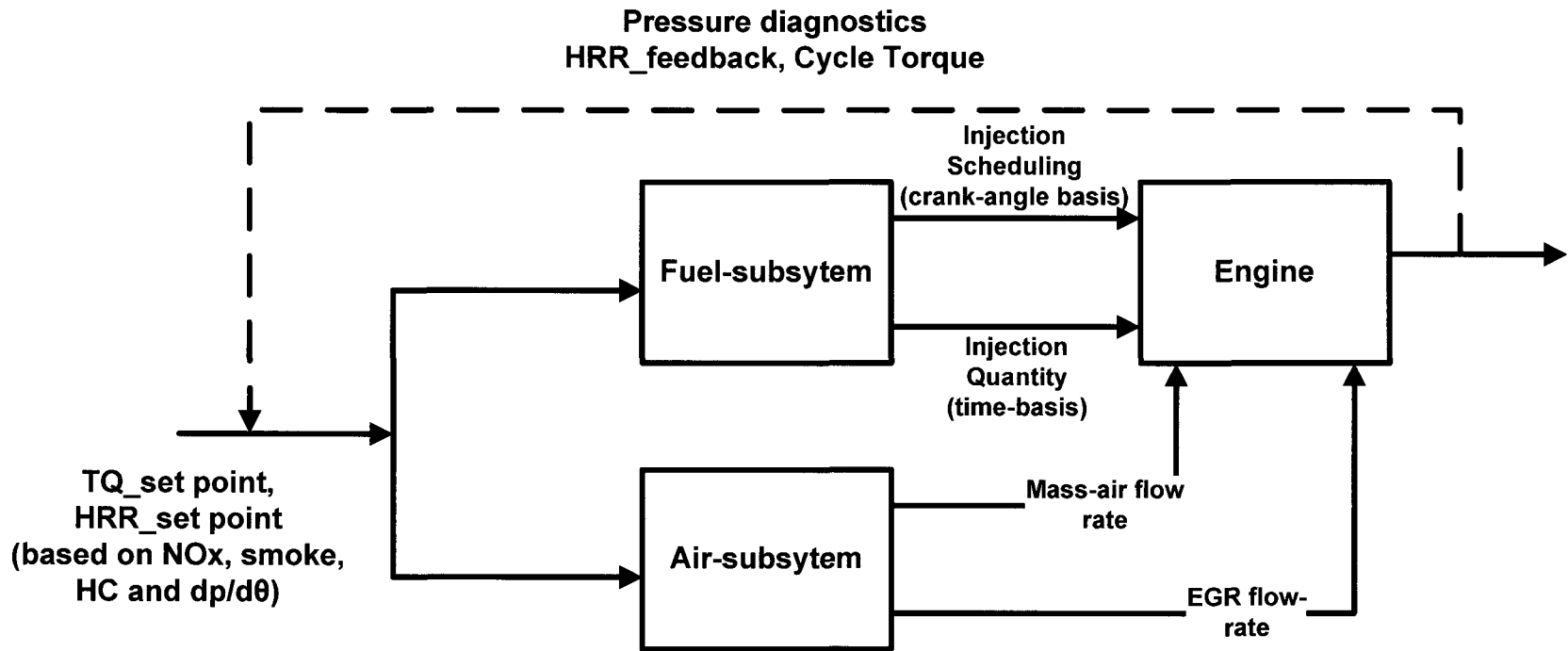
Figure 9-29: Major subsystems and their output for the implementation of EPC with prolonged ignition-delay and the injection and the combustion phasing are not coupled.

Table 9-4: Modes of process-control in fuel-subsystem during EPC combustion.

	Fuel-Subsystem	
	IMEP/TQ	HRR Control
Ignition-delay less than critical ignition delay (Single-shot close-to-TDC injection)	Manual	Close-loop control
Ignition delay greater than the critical ignition-delay (Multi-pulse HCCI injection)	Manual	Manual

Table 9-5: Modes of process-control in air-subsystem during EPC combustion.

	Air-Subsystem	
	IMEP/TQ	HRR Control
Ignition-delay less than critical ignition delay) (Single-shot close-to-TDC injection)	Manual	Manual
Ignition delay greater than the critical ignition-delay (Multi-pulse HCCI injection)	Manual	Manual

Table 9-3 was used as a guiding principle to formulate and decide the engine conditions necessary for the EPC combustion. Based on the steady-state testing (Figure 9-20, Figure 9-22 and Figure 9-23) it was decided that an EGR of 60% and a boost of 100kPa was necessary for an LTC operation of 8bar IMEP. Figure 9-30 shows that the engine was initially operating in conventional combustion at a boost of 50kPa. Then at time, t=9410seconds, a step change in boost was implemented from 50kPa to 100kPa and this was immediately followed by a step change in EGR. The emissions measurements, after the boost and the EGR reached their desired value showed simultaneous low NOx and soot, which validated that the engine was operating in the EPC combustion mode. Similarly, Figure 9-31, shows the transition out of the EPC combustion regime, wherein the EGR and the boost were reduced back to their original values. These experiments were performed with the closed-loop control on combustion phasing.
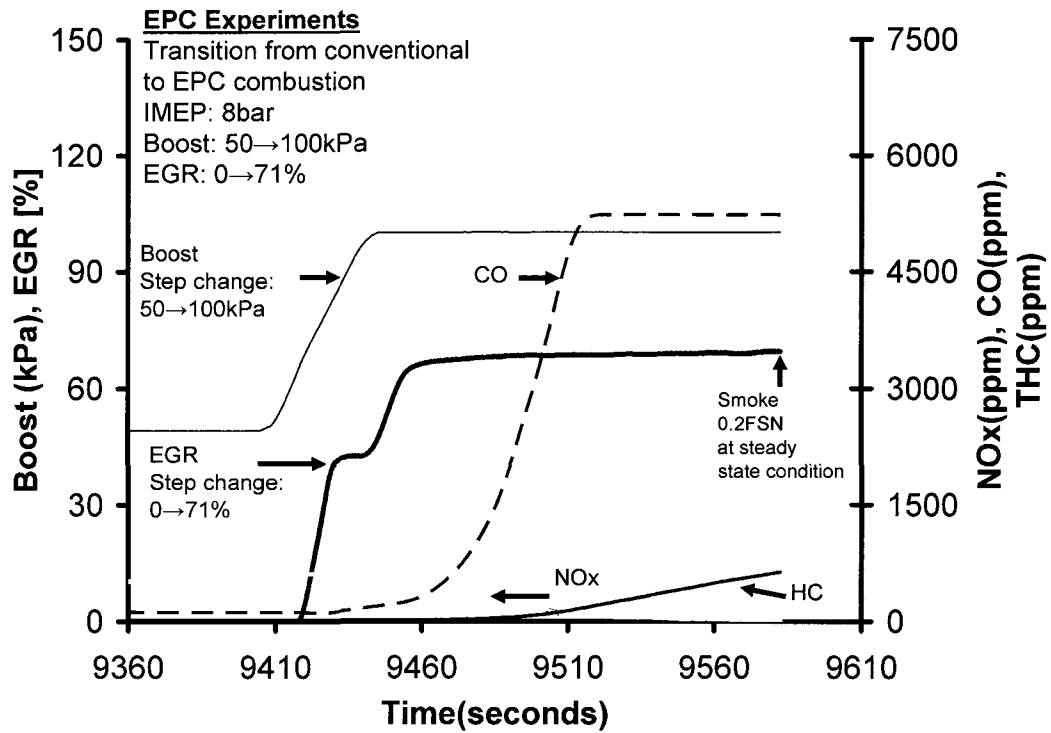
Figure 9-30: Transition from conventional combustion to EGR enabled EPC.
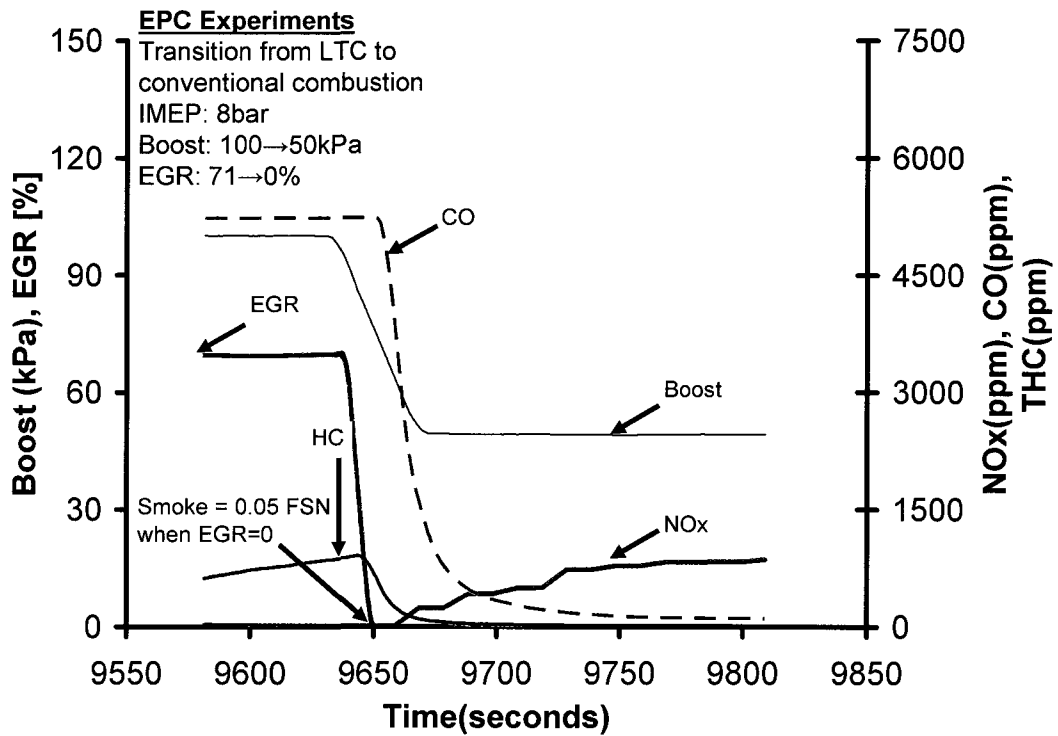
Figure 9-31: Transition from EGR enabled EPC to conventional combustion.

184

9.9 Revisiting the basic premise

The starting point of the research was the use of ϕ-T diagram to identify the local equivalence-ratio and the local flame temperature that can result in simultaneous low-NOx and low-soot. The studies such as the one shown in Figure 3-1, were made without taking into account the effect of EGR. This is significant since the present study has identified EGR as an important enabler for simultaneous NOx and smoke reduction. In the presence of EGR, the oxygen charge concentration is significantly altered and the reduced oxygen concentration has a significant impact on the flame-temperature. Therefore in this section, the NOx part of the ϕ-T diagram has been modified to account for the reduced oxygen concentrations in the presence of EGR. Also it was attempted to correlate the flame-temperature to the temperature at the start of combustion for the diesel combustion. Note, the discussion in the section is more suitable for the early multi-pulse injection strategy than the single-shot EGR enabled EPC.

The first step was to perform the Zeldovich calculation and compare it with the results published in the literature. The kinetics of the thermal NOx formation rate is typically much slower than the main hydrocarbon oxidation rate, and so most of the thermal NOx is formed after completion of combustion. Therefore, the thermal NOx formation process was treated as decoupled from the main combustion reaction mechanism and the NOx formation rate was calculated by assuming equilibrium values of the N_2 and the [O] values. The NOx concentrations were calculated over a time of 2ms similar to the original work by the authors. Note, that the adiabatic flame temperature is estimated based on type of fuel, amount of oxidant, type of oxidant (air or oxygen), and the initial temperature. For the case of diesel combustion, as discussed previously, the boost and the EGR decide the composition of the oxidant. The initial temperature corresponds to the temperature at the start of the combustion. The initial temperature and the flame temperature are related by the equation shown below:

$$h_{reactants}(T_i,P) = h_{products}(T_{ad},P)$$

T_i= Initial Temperature, T_{ad}= Adiabatic Flame Temperature
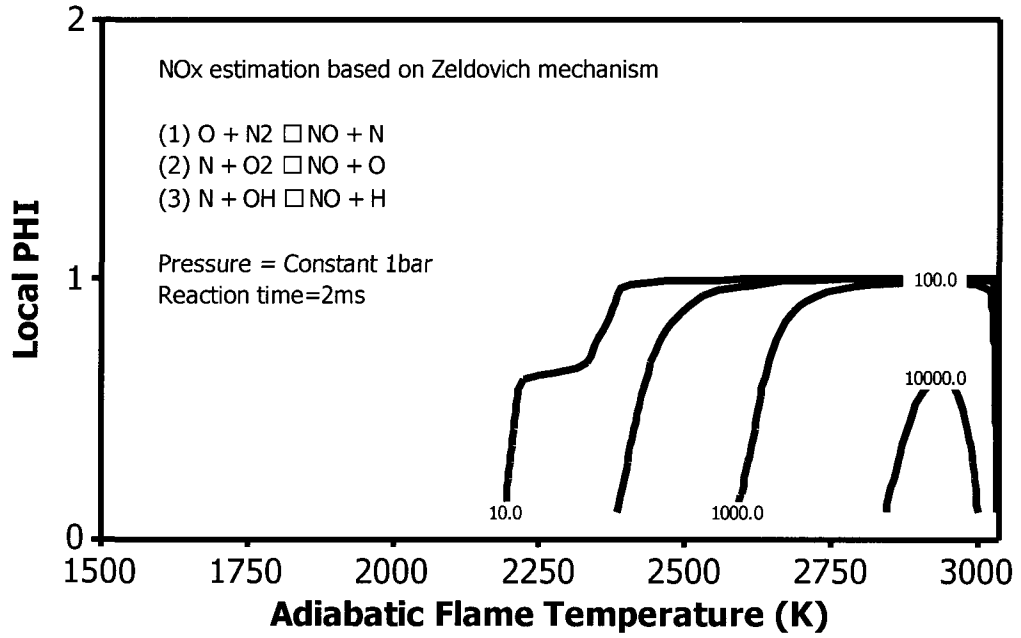
Figure 9-32: NOx estimations based on Zeldovich's mechanism.
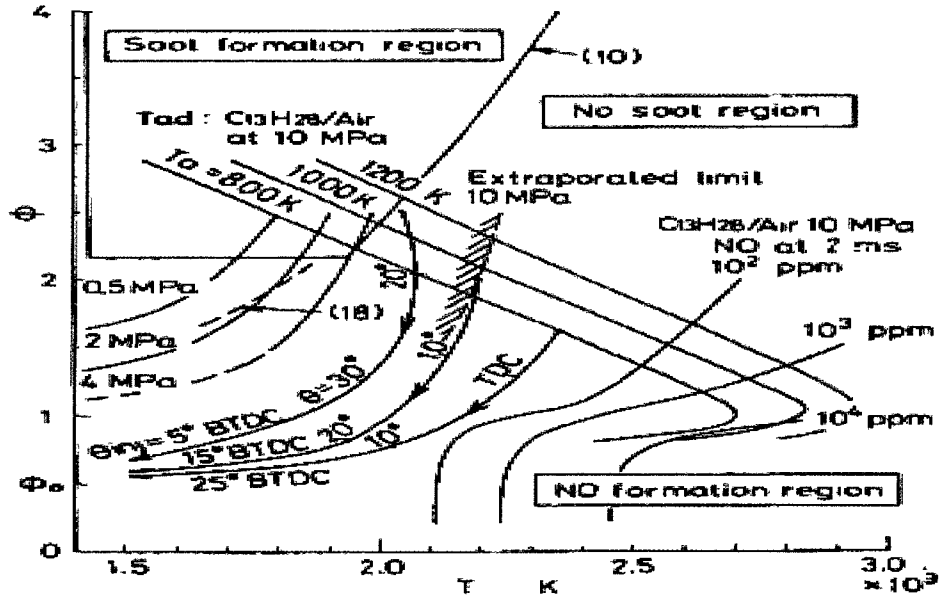
Figure 9-33: Original ϕ-T diagram [11].

Figure 9-32 and Figure 9-33 show a close match for the NOx predictions published in the literature and the computations done in this thesis. The next step then was to identify the flame temperature regions that actually exist in the engine. If a temperature of 1100K is assumed as the maximum temperature that exists before combustion, then only the region marked "A" of the ϕ-T actually exists during engine operating conditions. The Zeldovich equation was then used to estimate the estimate the NOx in the presence of EGR. Also, instead of using the flame-temperature a more engine specific parameter; temperature at the start of combustion was used as the x-coordinate. The modeling computations were able to predict the experimental results discussed earlier, such as a minimum intake-oxygen of 14% for low-NOx (Figure 9-35). The detailed procedure for calculation of NOx based on the Zeldovich mechanism is given in the Appendix. The ϕ-T diagram that includes the effect of EGR on soot formation is being currently prepared at the University of Windsor.
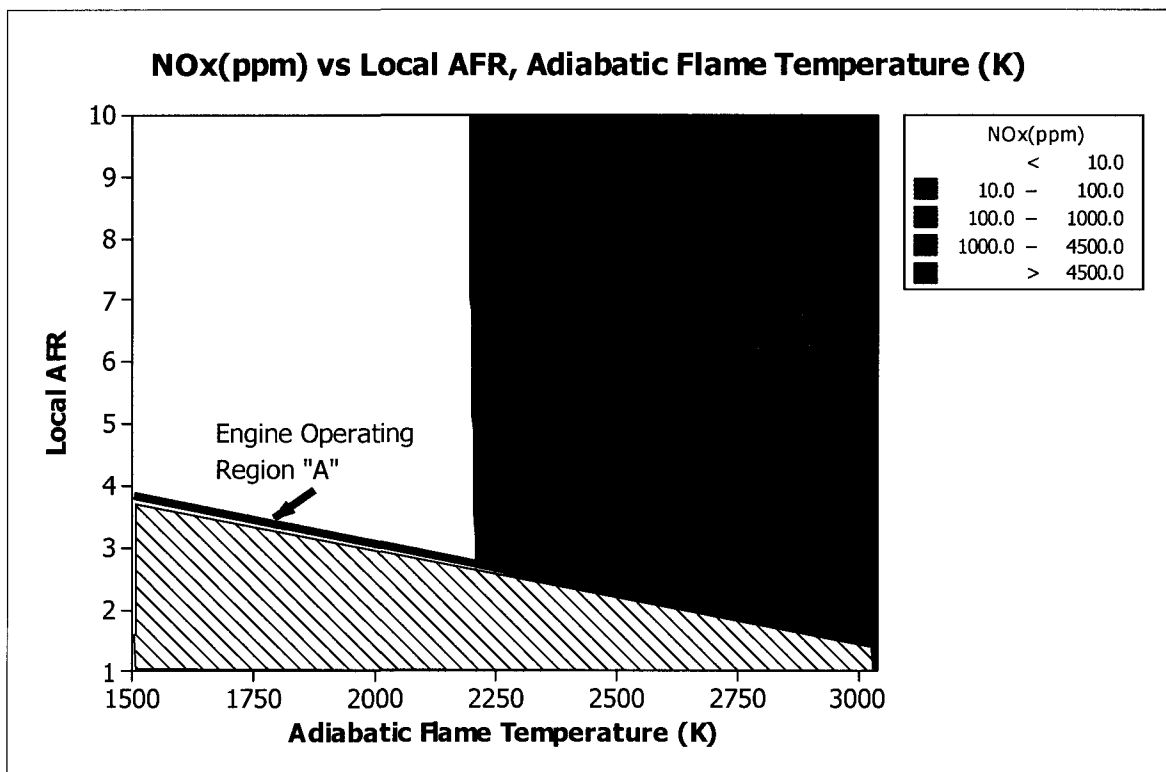
Figure 9-34: Actual engine operating condition in the ϕ-T diagram.
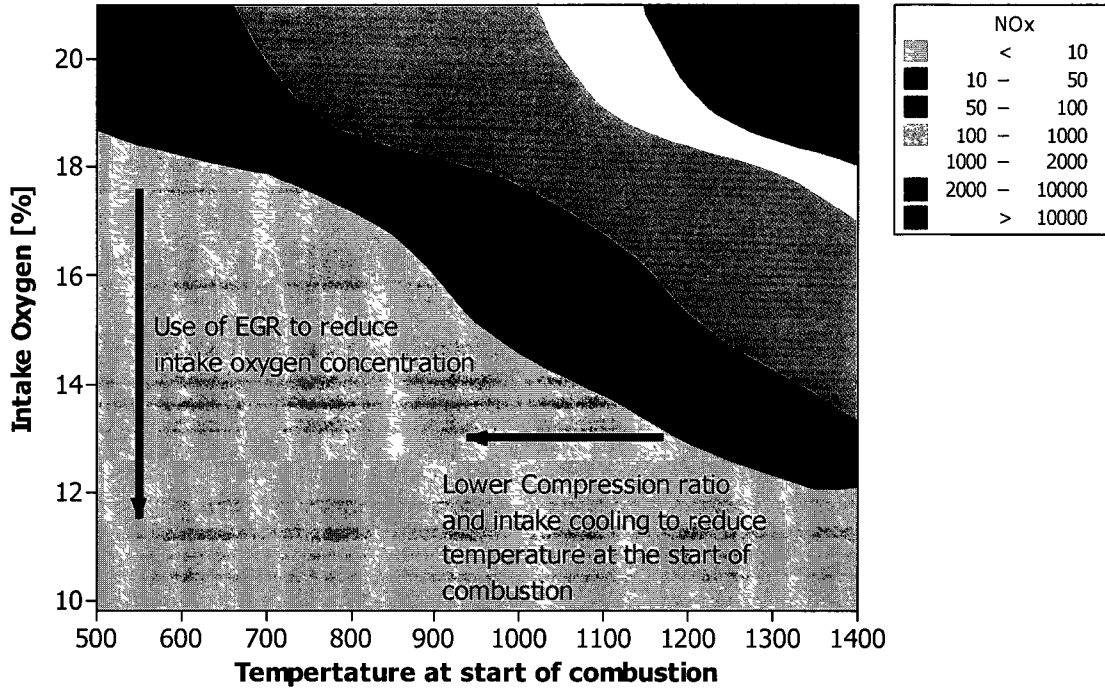
Figure 9-35: Modified ϕ-T diagram in presence of EGR.

CHAPTER X

10 CONCLUSIONS AND FUTURE WORK

10.1 Conclusions

Three types of EPC combustion strategy have been demonstrated. The major characteristics and their applicability ranges are given in Table 10-1. The details of the three combustion strategies are as follows:

a) Multi-pulse EPC: For this strategy a diluted near homogenous cylinder charge was prepared prior to the combustion with the implementation of precisely timed multi-pulse fuel-injection events early during the compression stroke and a heavy use of EGR. The EGR suppressed the auto-ignition of fuel injected during the compression stroke and immensely helped to gain the time necessary for the mixture preparation. It was possible to reduce the NOx, soot and HC simultaneously. This type of the combustion mode was largely applicable to mid-load engine operating conditions.

The significant contributions to this type of combustion mode were:

- Hiroyasu' phenomenological model based injection strategy selection to minimize HC.

- Development of principles for selection of boundary conditions based on a purely kinetic-based modeling.

- Development of minimum mixing duration guidelines for soot emissions.

b) EGR enabled EPC with single injection: This combustion mode was implemented with a single-injection close to top-dead center and a heavy use of EGR. A major advantage of this combustion mode was that the combustion phasing was closely coupled to the fuel injection event. The use of EGR helped to reduce the NOx for this combustion mode. Further, an increased application of EGR helped to lower the flame temperatures and

189

prolong the ignition delay thereby helping to attain simultaneous low-NOx and low-soot. This combustion mode was applied mainly at low-load engine operating conditions.

The significant contributions to this type of combustion mode were:

- Development and implementation of closed-loop cylinder pressure based to keep the combustion stabilization process during the application of high-EGR. It was possible to implement load, boost and RPM transients with the use of closed-loop on combustion phasing control. It was also possible to navigate into and out of this mode of combustion.

- Guidelines were developed for the implementation of this type of combustion. It was found that the NOx and soot could be characterized in terms of intake oxygen values. An intake oxygen of 13~14% was found to be sufficiently dilute for achieving low NOx and an intake oxygen of 9~10% was found to be sufficient for achieving simultaneous low-NOx and low-soot combustion.

- A minimum ignition delay of 1.5ms or an ignition-delay prolonging of 50% was found to be sufficient for producing the simultaneous low-NOx and low-soot combustion.

A limitation of this combustion mode was that the onset of the simultaneous low-NOx and low-soot combustion was preceded by a significant increase in the un-burnt hydrocarbons and carbon monoxide. This resulted in a significant decrease in the cycle thermal efficiency especially at elevated loads. However, higher injection pressure or boost in combination with higher EGR was found to be capable of mitigating the efficiency loss.

c) Combustion mode with a split heat-release characteristic: This combustion mode consisted of a part of fuel delivery very early during the compression stroke and a part of the fuel delivery close to the top-dead-centre. The fuel that was delivered early during the compression stroke had a significantly long ignition delay and the cylinder charge of enhanced homogeneity was prepared before the combustion. This part of the fuel underwent the kinetic control combustion process similar to multi-pulse EPC combustion.

The second part of the fuel was delivered towards the end of the combustion of the first heat-release. This part of fuel had a short ignition delay and had combustion characteristics similar to the conventional combustion.

The significant contributions to this type of combustion mode were:

- The split nature of the combustion limited the rate-of-pressure rise associated with the multi-pulse EPC combustion. The containment of rate-of-pressure rise served to extend the EPC application range to higher load levels.

- The conventional combustion of the second part of the fuel injected destroyed the carbon-monoxide produced earlier in the cycle, thereby improving the combustion efficiency. Synergy existed between the first and the second part of combustion for other aspects as well. For instance, the CO_2 produced during the combustion of the first part fuel served to enhance indirectly the EGR for the second part of combustion, thereby containing NOx without significant EGR addition.

- In addition, it was also possible to implement combustion phasing control directly using injection scheduling for the second part of heat-release rate. The combustion of the second part helped significantly in power production since the power production was configurable directly by injection-timing at the phasing for best-efficiency.

Major advantages and limitations for each of these combustion modes have been analyzed. The implementation of simultaneous low-NOx and low-soot combustion has been associated with fuel-efficiency penalty. The thesis has identified the major causes of this fuel-efficiency decrease as the un-burnt hydrocarbons, carbon-monoxide and combustion phasing. Specific strategies have been presented to overcome each of these limitations.

The concept of EGR reforming was investigated numerically, which showed that a small amount of gaseous-fuel in the form of hydrogen and carbon-monoxide is generated in the exhaust-loop, though without any significant energy penalty. The partial use of gaseous fuel has a potential to enhance the in-cylinder homogeneity and reduce the soot.

Table 10-1: Summary of EPC combustion techniques and their major characteristics

Mode	Loads	Implementation	CO + HC penalty	Phasing penalty	Injection and phasing correlation
Lean	Low-loads	Multiple shots and no EGR	Moderate	Yes	NO
Weak	Low to mid loads	SS+EGR	High	NO	Yes
	Mid-loads	Multiple shots + EGR	Moderate	Yes	No
HCCI-plus-late	Mid-loads with higher load potential	Multiple shots + EGR	Moderate to low	No	Yes

192

10.2 Future Work

In this thesis, EGR, injection scheduling and boost have been discussed as the enablers for the EPC combustion. These factors primarily modulate the air-fuel ratio to gain the time required for the formation of the homogeneous mixture. Another aspect of EPC combustion is to modulate the temperature history before the combustion is initiated to gain the time for mixture preparation. This temperature modulation is done primarily by the use of variable-valve timing or variable compression ratio. As a next step, the effect of temperature modulation on EPC needs to be examined. The EPC combustion has been examined primarily at 1200 and 1500RPM at loads up to 9bar IMEP. The EPC combustion mechanism needs to be investigated at higher RPM and higher loads also. At higher RPM the time available for homogenous mixture preparation is considerably reduced, while at higher loads the quantity of the fuel to be homogenized is significantly higher. Both these factors make the implementation of EPC combustion very challenging at high-loads and high speeds.

REFERENCES

1. Diesel R., "Method for Converting Heat to Work", US Patent 0542846.

2. Diesel R., "Internal Combustion Engine", US Patent 0608845.

3. Cummins C.L., Diesel's Engine: From Conception To 1918. Carnot Press, 1993

4. Heywood J., Internal Combustion Engine Fundamentals, McGraw-Hill Science Engineering, 1988.

5. Aoyagi Y., Kamimoto T., Matsui Y., and Matsuoka S., "A Gas Sampling Study on the Formation Processes of Soot and NO in a Di Diesel Engine", SAE 880423.

6. Hiroyasu H., Nishida K., Suzuki M., and Oda H., Yoshikawa S., and Arai M., "Total In-Cylinder Sampling Experiment on Emission Formation Processes in a D.I. Diesel Engine", SAE 902062.

7. Zhao H., Lowry G., and Ladommatos N., 1996, "Time-Resolved Measurements and Analysis of In-Cylinder Gases and Particulates in Compression-Ignition Engines", SAE 961168.

8. Donahue R.J., Borman G.L., Bower G.R., 1994, "Cylinder-Averaged Histories of Nitrogen Oxide in a D.I. Diesel With Simulated Turbocharging", SAE 942046.

9. Shimazaki N., Hatanaka H., Yokota, K., and Nakahira T., 1996, "A Study of Diesel Combustion Process Under the Condition of EGR and High-Pressure Fuel Injection With Gas Sampling Method", SAE 960030.

10. Kamimoto T., Yokota H., Kobayashi H., 1987, "Effect of High Pressure Injection on Soot Formation Processes in a Rapid Compression Machine to Simulate Diesel Flames", SAE 871610.

11. Kamimoto T., and Bae M.H., "High Combustion Temperature for Reduction of Particulate in Diesel Engines', SAE Paper 880423

12. Uyehara O.A., 1980, "Diesel Combustion Temperature on Soot", SAE 800969.

13. Frenklach M., Taki S., and Matula R.A., "A Conceptual Model for Soot Formation in Pyrolysis of Aromatic Hydrocarbons." Combustion and Flame, 49, p.275, 1983.

14. Kitamura T., Ito T., Senda J., and Fujimoto H., "Mechanism of Smokeless Diesel Combustion with Oxygenated Fuels Based on the Dependence of the Equivalence Ratio and Temperature on Soot Particle Formation", Internal Journal of Engine Research, p. 223-248, 2002.

15. Epsey C., and Dec J., "Diesel Engine Combustion Studies in a Newly Designed Optical-Access Engine Using High-Speed Visualization and 2-D Laser Imaging", SAE 930971.

16. Mellor A.M., Mello J.P., Duffy K.P., Easley W.L., Faulkner J.C., 1998. "Skeletal Mechanism for NOx Chemistry in Diesel Engines", SAE 981450.

17. Turns S.R., An Introduction to Combustion-Concepts and Applications. 2nd Edition, Mc-Grawhill, 2000

18. http:// www.dieselnet.com Accessed 2007.

19. http://www.epa.gov/ttn/catc/dir1/fnoxdoc.pdf. Accessed 2008

20. Zheng M., Reader, G.T., and Hawley J.G., "Diesel Engine Exhaust Gas Recirculation-A Review on Advanced and Novel Concepts", International Journal of Energy Conversion and Management, Vol. 45, Issue 6, pp. 883-900, 2004.

21. Zheng M., Irick D.K., and Hodgson J., "Stabilizing Excessive EGR with an Oxidation Catalyst on a Modern Diesel Engine", ASME ICE-Vol.38, 2002-ICE-455.

22. Buchwald R., Lautrich G., Maiwald O., and Sommer A., "Boost and EGR System for the Highly Premixed Diesel Combustion", SAE 2006-01-0204.

23. Leet J.A, Simescu S., Froelund K., Dodge L.G., "Emissions Solutions for 2007 and 2010 Heavy-Duty Diesel Engines", SAE 2004-01-0124.

24. Krueger U., Pantow E., Lutz R., Dreisbach R., Glensvig M., "High Performance Cooling and EGR Systems as a Contribution to Meeting Future Emission Standards", SAE 2008-01-1199.

25. Zheng M and Reader G.T. et al., "Adaptive Control to improve Low Temperature Diesel Engines Combustion", 12th Diesel Engine-Efficiency and Emissions Reduction (DEER) Conference, 2006.

26. Onishi S., Hong S., Shoda K., Do P., and Kato S., "Active Thermo-Atmosphere Combustion (Atac)--A New Combustion Process for Internal Combustion Engines", SAE Paper No.790501.

27. Noguchi M., Tanaka Y., Tanaka T., and Takeuch Y., "A Study on Gasoline Engine Combustion By Observation of Intermediate Reactive Products During Combustion", SAE Paper No. 790840.

28. Iida N., "Combustion Analysis of Methanol-Fueled Active Thermo- Atmosphere Combustion (Atac) Engine Using a Spectroscopic Observation", SAE Paper No. 940684.

29. Najt P., and Foster D.E., "Compression-Ignited Homogeneous Charge Combustion", SAE Paper No. 830264.

30. Thiring R.H., "Homogeneous Charge Compression Ignition (HCCI) Engines", SAE Paper No. 892068.

31. Ryan T. W., and Callahan T. J., "Homogeneous Charge Compression Ignition of Diesel Fuel", SAE Paper No. 961160.

32. Christensen M., Hultqvist A. and Johansson B., "Demonstrating the Multi-fuel Capability of a Homogeneous Charge Compression Ignition Engine with Variable Compression Ratio", SAE Technical Paper 1999-01-3679.

33. Christensen M., Johansson B., Amneus P.J.H., Mauss F.,"Supercharged Homogeneous Charge Compression Ignition", SAE Paper No.980787

34. Stanglmaier R.H. and Roberts C.E., "Homogeneous Charge Compression Ignition, HCCI: Benefits, Compromises and Future Engine Applications", SAE Technical Paper 1999-01-3682.

35. Zheng M., Mulenga M.C., Reader G.T., Wang M. and Ting D.S-K., "Influence of Biodiesel Fuel on Diesel Engine Performance and Emissions in Low Temperature Combustion", SAE Paper No. 2006-01-3281.

36. Takeda Y., and Keiichi N., "Emission Characteristics of Premixed Lean Diesel Combustion with Extremely Early Staged Fuel Injection", SAE Paper No. 961163.

37. Iwabuchi Y., Kawai K., Shoji T., and Takeda Y., "Trial of New Concept Diesel Combustion System - Premixed Compression-Ignition Combustion", SAE Paper No., 1999-01-0185.

38. Shimazaki N., Akagawa H., and Tsujimura K., "An Experimental Study of Premixed Lean Diesel Combustion", SAE Paper 1999-01-0081.

39. Helmantel A., and Denbratt I., "HCCI Operation of a Passenger Car Common-Rail DI Diesel Engine with Early Injection of Conventional Diesel Fuel", SAE Paper No. 2004-01-0935.

40. Jhavar R., and Rutland C., "Effects of Mixing on Early Injection Diesel Combustion", SAE Paper No. 2005-01-154, 2005.

41. Jacobs T.J., Bohac S.V., Assanis D.N., and Szymkowicz P.G., "Lean and Rich Premixed Compression Ignition Combustion in a Light-Duty Diesel Engine", SAE Paper No. 2005-01-0166.

42. Su W., Wang H., Liu B., "Injection Mode Modulation for HCCI Diesel Combustion", SAE Paper No.2005-01-0117.

43. Gill K., Zhao H., Sison K., and Marriner C., "In-cylinder Studies of Multiple Diesel Fuel Injection in a Single Cylinder Optical Engine", SAE Paper No. 2005-01-09515.

44. Zheng M., Reader G.T., Tan Y., and Wang M., "Adaptive Combustion Control to Improve Diesel HCCI Cycle Fuel Efficiency", ASME No. ICEF2007-1630, p.8.

45. Zheng M., Tan Y., Mulenga M.C., and Wang M., "Thermal Efficiency Analyses of Diesel Low Temperature Combustion Cycles", SAE 2007-01-4019.

46. Kimura S., Aoki O., Ogawa H., Muranaka S., and Enomoto Y., "New Combustion Concept for Ultra-Clean and High-Efficiency Small Di Diesel Engines", SAE Paper No. 1999-01-3681

47. Kimura S., Aoki O., Kitahara Y., and Aiyoshizawa E., "Ultra-Clean Combustion Technology Combining a Low-Temperature and Premixed Combustion Concept for Meeting Future Emission Standards," SAE Paper 2001-01-0200.

48. Kawamoto K., Araki T., Shinzawa M., Kimura S., Koide S., and Shibuya M., "Combination of Combustion Concept and Fuel Property for Ultra-Clean DI Diesel," SAE Paper Number 2004-01-1868.

49. Akihama K, Takatori Y, Inagaki K, Sasaki S, Dean A. Mechanism of the smokeless rich Diesel combustion by reducing temperature. SAE paper 2001-01-0655, 2001.

50. National Instruments Corporation, LabVIEW 7.1, 2004

51. Lancaster D.R., Krieger R.B., and Lienesch J.H., "Measurement and Analysis of Engine Pressure Data", SAE Paper 750026.

52. Zheng M., "Thermodynamic Modeling and Experimental Investigation Experimental Investigation of a Synthetic Atmosphere Diesel Engine System", Ph.D. Thesis, University of Calgary, 1993.

53. Hiroyasu H., and Arai M., "Structure of Fuel Sprays in Diesel Engines", SAE Paper 900475.

54. Ladommatos N., Abdelhalim S.M., Zhao H., and Hu Z., "The Dilution, Chemical, and Thermal Effects of Exhaust Gas Recirculation on Diesel Engine Emissions-Part 1: Effect of Reducing Inlet Charge Oxygen", SAE Paper 961165.

55. Ladommatos N., Abdelhalim S.M, Zhao H., and Hu Z., "The Dilution, Chemical, and Thermal Effects of Exhaust Gas Recirculation on Diesel Engine Emissions -- Part 2: Effects of Carbon Dioxide", SAE Paper 961167.

56. Ladommatos N., Abdelhalim S.M., Zhao H., and Hu Z., "The Dilution, Chemical, and Thermal Effects on Exhaust Gas Recirculation on Diesel Engine Emissions-- Part 3: Effects of Water Vapor", SAE Paper 971659.

57. Kumar R., and Zheng M., "Fuel Efficiency Improvements of Low Temperature Combustion Engine", SAE Paper 2008-01-0841.

58. Miles P., "In-cylinder Flow and Mixing Processes in Light-Duty, Low-Temperature Diesel Combustion Systems", 3rd International Symposium on Homogeneous Charge Compression Ignition (HCCI), San Ramon, CA, 2006.

59. Soylu S, "Examination of Combustion Characteristics and Phasing Strategies of a Natural Gas HCCI Engine", Energy Conversion and Management 46 (2005), pp.101-119.

60. Zheng M., Reader G.T., Kumar R, Mulenga M.C., Asad U., Tan Y., and Wang M., "Adaptive Control to Improve Low Temperature Diesel Engine Combustion", 2006 Diesel Engine Emission Reduction Conference.

61. de Ojeda W., and Karkkanien A., "Multicylinder Diesel Engine Design for HCCI", 2006 Diesel Engine Emission Reduction Conference.

62. Documentation for Injection Analyzer, IAV, Accessed 2008.

63. Johansson B., "The Combustion, Thermodynamic, Gas Exchange and Mechanical Efficiencies of HCCI Engines", Keynote Presentation at SAE Powertrain Conference, Toronto.

64. Cursente V., Pacaud P., Mendez S., Knop V., De Francqueville L., "System Approach for Compliance with Full Load Targets on a Wall Guided Diesel Combustion System", SAE Paper 2008-01-0840.

65. Sjoberg M., and Dec J.E., "Combined Effects of Fuel Type and Engine Speed on Intake Temperature Requirements and Completeness of Bulk-Gas Reactions for HCCI Combustion", SAE 2003-01-3173.

66. Aceves S.M., Smith J.R., Westbrook C., and Pitz W., 1999, "Compression Ratio Effect on Methane HCCI Combustion," ASME Journal of Gas Turbines and Power, Vol. 121, pp. 569-574, 1999.

67. Duffy K.P., Hardy W.L., and Michael P. Liechty, "Effects of Fuel Property Changes on Heavy-Duty HCCI Combustion", SAES paper NO. 2007-01-0191

68. Bozzano G., Dente M., Faravelli T., and Ranzi E., "Fouling phenomena in pyrolysis and combustion processes", Applied Thermal Engineering Volume 22, Issue 8, June 2002, Pages 919-927

69. Kulkarni B.D., and Ramachandran P.A., "A Simple Method for Calculation of Effectiveness Factors under Conditions of Catalyst Fouling", The Chemical Engineering Journal, Volume 19, Issue 1, 1980, Pages 57-66.

70. Bartholomew C.H., "Mechanisms of Catalyst Deactivation", Applied Catalysis A: General, Volume 212, Issues 1-2, 30 April 2001, Pages 17-60.

71. Nagaki H., Furutani H., and Takahashi S., "Acceptability of Premixed Hydrogen in Hydrogen Diesel Engine", SAE 1999-01-2521

72. Kumar S.M., Ramesh A., and Nagalingam B., "Use of hydrogen to enhance the performance of a vegetable oil fuelled compression ignition engine", International Journal of Hydrogen Energy, Volume 28, Issue 10, October 2003, pp 1143-1154.

73. Surovikin V F., "Analytical Description of the Processes of Nucleus-Formation and Growth of Particles of Carbon Black in the Thermal Decomposition of Aromatic Hydrocarbons in the Gas Phase," Khimiya Tverdogo Topliva, 10 (1), pp. 111-122 (1976).

74. Nagle J., and Strickland-Constable R.F., "Oxidation of Carbon Between 1000-2000°C," Proceedings. of the Fifth Conference. on Carbon, pp.154-164 (Pergamon Press, London, 1962).

75. Zheng M., Kumar R., Tan Y., and Reader G.T., "Heat Release Pattern Diagnostics to Improve Diesel Low Temperature Combustion", SAE Paper 2008-01-1726.

76. Tomazic D., and Pfeifer A., "Cooled EGR - A Must or An Option for 2002/04", SAE Paper 2002-01-0962.

77. Ryan T., "Combustion Targets for Low Emissions and High Efficiency", Diesel Engine Emission Reduction 2003.

78. Kodama Y., Nishizawa I., Sugihara T., and Sato N., "Full-Load HCCI Operation with Variable Valve Actuation System in a Heavy-Duty Diesel Engine", SAE Paper No. 2007-01-0215.

11 APPENDIX

11.1 Fuel-Injection Strategies at Clean-Diesel Engine Laboratories

A wide-range of injection-strategies were investigated at the Clean Diesel Engine Laboratory to achieve the EPC type of combustion. Based on the method of fuel-delivery these injection strategies can be sub-divided into intake-port injection, in-cylinder and EGR reforming strategies (Figure 11-1). In this thesis, the primary emphasis was on in-cylinder injection strategies, therefore only a discussion pertaining to in-cylinder injection strategy has been presented here. Depending on the relationship between the injection-strategy and the combustion-phasing, the in-cylinder injection strategies can be divided into two categories:

a) Combustion-phasing decoupled injection-strategy: This type of injection strategy was characterized by a very long-ignition delay, typically greater than 2milli-seconds and in this injection strategy; the combustion phasing was largely decoupled from injection timing and was dominated by the kinetics of the chemical reactions,

b) Combustion-phasing coupled injection-strategy: This type of injection strategy was characterized by a shorter ignition delay and with this injection-strategy the control of the combustion phasing was closely coupled to the fuel injection event.

Note that the fuel delivered in a single or multiple injection events can fall under either category depending on duration of the ignition-delay. For instance, if all the fuel was delivered in a single-injection event at 60°CA BTDC and the combustion was initiated close to the TDC, then this type of combustion would experience a prolonged ignition delay and the combustion phasing would be controlled primarily by EGR or boost . In such a case the single injection event strategy falls under the category of combustion-phasing decoupled injection strategy. However, if all the fuel was delivered at 20°CA BTDC and a direct correlation exists between the injection-timing and the combustion-phasing then this single-injection event strategy would be a representative of combustion-phasing coupled injection-strategy. Similarly, the multiple-injection event strategy can be considered as a combustion-phasing decoupled injection-strategy or the combustion-

202

phasing coupled injection strategy depending on the minimum ignition delay for the injections.

The multiple-event injection delivery that falls under the combustion-phasing decoupled injection strategy was further classified as sparse and dense injection-strategy. In the sparse injection strategy the fuel was delivered in 2~3 injection events very early during the compression stroke and a significant dwell existed between the injection events. An injection event detailed in Section 6.1.3 can be considered as representative of sparse injection strategy. As mentioned before, this type of injection delivery was associated with high HC due to poor vaporization of the fuel and the cylinder wall impingement. The dense injection strategy evolved as a solution to overcome the problem of high HC associated with the sparse injection strategy. In this injection strategy the fuel was delivered in a series of injection events of equal duration. The timing and the duration of the injection events was decided based on the spray-penetration calculations proposed by the Hiroyasu model. The typical heat-release rate associated with the dense injection strategy is shown in Figure 6-12.
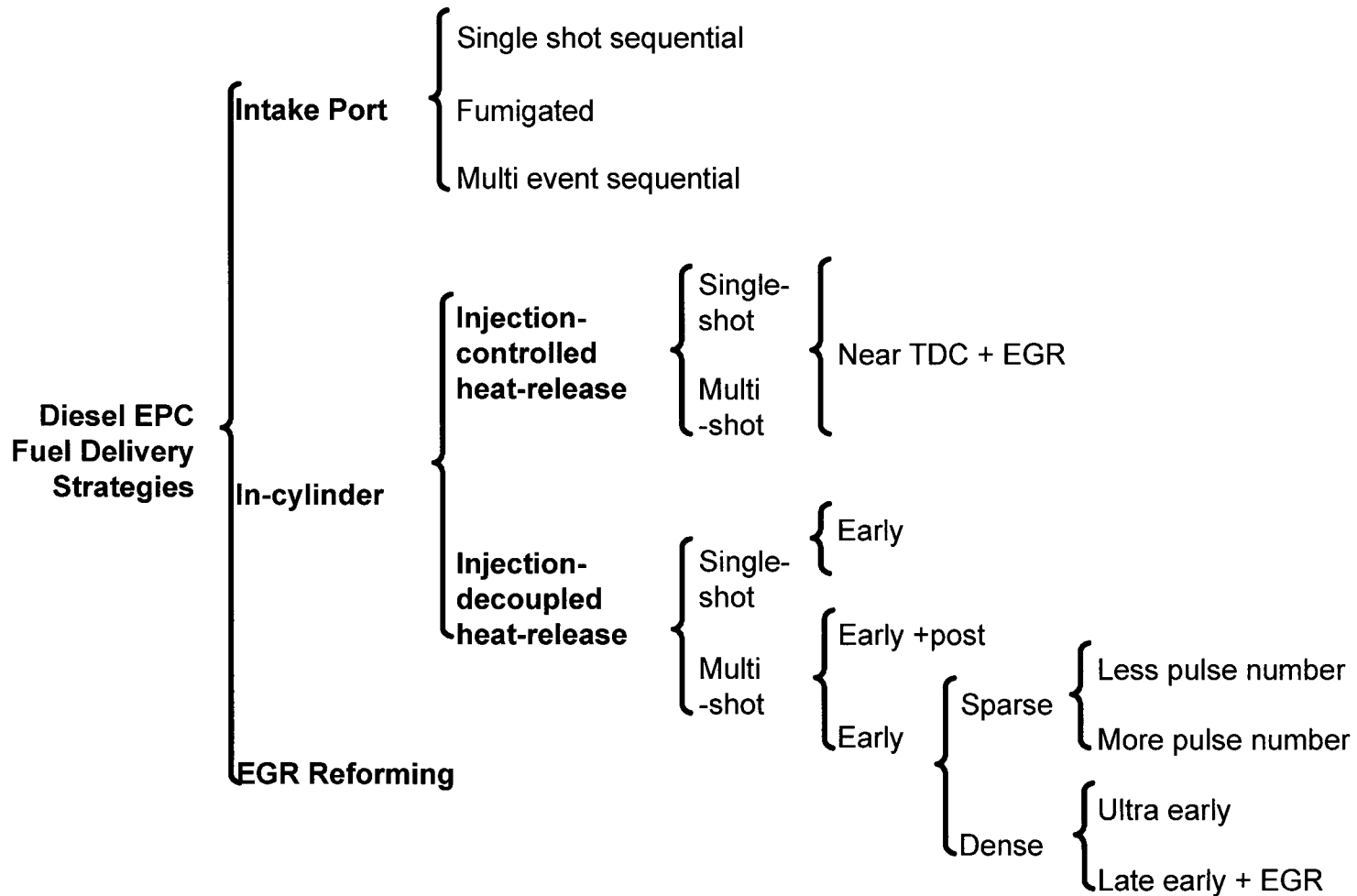
Figure 11-1: Injection strategies investigated for EPC combustion

11.2 Engine Instrumentation

This section provides details of principal components that were used during the course of experiments.

Dynamometer: An eddy current dynamometer (Manufacturer: Schenck Pegasus, Model No.WS-230-F) was for the tests. The engine was connected to the dynamometer via a drive-shaft and an adapter shaft. An empty transmission case was mounted to the engine and the adapter shaft placed inside it. One end (side A) of the adapter shaft was inside the transmission case and was connected to the flywheel and the other end came out of the transmission case (side B). The driveshaft with universal joints at both the ends was connected between the side B and the dynamometer.

Working principle of dynamometer: An eddy-current dynamometer was used to measure the engine speed and the torque produced by the engine during its operation. An eddy current dynamometer consists of a rotor and a stator part. The rotor is coupled to the engine and it rotates at the same speed as the engine. The rotor is connected to the stator electromagnetically. The strength of the electromagnetic coupling between the rotor and the stator decides the resistance offered to the engine rotation. For all the tests the dynamometer was run in the constant engine speed mode.

Encoder: The Ford engine had a baseline crank and a cam position sensor. However, the least-count of the crank sensor was only 6°CA which limited the resolution of the fuel-injection strategy. Therefore, for all the experiments a rotary incremental encoder with a crank-angle resolution of 0.1°CA was set-up and used. (Manufacturer: Gurley Precision Instruments, Model No: 9125S-03600H-5L01-C18SQ-06EN). The encoder was a solid shaft type of encoder; therefore, a special mating, called encoder adapter was prepared and mounted on the crank-shaft pulley. The encoder adapter had a circularity of less than 0.02mm after it was installed on the crank pulley. The encoder was mounted on a bracket using an intermediate adjusting plate. The use of an adjusting plate was to facilitate the alignment between the encoder and the encoder on the engine. The encoder adapter and the encoder were joined together using a flexible coupling (Manufacturer: Gurley Precision Instruments, Model Number: SCA-06E-06E) Since an incremental encoder

was used, it was necessary the encoder had a reference signal in addition to the 0.1°CA signal. The encoder was aligned at the time of installation so that the reference signal coincided with the physical TDC of the engine.

The cylinder pressure data was recorded on the crank-angle basis; this was achieved by using the output of the shaft encoder as an external clock for the data-acquisition system.

Working principle of encoder: The optical encoder operates on the principle of the photo-electrical scanning of very fine gratings. The scanning unit of an encoder consists of a light source, a condenser lens for collimating the light beam, the scanning reticule with the index gratings, and silicon photovoltaic cells. When the scale is moved relative to the scanning unit, the lines of the scale coincide alternately with the lines or spaces in the index grating. The periodic fluctuation of light intensity is converted by photovoltaic cells into electrical signals.

Cylinder pressure transducer: A piezo-electric type of glow-plug mounted, un-cooled pressure transducer was used for in-cylinder pressure measurement. (Manufacturer: AVL, Model Number: GU-13P). The membrane of the pressure transducer was flush-mounted to minimize any resonance effect.

Working principle of piezo-electric pressure transducer: The in-cylinder pressure transducers are based on the principle of piezo-electricity. Piezoelectricity is the ability of some materials, such as quartz to generate an electric charge in response to applied mechanical force/pressure. As the cylinder in-cylinder pressure increases during the compression and the combustion process the piezo-electric crystals of the pressure transducer become electrically charged and produce charge (measure in pico-columbs) in direct proportion to the in-cylinder pressure. The AVL pressure transducer is based on the longitudinal effect which means that the crystal charges in the x-plane for the force acting on the x-plane. An alternative of the longitudinal effect is the transverse effect where the crystal charges on the x-plane for force acting on the y-plane. The output of the signal is transferred by means of a highly insulating, low-noise cable to the charge amplifier unit where it is converted to the voltage signal.

The engine coolant (temperature) and the engine lubricating oil (pressure and temperature) were maintained constant independent of engine operating conditions using special conditioning units. (Manufacturer: FEV, Model Number: Coolcon and Lubcon)

Fuel-flow measurement: The fuel-flow measurements were done on a high-precision volumetric-flow meter (Manufacturer: Ono-Soki, Model No. 2140H). The fuel-flow detector had a resolution of 0.1 ml and an accuracy of +/- 0.2% of reading over the entire range from 0.3 to 120 liters/hr.

Mass-air flow meter: Two mass-air flow meters were installed as part of the engine instrumentation. The first one was the hot-film mass air flow meter (Manufacturer: Bosch, Model No.EH-047820), that was used when the engine was tested in the naturally-aspirated condition. The hot-film mass air flow meter is a type of thermal flow-meter that correlates the sensor thermal characteristics to the engine's mass air-flow rate. The sensor filament includes temperature sensor and a heating area that is exposed to the engine's air flow. As the air flows past the sensor, the sensor cools, decreasing its resistance, which in turn allows more current to flow through the circuit. As more current flows, the wire's temperature increases until the resistance reaches equilibrium again. The amount of current required to maintain the wire's temperature is directly proportional to the mass of air flowing past the wire.

For engine tests where the boost was higher than 1bar (absolute) an alternate method was used to evaluate the mass-air flow rate. In this scenario, the volumetric flow-rate was first measured using a positive displacement method and then combined with the density term to give the mass air flow-rate (Manufacturer: Dresser Inc, Model No.5M175). In this method, the gas volumes are measured by correlating it with the rotating characteristics of two impellers in a chamber of fixed volume.

11.3 US-FTP Emission Norms

The Clean Air Acts Amendment (CAAA) of 1990 introduced two sets of standards for light-duty vehicles.

Tier 1 standards: These sets of rules were published as a final rule in 1991 and were phased in progressively during 1994 to 1997.

Tier 2 standards: These sets of rules were adopted in December 1999, and will be implemented from 2004 to 2009.

The Tier 1 standards were applied to all new light-duty vehicles (LDV). A vehicle was classified as an LDV if the gross vehicle weight is less than 8500 lbs. Note that the gross vehicle weight rating (GVWR) includes the weight of the vehicle and the cargo. The LDV were further sub-divided into:

a) Passenger cars

b) Light-light duty trucks (less than 6000lbs GVWR)

c) Heavy-light duty trucks (between 6000 to 8500lbs GVWR)

For Tier 2, the applicability of Tier 1 standards was extended to cover the heavier vehicle categories. The emission regulation was extended to vehicles with a GVWR between 8500~10,000 lbs and were used for personal transportation. The vehicle categories used for Tier 2 standard is given below:

Table 11-1: Vehicles categories used in EPA Tier 2 Standards

Vehicle Category			Abbreviation	Requirements
Light-Duty Vehicle			LDV	Max. 8500 lb GVWR
Light-Duty Truck			LDT	Max. 8500 lb GVWR, Max. 6000 lb curb weight and max 45 ft2 frontal area
	Light-light duty truck		LLDT	Max. 6000 lb
		Light-duty truck 1	LDT1	Max 3750 lb LVW
		Light-duty truck 2	LDT2	Min 3750 lb LVW
	Heavy light-duty truck		HLDT	Min. 3750 lb
		Light duty truck	LDT3	Max 5750 lb ALVW
		Light-duty truck	LDT4	Min 5750 lb ALVW
Medium-Duty Passenger Vehicle			MDPV	Max 10000lb GVWR

LVW: Loaded vehicle weight = curb weight + 300 lb

ALVW: Adjusted loaded vehicle weight = Average GVWR and curb weight

Tier 2 Certification Bins

The Tier 2 emissions standards are structured into 8 permanent and 3 temporary certification levels of different stringency, called "certification bins". In addition the vehicle manufacturers also have to maintain an average fleet standard for NOx. The average NOx emissions for the entire light-duty fleet sold by each manufacturer have to meet the average NOx standard of 0.07 g/mi. The temporary certification bins (bin 9,10 and MDPV bin 11) are available only during the phase-in period and expire after the

2008 model year. For every vehicle manufacturer, the Tier 2 vehicles are the one's that meet the requirements of one of the available bins and are used to meet the requirement that a percentage of the fleet have an average NOx emission of 0.07 g/mile. During the phase-in period, the part of the fleet not satisfying the 0.07 g/mile NOx average is referred to as the interim non-Tier 2 vehicles. They must still meet the requirements of one of the available bins but have more relaxed fleet average requirements.

The emission standards for all pollutants (certification bins) when tested on the Federal Test Procedure (FTP) are shown in Table A.2. Typically, "intermediate useful life" exhaust emission standards or "full useful life" are applicable for the test vehicles. The "intermediate useful life" is for five years or 50,000 miles, whichever occurs first. Similarly, "full useful life" period for LDVs and light LDTs is considered as 120,000 miles or ten years whichever occurs first and for heavy LDTs and MDPVs, it is 11 years or 120,000 miles whichever occurs earlier. Additionally, the manufacturers may optionally adhere to the Tier 2 exhaust emission standards for 150,000 miles and gain NOx credits or opt out of intermediate life standards. In such a case, the useful life is 15 years or 150,000 miles, whichever occurs first. For interim non-Tier 2 LDV/LLDTs, the useful life is 10 years or 100,000 miles, whichever occurs earlier.

The emission regulations in Canada are decided by Environment Canada and Transport Canada. Based on the Canadian Environmental Protection Act 1999 (CEPA 1999), Environment Canada regulates emissions from engines other than those used in aircraft, railway locomotives and commercial marine vessels. The emissions from aircraft, railway locomotives and commercial marine vessels are regulated by Transport Canada. The general approach to setting vehicle emissions standards in Canada is to synchronize with the US EPA federal standards as much as possible. This process was initiated in 1988, for the on-road vehicle emission standards. In February 2001, the Minister of the Environment in the Federal Agenda on Cleaner Vehicles, Engines and Fuels set out a number of policy measures that would continue the harmonization of on-road emissions standards as well as to expand this harmonization by developing emission standards for off-road engines and standards for fuels that are aligned with those of the federal US EPA requirements

Table 11-2: Tier 2 emission standards, FTP 75 g/mi [18]

Bin	Intermediate Life (5 years or 50,000 miles)					Useful Life				
	NMOG*	CO	NOx	PM	HCHO	NMOG*	CO	NOx[+]	PM	HCHO
Temporary Bins										
11 MDPV[c]						0.28	7.3	0.9	0.12	0.032
10[a,b,d,f]	0.125	3.4	0.4	-	0.015	0.156	4.2	0.6	0.08	0.018
9[a,b,e,f]	0.075	3.4	0.2	-	0.015	0.090	4.2	0.3	0.06	0.018
Permanent Bins										
8[b]	0.1	3.4	0.14	-	0.015	0.125	4.2	0.2	0.02	0.018
7	0.075	3.4	0.11	-	0.015	0.09	4.2	0.15	0.02	0.018
6	0.075	3.4	0.08	-	0.015	0.09	4.2	0.10	0.01	0.018
5	0.075	3.4	0.05		0.015	0.09	4.2	0.07	0.01	0.018
4	-	-	-		-	0.07	2.1	0.04	0.01	0.011
3	-	-	-		-	0.055	2.1	0.03	0.01	0.011
2	-	-	-		-	0.01	2.1	0.02	0.01	0.004
1	-	-	-		-	0.00	0.0	0.00	0.0	0.000

- * for diesel fueled vehicle, NMHC (non-methane hydrocarbons)) is considered as NMOG (non-methane organic gases)

- [+] average manufacturer fleet NOx standard is 0.07 g/mi for Tier 2 vehicles

- a - Bin deleted at end of 2006 model year (2008 for HLDTs)

- b - The higher temporary NMOG, CO and HCHO values apply only to HLDTs and MDPVs and expire after 2008

- c - An additional temporary bin restricted to MDPVs, expires after model year 2008

- d - Optional temporary NMOG standard of 0.195 g/mi (50,000) and 0.280 g/mi (full useful life) applies for qualifying LDT4s and MDPVs only

- e - Optional temporary NMOG standard of 0.100 g/mi (50,000) and 0.130 g/mi (full useful life) applies for qualifying LDT2s only

- f - 50,000 mile standard optional for diesels certified to bins 9 or 10

Tier 2 Emission standard phase-in

The Tier 2 standards are being phased-in between 2004 and 2009, as shown in Table A.3. For the new passenger cars (LDVs) and LLDTs, Tier 2 standards phase-in begins in 2004, with full implementation by the 2007 model year whereas for the HLDTs and MDPVs, the Tier 2 standards are phased from the beginning of 2008, with the full compliance to be achieved by 2009.

Up through and including model year 2008, manufacturers must calculate separate fleet average NOx emissions for the portion of their fleet of LDV/LLDT and HLDT/MDPV Tier 2 vehicles being phased-in. Both must comply with the 0.07 g/mile standard (equivalent to bin 5) for the required phase-in percentage for that year.

During the phase-in period, vehicles not used to meet the Tier 2 FTP phase-in requirements must still comply with the full useful life and intermediate useful life FTP exhaust emission standards for one of the available bins listed in Table 2 (i.e., at least bin 10 for LDV/LDTs and bin 11 for MDPVs).

During the period 2004-2007, all passenger cars (LDVs) and LLDTs not certified to the primary Tier 2 standards (i.e., the 0.07 g/mile fleet average NOx) must meet an interim average standard of 0.30 g/mi NOx, equivalent to bin 9 and the NLEV standards for LDVs.

During the period 2004-2008, HLDTs and MDPVs not certified to the final Tier 2 must meet an interim average standard of 0.20 g/mi NOx (equivalent to bin 8) following the schedule in Table 2. Those vehicles not covered by the phase-in requirements are still subject to the emission standards listed in Table 1 (i.e., bin 10, 0.6 g/mi NOx, for HLDTs and bin 11, 0.9 g/mi NOx, for MDPVs).

Through model year 2007, a manufacturer may opt to certify diesel engines for MDPVs through the heavy-duty diesel engine requirements instead of the entire vehicle through the light-duty regulations. These vehicles cannot be used for compliance with phase-in requirements for interim non-Tier 2 MDPVs

Table 11-3: Phase-in percentages for Tier 2 requirements

Model Year	LDV/LLDT		
	Tier 2a	Tier 2b	Interim Non-Tier2c
2004	25		25
2005	50		50
2006	75		75
2007	100		100
2008	100	50	100
2009 and subsequent	100	100	

a - Percentage of LDV/LLDTs that must meet Tier 2 requirements

b - Percentage of HLDT/MDPVs that must meet Tier 2 requirements

c - Percentage of non-Tier 2 HLDT/MDPVs that must meet interim non-Tier 2 fleet

average NOx requirements

11.4 Evolution of Diesel Engine Oils

A brief history about the evolution of diesel engine oil has been provided in this section and a quick look at the Table 11-4 shows that implementation of every major emission benchmark was preceded by the introduction of appropriate engine oils. For instance, implementation of high-rates of EGR was possible in for meeting the Year 2004 emission norms primarily because of the development of the engine oil that was able to sustain engine durability in the presence of EGR. A similar advancement in the oil properties are again needed to meet the future emission norms and its essential that the engine oil developments are in alignment with the development of newer combustion strategies such as the EPC.

Table 11-4: Evolution of diesel engine oil with increasingly stringent emission norms

API-Designation	Year	Purpose or reason for change
CD	Before 1988	Deposits/Corrosion
CE	1988	Oil Consumption
CF-4	1990	Fuel Efficiency/PM
CG-4	1995	PM and Sulfur reduction
CH-4	1999	NOx reduction with injection timing retarding
CI-4	2002	Sustain engine durability in presence of EGR
(PC-10)	2007	After-treatment compatible

11.5 Modeling Equations

Governing equations for KIVA

The mass, momentum and energy equations coupled with the turbulence equations is solved for the fluid-phase

Conservation of mass:

$$\frac{\partial \rho}{\partial t} + \nabla.(\rho \vec{u}) = \dot{\rho}^s$$

(11.1)

Conservation of momentum:

$$\frac{\partial(\rho\vec{u})}{\partial t} + \nabla.(\rho\vec{u}\vec{u}) = \rho\vec{g} + \vec{F}^s - \frac{1}{\alpha^2}\nabla p + \nabla.\vec{\sigma} - A_0\nabla\left(\frac{2}{3}\rho k\right)$$

(11.2)

Conservation of energy:

$$\frac{\partial(\rho I)}{\partial t} + \nabla.(\rho\vec{u}I) = -\nabla.\vec{J} + \dot{Q}^c + \dot{Q}^s - p\nabla.\vec{u} + (1 - A_0)\vec{\sigma}\nabla\vec{u} + A_0\rho\varepsilon$$

(11.3)

Turbulent kinetic energy:

$$\frac{\partial(\rho k)}{\partial t} + \nabla.(\rho\vec{u}k) = -\frac{2}{3}\rho k\nabla.\vec{u} + \vec{\sigma}\nabla\vec{u} + \nabla.\left[\frac{\mu}{Pr_k}\nabla k\right] - \rho\varepsilon + \dot{W}^s$$

(11.4)

Turbulent kinetic energy dissipation:

$$\frac{\partial(\rho\varepsilon)}{\partial t} + \nabla.(\rho\vec{u}\varepsilon) = -\left(\frac{2}{3}c_{\varepsilon1} - c_{\varepsilon2}\right)\rho\varepsilon\nabla.\vec{u} + \nabla.\left[\frac{\mu}{Pr_\varepsilon}\nabla\varepsilon\right] + \frac{\varepsilon}{k}\left(c_{\varepsilon1}\vec{\sigma}\nabla\vec{u} - c_{\varepsilon2}\rho\varepsilon + c_s\dot{W}^s\right)$$

(11.5)

Heat flux:

$$\vec{J} = -K\nabla T - \rho D\sum_m h_m\nabla\left(\frac{\rho_m}{\rho}\right)$$

(11.6)

216

Equations of state:

$$p = R_0 T \sum_m \left(\frac{\rho_m}{\rho} \right)$$

(11.7)

$$I(T) = \sum_m \left(\frac{\rho_m}{\rho} \right) I_m(T)$$

(11.8)

$$c_p(T) = \sum_m \left(\frac{\rho_m}{\rho} \right) c_{pm}(T)$$

(11.9)

$$h_m(T) = I_m(T) + \frac{R_0 T}{W_m}$$

(11.10)

Conservation of mass is also written for each of the N individual species considered in the reaction as follows:

$$\frac{\partial \rho_m}{\partial t} + \nabla \cdot (\rho_m \vec{u}) = \nabla \cdot \left[\rho D \nabla \left(\frac{\rho_m}{\rho} \right) \right] + \dot{\rho}_m^c + \dot{\rho}_m^s \delta_{m1}$$

Mass consistency check:

$$\sum_{m=1}^{N_c} \frac{\rho_m}{\rho} = 1$$

The description of the unknown is shown below:

ρ = total mass density

$\vec{u}$ = u_1, u_2, u_3 fluid velocity

I = specific internal energy

k = turbulent kinetic energy

ε = turbulent kinetic energy dissipation

$\vec{J}$	=	heat flux vector

p	=	fluid pressure

T	=	temperature

ρ_m	=	density of chemical species from 1...N

The description of the parameters and the constants appearing in the equation is given below:

α	=	dimensionless quantity with pressure gradient scaling method

μ	=	first viscosity coefficient

λ	=	second viscosity coefficient

$\vec{\sigma}$	=	viscous stress tensor

δ	=	knocker's delta function

h_m	=	enthalpy of chemical species, m

c_p	=	specific heat at constant pressure for the fluid phase

c_{pm}	=	specific heat at constant pressure for species, m

$\vec{g}$	=	acceleration due to gravity

A_0	=	0 for laminar model, 1 for turbulence model

A_3	=	$-2/3$ for turbulent flows

D	=	diffusion coefficient for Fick's law

$\vec{I}$	=	unit tensor

I_m =   specific internal energy of species, m

K   =   ratio of diffusion to transport coefficient

Pr   =   Prandtl number

R_0 =   Universal gas constant

S_c =   Schimdt number

W_m =   molecular weight of species, m

The constants used in the turbulence model are as follows:

$c_{\varepsilon 1}$ =   1.44

$c_{\varepsilon 2}$ =   1.92

$c_{\varepsilon 3}$ =   -1.0

Pr_k =   1.0

Pr_ε =   1.3
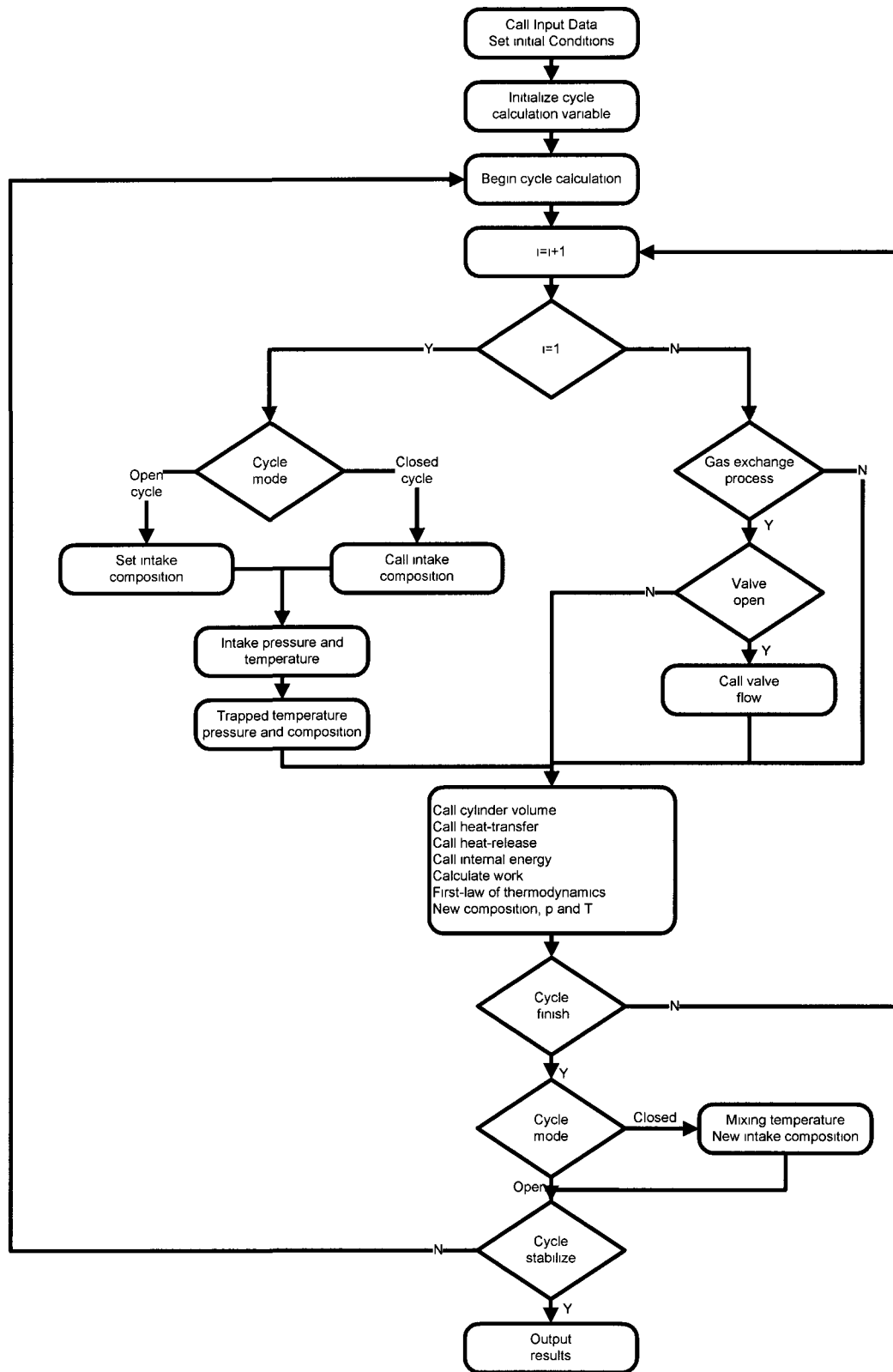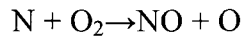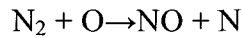
c_s =   1.5

Figure 11-2: Basic flow-chart for implementation of zero-dimensional engine cycle simulations.

11.6 NOx Estimation Using Zeldovich mechanism

The two main reactions of the Zeldovich mechanism are:

$N_2 + O \rightarrow NO + N$

$N + O_2 \rightarrow NO + O$

$$k_{1f} = 1.8 \times 10^{11} \exp[-38370/T(K)], \ m^3/kmol - s$$

$$k_{1r} = 3.8 \times 10^{10} \exp[-425/T(K)], \ m^3/kmol - s$$

$$k_{2f} = 1.8 \times 10^{7} \exp[-4680/T(K)], \ m^3/kmol - s$$

$$k_{2r} = 3.8 \times 10^{6} \exp[-20820/T(K)], \ m^3/kmol - s$$

Since the second reaction is much faster than the first, the steady-state approximations can be used to estimate the N-atom concentration. During the conventional combustion, the NO formation reaction is typically much slower than other reactions involving O2 and O. Thus, O2 and O are assumed to be in equilibrium given by:

$O_2 \leftrightarrow 2O$
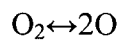
Therefore, for the global mechanism:

$N_2 + O_2 \rightarrow 2NO$
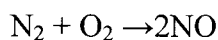
$$\frac{d[NO]}{dt} = k_G [N_2]^m [O_2]^n$$

After ignoring the reverse reaction, it can be written as

$$\frac{d[NO]}{dt} = k_{1f} [N_2][O] + k_{2f} [N][O_2]$$

$$\frac{d[N]}{dt} = k_{1f} [N_2][O] - k_{2f} [N][O_2]$$

with the steady-state approximation of $d[N]/dt = 0$

$$[N]_{SS} = \frac{k_{1f}[N_2][O]}{k_{2f}[O_2]} \text{ , substituting in the rate equation for NO}$$

$$\frac{d[NO]}{dt} = 2k_{1f}[N_2][O]$$

in part-per-million

$$\frac{d\chi_{NO}}{dt} = \frac{R_u T}{P} \frac{d[NO]}{dt}$$

$$\int_0^t d[NO] = \int 2k_{1f}[N_2][O]$$

11.7 Carbon Monoxide Formation

The effect of important factors namely; pressure, temperature and oxygen concentration were computed using Aurora part CHEMKIN as shown below.

11.7.1 Effect of temperature
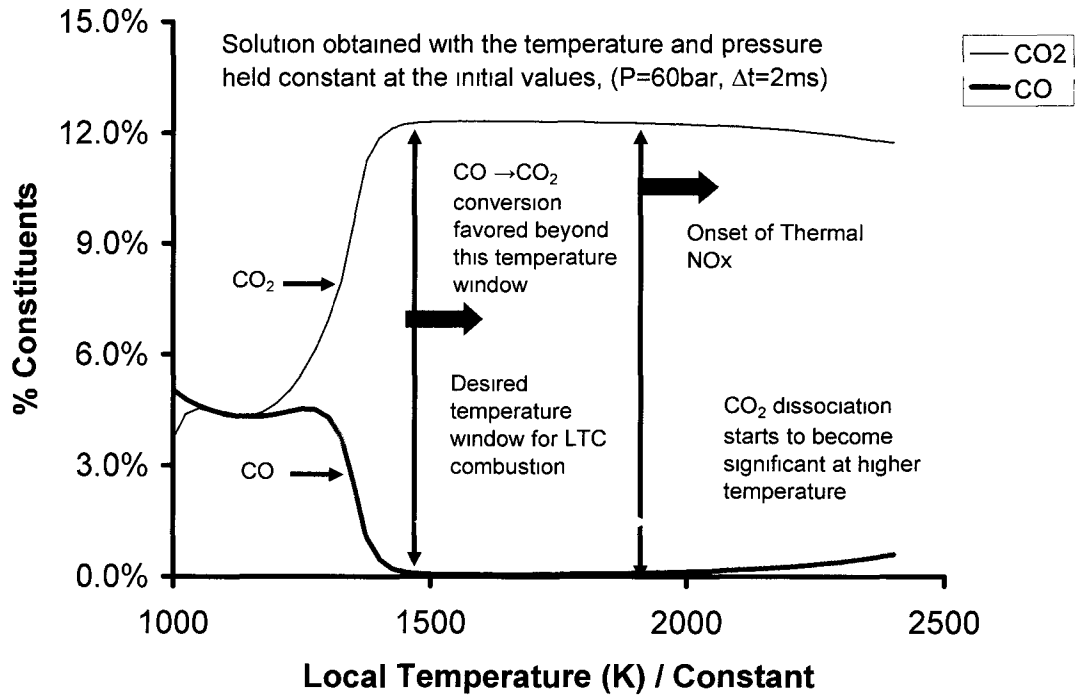

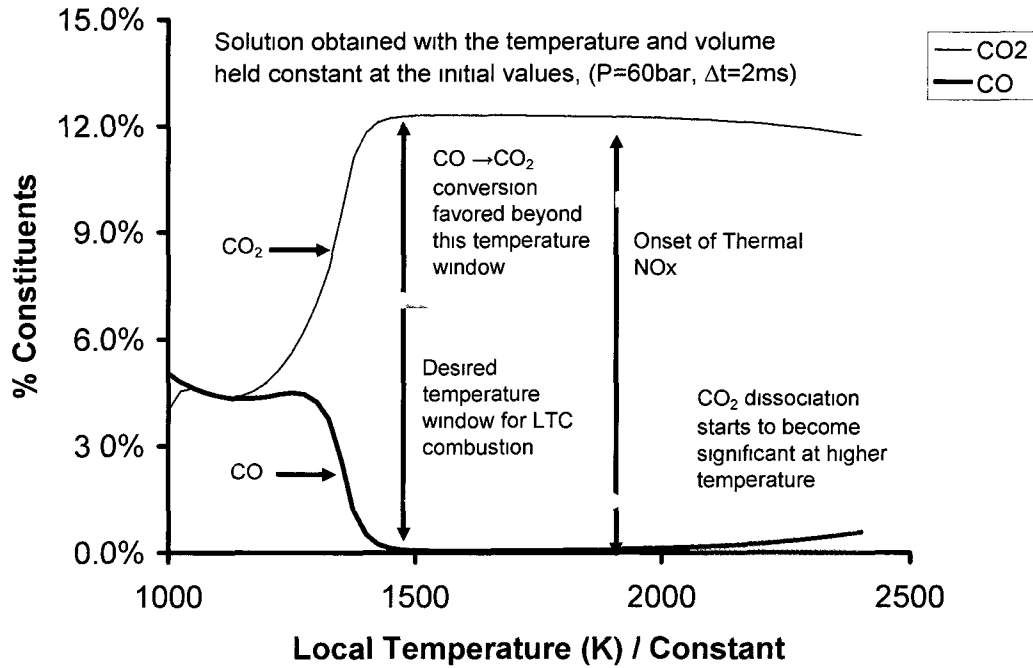Figure 11-3: Effect of temperature on CO oxidation (constant temperature and pressure assumption).

Figure 11-4: Effect of temperature on CO oxidation (constant temperature and volume assumption).
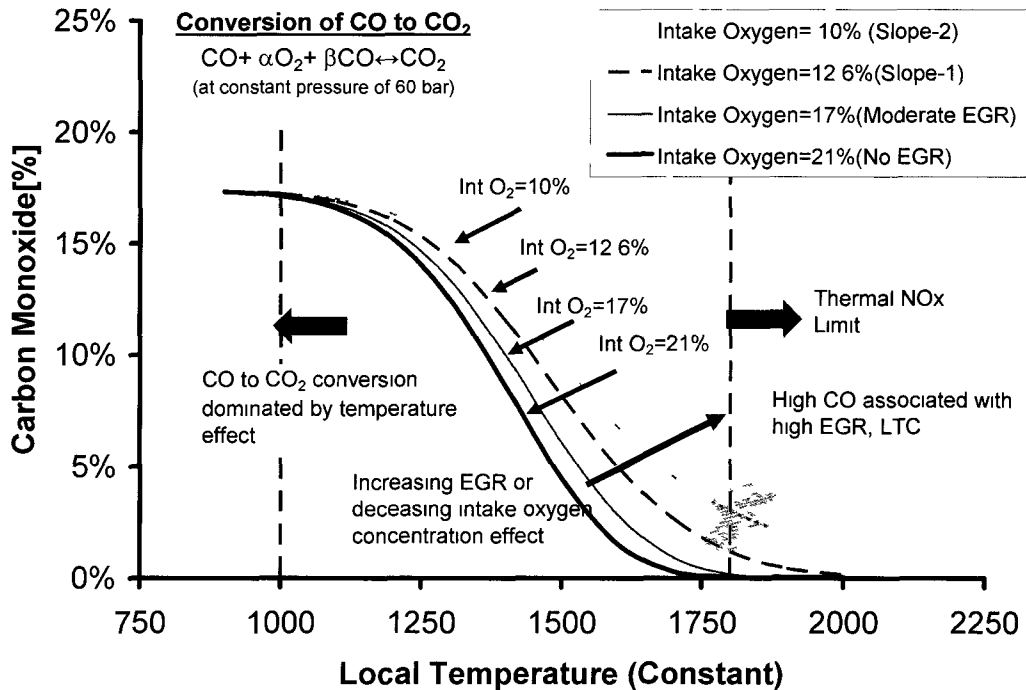
11.7.2 Effect of oxygen concentration

Figure 11-5: Effect of oxygen concentration on CO conversion.
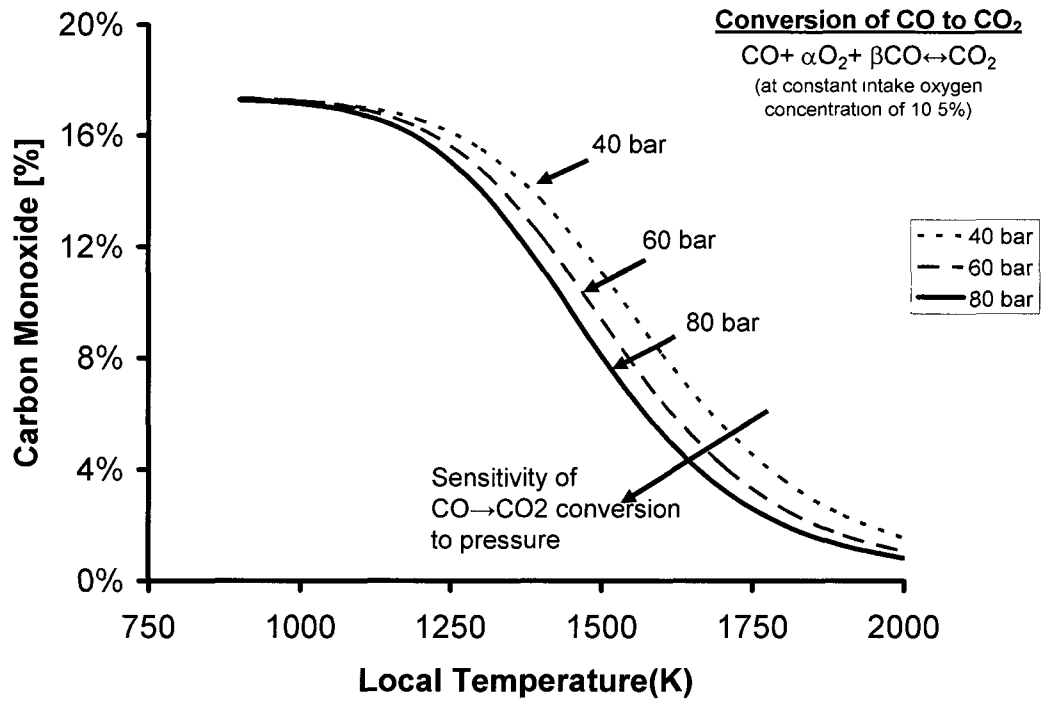
11.7.3 Effect of pressure

Figure 11-6: Effect of oxygen pressure on CO conversion.

11.8 Various Methods of Expressing EGR

Various methods of expressing EGR were found in the literature. Some of the commons expressions are listed in the following table;

Table 11-5: Some of commonly used methods to evaluate EGR in the literature

EGR Expression	Explanation of Term	Operating Conditions	References
$d = \dfrac{(CO_2)_i}{(CO_2)_e}$	d= charge dilution fraction $(CO_2)_i$ = volume % of CO_2 at the intake $(CO_2)_e$ =volume % of CO_2 at the exhaust	SI engine	Benson, 1971
$\%EGR = \dfrac{CO_2, \text{int}ake}{CO_2, exhaust}$		Single cylinder, DI Cooled EGR, 0~20% EGR	Yu, 1981
$\%EGR = \dfrac{V_o - V_{air}}{V_o}$	V_o = Flow rate of inlet fresh air without EGR V_{air} = Flow rate of inlet fresh air with EGR	DI diesel engine Cooled and un-cooled EGR, 0~70% EGR investigated	Narusawa, 1990
$\%EGR = \dfrac{\dot{m}_o - \dot{m}}{\dot{m}_o}$	$\dot{m}_o$ = Mass flow rate of fresh air without EGR $\dot{m}$ = Mass flow rate of fresh air with EGR	DI diesel engine Cooled EGR, 0~40% EGR	Yoshikawa, 1993
$\%EGR = \dfrac{(CO_2)_{in} - (CO_2)_{amb}}{(CO_2)_{exh} - (CO_2)_{amb}}$		DI Diesel, un-cooled EGR, 0~10% EGR	Pierpont, 1995

226

11.9 Glossary of Terms

Brake mean effective pressure: The work accomplished during one engine cycle divided by the engine swept volume. The term "brake" denotes the actual torque/power available at the engine flywheel as measured on a dynamometer.

Brake specific fuel consumption: BSFC is measure of engine efficiency and is calculated as the ratio of the engine fuel consumption to the engine power output (as measured at the flywheel). BSFC has units of grams of fuel per kilowatt-hour (g/kWh) or pounds mass of fuel per brake horsepower-hour (lb/bhp-hr).

Cetane number: Cetane number is a measure of easiness of ignition quality for the diesel fuel. The higher the cetane number, the easier the fuel ignites after ignition. Cetane number is determined by an engine test using two reference fuel blends of known cetane numbers. The reference fuels are prepared by blending normal cetane (n-hexadecane), having a value of 100, with heptamethyl nonane, having a value of 15.

Common-rail injection: A diesel fuel injection system that employs a common pressure accumulator is called a common-rail injection system. In the common rail injection system the injection pressure is independent from engine speed and load. Therefore, the injection parameters can be freely controlled. Usually common-rail engines have the ability to perform multi-pulse injection.

Compression Ignition: The form of ignition, where the rapid compression of air within the cylinders generates the heat required to ignite the fuel as it is injected.

Direct injection: Diesel engines in which the fuel is injected directly into the combustion chamber.

Homogeneous mixture: A cylinder charge of uniform composition.

Ignition delay: The time duration between the start of injection and the start of combustion.

In-direct injection: Diesel engines in which the combustion chamber is divided into a pre-chamber and main chamber. The combustion starts in the pre-chamber and propagates to the cylinder.

Stoichiometric: The quantity of oxidizer that is just the right amount needed to completely burn the fuel. If more than the stoichiometric quantity of the oxidizer is supplied, the mixture is said to be fuel lean, while supplying less than stoichiometric amount of oxidizer results is a rich mixture.

Weaken mixture: Cylinder charge that contains less than 21% oxygen at the intake due to the application of EGR.

VITA AUCTORIS

NAME: Raj Kumar

PLACE OF BIRTH: Madurai, India

DATE OF BIRTH: May 9th, 1973

EDUCATION: University of Windsor, Windsor, Ontario, Canada
2003-2008, PhD

University of Tennessee, Knoxville, USA
2000-2002, M.A.Sc

Delhi College of Engineering, Delhi, India
1991-1995, B.Eng

LIST OF PUBLICATIONS

a) Peer Reviewed Publications

2) M. Zheng, **R. Kumar**, Y. Tan and G.T. Reader, "Heat Release Pattern Diagnostics to Improve Diesel Low Temperature Combustion", SAE Paper 2008-01-1726.

3) **R. Kumar** and M. Zheng, "Fuel Efficiency Improvements of Low Temperature Combustion Diesel Engines", SAE Paper 2008-01-0841

4) W. de Ojeda, **R. Kumar**, P. Zoldak and R. Espinosa, "Development of a Fuel Injection Strategy for Diesel LTC", SAE 2008-01-0057.

5) **R. Kumar**, M. Zheng, U. Asad and G.T. Reader, "Heat-Release Based Adaptive Control to Improve Low Temperature Diesel Engine Combustion", SAE Paper 2007-01-0771, 2007.

6) M. Zheng, U. Asad, **R. Kumar**, G.T. Reader, M.C. Mulenga, M. Wang and J.S. Tjong, "An Investigation of EGR Treatment on the Emission and Operating Characteristics of Modern Diesel Engines", SAE Paper 2007-01-1083, 2007.

7) M. Zheng, **R. Kumar**, and G.T. Reader, "Adaptive Fuel Injection Tests to Extend EGR Limits on Diesel Engines", SAE Paper 2006-01-3426, 2006.

8) M. Zheng, G.T. Reader, D. Wang, J. Zuo, **R. Kumar**, M.C. Mulenga, U. Asad, D.S.K. Ting and M. Wang, "A Thermal Response Analysis on the Transient Performance of Active Diesel After-treatment", **SAE Transactions Journal of Fuels and Lubricants**, Paper 2005-01-3885, 2005.

9) **R. Kumar**, M. Zheng and G.T. Reader, "Preliminary Energy Efficiency Analysis on Multi-Pulse Injection Schedule in a Diesel Engine", ASME-ICEF 2005-1212, 2005.

10) **R. Kumar**, M. Zheng, G.T. Reader, S.J. Ko, and D.S.K. Ting, "Preliminary Energy Efficiency Analysis of an EGR Fuel-Reformer", **SAE Transactions Journal of Fuels and Lubricants**, Paper 2004-01-2918, 2004.

11) **R. Kumar**, G.T. Reader and M. Zheng, "A Preliminary Study of Ignition Consistency and Heat Release Analysis for a Common-Rail Diesel Engine", SAE Paper 2004-01-0932, 2004.

b)   Other Publications

12) X. Han, U. Asad, **R. Kumar**, M.C. Mulenga, S. Banerjee, M. Wang, G.T. Reader and M. Zheng, "Empirical Studies of Diesel Low Temperature Combustion on a Modern Diesel Engine", Combustion Institute/Canadian Section (CI/CS), 2007.

13) W. de Ojeda, P. Zoldak, R. Espinoza, **R. Kumar**, C. Xia, and D. Cornelius, "Multicylinder Diesel Engine Design for HCCI operation", Diesel Engine Efficiency R and D, Session of 13th Diesel Engine-Efficiency Emissions Research (DEER) Conference, 2007.

14) M. Zheng, G.T. Reader, **R. Kumar**, M.C. Mulenga, U. Asad, Y. Tan and M. Wang, "Adaptive Control to Improve Low Temperature Diesel Engine Combustion", Advanced Combustion Technologies Session of the 12th Diesel Engine-Efficiency Emissions Research (DEER) Conference, 2006.

15) **R. Kumar**, M. Zheng, G.T. Reader, M.C. Mulenga, W. Bombardier, S. Ko and M. Wang, "A Study on the Energy and Emission Efficacy of Multi-Pulse Fuel Injection on Low-Temperature Combustion", Combustion Institute/Canadian Section (CI/CS), 2006.

16) **R. Kumar**, Yue Wu, G.T. Reader, and M. Zheng, "Effect of Heat-Release Rate Shaping on Engine Indicated Mean Effective Pressure", Combustion Institute/Canadian Section (CI/CS) 2004.

17) M. Zheng, G.T. Reader, **R. Kumar**, M.C. Mulenga, U. Asad, Y. Tan and M. Wang, 3 Confidential Industrial Reports for Year 2004, 2005 and 2006.

18) M. Zheng and **R. Kumar**, "Implementation of Multiple-Pulse Injection Strategies to Enhance the Homogeneity for Simultaneous low-NOx and low-soot Diesel Combustion", Manuscript submitted to International Journal for Thermal Sciences.